P 2 mic

NASA TECHNICAL MEMORANDUM

NASA TM X-62,310

NASA TM X-62,310

PRELIMINARY ASSESSMENT OF THE MICROWAVE LANDING SYSTEM REQUIREMENTS FOR STOL OPERATIONS

Clifford N. Burrous, Stuart C. Brown, Tsuyoshi Goka, and Kun E. Park

Ames Research Center
Moffett Field, California 94035

October 1973

ABSTRACT

This report describes the results of an investigation made to assess the Microwave Landing System (MLS) Requirements for use by civil STOL aircraft. A set of requirements was proposed for general use by the RTCA SC-117. The principal MLS characteristics investigated in the report were signal accuracy and volume of coverage. The study utilized a nonlinear six-degree-of-freedom digital simulation of a De Havilland Buffalo C-8A aircraft. Fully automatic control of timed curve flight down to touchdown was simulated.

Selected MLS accuracy and coverage parameters for the azimuth, primary elevation, flare elevation and DME signals were varied. The resulting STOL aircraft system performance in following a representative curved flight path was statistically determined. Coverage requirements for STOL aircraft operating in the terminal area environment were also investigated.

TABLE OF CONTENTS

PRELIMINARY ASSESSMENT OF THE MICROWAVE LANDING SYSTEM REQUIREMENTS FOR STOL OPERATIONS

Clifford N. Burrous, Stuart C. Brown, Tsuyoshi Goka,
and Kun E. Park
Ames Research Center

I. INTRODUCTION

A program is in progress to develop an advanced universal Microwave Landing System (MLS) which is intended to eventually replace the present-day ILS system (ref. 1). The new system is to provide a signal in space of sufficient accuracy and volume to allow up to category IIIC landings and to satisfy future terminal area approach navigation requirements. The expanded coverage requirements are directed toward providing relief to the terminal area traffic problem by allowing curved approaches and multiple final approach paths. The system is intended for use by all types of aircraft, and the Radio Technical Commission for Aeronautics (RTCA) Special Committee (SC)-117 has prepared a preliminary set of requirements for it. Several groups (refs. 2-8) have investigated the suitability of the requirements for CTOL aircraft. The NASA Ames Research Center, under the Task Order of reference 9, has conducted an investigation of the adequacy of these requirements for use by civil STOL aircraft. The requirements assessed include the following MLS characteristics:

(1) Available functions (Azimuth, Elevation, DME, etc.)

(2) Information rate

(3) Information accuracy

(4) Volume of coverage

The emphasis in this report is on the last two characteristics.

The MLS provides a signal in space to be utilized by the airborne avionics to perform sensing and guidance functions which determine the course to be followed by the aircraft. The control system utilizes this guidance information to determine the proper commands to the aircraft control system. To evaluate overall suitability of the MLS characteristics for STOL operational requirements, a spectrum of airborne avionics capability should be considered. In this initial effort, the approach taken was to select an available controlled aircraft simulation which could be used to evaluate at least a number of the more critical requirements.

The primary tool used for this investigation was an extensive digital simulation facility (ref. 10) which was developed for the joint DOT/NASA Operating Experiments Program. The STOL aircraft simulated was a De Havilland Buffalo C-8A aircraft. The level of automation available for the airborne part of the simulation ranged from a manual mode with raw data displays to a fully automatic mode with timed curved flight to touchdown. Only the fully automatic mode was used in the present study. Selected MLS accuracy and coverage parameters for the azimuth, primary elevation, flare elevation, and DME signals were varied. These parameters included random uncorrelated and correlated noise, bias errors, data rate, and horizontal coverage. The resulting STOL aircraft system performance in following a representative curved flight path was statistically determined. The performance parameters included averaged aircraft vertical and horizontal position and attitude dispersions of selected points along the flight path including touchdown.

Coverage requirements for STOL aircraft operating in the terminal area were also investigated. Two representative STOL curved flight paths were selected and effects of MLS coverage on the ability of the aircraft to follow these flight paths were determined.

II. SYSTEM DESCRIPTION

A general description of the computer simulation and the components to be represented are described in this section. First an overall description of the simulation equipment is given. Then the aircraft, and its controls are described. Next the simulation of the MLS navigation system, the siting, and the associated filtering is discussed. Finally, the particular flight paths chosen, and the environmental disturbances selected are introduced.

A. STOLAND Simulation Equipment System Features and Functions

STOLAND was developed to facilitate flight and simulator research in V/STOL terminal area navigation, and guidance and control concepts; the resultant research tool is an integrated digital system using ARINC specified airborne hardware.

The simulation facility (Fig. 1) consists of: a) an EAI 8400 digital computer to simulate the aircraft (C-8), Navaids (TACAN, VOR/DME, MLS, etc.) plus winds and turbulence, b) an Avionics equipment rack containing ARINC specified airborne hardware including a Sperry 1819A digital computer, cockpit display generators, together with an airborne hardware simulator and data adaptor for transforming the Navaid information generated on the 8400 to the form received by the airborne receivers, c) a simulation cockpit (Fig. 2) containing standard airborne instrumentation together with advanced display and mode select system, d) an EAI 8800 analog and logic computer simulating the control surface servos and interlock logic, and e) a data conversion rack to electrically interface all these subsystems.

The STOLAND airborne hardware block diagram is shown in Fig. 3; note that all the navigation sensors including the MLS are included. The data adapter acts as an interface between various elements of the system and also

between the system and the aircraft. Communication with the computer is by means of high-speed parallel data transfer (18 and 36 bit). Nonetheless, serial data communication is used extensively to minimize interface wiring difficulties. Interfaces contained in the data adapter meet the requirements of standard ARINC characteristics 547 (VHF/NAV receivers), 552 (radio altimeter), 568 (DME), and 561 (INS), as well as MLS equipment which falls under the research or prototype category.

A key element of the validation facility is the airborne hardware simulator (AHS), which provides an exact electrical interface for all airborne sensors and subsystems that interface with the data adapter. An illustration of the AHS function and its importance in the system validation concept can be given with the DME as an example. The DME error model (including quantization effects) is computed in the simulation equations (on the 8400) and the numerical value which would be measured by the DME receiver is transmitted to the AHS. Within the AHS, DME data is encoded into the six-wire, serial digital format used by actual airborne DME hardware; it is then transmitted to the data adapter at the same data rate and with the identical electrical characteristics used by the DME receiver. This serial data must be decoded, stored, and transmitted to the airborne digital computer by circuit elements within the data adapter. In this manner, the AHS allows an exact duplication of all airborne data traffic that must enter and leave the STOLAND computer complex. Not only are the hardware interfaces of the data adapter thoroughly exercised by this procedure, but also all of the computer's software - for input-output, data acquisition, and analog-digital conversion - can be validated. To the extent that the entire real-time data flow and system accuracies are exactly duplicated, a flight in the simulator becomes truly representative

of a real flight, insofar as the avionics computer complex is concerned.

Besides conventional flight instrumentation, the cockpit (Fig. 2) contains an electromechanical horizontal situation indicator (HSI), an electronic attitude direction indicator (EADI), and a multi-function display (MFD) for presenting a complex moving map that shows the selectable flight path. A keyboard is provided for data entry into the computer and the mode select panel is the primary means for selecting guidance and control modes and setting flight path reference values.

Four levels of automation are available with the system (Fig. 4). These range from raw data display and unaugmented manual control (Manual I) to fully automatic flight in 4D to touchdown (Automatic II). Only the fully automatic mode was used in the present study.

B. Aircraft

The STOL aircraft simulated in this study is a prototype version of the De Havilland DHC-5. This aircraft was designated CV-7A by the U.S. Army and later redesignated C-8A by the U.S. Air Force. See Figure 5 for the various physical and performance specifications (ref. 11).

The simulation model includes the six-degree-of-freedom nonlinear equations of motion; the kinematic and nonlinear aerodynamic equations; a GET64-10 turbo-prop engine model; pitch, roll, and yaw parallel control servo models; and a simulated servo-interlock-unit (SIU).

C. Control Laws

The aircraft control system functions are programmed in the airborne digital computer. Generally, the sensing and frequency ranges used are comparable with present-day advanced autopilots. Block diagrams and equations

of the principal control functions are listed in Figures 6 to 20. The diagrams and equations are intended to show only the form of the control laws used since many of the constants listed are in bit scaling form rather than in dimensional form. The curved flight path guidance and control portion of the system has not been shown. Although implemented digitally, the equations are shown in a more convenient analog form.

D. MLS Model and Signal Processing

The portion of the simulation concerned with the MLS signals and their initial processing is shown in Figure 21. Geometry for the MLS navigation is shown in Figure 22. Aircraft position coordinates are converted into MLS coordinates using planar angle equations (Fig. 23). Error quantities are then added to the MLS signals. Provision was made in the computer program for varying the following quantities.

- Accuracy
  - Random Noise
  - Bias Errors
  - Granularity
  - Correlated Noise
- Data Rate
- Coverage

The conversion of the MLS position coordinates to inertially referenced x, y, z coordinates in the airborne computer is given by the planar angle equations in Figure 24. The z coordinate is blended from the EL_1 antenna source to the EL_2 antenna source between 400 and 200 ft. The X_R', Y_R', Z_R' quantities are then sent to the navigation filters along with the resolved acceleration signals. The filtered position and velocity signals are then transmitted to appropriate portions of the guidance and control systems.

E. STOLport Geometry

The MLS siting geometry for a representative STOLport is shown in Figure 25. This configuration was used for all of the results presented. Because of the short runway, the EL_I transmitter was situated relatively close to the threshold. The distance between the two elevation antennas was made as large as feasible after considerations of aircraft landing dispersion and stopping distance requirements.

F. Navigation Filtering

The filters used for this preliminary MLS study are fixed configuration complementary filters that are intended for use with a variety of navigation aids and control system modes. As shown in Figure 21, the filter combines resolved accelerometer information with navigation aid derived position information given in an earth-referenced rectangular coordinate system. The outputs are filtered position and velocity information. The filter block diagram is shown in Figure 26. Note that the horizontal channel involves three integrators whereas the vertical channel involves two. The loop containing ω_1 in the horizontal filter is used only for filter initialization.

For the basic complementary filter configuration, two sets of filter gains were used (Fig. 27); one moderately low gain configuration to be called the nominal frequency filter, the other a high gain configuration to be called the high frequency filter. For the former case, the gains were chosen based on an airborne filter presently being tested in a Convair CV-340. The position signal error cutoff frequency was about 0.1 radian/sec for the horizontal and of 0.9 radian/sec for the vertical (see Fig. 28). The high frequency, which results in about three times the bandwidth of the previous filter, was treated to assess the relative weightings between MLS error signals and the accelerometer error signals in obtaining the estimates. The problem

of selecting the relative weighting between MLS position and accelerometer errors is a very difficult one. By testing two distinctly separate filter bandwidths, we believe we have gained considerable insight into the problem.

Finally, the filter configuration without the accelerometer measurements was tested to arrive at some qualitative conclusions about the need for on-board accelerometers.

(1) Complementary Filter Equations

The filter state equations after initialization (i.e., after the ω_1 loop is opened) are given by (see Fig. 26 for the block diagram):

$$\frac{d}{dt}\begin{bmatrix}\hat{Y}_R\\ \hat{\dot{Y}}_R\\ B\end{bmatrix} = \begin{bmatrix}-\omega_2 & 1 & 0\\ -\omega_3 & 0 & 1\\ -\omega_4 & 0 & 0\end{bmatrix}\begin{bmatrix}\hat{Y}_R\\ \hat{\dot{Y}}_R\\ B\end{bmatrix} + \begin{bmatrix}\omega_2 & 0\\ \omega_3 & 1\\ \omega_4 & 0\end{bmatrix}\begin{bmatrix}Y_R'\\ \ddot{Y}_R\end{bmatrix}$$

$$\frac{d}{dt}\begin{bmatrix}\hat{Z}_R\\ \hat{\dot{Z}}_R\end{bmatrix} = \begin{bmatrix}-\omega_2 & 1\\ -\omega_3 & 0\end{bmatrix}\begin{bmatrix}\hat{Z}_R\\ \hat{\dot{Z}}_R\end{bmatrix} + \begin{bmatrix}\omega_2 & 0\\ \omega_3 & 1\end{bmatrix}\begin{bmatrix}Z_R'\\ \ddot{Z}_R\end{bmatrix}$$

where

$\hat{Y}_R$, $\hat{\dot{Y}}_R$ = smoothed Y-position and velocity,

B = estimated accelerometer drift term,

$\hat{Z}_R$, $\hat{\dot{Z}}_R$ = smoothed Z-position and velocity,

Y_R', Z_R' = MLS induced position measurements,

$\ddot{Y}_R$, $\ddot{Z}_R$ = inertially resolved accelerations.

The X-channel has the same equation as Y-channel.

The two equations are given in frequency domain form as follows:

$$\begin{bmatrix}\hat{Y}_R(S)\\ \hat{\dot{Y}}_R(S)\\ B(S)\end{bmatrix} = \frac{1}{\det_1}\begin{bmatrix}\omega_2 S^2 + \omega_3 S + \omega_4 & S\\ S(\omega_3 S + \omega_4) & S(S + \omega_2)\\ \omega_4 S^2 & -\omega_4\end{bmatrix}\begin{bmatrix}Y_R'(S)\\ \ddot{Y}_R(S)\end{bmatrix}$$

$$\begin{bmatrix} \hat{Z}_R(S) \\ \hat{\dot{Z}}_R(S) \end{bmatrix} = \frac{1}{\det_2} \begin{bmatrix} \omega_2 S + \omega_3 & 1 \\ \omega_3 S & S + \omega_2 \end{bmatrix} \begin{bmatrix} Z_R'(S) \\ \ddot{Z}_R(S) \end{bmatrix}$$

where

$$\det_1 = S^3 + \omega_2 S^2 + \omega_3 S + \omega_4$$

$$\det_2 = S^2 + \omega_2 S + \omega_3$$

The table in Figure 27 summarizes the filter gains, and the frequency responses of selected transfer functions are plotted in Figure 28.

(2) Noncomplementary Filter

Without the accelerometer measurement, it is felt (based on an IBM 360 study) that at least three integrators are needed for the lateral channel for adequate filter tracking capability and for sufficiently smooth state estimation. This can be done with the basic configuration by closing the switch S_1 in the accelerometer drift compensation loop of Figure 26. For the vertical channel a two-state filter is used. The filter state equations are given by removing the acceleration terms from the complementary filter equations previously given. For this reason the equations will not be explicitly given for this case.

For the horizontal channel the filter gains are so chosen that the characteristic polynominal is of the form $S^3 + \omega_2 S^2 + \omega_3 S + \omega_4 = (S + \alpha)^3$.

For the vertical channel the filter gains are chosen so that the characteristic polynominal is of the form $S^2 + \omega_2 S + \omega_3 = (S + \alpha)^2$. Then the parameter α and the localizer tracking control law gains are "tuned" for satisfactory filter performance. It should be stressed here that in choosing the filters as well as the control gains, the smoothness of the control motions were more heavily weighted as long as the filter tracking performance was acceptable.

The final filter gains are summarized in Tables 3 and 4 (Fig. 27). The frequency response curves are found in Figure 29.

G. Flight Paths

Two typical STOL flight paths were chosen for the study - one 90° and the other an 180° final turn (Figs. 30-33). These paths were chosen to utilize the STOL aircraft's steep descent capability. One and one-half minute of straight-in final approach was selected to allow for the pilot's final system checks. The flight paths were flown at a constant approach speed so that the longitudinal control could be more readily monitored. (See Section IIIC for additional discussion of flight paths.)

H. Environmental Model

Reasonable combinations of environmental conditions were selected for the MLS simulations in accordance with reference 12. The variation of the wind and turbulence models with altitude is shown in Figure 34. The wind direction selected was from 30° with respect to the runway direction. The effective height of the aircraft at touchdown was 10 ft. Moderate size wind and turbulence were chosen for the real-time simulation because the main objective was to assess the MLS errors for STOL operations. The wind model was used in all the simulation results but turbulence was added only when indicated.

III. DATA

This section contains all of the data analysis for this task, and Section IIIF includes a table of the statistical mean and standard deviations for each set of conditions. Before proceeding with the analysis, several details need to be mentioned which were not covered in the general systems description.

A. Simulation Conditions and Criteria

Figure 35 shows the two sets of MLS (bias and random) error combinations which were utilized in Section IIIB2, 3, and 4. The first set, to be called the CAT III combination, was established by converting the RTCA-117 CAT III MLS touchdown displacement errors to angular errors for the STOLport MLS siting shown in Figure 25. These angles became significantly larger than those shown in DO-148 because the STOLport is one-seventh the length of the RTCA-117 14,000 ft CTOL runway. The CAT III errors are the smallest used in this simulation and they form the base for all other data. The second set, to be called the CAT II MLS error combination, was not derived from DO-148. The combination was developed by increasing MLS random and bias errors so that the controlled aircraft tracking errors (in the presence of the assessed wind and turbulence) would be somewhat greater than the present CTOL CAT II touchdown and decision height criteria. No attempt was made, however, to include all of the factors contributing to total aircraft dispersions (all MLS errors listed are $\pm 1\ \sigma$).

All runs were made with the following conditions:

- 6° glideslope
- Flight path no. 1 (except Sec. IIIC)
- Initialization at y = -20,000 ft with stability achieved prior to WP. no. 2 after the addition of wind (except Sec. IIIC)
- All runs included the wind of Section III
- MLS coverage limits of ±60° azimuth horizontal and 20° elevation vertical (except Sec. IIIC). The other coverage parameters were not limited.
- MLS data rate = 5.0 Hz except EL_2 = 10.0 Hz (except Sec. IIID).
- STOLAND operation in Automatic II (synonymous to autoland)

- The 8400 computer printout was initiated by altitude at all points except the start of G/S which was triggered by lateral position from the runway centerline
- 10 runs for all random errors
- 3 runs for all individual bias errors
- The MLS resolutions as shown in Figure 36

All the figures of dispersions at touchdown and at various altitudes were plotted with ±1 σ dimensions.

Figure 37 lists all of the symbols used in the time history strip chart recordings. The sample time histories in this report are taken from a multiplexed strip chart recorder; hence there are generally two sets of data shown on each recording. The left-hand scale on these figures represents the continuous solid trace and the second scale represents the discontinuous trace. For example, the fourth trace from the top of Figure 62 shows a continuous solid line for the aircraft lateral (Y) position (off scale initially), and the discontinuous unconnected data is the aircraft lateral acceleration ($\ddot{Y}_B$). The ratio of total aileron position to the wheel position shown is 0.5.

MLS error combination data were taken with fixed positive bias levels with no random selection of bias for each run. Therefore, a true ensemble mean and standard deviation for each set of runs was not obtained. However, since only a limited number of runs were feasible for each set of conditions, it was felt that a more clear presentation of the separate effects of the MLS random and bias errors could be achieved by this procedure. When necessary, estimates of the combined effects have been made.

One of the most difficult parts of this task is the comparison of the simulation results to a known STOL criteria. There are no real FAA or ICAO specifications for any category of STOL touchdown or decision height dispersions. In lieu of such standards the results are compared to the existing ILS/MLS/CTOL

specifications shown in Figure 38. Note that the FAA criteria (parts A and B) are based on aircraft errors due to all sources, whereas the ICAO (part C) and RTCA (part D) criteria pertain only to ILS and MLS error sources. One of the objectives of the Joint DOT/NASA STOL Operating Experiments Program is to develop a data base for establishing such criteria.

B. Accuracy

This section includes the evaluations of individual and combination MLS errors. The data presented in subsections 1 and 2 were taken with the nominal airborne complementary navigation filters described in Section II. Other forms of airborne filtering were evaluated in subsections 3 and 4.

1. Individual MLS Errors

All of the individual MLS error data presented in this subsection were evaluated with the nominal airborne complementary filter discussed in Section II. (Individual MLS error sources were not evaluated with any of the other forms of airborne filtering.)

(a) Bias Errors

Each bias error was evaluated separately except for certain combinations of EL_1 and EL_2. Since no random errors were included in the bias runs, only three runs were made at each error condition. During the assessment of each bias error all other bias errors were held at the low CAT III levels defined in Figure 35.

Azimuth Bias

The effect of azimuth bias errors can actually be evaluated analytically, however, simulations were conducted in order to validate the theoretical conclusions. The three levels of azimuth biases evaluated include +0.124°, +0.2°, +0.4°, and -0.4°.

Figure 39 shows the effect of azimuth bias on lateral touchdown dispersion. (The data are normalized in X.) The actual (mean) lateral touchdown points are in good agreement with the theoretical points at the higher positive angles but vary somewhat elsewhere. An MLS azimuth bias of 0.4° produces ≈14 ft (1 σ) of lateral touchdown error which slightly exceeds the 1 σ ± 13.5 ft FAA CTOL lateral touchdown criteria (ref. 12).

Figures 40 and 41 show the effect of positive azimuth biases on aircraft positions at 100 ft and 200 ft altitudes. The actual (mean) aircraft positions are displaced further to the right (similar to the touchdown points) and lower than the theoretical points. The aircraft is within the AC 120-20 CTOL CAT II window even with 0.4° of azimuth bias (at either altitude), however, this value is too large to allow for reasonable values of random azimuth noise, horizontal turbulence, etc. Figure 42 shows the effect of ±0.4° azimuth bias on the entire flight path.

Elevation Bias

Figure 43 demonstrates the effect of EL_1 and EL_2 biases on touchdown dispersions. The combinations with equal (or near equal) error magnitudes were chosen to simulate a single elevation antenna, since, in all cases a blending of EL_1 and EL_2 data occurred in the 400 to 200 ft altitude area. Notice that the ±0.2° elevation error case results in approximately 200 ft of longitudinal touchdown dispersion (1 σ total), which is unacceptable for this single error source.

Figure 44 shows the effect of the same elevation biases at the 100 and 200 ft altitudes. Again the ±0.2° biases exceed the 1 σ AC 120-20

window specifications. The other values of elevation bias shown would probably allow enough latitude for the addition of reasonable levels of elevation random noise, vertical turbulence, etc. The apparent discrepancy of positive elevation biases causing the aircraft to be low at either elevation can be explained by the fact that

$$\theta_{measured} = \theta_{actual} + \theta_{bias}$$

and the vertical control system feedback tends to force $\theta_{measured}$ to equal the air selectable $\theta_{nominal}$, hence

$$\theta_{actual} = \theta_{nominal} - \theta_{bias}$$

For +0.2° elevation bias and a 6.0° selected θ, θ_{actual} equals 5.8° and the aircraft will in fact be low at the 100 and 200 ft elevations. The fact that the flights which are lower at the 100 and 200 ft elevations produce longer longitudinal touchdown is explained by the trend toward longer flares with lower glideslopes.

DME Bias

Figure 45 demonstrates the dramatic effect of DME bias on longitudinal touchdown. (This is a conventional exponential flare law as described in Sec. II.) The ±300 ft biases are clearly unacceptable. The ±100 ft values produce an X dispersion of 240 ft, and are thus also too high when combined with other errors such as DME random noise, elevation bias and random errors, turbulence, different winds, etc. Figure 46 illustrates the rapid increase in aircraft sink rate ($\dot{h}$) as the DME bias exceeds either plus or minus 100 ft. The increase in sink rate with negative DME biases is caused by the lower flare initiation and subsequent incomplete flare and short/hard landing. With positive DME biases the aircraft tends to float and then drops the last several feet of altitude to touchdown. The effect of DME bias on Δh at

either elevation is small and not well correlated as shown in the tables of Section IIIF. The last two figures show that autoland touchdown performance is very sensitive to DME bias. If the DME range and EL_1 or EL_2 elevation angle are used to compute altitude as in this simulation, STOL operations will require the DME bias errors to be less than ±100 ft. Depending on the magnitude of the other errors which affect longitudinal touchdown, the DME bias can probably be greater than the ±20 ft RTCA-117 CAT III specification. Figure 47 shows the effect of ±300 ft DME bias on the horizontal portion of the entire flight path.

(b) Random Noise

Ten runs were made for each set of random error conditions. As in the individual bias error cases, the effects of random errors were only assessed for the nominal complementary filter. All individual random error runs include the CAT III random and bias error background on all functions except the one error under study. (All data were taken with the wind of Sec. II included.) All of the figures in this section are drawn with 1 σ total dimensions.

Azimuth Random Noise

Figure 48 shows the effect of azimuth random noise on lateral touchdown. dispersion. Notice the mean is shifted approximately 1 ft and the dispersion is increased 50% with an increase of azimuth random noise from 0.112° to 0.3°. However, the lateral touchdown dispersion caused by the 0.3° random azimuth error will not be within the present AC 20-57A CTOL CAT II autoland lateral dispersion specification when combined with reasonable values of azimuth bias and turbulence. Figures 49 and 50 illustrate the effect of random azimuth noise on lateral dispersion at the 100 and 200 ft elevations, respectively. The 0.3° random error increases the dispersion by a factor of 4 or 5, but when coupled with reasonable values of azimuth bias errors and turbulence the total lateral dispersion may still be within the ±72 ft (2 σ) AC 120-20 CTOL

specification. The effect of the 0.3° random azimuth error for the entire flight path (FP no. 1) can be seen in Figure 51.

DME Random Noise

Figure 52 compares the effect of 20 ft and 300 ft DME random noise on touchdown dispersions. The 170 ft (1 σ total) longitudinal dispersion caused by the 300 ft DME random error is excessive even if the related DME bias error were under ±100 ft. The effect of the 300 ft DME random noise prior to the final turn in flight path no. 1 is shown in Figure 53.

Elevation Random Noise

Figures 54 through 58 show the effect of EL_1 and EL_2 random errors on touchdown performance and aircraft position at various altitudes. Basically, all of these figures demonstrate that elevation errors in EL_1 and/or EL_2 have very little effect on vertical guidance with the nominal vertical complementary filter. Figure 58A shows a significant increase in $\dot{h}$, Δh, and forward velocity oscillations prior to EL_2 blending (400 to 200 ft altitude) when the EL_1 random noise is increased from 0.032° to 0.15°. Notice that the flare performance is adequate in both cases with CAT III EL_2 errors.

(c) Correlated Noise

A preliminary assessment of the effects of correlated noise was made. The low frequency noise component will always be present to some extent in the signal even though most of the noise energy will be concentrated at the higher frequencies. A principal source of this noise is multipath effects although other causes, such as filtering in the airborne receiver, may also result in correlated noise at the airborne receiver output. No attempt was made to assess the magnitude of these sources of the correlated noise. Instead, noise parameters were selectively varied to provide information

on the magnitudes necessary to cause interference with aircraft tracking performance. Only effects of correlated noise in the azimuth angle measurement were investigated in this initial assessment.

Comparisons of azimuth correlated noise (T = 2 sec) with uncorrelated (white) noise are summarized in Figures 59 and 60. A magnitude of 0.3° was selected in order to more clearly show trends and allow comparisons to the same magnitude of azimuth uncorrelated noise. The previously described CAT III values of random and bias errors were used for the other MLS quantities together with the nominal wind disturbance. The correlated noise case produces considerably greater lateral position and rate errors for all locations. A comparison of touchdown dispersions is shown in Figure 61. Both the mean and standard deviations are larger for the correlated noise case. The increase in the former quantity is believed to reflect the deterioration in decrab control in the crosswind. Note that the overall lateral dispersion due only to random errors approximately equals the proposed 12 ft lateral standard deviation limit for STOL aircraft discussed in Section III. Typical time histories of these responses are shown in Figures 62 and 63. Note the large increase in lateral acceleration and position, and yaw angle for the correlated noise case. An X-Y plot of the case with azimuth correlated noise is shown in Figure 64.

It is seen that even with the use of acceleration signals in the filtering, the presence of correlated noise results in a much more difficult filtering task than is the case with only white noise. Hence, in addition to the limits on magnitudes of the random noise for the MLS variables, a specification may be required which describes the frequency content required as well.

2. MLS Error Combinations (with the Nominal Complementary Filter)

This section contains the results obtained with the CAT III (RTCA) and CAT II MLS random and bias error combinations shown in Figure 35. The nominal complementary navigation filtering was utilized for all runs and the wind described in Section II was present. The CAT III and CAT II errors were also run with turbulence (Sec. II), and the results are compared in subsections b, d, and e.

(a) CAT III (RTCA) Random and Bias Errors Without Turbulence

Figures 65 and 66 show the effect of the CAT III random and bias errors on dispersions at touchdown and at the 100 and 200 ft elevations. As expected, the dispersions are well within the applicable standards. Figure 67 shows a sample time history of these runs. (This data will be used repeatedly as a comparison for the other levels of MLS errors, turbulence and forms of airborne filtering.)

(b) CAT III MLS Random and Bias Errors With Turbulence

The effects of CAT III MLS random and bias errors and turbulence are shown in Figures 68 through 71. A substantial increase is noted in touchdown dispersion and Δh dispersions at the two elevations. The longitudinal dispersion is increased by a factor of 4.5 with turbulence (Fig. 68) and is very close to the limit of the tentative 700 ft (1 σ total) STOL criteria (first part of Sec. III). The lateral touchdown distribution is increased by a factor of 3 but still is within the AC 20-57A CTOL criteria. With turbulence, the Δh distribution at 100 ft altitude increases by a factor of 3.2 and falls just outside of the AC 120-20 specification. Figure 71 shows a typical time history with turbulence. Comparing this time history to CAT III without turbulence (Fig. 67) shows a substantial increase in the variations of $\dot{h}$ and Δh is seen.

(c) CAT II MLS Random and Bias Errors Without Turbulence

Figures 72 through 75 show the comparison between CAT II and CAT III MLS random and bias errors without turbulence on dispersions at touchdown, 100 ft and 200 ft altitudes and the localizer intercept point. The 173 ft increase in the mean longitudinal touchdown point with CAT II errors is primarily due to the increase in DME bias from +20 ft to +100 ft. (The individual DME bias data of Sec. IIIA1a shows an increase in X_{TD} of 115 ft. The 3-to-1 increase in positive elevation bias and 5-to-1 increase in DME random noise also contribute to the longer X_{TD}.) If random bias errors are assumed, estimates indicate that the system does not meet the tentative STOL touchdown criteria with CAT II MLS errors for longitudinal dispersions although lateral dispersions are within limits.

The 10 ft increase in the mean y at 100 ft elevation shown in Figure 73 can be attributed to the increase in azimuth bias from +0.124° to +0.3° (see Sec. IIIA1a), however the Δh and y dispersions are within the AC 120-20 CAT II ILS/CTOL window. A sample time history with CAT II MLS random and bias errors without turbulence is shown in Figure 76. Compared to the CAT III MLS errors (Fig. 67), the CAT II errors produce greater variations in nearly all parameters. (The aircraft does flare with the CAT II errors, but it tends to float excessively.) X-Y plots of the 90° final turn flight path trajectory for CAT II and CAT III MLS errors are shown in Figures 77 and 78, respectively. As can be seen, the aircraft tracks the horizontal flight path quite well with either set of MLS errors.

(d) CAT II MLS Random and Bias Errors With Turbulence

Figure 79 compares the touchdown performance with and without turbulence with CAT II MLS error conditions. This level of turbulence increases the longitudinal and lateral touchdown distributions by a factor of approximately 3.5. (Adding the same turbulence to CAT III MLS errors causes a 4.5 and 3

increase in these dispersions, respectively.) The 1 σ total longitudinal touchdown footprint of Figure 79 exceeds the tentative STOL criteria of Figure 38 by a few feet. The 730 ft extremity of this dispersion is over one-third of the runway length. A fully loaded C-8A aircraft can stop in 700 to 1200 ft, leaving a safety margin of nearly 700 ft; however, preliminary results with 15 knots headwinds and tailwinds indicate that the longitudinal dispersions may increase by approximately another 200 ft. These variations coupled with runway altitude variations could reduce the safety margin to an unacceptable level. The lateral touchdown dispersion exceeds the tentative STOL specification (±14 ft compared to ±12 ft).

Figure 80 compares the dispersions at 100 ft with and without turbulence with the CAT II MLS errors. Again, the turbulence causes the G/S tracking performance to fall outside of the ±6 ft AC 120-20 vertical specification interpretation.

(e) Comparison of CAT III and CAT II MLS Errors With Turbulence

Figure 82 compares the touchdown performance with CAT II and CAT III MLS errors and turbulence. The mean longitudinal touchdown point is increased by 130 ft due to the CAT II MLS errors. (Primarily the 3-to-1 and 5-to-1 increase in positive EL and DME biases, respectively.) Notice that the 1 σ longitudinal dispersions are very similar (approximately 200 ft).

As previously stated, the addition of turbulence to either combination of MLS errors causes the longitudinal touchdown footprint to reach the 600 or 700 ft mark. This is a substantial portion of the runway length.

The mean lateral touchdown point is increased from +1 ft to +9 ft due to the CAT II MLS errors. This is primarily due to the larger CAT II 0.3° azimuth bias as shown by Figure 39. The 1 σ lateral standard deviations are almost identical.

Figure 83 shows the dispersions at 100 ft altitude for CAT II and III MLS errors with turbulence. Neither are outside the AC 120-20 ±32 ft CTOL 100 ft horizontal window specification; however, both fall slightly above the ±6 ft vertical window criteria. The CAT II lateral mean and standard deviations are approximately four and two times larger, respectively, than the CAT III case because of the approximate 3-to-1 and 2-to-1 increase in azimuth bias and random errors, respectively. Figure 83B shows a sample time history with CAT II MLS errors with turbulence.

3. Complementary Filter Variations

The complementary filter characteristics and the nominal values used were described in Section II. In this section, the changes in aircraft response will be examined which result from an increase in the cut-off frequency of the position error response of the horizontal and vertical filters. The filter gains for both the horizontal and vertical filters were adjusted to increase the filter breakpoint frequencies by a factor of 3, while the frequency response shape for position errors was maintained. These adjustments resulted in an increase in the position error cutoff frequency from about 0.5 rad/sec to 1.5 rad/sec for the horizontal filter and from about 1.0 rad/sec to 3.0 rad/sec for the vertical filter. The design of a complementary filter involves tradeoffs between filtering the high frequency portion of the position signal relative to the low frequency portion of the acceleration signal. The transfer function relations are given in a previous section. Increasing the filter gains (increase in position error cutoff frequency) results in a deterioration of the position error filtering while improving the low frequency acceleration filtering. Hence the increased gain setting represents a filter adjustment which relies more on the MLS position information and it could be indicative of a compromise needed to further reduce acceleration errors associated with a minimum cost accelerometer installation.

Comparisons of vertical and lateral dispersions at several waypoints for the nominal and high frequency filter are shown in Figures 84, 85, 86, and 87. The previously described CAT II values of random and bias MLS errors were used together with the nominal wind disturbance. Touchdown conditions are not shown since CAT II specifications are primarily intended for use above a decision height. The errors for the high frequency filter are seen to be much larger than those for the nominal filter for all cases. The relatively large lateral dispersions can also be seen from the X-Y plot (Fig. 88) and the example time histories (Figs. 89 and 76). Both the lateral and vertical errors for the high frequency filter at the 100 ft altitude exceed those considered to be maximum allowable values (6 ft vertical and 36 ft lateral, 1 σ). The use of a randomly selected bias in the simulation would not alter this situation. Since no margin is allowed for effects of other conditions such as turbulence or different wind magnitudes, the high frequency filter is not considered to provide adequate performance with this random noise level.

4. Noncomplementary Filter

After the filter and lateral control gains were adjusted as described in Section II, ten (10) statistical runs were made with the noncomplementary filter with CAT III random and bias errors and with the standard steady-wind and turbulence.

For comparison, the data are discussed with the runs made with the nominal complementary filter and the same MLS errors and wind conditions. The readers are referred to that section for additional information.

(a) Flare and Touchdown

The flare and touchdown performance is not satisfactory as can be seen by the excessive "floating" (see $\dot{h}$ in Fig. 90 and h in Fig. 94). The reason for this is that the aircraft dynamics are too rapid for the vertical

filter to provide usable estimates for the control system. Most likely this problem will not be cured by making the EL_2 signal more accurate or by increasing the sampling rate. Therefore for automatic landing, vertical acceleration information is probably needed to perform a satisfactory flare and touchdown.

(b) Localizer Capture and Tracking (Figure 93)

As might be expected, without the accelerometer information, the aircraft overshoots the runway centerline at the end of the 90^{o} turn. The maximum overshoot was less than 300 ft and gradually steadied out to a maximum of 23 ft at an altitude of 100 ft.

The aircraft cross-track error can be visualized by looking at X in Figure 92 and Y in Figure 91. Before the turn, the standard deviation in crosstrack error (X) is less than 20 ft; after the turn it doubles to approximately 50 ft; at the altitude of 200 ft it has decreased to about 5 ft. Except at the localizer intercept point, these variances compare favorably with the complementary filter case, despite the fact that the control gains were nearly halved.

As can be seen from a comparison with results from a previous section, the body x and y accelerations do not deteriorate materially either in magnitude or in frequency in the absence of acceleration inputs. From these data we may conclude that if enough time is available on the localizer, and if the aircraft turn rate is less than 2.3°/sec, then the noncomplementary filter can capture and stay on the localizer without excessive lateral acceleration and without excessive control motions. To state the effect inversely, if MLS high frequency errors become somewhat larger than those simulated here, then in order to obtain the suitable aircraft tracking and control performance, either the time on the localizer should increase and/or the turn rate should decrease. Therefore the impact of larger MLS higher

frequency errors with the noncomplementary filter will be the sharing of the extended runway common path with other aircraft for longer periods of time.

(c) Glideslope Capture and Tracking

The vertical filter without the accelerometer input performed comparably with the nominal complementary filter except at the initial overshoot at the glideslope initiation. For example, the standard deviations of Δh at altitudes of 100 and 200 ft are within a foot or so of each other, and the means of Δh are within 3 ft (Fig. 91A, B).

(d) Conclusions

Although acceptable tracking performance in both the horizontal and vertical channel were obtained during the landing approach under the CAT III noise level, performance during the automatic flare and landing requires at least the vertical acceleration information.

If the random noise is increased somewhat above the CAT III level, preliminary results indicate that the performance may be satisfactory if the magnitudes of the flight path maneuvers are reduced so that lower control gains can be used. The reduction in maneuvers include increasing the radius of turn as well as separating the one-segment 6° glide path transition into a two-segment approach.

C. MLS Coverage Requirements

The MLS coverage requirements for STOL operations were assessed in a somewhat different manner than the accuracy requirements. As discussed in Section II, the two STOL flight paths utilized in this study were heavily influenced by the FAA Flight Inspection Division's STOL approach procedures for ten real-life STOLports (ref. 13), plus NASA simulation and flight experiments with curved, descending IFR STOL approaches (refs. 14, 15).

Three of the ten STOLports studied in reference 13 required curved descending approaches and the maximum required turn was approximately 110° with a 5000 ft radius.

Figure 95 illustrates some of the basic coverage elements and summarizes the recommendations of references 14 and 15. The three elements of coverage include a minimum straight-in final approach, a minimum final turn radius and a minimum initial straight leg before any maneuver. Many factors influence the dimensions of these elements; however, one can see that the azimuth coverage requirement increases if 1) the final turn radius is increased, 2) the final approach distance is decreased, or 3) the initial approach angle is increased.

The MLS must provide elevation coverage above the potential 6° to 10° STOL glideslope angles plus a reasonable margin to allow for MLS vertical elevation coverage intercept prior to descent (see Fig. 100).

The two flight paths used in this study are repeated in Figure 96. The 90° final turn flight path (F.P. no. 1) approximates the STOL approaches in the FAA study (ref. 13). The final approach distance was selected on the basis of references 13, 14, and 15 and observations of glideslope tracking performance. Flight Path no. 2 (180° final turn) was selected as a worst case approach, and it exceeded the requirements of any of the recommended STOLport approaches of reference 13. Hence, the method used to determine MLS coverage requirements for STOL operations was to vary the simulated MLS coverages and assess the azimuth, elevation, and DME coverage required for the typical and worst-case flight paths shown in Figure 96. The results for each flight path are shown in the following two subsections.

1. Flight Path No. 1 (90° Final Turn)

Figures 97 and 98 demonstrate the effect of varying the azimuth horizontal coverage on F.P. no. 1 from ±60° to ±40°. In order to simulate a reasonable

en-route navigation aid error, the following TACAN errors were included: DME bias = +1000 ft, DME random noise = 172 ft (1 σ), bearing bias = +1.5° (the bearing random noise was inadvertently omitted). The MLS errors were the standard CAT III random and bias levels. The related EL_1 and EL_2 vertical coverage was 20° and all other coverages were unlimited. The present simulation requires that all three MLS functions (azimuth, elevation, and DME) be valid before MLS guidance can be utilized.

Figure 98 shows the horizontal transition from TACAN to MLS, for 40° and 60° of azimuth horizontal coverage. Figure 97 shows several parameters over the region from the TACAN/MLS transition through the start of the 6° G/S descent (Waypoint no. 4). The data on the left shows that for an azimuth horizontal coverage of ±60° the aircraft has had adequate time to stabilize after the TACAN/MLS transition prior to any maneuver (G/S descent at W.P. no. 4). However, the right-hand side of Figure 97 shows that reducing the azimuth horizontal coverage to ±40° leaves just enough (or insufficient in some cases) time for several aircraft position and state quantities to stabilize prior to W.P. no. 4. The aircraft made a successful autoland in both cases, however, pilots generally prefer to be stabilized prior to such a maneuver. On this basis ±40° is probably the absolute minimum azimuth horizontal coverage for F.P. no. 1. (The cost difference between ±60° vs ±40° of azimuth horizontal coverage may not be substantial). Waypoint no. 4 is at an azimuth vertical angle of 7.7°, hence an azimuth vertical coverage of approximately 10° would be satisfactory for this flight path.

Assuming the EL_1 siting of Figure 25, 40° of EL_1 horizontal coverage would just be adequate (45° or more would be preferred). The EL_1 vertical angle at W.P. no. 4 is 8.77°, hence an EL_1 vertical coverage of 10° would allow for a +300 ft elevation error.

Figure 97A is a typical F.P. no. 1 time history showing the vertical transition from TACAN to MLS coverage with a 125 ft altitude error in the TACAN coverage area. The azimuth horizontal coverage is ±60° and the TACAN-to-MLS transition starts at that point (just after W.P. no. 2) due to the "combined" MLS validation scheme discussed above. The pitch angle, flight path angle, $\dot{h}$ and Δ elevator parameters are all restabilized within ≈25 sec or 3000 ft (similar to the horizontal parameters of Figs. 97 and 97A). This leaves the aircraft stable long before the start of G/S descent at W.P. no. 4. With 40° azimuth horizontal coverage and the same MLS valid arrangement, the aircraft is barely stable in the vertical axis prior to W.P. no. 4 (just as it is in the horizontal axis). If the azimuth and elevation valids were independent the vertical transition of Figure 97A imposes no greater EL_1 coverage requirements than those stated above (EL_1 horizontal is the limiting parameter).

The characteristics of STOL aircraft and short haul air transportation operations preclude the necessity of the proposed 20 nmi MLS range. A more likely range figure is 10 nmi. This only affects the initial equipment and maintenance cost of the final power output stage for each airborne and ground function and may not be a significant percentage of the total system cost.

The use (and accuracy) of area navigation in STOL aircraft will also affect the MLS coverage requirements.

2. Flight Path No. 2 (180° Final Turn)

Figures 99 and 100 demonstrate the azimuth and elevation coverage requirements for F.P. no. 2. For this flight path the 2160 ft initial level flight does not fall within the 20° EL_1 vertical coverage until approximately 1500 ft before W.P. no. 3 (see Figs. 96 and 100). (This intersection happens to coincide closely with an azimuth horizontal coverage of 40°.) With the

MLS valid situation used, the MLS capture is delayed until the 20° EL_1 vertical coverage is intersected even if the azimuth horizontal coverage is ±60°. Figure 99 shows the large horizontal transient experienced with these TACAN errors and such a late MLS capture (or ±40° effective azimuth horizontal coverage). The flare and touchdown were satisfactory. One solution to this problem would be to provide ±60° azimuth horizontal coverage and separate valids for the MLS azimuth and elevation functions. Another solution would be to alter the flight path, however, a 2160 ft altitude level-flight prior to G/S intercept is not unreasonable (ref. 13). Figure 100 points to a potential problem concerning the vertical coverage requirements of EL_1. That is, a vertical coverage of considerably more than that required for 6° to 10° STOL glideslopes can be required for flight paths such as F.P. no. 2.

The 20° azimuth vertical coverage is adequate for this flight path. Forty degrees of EL horizontal coverage intersects F.P. no. 2 at approximately W.P. no. 3 which is just adequate.

Assuming independent azimuth and elevation valids and the same altitude error and vertical transition as shown in Figure 97A, the minimum EL_1 vertical and horizontal coverages for aircraft stability at W.P. no. 4 are approximately 15° and 40°, respectively.

3. Backcourse Coverage

The MLS backcourse coverage requirements were not assessed in this simulation; however, there are a few general comments which can be made on this subject. First, most of the presently proposed methods of obtaining backcourse MLS guidance require a second azimuth antenna installation, and this increases the total ground equipment cost substantially. (Approximately 20% compared to essentially zero for ILS.)

Most of the SID's do not utilize the ILS; however, the increased azimuth capability of MLS may make such procedures desirable in the future depending on the cost/benefit tradeoff.

The MLS could provide much greater accuracy in the backcourse for missed approaches (tens of feet errors compared to hundreds of feet for present enroute navigation aids). However, without DME or elevation information the airborne altimeters would still have to provide vertical guidance.

If the front and backcourse azimuth functions are both physically located off the stop end of the runway, as shown in Figure 101, an appreciable zone of silence would be encountered in a straight missed approach. The pilot workload and other problems associated with two transitions between the MLS and enroute navigation aids may outweigh the advantages of greater backcourse horizontal guidance accuracy. Backcourse coverage would not accommodate the missed approach procedures which call for a turn prior to the runway threshold.

4. Other Coverage Considerations

The Battelle Columbus Laboratory conducted a brief study of the MLS coverage requirements for STOL operations as part of NASA contract NAS2-6889 (ref. 16). Although space does not permit including all of the results of that study, some of the key conclusions and figures will be repeated here. Figure 102 shows the airspace within the MLS required for a family of path stretching maneuvers which would provide 60 sec of delay for three different values of azimuth coverage. The crosshatched area is the airspace required for ±60 sec of time adjustment and the dotted area is the same area shifted one-half mile to allow for adjustment of typical enroute cross track errors. The common path gate is 2 nmi for all examples. (This is close to the value used in F.P. no. 1 and no. 2.) The following table shows the reduction in common path length which results as the MLS azimuth horizontal coverage is increased.

MLS Azimuth Coverage	Common Path for Displaced Fan Family With 60 Sec Time Adjustment
±20°	11.0 nmi
±40°	7.0 nmi
±60°	6.0 nmi

As shown, a coverage increase from 20° to 40° can significantly decrease the required common path. (For short haul aircraft operations significant increases in final approach length can affect operating economics.)

Figure 102 and other data points out that if a large time of arrival control authority is required, excessive common path lengths will result if that authority is exercised solely within the MLS coverage. Hence, there is a need to perform some of this time control outside of the MLS coverage.

Figure 103 shows the increased capacity which results by reducing the common path length for two different combinations of aircraft speed mixes. Along this line, it appears possible to allot separate regions of the MLS coverage to two different speed aircraft with 20 nmi range and ±20° azimuth horizontal coverage.

Lastly, the Battelle study points out that the parallel STOL/CTOL runway situation places the most demands on the accuracy and coverage of the MLS due to the merging traffic and possible dedication of one-half of the azimuth coverage to each class of aircraft.

D. Data Rate

The MLS data rate for all previous data was 5.0 Hz for all functions except EL_2, which was 10.0 Hz. This appears to be an adequate value even with turbulence. (See the sample time histories in Sec. A.) Figure 104 shows a time history with all data rates equal to 5.0 Hz including EL_2. Figure 105 is a time history for an EL_2 data rate of 10.0 Hz with 5.0 Hz for all other

functions. Both time histories were taken with CAT III MLS errors (except EL_1 and EL_2 random errors were 0.15°), no turbulence and the nominal complementary filter. There is no obvious difference between the two runs in the region that EL_2 data are utilized, primarily flare.

E. Functions

The number of MLS functions was not varied in this study; however, successful simulations and flight tests have been made with the same facility and a tilted conical MLS system (MODILS), which has a single elevation antenna. This system has been successfully operated with a mixture of radio altimeter and MODILS derived elevation information.

F. Data Summary Tables

The following tables summarize MLS bias errors, MLS random errors, and MLS error combinations.

SUMMARY OF MLS ERROR COMBINATIONS

TOP ROW = MEAN
SECOND ROW = 1 SIGMA DEVIATION

CONDITION (Key Difference)	AT TOUCHDOWN					AT ALT. = 100 FT.					AT ALT. = 200 FT.					AT LOCALIZER INTERCEPTION					AT GLIDE SLOPE CAPTURE					
	X	Y	$\dot{Y}$	$\ddot{Y}$	Z	ΔZ	Y	$\dot{X}$	$\dot{Y}$	$\dot{Z}$	ΔZ	Y	$\dot{X}$	$\dot{Y}$	$\dot{Z}$	ΔZ	Y	$\dot{X}$	$\dot{Y}$	$\dot{Z}$	X	Y	$\dot{X}$	$\ddot{Y}$	ALT	$\dot{Z}$
CAT III Random & Bias;	340	+2.2	0.23	-2.3	-1.8	-0.8	+7.3	104	0.1	-11.0	-1.1	+8.6	104	-0.4	-10.8	14.1	-33.9	103	N.A.	-9.9	-13968	81.6	-0.3	118	N.A.	-1.7
Wind; Nominal Comp. - filter	44	1.8	0.02	1.3	0.1	1.4	1.6	0.2	0.7	0.2	1.5	1.9	0.2	1.0	0.17	9.9	6.8	1.2	N.A.	1.2	10	0.6	1.3	4.1	N.A.	0.7
CAT III Random & Bias; Wind &	403	0.5	0.22	-2.1	-2.1	-2.5	+5.2	104	+0.12	-10.9	-1.4	+7.9	103	-0.2	-10.8	-9.6	-36.0	103	N.A.	-9.3	-13974	81.2	0.8	118	N.A.	-1.5
Turb.; Nominal Comp. Filter	195	5.4	0.24	2.1	0.5	4.5	2.1	2.0	0.95	1.1	5.3	2.5	1.4	0.6	1.0	11.8	5.9	3.1	N.A.	1.4	12.7	1.1	0.9	5.5	N.A.	2.7
CAT II Random & Bias; Wind;	513	+4.2	+0.07	-2.4	-2.3	-0.9	+16.0	104	-0.6	-10.6	-2.8	+23.0	103	-1.1	-10.7	-21.2	11.9	101	5.1	-10.8	-13925	81.3	0.2	114	2135	N.A.
Nominal Comp. Filter	59	1.7	+0.08	1.3	0.4	2.0	3.8	0.3	0.7	0.2	2.2	3.8	0.4	1.4	0.4	18.9	14.9	2.6	3.8	2.6	248	0.8	1.5	2.0	19.4	N.A.
CAT II Random & Bias; Wind;	425	+13.1	+0.13	-2.2	-2.7	-3.6	+29.4	105	-1.2	-10.6	-4.9	+32.0	104	-0.9	-10.4	-12.3	39.0	107	2.3	-8.8	-13954	82.9	-3.9	110	2140	N.A.
High Frequency Comp. Filter	96	9.0	0.07	4.1	0.4	4.3	14.0	0.7	4.2	1.1	8.1	14.5	1.3	5.9	1.0	43.0	37.8	2.2	6.2	2.0	52.3	2.0	4.8	4.3	37.7	N.A.
CAT III Random & Bias; Wind &	N.A.	N.A.	N.A.	N.A.	N.A.	-4.9	+12.9	104	0.1	-10.4	-5.8	+12.7	103	+0.2	-11.8	-3.8	116.8	100	17.1	-10.8	-13971	81.2	0.03	113	2149	N.A.
Turb.; Non-Comp.-Filter	N.A.	N.A.	N.A.	N.A.	N.A.	4.6	5.0	1.3	0.8	1.3	4.2	6.6	1.4	0.9	1.4	10.0	48.6	2.9	2.6	1.6	18.2	1.3	1.1	4.1	17.8	N.A
CAT II Random & Bias; Wind,	533	9.2	0.18	-1.2	-2.3	-2.0	19.5	104	-0.11	-10.0	-3.0	21.4	103	-0.9	-10.5	-17.6	17.3	101	3.5	8.9	-13924	80.9	1.1	115	2134	N.A.
Turb.; Nominal Comp. Filter	202	5.3	0.14	2.1	0.7	5.6	4.4	1.1	1.0	3.3	7.2	5.0	2.0	1.5	1.2	14.9	11.2	3.5	2.4	2.7	16.1	1.6	2.4	2.9	16.5	N.A.

SUMMARY OF MLS RANDOM ERRORS

TOP ROW = MEAN
SECOND ROW = 1 SIGMA DEVIATION

CONDITION	AT TOUCHDOWN					AT ALT. = 100 FT.					AT ALT. = 200					AT LOCALIZER INTERCEPTION					AT GLIDE SLOPE CAPTURE					
(Key Difference)	X	Y	Ψ	$\dot{Y}$	$\dot{Z}$	ΔZ	Y	$\dot{X}$	$\dot{Y}$	$\dot{Z}$	ΔZ	Y	$\dot{X}$	$\dot{Y}$	$\dot{Z}$	ΔZ	Y	$\dot{X}$	$\dot{Y}$	$\dot{Z}$	X	Ψ	$\dot{X}$	$\dot{Y}$	Z	$\dot{Z}$
DMER = 20'	340	+2.2	+0.23	-2.3	-1.8	-0.8	+7.3	104	0.1	-11.0	-1.1	+8.6	104	-0.4	-10.8	14.1	-33.9	103	N.A.	-9.9	-13968	81.6	-0.3	118	N.A.	-1.7
	44	1.8	0.02	1.3	0.1	1.4	1.6	0.2	0.7	0.2	1.5	1.9	0.7	1.0	0.17	9.9	6.8	1.2	N.A.	1.2	10	0.6	1.3	4.1	N.A.	0.7
DMER = 300'	402	+1.1	0.18	-2.0	-1.9	-0.7	+8.7	104	-0.1	-10.8	-1.1	+10.5	103	-0.4	-11.1	-8.2	-43.3	102	1.8	-9.4	-13921	81.1	0.5	114	N.A.	-11.9
	86	3.5	0.08	1.3	0.4	1.3	3.6	0.3	1.0	0.4	1.9	2.8	0.4	0.5	0.5	7.6	35.4	0.9	2.4	1.3	8.	3.0	6.2	1.9	N.A.	1.7
AZ RANDOM = 0.112°	340	+2.2	+0.23	-2.3	-1.8	-0.8	+7.3	104	+0.1	-11.0	-1.1	+8.6	104	-0.4	-10.8	14.1	-33.9	103	N.A.	-9.9	-13968	81.6	-0.3	118	N.A.	-1.7
	44	1.8	0.02	1.3	0.1	1.4	1.6	0.2	0.7	0.2	1.5	1.9	0.7	1.0	0.17	9.9	6.8	1.2	N.A.	1.2	10	0.6	1.3	4.1	N.A.	0.7
AZ RANDOM = 0.3°	294	+3.3	+0.26	-2.1	-1.7	-0.6	+8.0	104	-0.9	-11.0	-0.4	+12.2	104	-0.3	-10.9	-6.6	-41.7	102	2.0	-9.3	-13973	81.3	-0.3	114	2148	N.A.
	39	2.8	0.09	1.3	0.08	1.1	6.6	0.3	1.8	0.1	1.1	10.0	0.24	2.6	0.13	4.4	3.0	0.8	4.3	0.5	14	0.8	1.6	0.7	28	N.A.
AZ CORRELATED = 0.3°	322	+6.7	+0.24	-1.2	-1.8	-0.5	+6.2	104	+1.7	-11.0	-0.08	+9.8	104	-4.5	-10.9	-7.6	-1.5	101	5.6	-9.2	-13971	81.6	-1.2	114	2153	N.A.
	65	10.7	0.11	2.5	0.1	1.8	15.6	0.4	4.8	0.2	2.2	19.6	0.5	3.8	0.15	3.5	4.6	1.5	103	0.7	30	2.1	3.5	2.3	7.6	N.A.
EL_1 RANDOM = 0.042°	340	+2.2	+0.23	+2.3	-1.8	-0.8	+7.3	104	+0.1	-11.0	-1.1	+8.6	104	-0.4	-10.8	14.1	-33.9	103	N.A.	-9.9	-13968	81.6	-0.3	118	N.A.	-1.7
EL_2 RANDOM = 0.032°	44	1.8	0.02	1.3	0.1	1.4	1.6	0.2	0.7	0.2	1.5	1.9	0.7	1.0	0.17	9.9	6.8	1.2	N.A.	1.2	10	0.6	1.3	4.1	N.A.	0.7
EL_1 RANDOM = 0.15°	338	2.6	0.22	-2.2	-1.8	+0.09	+8.9	104	-0.4	-10.9	+0.08	+11.3	103	0.03	-10.8	-1.0	-27.1	102	2.1	-8.7	-13971	81.3	-0.2	115	2146	N.A.
EL_2 RANDOM = 0.032°	31	2.7	0.04	0.6	0.1	1.2	2.7	0.2	1.2	0.2	1.6	2.8	0.3	1.0	0.17	13.0	10.3	2.3	2.5	2.4	5.3	0.5	0.7	1.9	7.2	N.A.
EL_2 RANDOM = 0.150°	337	+1.1	0.26	-1.8	-1.8	-0.6	+5.0	105	-0.3	-11.1	-0.6	+8.8	103	-0.3	-10.8	-13.8	-33	102	1.5	-9.8	-13976	81.4	0.3	116	2144	N.A.
EL_1 RANDOM = 0.150°	49	2.8	0.05	1.2	0.1	1.4	2.9	0.1	0.7	0.2	1.2	2.5	0.2	0.9	0.3	19.0	6.4	5.6	1.8	2.6	2	0.8	1.4	2.1	9.3	N.A.

SUMMARY OF MLS BIAS ERRORS

TOP ROW = MEAN
SECOND ROW = 1 SIGMA DEVIATION

CONDITION (Key Difference)	AT TOUCHDOWN X	Y	Ÿ	Ẏ	Ż	AT ALT. = 100 FT. Δh	Y	Ẋ	Ẏ	Ż	AT ALT. = 200 FT. Δh	Y	Ẋ	Ẏ	Ż	AT LOCALIZER INTERCEPTION Δh	Y	Ẋ	Ẏ	Ż	AT GLIDE SLOPE CAPTURE X	Ÿ	Ẋ	Y	ALT	Ż
AZ Bias = +0.124°	324	-1.6	0.24	-2.4	-1.7	-2.9	+5.8	104	-0.2	-11.0	-1.1	+7.0	103	-0.5	-11.1	-5.9	-35.0	103	0.8	-9.2	-13979	81.5	0.1	115	2145	N.A.
	4.0	1.7	0.01	0.3	0.04	0.6	4.4	0.09	0.1	0.2	1.1	2.6	0.2	1.7	0.02	0.2	1.3	0.1	0.1	0.1	2.5	0.2	0.2	0.4	2.0	N.A.
AZ Bias = +0.4°	326	+11.9	0.23	-2.5	-1.8	-2.7	+22.5	104	-0.4	-11.0	-0.7	+28.6	103	-1.1	-11.2	-5.9	28.1	103	-0.1	-9.2	-14017	81.2	0.7	115	N.A.	-0.4
	50	3.8	0.03	0.4	0.2	1.0	1.5	0.14	0.6	0.1	1.2	3.8	0.2	0.4	0.1	1.2	1.4	0.3	0.2	0.1	1.1	0.1	0.3	0.5	N.A.	0.2
AZ Bias = -0.4°	309	-16.6	0.25	-1.6	-1.8	-2.8	-23.7	104	0.8	-11.1	-0.4	-29.8	103	0.6	-11.2	-5.0	-15.6	103	1.7	-9.1	-13902	81.6	-0.4	116	2131	N.A.
	7.8	4.8	0.004	0.3	0.05	0.2	2.1	0.25	0.2	0.1	0.5	1.3	0.1	0.1	0.04	0.3	1.1	0.1	0.2	0.1	1.1	0.1	0.2	0.1	0.7	N.A.
EL_1 = 0.036° EL_2 = 0.032	324	-1.6	0.24	-2.4	-1.7	-2.9	+5.8	104	-0.2	-11.0	-1.1	+7.0	103	-0.5	-11.1	-5.9	-35.0	103	0.8	-9.2	-13979	81.5	0.1	115	2145	N.A.
	4.0	1.7	0.01	0.3	0.04	0.6	4.4	0.1	0.1	0.2	1.1	2.6	0.2	1.7	0.02	0.2	1.3	0.1	0.1	0.1	2.5	0.2	0.2	0.4	2.0	N.A.
$EL_{1\ \&\ 2}$ Bias = +0.2°	421	+0.7	0.15	-2.1	-2.1	-7.5	+8.0	104	-0.2	-10.6	-7.1	+8.5	104	-0.2	-10.7	-44.9	-35.1	102	2.6	-8.7	-13981	81.1	0.5	114	2105	N.A.
	51	1.4	0.05	1.0	0.3	2.9	2.7	0.2	0.2	0.2	1.9	1.9	0.3	0.3	0.1	0.8	1.8	0.4	0.1	0.06	0.3	0.1	0.3	0.1	1.5	N.A.
$EL_{1\ \&2}$ Bias = -0.2°	230	+3.3	0.4	-1.8	-1.9	+0.9	+8.1	104	-0.1	-11.4	+5.7	+9.9	103	-0.3	-11.5	42.3	-22.4	103	4.3	-10.2	-13968	81.2	0.5	115	2202	N.A.
	24	2.4	0.2	0.5	0.07	0.5	1.3	0.07	0.2	0.1	1.4	1.6	0.2	0.3	0.2	1.9	2.8	0.5	0.2	0.2	2.2	0.1	0.2	0.2	0.5	N.A.
EL_1 = -0.1	285	+6.1	0.2	-1.9	-1.8	-0.9	8.2	104	0.07	-11.2	+2.8	+9.4	103	-0.2	-11.4	23.8	-28.0	103	4.0	-9.7	-13974	81.3	0.5	115	2179	N.A.
EL_2 = -0.05	17.5	1.9	0.01	0.2	0.07	0.3	2.2	0.03	0.2	0.2	1.4	1.4	0.3	0.05	0.06	0.4	1.1	0.2	0.2	0.1	2.5	0.2	0.3	0.3	0.6	N.A.
DME Bias = +20'	324	-1.6	+0.2	-2.4	-1.7	-2.9	+5.8	104	-0.2	-11.0	-1.1	+7.0	103	-0.5	-11.1	-5.9	-35.0	103	0.8	-9.2	-13979	81.5	0.1	115	2145	N.A.
	4.0	1.7	0.02	0.3	0.04	0.6	4.4	0.09	0.1	0.2	1.1	2.6	0.2	1.7	0.02	0.2	1.3	0.1	0.1	0.1	2.5	0.2	0.2	0.4	2.0	N.A.
DME Bias = -20'	292	+5.3	0.23	-2.3	-1.8	-3.5	+9.2	104	+0.05	-10.9	-1.8	+8.3	103	-0.2	-11.1	-4.3	-32.2	103	1.4	-9.2	-14012	81.3	0.4	115	2149	N.A.
	14	1.5	0.02	1.3	0.1	0.1	4.8	0.05	0.7	0.1	0.5	2.4	0.05	0.4	0.05	0.3	1.3	0.1	0.3	0.1	1.7	0.2	0.3	0.8	2.1	N.A.
DME Bias = +100'	439	-0.2	+0.1	-2.9	-2.3	-2.7	+8.5	104	+0.4	-11.0	-0.8	+12.1	103	0.1	-11.1	-6.5	-35.9	103	0.2	-8.9	-13903	81.2	0.4	114	2133	N.A.
	29	1.4	0.07	0.9	0.1	0.2	1.1	0.03	0.2	0.07	1.0	4.2	0.2	0.8	0.02	0.1	0.6	0.2	0.04	0.1	2.8	0.2	0.3	0.2	2.4	N.A.
DME Bias = -100'	203	+6.0	+0.5	-1.4	-1.9	-3.8	+6.0	104	-0.6	-10.9	-2.4	+9.5	103	-0.1	-11.2	-2.8	-27.0	103	2.3	-9.2	-14083	81.6	-0.2	115	2160	N.A.
	16	2.5	0.09	0.08	0.02	0.07	5.3	0.04	0.3	0.01	0.3	3.1	0.04	0.1	0.02	0.3	0.6	0.1	0.3	0.04	3.0	0.3	0.5	0.5	2.6	N.A.
DME Bias = +300'	614	+2.1	0.1	-1.7	-3.4	-1.7	+9.6	104	-0.04	-10.8	-0.8	+9.6	103	-0.4	-11.0	-12.5	-45.3	102	1.5	-9.2	-13729	80.9	1.3	114	2106	N.A.
	22	1.2	0.02	0.3	0.09	0.3	2.4	0.03	0.2	0.1	0.7	1.9	0.2	0.2	0.05	0.4	0.8	0.1	0.1	0.01	2.2	0.2	0.4	0.8	1.5	N.A
DME Bias = -300'	28	+5.8	1.2	-0.4	-4.1	-3.7	+5.7	104	-0.06	-11.2	-1.8	+7.2	104	-0.2	-11.2	-1.2	-18.0	103	3.6	-9.6	-14260	81.7	-0.4	116	2184	N.A.
	8.5	4.3	0.1	0.1	0.1	1.1	0.6	0.2	0.1	0.1	1.1	5.5	0.2	0.05	0.05	1.2	1.6	0.1	0.02	0.1	2.0	0.05	0.05	0.5	0.6	N.A.

IV. CONCLUSIONS

Conclusions are presented throughout the body of this report in each major subsection; however, the more general conclusions are summarized here. The order is the same as the body of the report and there has been no attempt to list them in order of importance.

Two miles appears to be an adequate (straight-in) final approach distance for the flight paths and errors investigated.

Since STOLport runway lengths are typically 15 to 25% of CTOL runway lengths, much larger MLS angular errors can be tolerated for STOL operations. For example, the 10 ft touchdown azimuth bias error specified in DO-148 (for the 14,000 ft CAT III MLS configuration) converts to an angular error of ≈0.05°. For the 2000 ft STOLport of this study, the same 10 ft touchdown bias represents an angular error of ≈0.3°.

The mean STOL longitudinal touchdown point is very sensitive to DME and elevation bias; however, ±30 ft and ±0.07°, respectively, appear to be within acceptable limits for CAT III operations.

With the nominal complementary filter, the range of EL_1 and EL_2 random MLS errors assessed (0.032° to 0.15°) had a very small effect on longitudinal touchdown and 100/200 ft elevation vertical standard deviations.

The 1 σ lateral dispersions of the aircraft were reduced to somewhat less than one-half of the corresponding 1 σ values of the MLS azimuth random errors (with nominal complementary filtering and no turbulence).

Azimuth correlated noise (time constant = 2 sec) has a significantly larger effect on aircraft dispersions than the same magnitude of uncorrelated (white) azimuth noise. The crosstrack dispersions at 100 ft and 200 ft elevations are approximately twice those caused by the same magnitude of uncorrelated azimuth noise. The lateral touchdown disperions are ≈65% greater. Hence, specifications which describe the frequency content as well as the magnitude of

the random errors in the received MLS signals may be required.

The noncomplementary filter configuration provided acceptable tracking performance in both the horizontal and vertical channels for the landing approach with CAT III MLS error combinations. The flare maneuver was not satisfactory, and it appears that measured vertical acceleration information is required. For noise levels somewhat higher than the CAT III values, preliminary results showed that the performance may be satisfactory if the magnitudes of the nominal flight path maneuvers are reduced so that lower control gains can be used.

Comparisons of system performance with CAT III and with CAT II (Fig. 35) MLS errors (without turbulence and with the nominal complementary filters) show that the following parameters are affected only slightly.

- Longitudinal and lateral touchdown standard deviation due to random errors
- Lateral touchdown standard deviation due to random errors
- Vertical dispersion at 100 and 200 ft altitudes

The dispersions which are significantly increased include:

- Mean longitudinal touchdown point
- Lateral crosstrack errors at 100 and 200 ft

The levels of turbulence (2.0 fps horizontal and 0.8 to 1.5 fps vertical) assessed in this report have a significant effect on the longitudinal and lateral touchdown dispersions, and the vertical dispersions at 100 and 200 ft ft elevation. The addition of the turbulence to the CAT III or CAT II MLS errors causes these dispersions to increase by a factor of at least 3. Note that the dispersions due to turbulence are being compared with dispersions due to random errors only; bias errors are fixed for each set of runs. The deviations in crosstrack errors (Y) at the 100 and 200 ft altitudes are not increased substantially by the lateral turbulence. The above comparison

points out the well-known fact that a significant part of the control design of a STOL aircraft is the requirement to make it sufficiently insensitive to environmental disturbances.

The selection of the level of MLS errors that can be tolerated, in combination with all the other error sources, is difficult for the following reasons:

a) The environmental disturbances such as turbulence cause a large increase in the longitudinal touchdown and 100 and 200 ft elevation vertical dispersions. Reducing the MLS errors below the CAT III levels (Fig. 35) would not significantly reduce the above dispersions since their sensitivity to turbulence is three to four times that of most of the MLS random errors.

b) Variations in wind direction cause an additional increase in dispersions. Only the 12Kt 30° wind was simulated in this study, but limited runs with 15Kt headwinds and tailwinds indicate additional longitudinal touchdown dispersions of a few hundred feet.

c) The MLS bias errors that were included in the MLS error combinations were discrete positive levels with no random selection over a range. Hence the offsets caused by these biases are representative of the worst case conditions in one direction only.

d) It is impractical to study all of the possible error combinations in a Monte Carlo fashion with a real-time simulation facility.

e) There are many tradeoffs that can be made between the individual MLS errors, the control system, siting, etc. Observation of the system performance with the CAT II and CAT III MLS error combinations shows that there is little leeway with the errors that affect the longitudinal touchdown and Δh (at 100 ft) dispersions; however, it appears that the azimuth bias can be increased above the CAT III levels.

f) The decision heights, windows, and touchdown dispersion criteria have not been developed for STOL operations.

g) This simulation included only one type of STOL aircraft.

Even with the above uncertainties, it appears that the CAT III MLS errors of Figure 35 can be tolerated in STOL terminal area operations. MLS equipment with even better specifications will be readily available because much more stringent MLS specifications are required for CTOL aircraft due to the much longer CTOL runways.

The system performance is well within the applicable standards with the CAT III MLS errors and nominal complementary filtering and without turbulence (Figs. 35 and 38). The addition of the turbulence of Figure 34 causes the longitudinal touchdown dispersion and vertical error at 100 ft altitude to equal or slightly exceed the tentative STOL criteria and AC 120-20.

Without turbulence, the system performance with CAT II MLS errors and nominal complementary filtering meets the tentative STOL criteria for longitudinal and lateral touchdown dispersions (although the mean longitudinal touchdown point is long). The longitudinal and lateral dispersions at 100 ft altitude were within the overall limits given by AC 120-20. The addition of turbulence to the CAT II MLS errors causes both the longitudinal and lateral touchdown dispersions to exceed the tentative STOL criteria of Figure 38. At 100 ft elevation the vertical dispersions slightly exceed AC 120-20, but the crosstrack errors meet this specification.

Aircraft tracking performance deteriorated significantly when the complementary filter frequency response was increased by a factor of 3 with CAT II level noise. Dispersions at the glide path localizer, and altitude intercepts doubled or tripled. Hence, complementary filter parameters must be chosen with care to reflect a realistic installation in order to obtain a realistic evaluation of the MLS random errors.

The proposed CAT II levels of random noise are acceptable only for aircraft equipped with appropriate complementary filtering equipment. Dispersions were too large for the increased frequency complementary filter and, although not shown, also for the noncomplementary filter (see pg. 37).

The following table summarizes the minimum required MLS coverages for the two STOL flight paths evaluated in this report with the errors (Fig. 98) for a Navaid located near the airport and the combined MLS valid arrangement. Aircraft settling time prior to the start of G/S descent was the criteria used.

	Flight Path No. 1	Flight Path No. 2
Range	10 nmi	10 nmi
Azimuth and DME Horizontal	±40°	±60°
Azimuth and DME Vertical	10°	20°
Elevation no. 1 Horizontal	±45°	±40°
Elevation no. 1 Vertical	10°	30°

If the azimuth and elevation valids are independent the elevation vertical coverage can be reduced to ≈15° for F.P. no. 2.

Backcourse azimuth coverage may not be cost effective for STOL operations at this time. Backcourse coverage would increase the position accuracy for missed approaches; however, such coverage would not accommodate the missed approach procedures which call for a turn prior to the runway threshold. If the front and backcourse azimuth antennas are co-located off the stop end of the runway, an appreciable zone of silence would be encountered in a straight go-around.

Sixty seconds of fan pattern type pathstretching to achieve time-of-arrival control can be obtained within the MLS horizontal coverages evaluated with different range and common path length penalties. For one type of fan pattern, the common path varies from 12 nmi with 20° of azimuth horizontal coverage to 6 nmi with 60° of coverage.

An MLS range of 10 nmi appears to be adequate for STOL operations.

The nominal 5.0 Hz data rate for all MLS functions (except EL_2 at 10.0 Hz) was adequate for the range of conditions in this report.

The primary elevation antenna was located 100 ft upwind from the runway threshold. This location resulted in a longitudinal distribution which was within the desired touchdown zone.

V. ACKNOWLEDGEMENTS

The authors would like to express their gratitude to the following individuals for their contributions:

Gary Bear, Warren C. Birmingham, Dave C. Boze,

C. Francis Crane, Brian F. Doolin,

Jules Kanter, Jay Karmarkar, Henry C. Lessing,

Chester Ludlam, Larry A. Montgomery, Jr., Manuel M. Orozco,

Masayuki Omura, Ernie Trujillo, John S. White,

and the four MLS Contractors.

VI. REFERENCES

1. Anon.: National Plan for Development of the Microwave Landing System. DOT-NASA-DOD, AD 733268, July 1971.
2. Lanman, Maurice, H.: An Investigation of Microwave Landing Guidance System Signal Requirements for Conventionally Equipped Civilian Aircraft. FAA-RD-71-86, June 1971.
3. Lanman, Maurice H.: Microwave Landing System Signal Requirements for Conventional Aircraft. FAA-RD-72-86, July 1972.
4. Graham, D.; Clement, W. F.; and Hofmann, L. G.: Investigation of Measuring System Requirements for Instrument Low Visibility Approach. AFFDL-TR-70-102, February 1971.
5. Hofmann, L. G.; Clement, W. F.; Graham, D.; Blodgett, R. E.; and Shah, K. V.: Investigation of Measuring System Requirements for Low Visibility Landing. AFFDL-TR-71-151, December 1971.
6. Dillow, J. D.; Stolz, P. R.; and Zuckerman, M. D.: Analysis of Data Rate Requirements for Low Visibility Approach With a Scanning Beam Landing Guidance System. AFFDL-TR-71-177, February 1973.
7. Duning, E. K.; and Hemesath, N. B.: Curved Approach Path Study. FAA-RD-73-143, April 1973.
8. Benjamin, J.: A Review of Approach and Landing Guidance in Relation to Civil and Military Requirements. RAE TR 71186, September 1971.
9. Joint DOT, FAA and NASA-Ames Task Order DOT-FA73WAI-395 to NASA NMI-1052.151. Assess the Adequacy of the RTCA SC-117 Operational/Functional MLS Requirements for Civil STOL Use.
10. Young, L. S.; Hansen, Q. M.; Rouse, W. E.; and Osder, S. S.: Development of STOLAND, a Versatile Navigation, Guidance and Control System. NASA TM X-62183, 1972.

11. Taylor, J. W. R. (ed.): Jane's All the World's Aircraft 1968-1969. McGraw Hill Book Co., New York, 1969.

12. Anon.: Automatic Landing System. FAA Advisory Circular 20-57A, Washington, D. C., Jan. 12, 1971.

13. Anon.: Evaluation of STOL Microwave Facility Performance Requirement. FAA Standards Development Branch, NATIONAL FLIGHT INSPECTION DIV., Flight Standards Service, Washington, D. C., Jan. 1972.

14. Benner, M. S.; Sawyer, R. H.; and McLaughlin, M. D.: Simulation Studies of Curved Descending Instrument Approach Paths Using Two STOL Airplanes. Proposed Technical Note, NASA Langley Research Center, April 1969.

15. Gee, S. W.; Barber, M. R.; McMurty, T. C.: A Flight Evaluation of Curved Landing Approaches. NASA Flight Research Center, Edwards, Ca., 1972.

16. Welp, D. W.; Kuhner, M. B.; Ullman, D. G.; Brown, R. A.; and Yarbrough, E. R.: Effectiveness Evaluation of STOL Transport Operations, Quarterly Progress Report. July 1973.

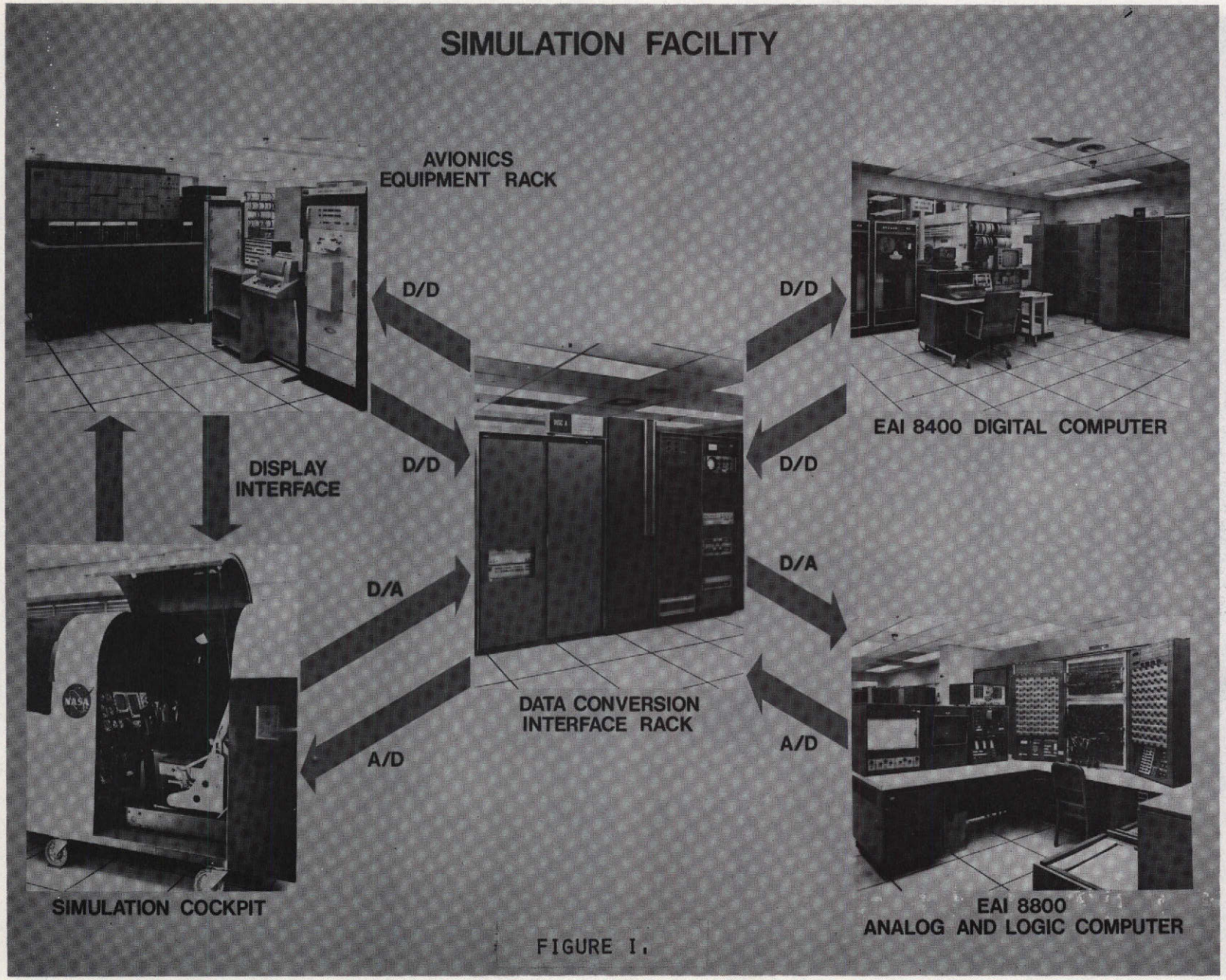
SIMULATION FACILITY
AVIONICS
EQUIPMENT RACK
D/D
D/D
D/D
D/D
EAI 8400 DIGITAL COMPUTER
DISPLAY
INTERFACE
D/A
D/A
DATA CONVERSION
INTERFACE RACK
A/D
A/D
SIMULATION COCKPIT
EAI 8800
ANALOG AND LOGIC COMPUTER

FIGURE I.

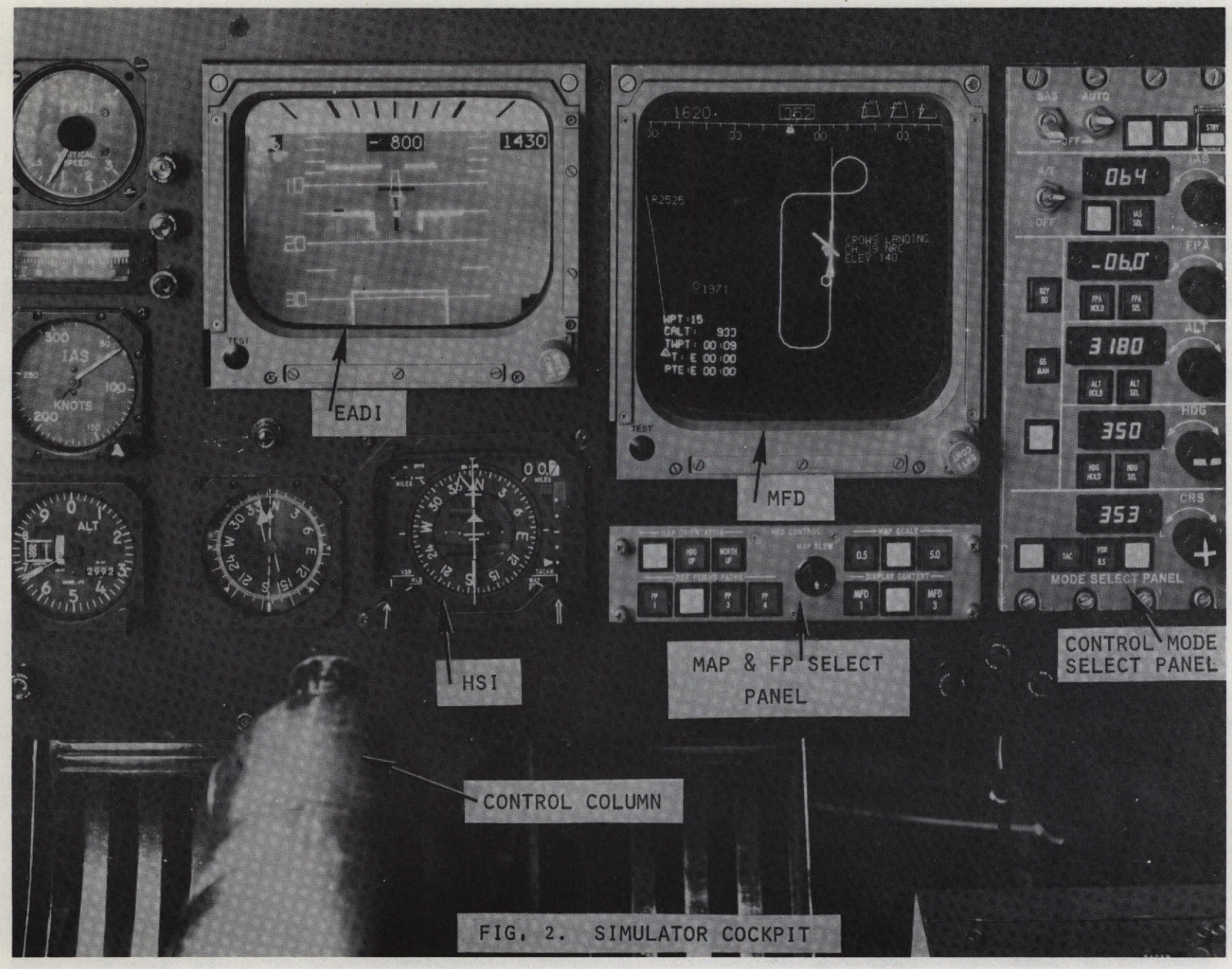

FIG. 2. SIMULATOR COCKPIT

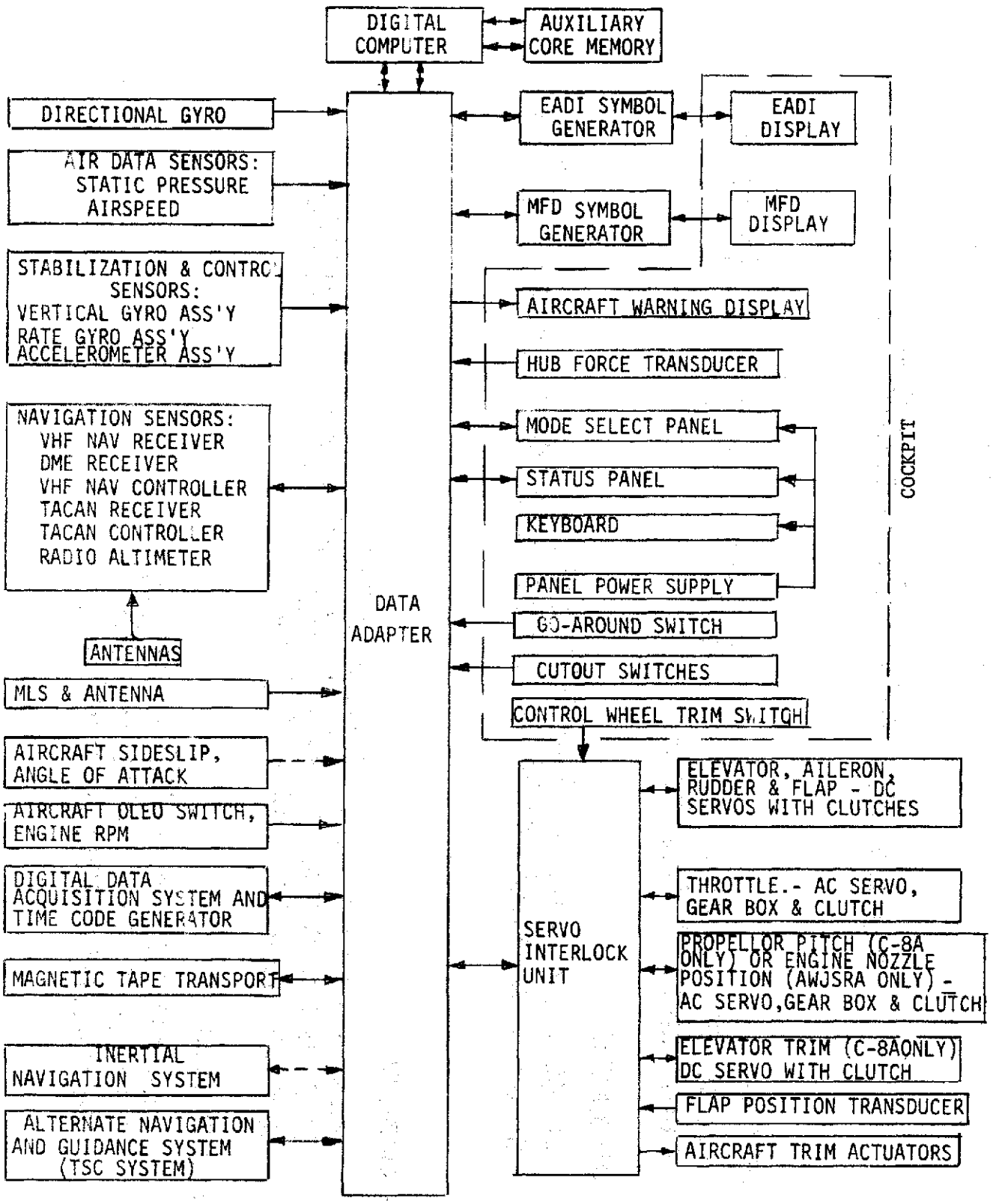

FIG. 3 - STOLAND HARDWARE BLOCK DIAGRAM

FIG. 4.1 STOLAND CONFIGURATIONS

- **AUTOMATIC II**

  "HANDS-OFF" TERMINAL AREA NAVIGATION, GUIDANCE AND CONTROL IN 4 DIMENSIONS TO TOUCHDOWN.

- **AUTOMATIC I**

  AUTOMATIC NAVIGATION AND MAP DISPLAY.
  GUIDANCE AND CONTROL TO 100 FEET ALTITUDE USING AUTOPILOT MODES

- **MANUAL II**

  AUTOMATIC NAVIGATION AND MAP DISPLAY.
  STEERING COMMANDS TO 100 FEET ALTITUDE FOR FLIGHT DIRECTOR.
  CWS (AUGMENTED) MODES AVAILABLE.

- **MANUAL I**

  RAW DATA DISPLAY (NO COMPUTATION).
  MANUAL CONTROL TO 200 FEET ALTITUDE.
  CWS (AUGMENTED) MODES AVAILABLE.

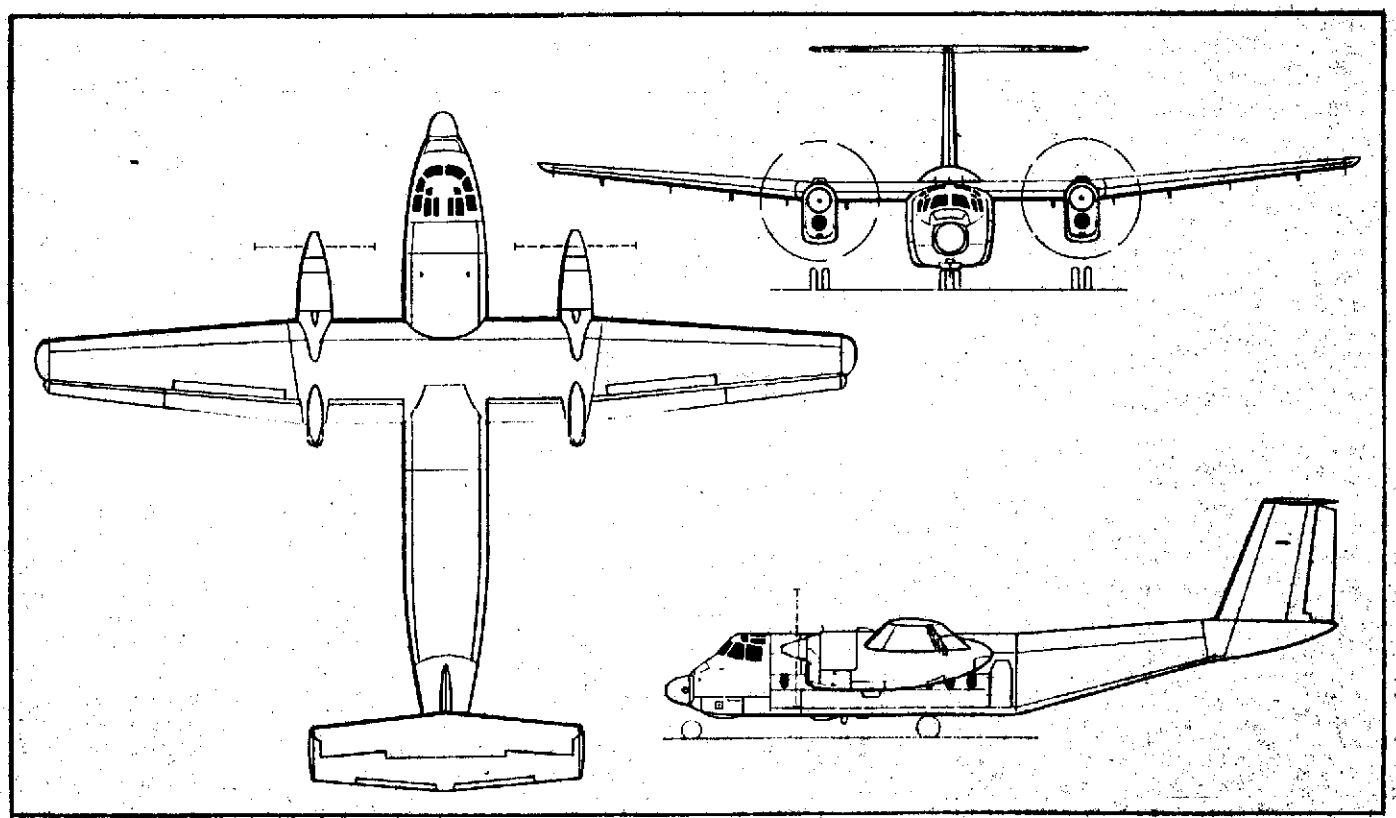

DHC-5 Buffalo twin-turboprop STOL utility transport

DHC-5 Buffalo STOL utility transport

Differences between the US and Canadian versions are as follows:

CV-7A. US model, with 2,850 eshp General Electric T64-GE-10 turboprops. Overall length 77 ft 4 in (23·57 m).

CC-115. Canadian Defence Force model, with 3,055 eshp General Electric T64/P2 turboprops. Overall length 79 ft 0 in (24·08 m). Otherwise similar to CV-7A, with only small differences in performance.

WINGS: Cantilever high-wing monoplane. Wing section NACA $64_3A417{\cdot}5$ (mod) at root, NACA 63_3A615 (mod) at tip. Aspect ratio 9·75. Chord 11 ft 9½ in (3·59 m) at root, 5 ft 11 in (1·19 m) at tip. Dihedral 0° inboard of nacelles, 5° outboard. Incidence 2° 30'. Sweepback at quarter-chord 1° 40'. Conventional fail-safe multi-spar structure of high-strength aluminium alloys. Full-span double-slotted aluminium alloy flaps, outboard sections functioning as ailerons. Aluminium alloy slot-lip spoilers, forward of inboard flaps, are actuated by Jarry Hydraulics unit. Spoilers coupled to manually-operated ailerons for lateral control, uncoupled for symmetrical ground operation. Electrically-actuated trim-tab in starboard aileron. Geared tab in each aileron. Rudder-aileron interconnect tab on port aileron. Outer wing leading-edges fitted with electrically-controlled flush pneumatic rubber de-icing boots.

FUSELAGE: Fail-safe structure of high-strength aluminium alloy. Cargo floor supported by longitudinal keel members.

TAIL UNIT: Cantilever structure of high-strength aluminium alloy, with fixed-incidence tailplane mounted at tip of fin. Elevator aerodynamically and mass-balanced. Fore and trailing serially-hinged rudders are powered by tandem jacks operated by two independent hydraulic systems manufactured by Jarry Hydraulics. Trim-tab on port elevator, spring-tab on starboard elevator. Electrically-controlled flush pneumatic rubber de-icing boot on tailplane leading-edge.

LANDING GEAR: Retractable tricycle type. Hydraulic retraction, nose unit aft, main units forward. Jarry Hydraulics oleo-pneumatic shock-absorbers. Goodrich main wheels and tyres, size 37·00 × 15·00-12, pressure 45 lb/sq in (3·16 kg/cm²). Goodrich nose wheels and tyres size 8·00 × 12·50, pressure 38 lb/sq in (2·67 kg/cm²). Goodrich multi-disc brakes.

POWER PLANT: Two General Electric T64 turboprop engines (details under entries for individual versions, above), each driving a Hamilton Standard 63E60-13 three-blade propeller, diameter 14 ft 6 in (4·42 m). Fuel in one integral tank in each inner wing, capacity 533 Imp gallons (2,423 litres) and rubber bag tanks in each outer wing, capacity 336 Imp gallons (1,527 litres). Total fuel capacity 1,738 Imp gallons (7,900 litres). Refuelling points above wings and in side of fuselage for pressure refuelling. Total oil capacity 10 Imp gallons (45·5 litres).

DIMENSIONS, EXTERNAL:

Wing span	96 ft 0 in (29·26 m)
Length overall:	
CV-7A	77 ft 4 in (23·57 m)
CC-115	79 ft 0 in (24·08 m)
Height overall	28 ft 8 in (8·73 m)
Tailplane span	32 ft 0 in (9·75 m)
Wheel track	30 ft 6 in (9·29 m)
Wheelbase	27 ft 11 in (8·50 m)
Cabin doors (each side):	
Height	5 ft 6 in (1·68 m)
Width	2 ft 9 in (0·84 m)
Height to sill	3 ft 10 in (1·17 m)
Emergency exits (each side, below wing leading-edge):	
Height	3 ft 4 in (1·02 m)
Width	2 ft 2 in (0·66 m)
Height to sill approx	5 ft 0 in (1·52 m)
Rear cargo loading door and ramp:	
Height	20 ft 9 in (6·33 m)
Width	7 ft 8 in (2·33 m)
Height to ramp hinge	3 ft 10 in (1·17 m)

DIMENSIONS, INTERNAL:

Cabin, excluding flight deck:	
Length, cargo floor	31 ft 5 in (9·58 m)
Max width	8 ft 9 in (2·67 m)
Max height	6 ft 10 in (2·08 m)
Floor area	243·5 sq ft (22·63 m²)
Volume	1,715 cu ft (48·56 m³)

AREAS:

Wings, gross	945 sq ft (87·8 m²)
Ailerons (total)	39 sq ft (3·62 m²)
Trailing-edge flaps (total, including ailerons)	280 sq ft (26·01 m²)
Spoilers (total)	25·2 sq ft (2·34 m²)
Fin	92 sq ft (8·55 m²)
Rudder, including tab	60 sq ft (5·57 m²)
Tailplane	151·5 sq ft (14·07 m²)
Elevators, including tab	81·5 sq ft (7·57 m²)

WEIGHTS AND LOADINGS:

Operating weight empty, including 3 crew at 200 lb (91 kg) each, plus trapped fuel and oil and full cargo handling equipment	23,157 lb (10,505 kg)
Max payload	13,343 lb (6,279 kg)
Max T-O weight	41,000 lb (18,598 kg)
Max zero-fuel weight	37,000 lb (16,783 kg)
Max landing weight	39,000 lb (17,690 kg)
Max wing loading	43·4 lb/sq ft (212 kg/m²)
Max power loading	7·2 lb/eshp (3·27 kg/eshp)

PERFORMANCE (CV-7A, at max T-O weight):

Max level speed at 10,000 ft (3,050 m)	271 mph (435 kmh)
Max permissible diving speed	334 mph (537 kmh)
Max cruising speed at 10,000 ft (3,050 m)	271 mph (435 kmh)
Econ cruising speed at 10,000 ft (3,050 m)	208 mph (335 kmh)
Stalling speed, 40° flaps at 39,000 lb (17,690 kg) AUW	75 mph (120 kmh)
Stalling speed, flaps up at max AUW	105 mph (169 kmh)
Rate of climb at S/L	1,890 ft (575 m) min
Service ceiling	30,000 ft (9,150 m)
Service ceiling, one engine out	14,300 ft (4,360 m)
T-O run on firm dry sod	1,040 ft (317 m)
T-O to 50 ft (15 m) from firm dry sod	1,540 ft (470 m)
Landing from 50 ft (15 m) on firm dry sod	1,120 ft (342 m)
Landing run on firm dry sod	610 ft (186 m)
Range with max fuel and 4,000 lb (1,815 kg) payload, with allowances for warm-up, taxying, take-off, climb, descent and 45 min reserve at cruise power 2,170 miles (3,490 km)	
Range with max payload, reserves as above,	507 miles (815 km)

FIG. 5 – DESCRIPTION OF THE C-8A (CV-7A)

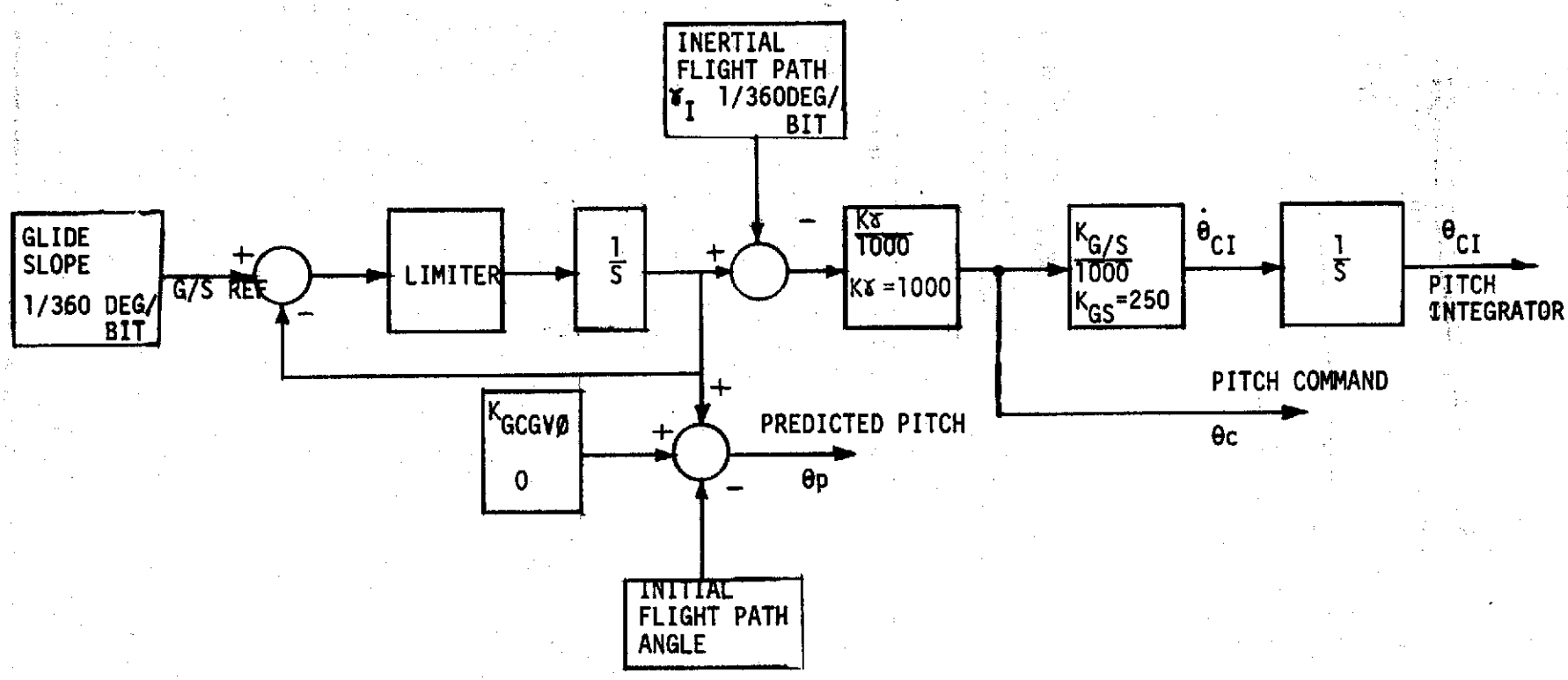

FIGURE 6.- GLIDE SLOPE CAPTURE CONTROL LAW

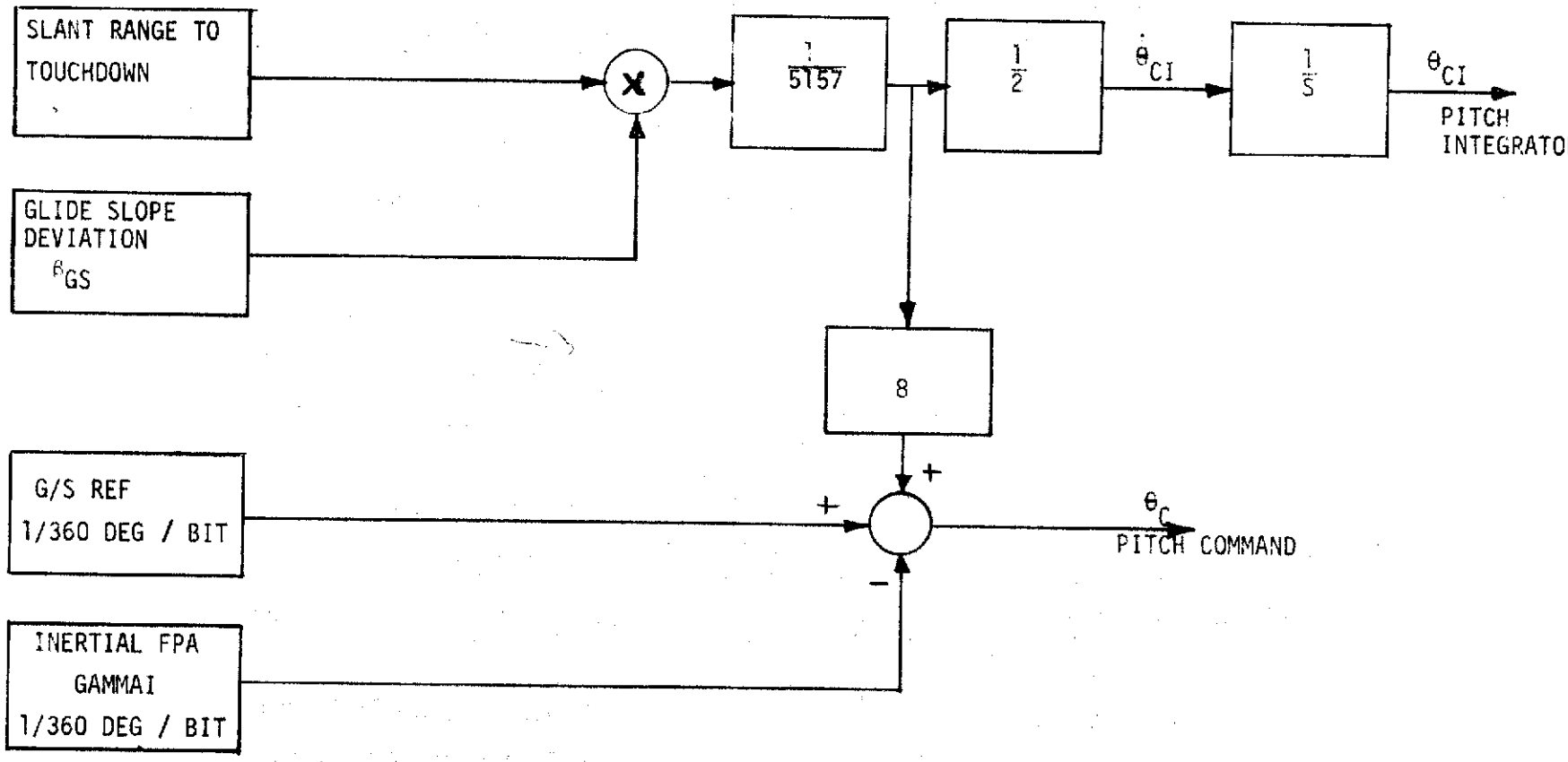

FIGURE 7. – GLIDE SLOPE TRACK CONTROL LAW

GLIDE SLOPE CAPTURE LAW

PITCH COMMAND

$$\theta_C = \frac{K\gamma}{1000}\left\{\gamma_{G/S\,REF}\left(\frac{1}{S+1}\right) - \gamma_I\right\}$$

PREDICTED PITCH

$$\theta_P = K_{GC}\,GV\phi - \gamma_0 + \gamma_{G/S\,REF}\left(\frac{1}{S+1}\right)$$

INPUT TO PITCH INTEGRAL COMMAND GENERATOR

$$\theta_{CI} = \theta_C\left(\frac{K_{GS}}{1000}\right)\frac{1}{S}$$

GLIDE SLOPE TRACKING LAW

PITCH COMMAND

$$\theta_C = 8\eta_{TD} \cdot \beta_{GS} + \gamma_{G/S\,REF} - \gamma_I$$

PITCH INTEGRAL INPUT

$$\theta_{CI} = \frac{1}{2S}\left(\eta_{TD} \times \beta_{GS}\right)$$

η_{TD} = TOUCHDOWN SLANT RANGE

β_{GS} = GLIDE SLOPE DEVIATION

FIGURE 8

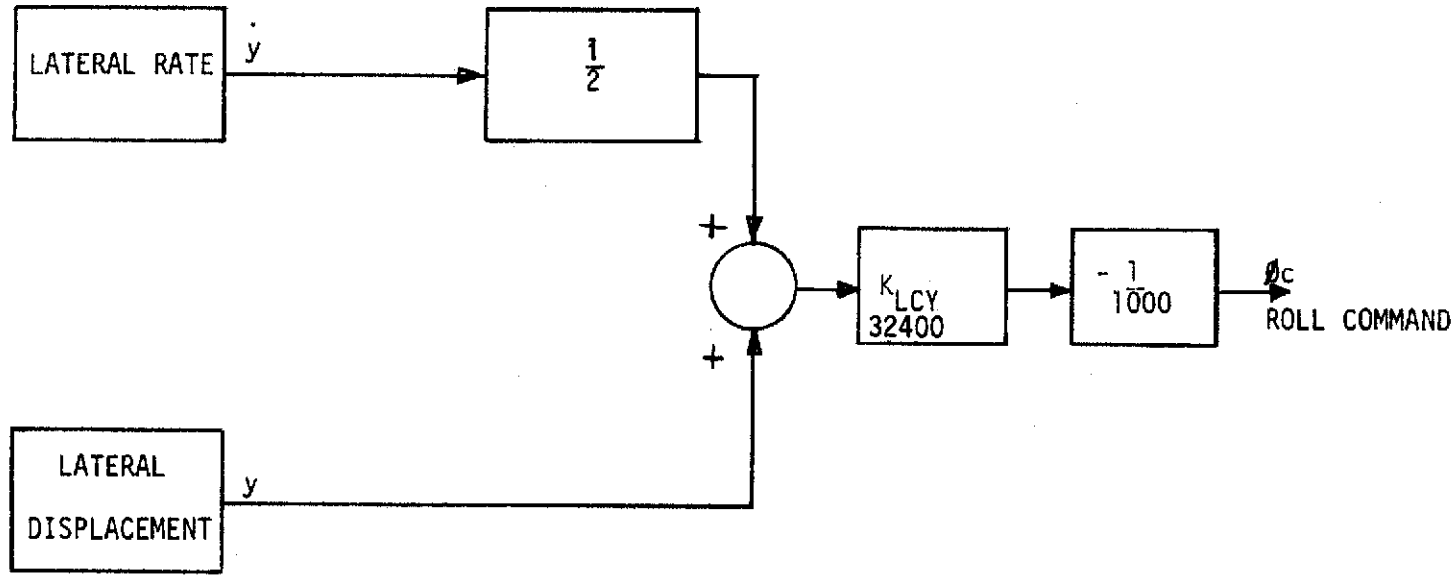

FIGURE 9.- MLS LOCALIZER CAPTURE CONTROL LAW

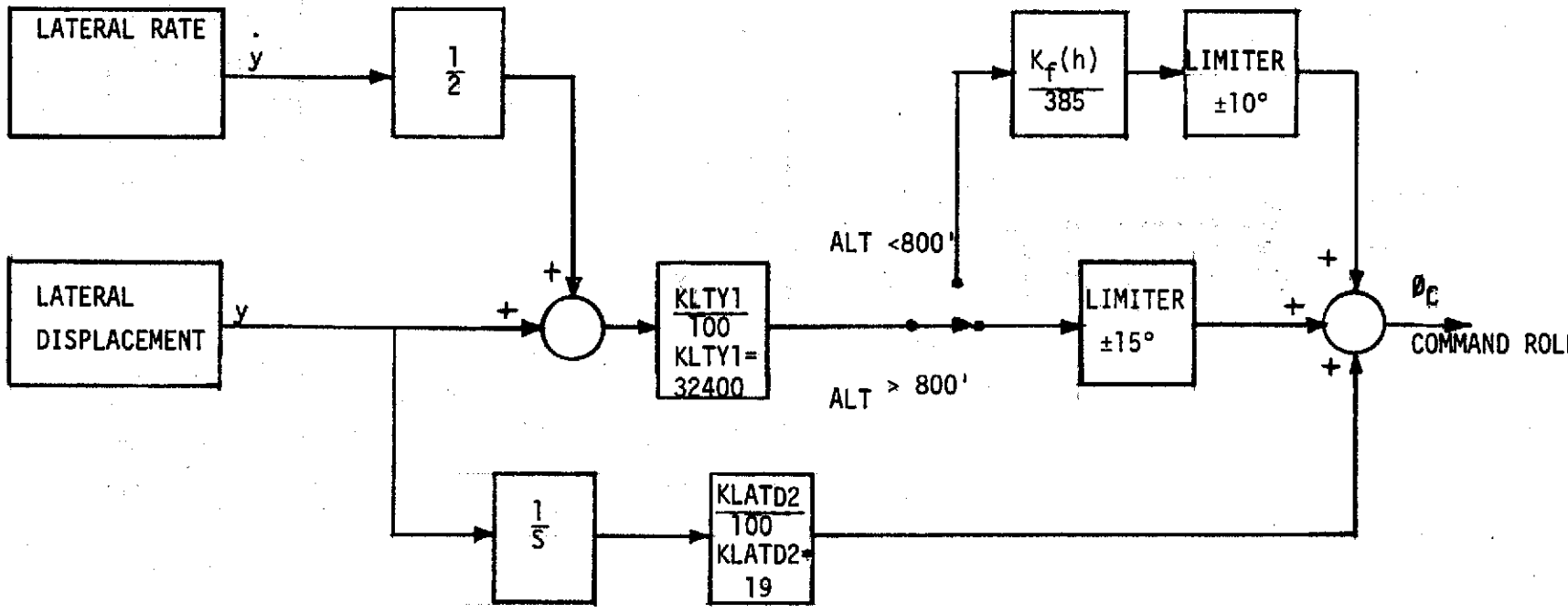

FIGURE 10.- MLS LOCALIZER TRACK CONTROL LAW

MLS LOCALIZER CAPTURE LAW

ROLL COMMAND

$$\phi_c = \left(\frac{\dot{Y}}{2} + Y\right)\frac{KLCY}{1000}$$

MLS LOCALIZER TRACK LAW

ROLL COMMAND : ALTITUDE < 800'

$$\phi_c = \left(\frac{\dot{Y}}{2} + Y\right)\left(\frac{K_{LTY1}}{1000}\right)\left(\frac{K_{f(h)}}{385}\right) + \left(\frac{Y}{5}\right)\left(\frac{K_{LATD2}}{1000}\right)$$

ALTITUDE > 800'

$$\phi_c = \left(\frac{\dot{Y}}{2} + Y\right)\left(\frac{K_{LTY1}}{1000}\right) + \left(\frac{Y}{5}\right)\left(\frac{K_{LATD2}}{1000}\right)$$

FIGURE 11

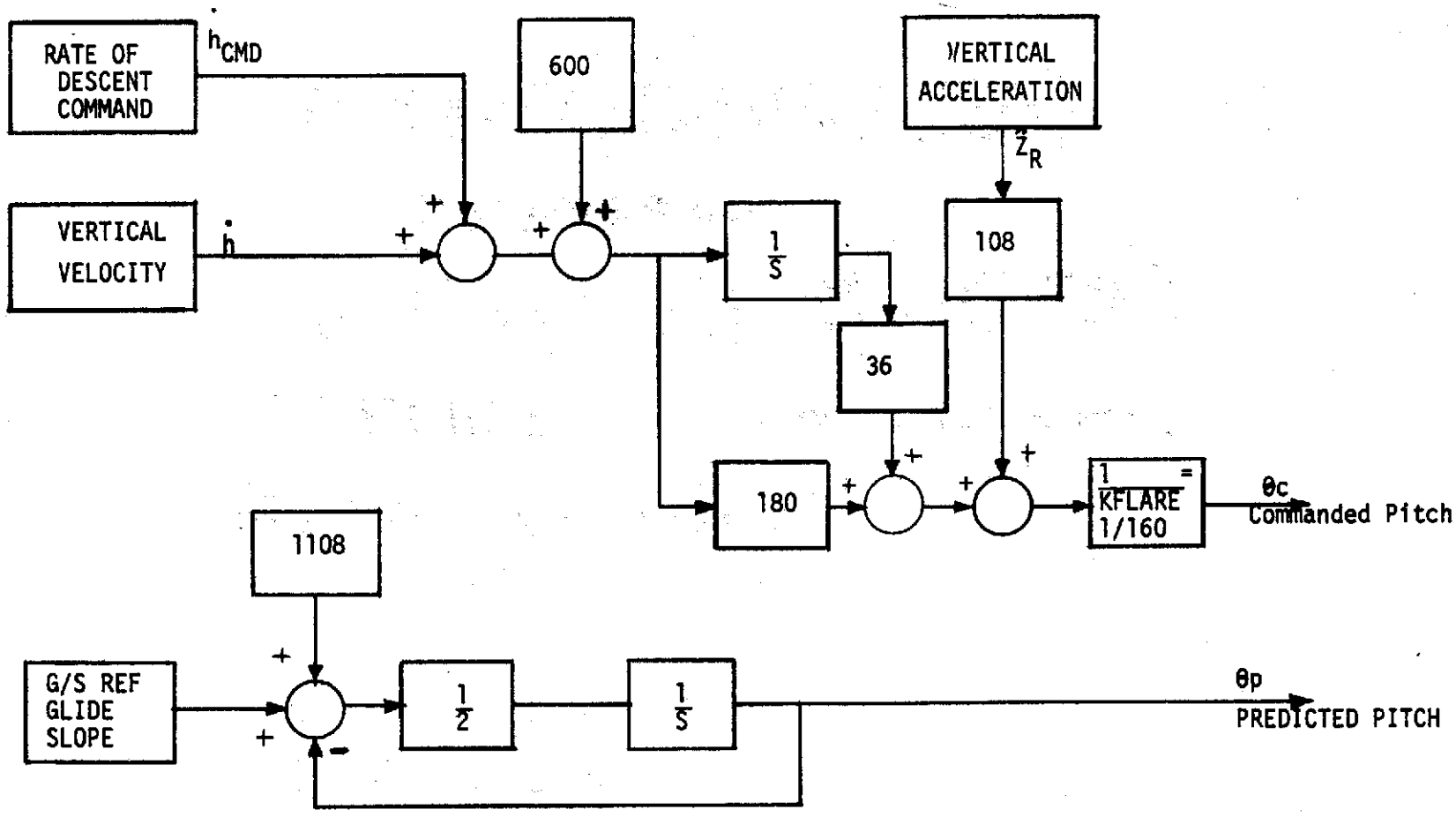

FIGURE 12.- FLARE GUIDANCE CONTROL LAW

FLARE INITIATION LAW

$$.5h - \dot{h} - 14.3 \geq 0$$

FLARE GUIDANCE CONTROL LAW

PITCH COMMAND

$$\theta_C = \left\{ \left(\dot{h}_{CMD} + \dot{h} - 600 \right) \left(\frac{36}{S} + 180 \right) + 108\, \ddot{Z}_R \right\} / K_{FLARE}$$

PREDICTED PITCH

$$\theta_P = \left(\theta_{G/S\ REF} + 1108 \right) \left(\frac{1}{2S+1} \right)$$

FIGURE 13

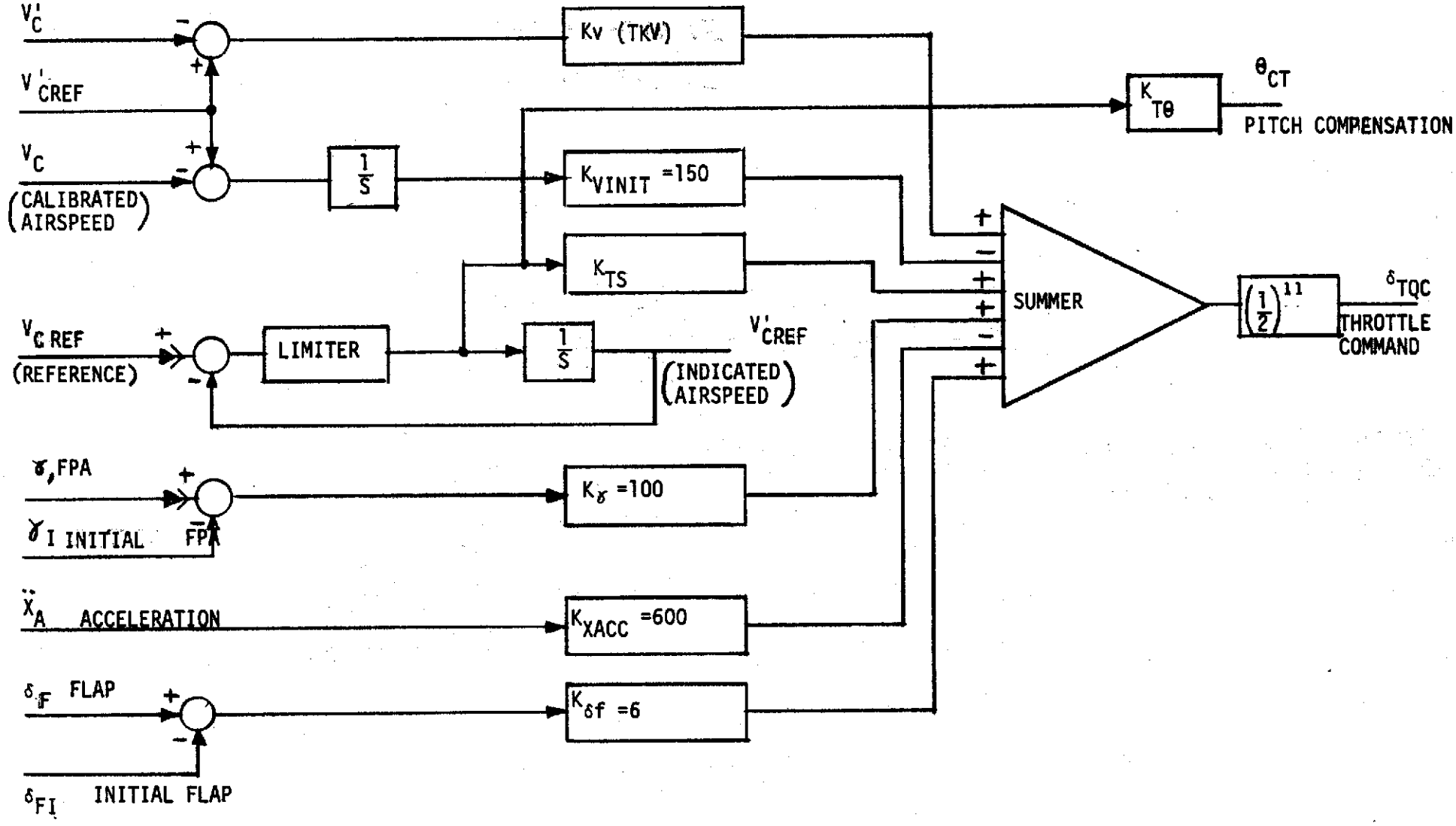

FIGURE 14.- AUTOTHROTTLE SPEED CONTROL LAW

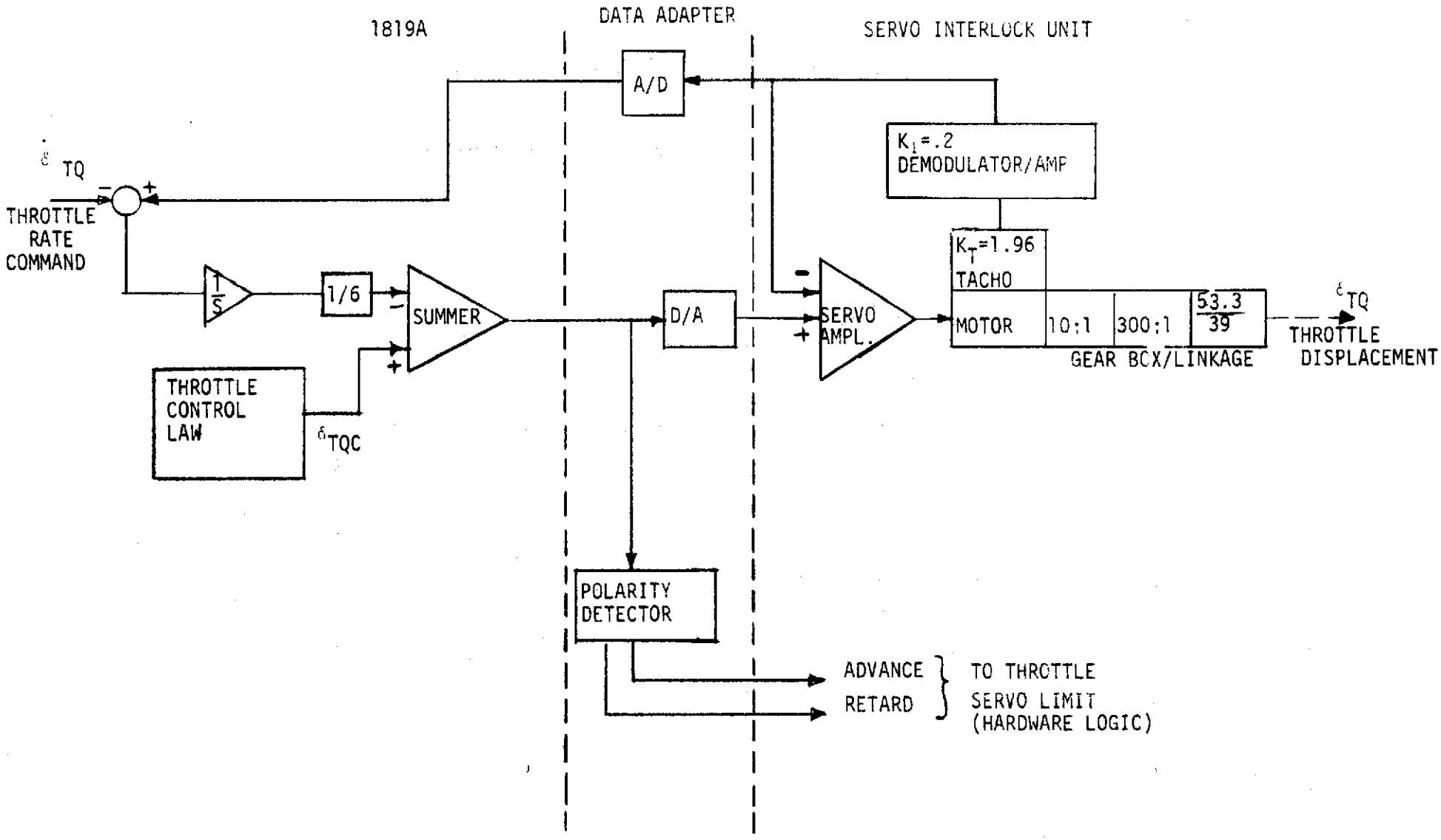

FIGURE 15. – AUTOTHROTTLE SERVO LOOP

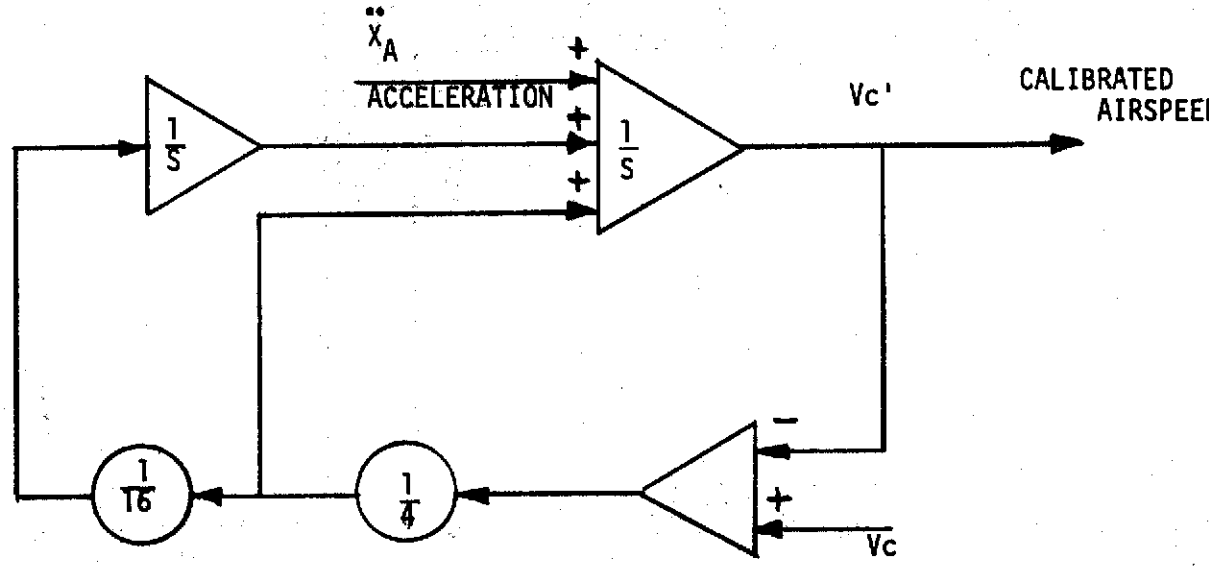

FIGURE 16.—AIRSPEED COMPLEMENTARY FILTER

AUTO THROTTLE CONTROL LAW

THROTTLE COMMAND

$$\delta_{TQC} = \left\{ -K_V\left(V_C' - V_{C\,REF}'\right) + \left(V_C - V_{C\,REF}'\right)\frac{K_{VINT}}{s} - K_{XACC}\,\ddot{X}_A \right.$$

$$\left. +(r - r_I)K_r + (\delta_f - \delta_{fI})K_{\delta_f} + K_{TS}\left(\frac{s}{s+1}\right)V_{C\,REF} \right\} \gamma_{TQ}$$

PITCH COMPENSATION

$$\theta_{CT} = K_\theta\, V_{C\,REF}\left(\frac{s}{s+1}\right)$$

AIRSPEED COMPLEMENTARY FILTER

$$V_C' = \frac{\left\{64s\left(\ddot{X}_A\right) + (16s+1)\,V_C\right\}}{(8s+1)^2}$$

FIGURE 17

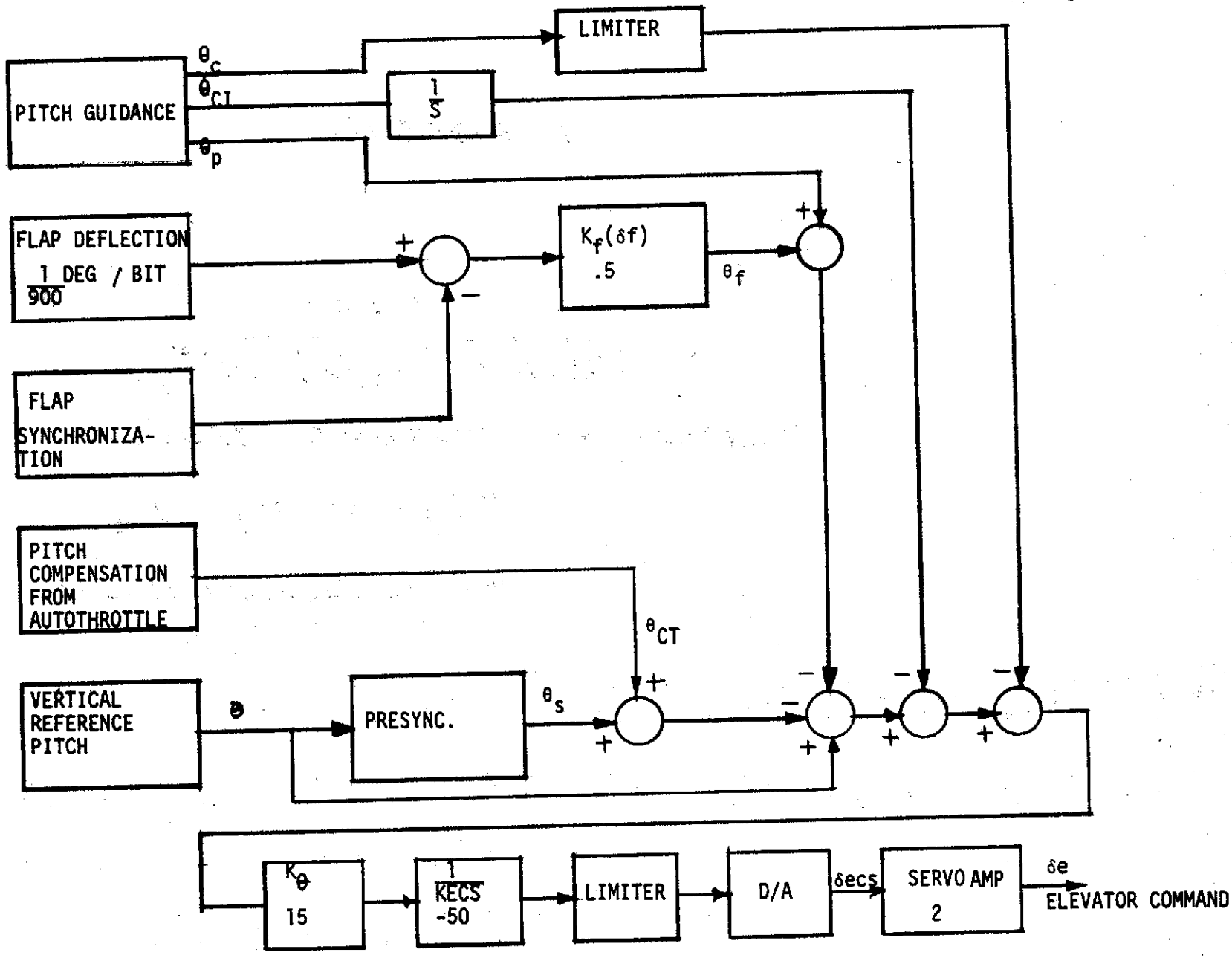

FIGURE 18.- LONGITUDINAL CONTROL SYSTEM

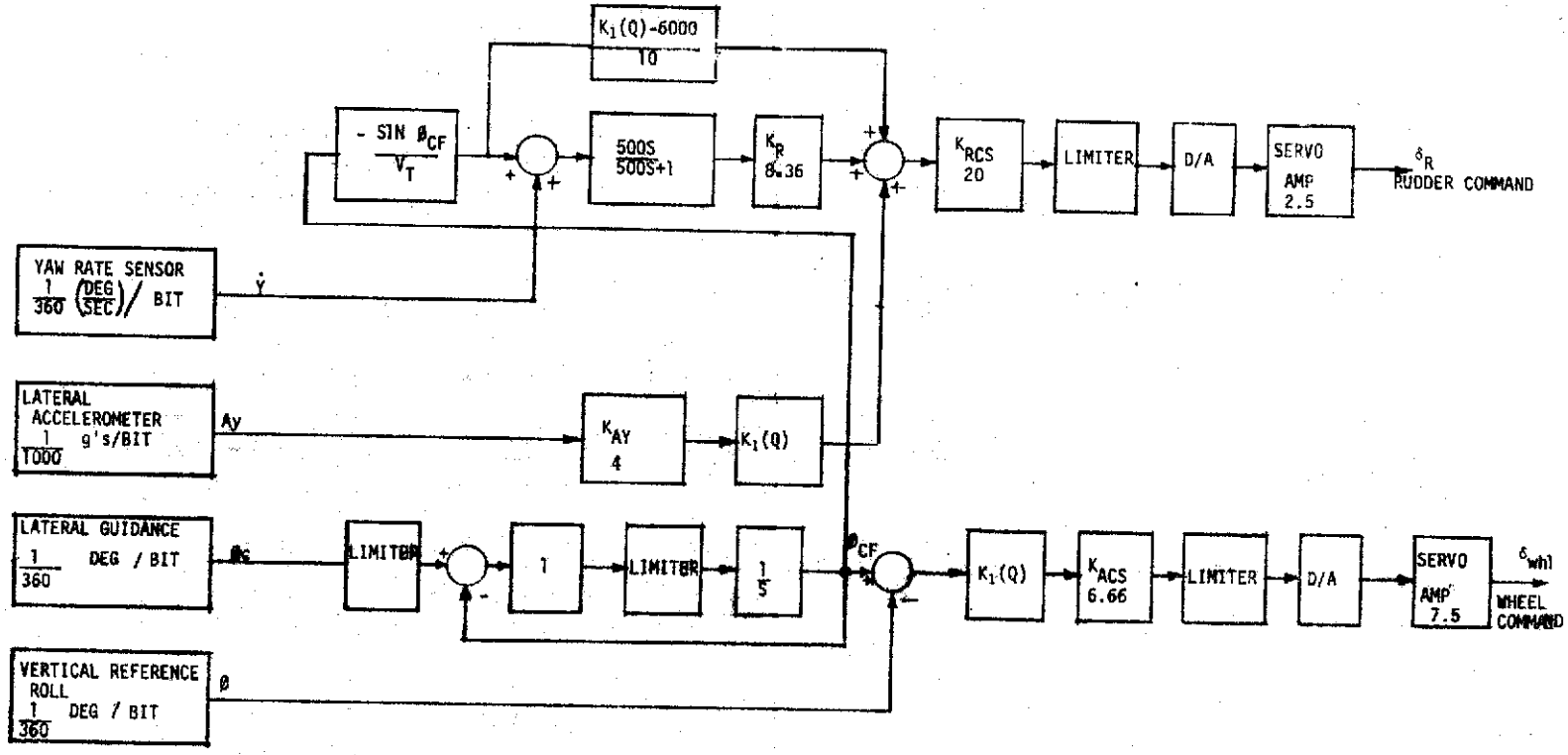

FIGURE 19.–LATERAL CONTROL SYSTEM

LATERAL CONTROL SYSTEM

RUDDER COMMAND

$$\delta_R = 2.5\, K_{ECS}\left\{-\left(\frac{K_1(Q)-6000}{10}\right)\left(\frac{\sin\phi_{CF}}{V_T}\right)+K_R\left[\frac{-\sin\phi_{CF}}{V_T}+\dot{\psi}\right]\left(\frac{500\,s}{500s+1}\right)\right.$$

$$\left.+K_1(Q)\,K_{AY}\,A_Y\right\}$$

WHERE

$$\phi_{CF} = \frac{\phi_C}{(s+1)}$$

WHEEL COMMAND

$$\delta_{CF} = K_{ACS}\,K_1(Q)\left\{\phi_{CF}-\phi\right\}(7.5)$$

LONGITUDINAL CONTROL SYSTEM

ELEVATOR COMMAND

$$\delta_e = \frac{-2}{K_{ECS}}\left\{K_\theta\left[\theta-\left(\theta_s+\theta_p+\frac{\dot{\theta}_{CI}}{s}+\theta_c+\theta_f+\theta_{CT}\right)\right]\right\}$$

WHERE

$$\theta_f = K_f(\delta_f)\left[\delta_f-\delta_{fo}\right]$$

FIGURE 20

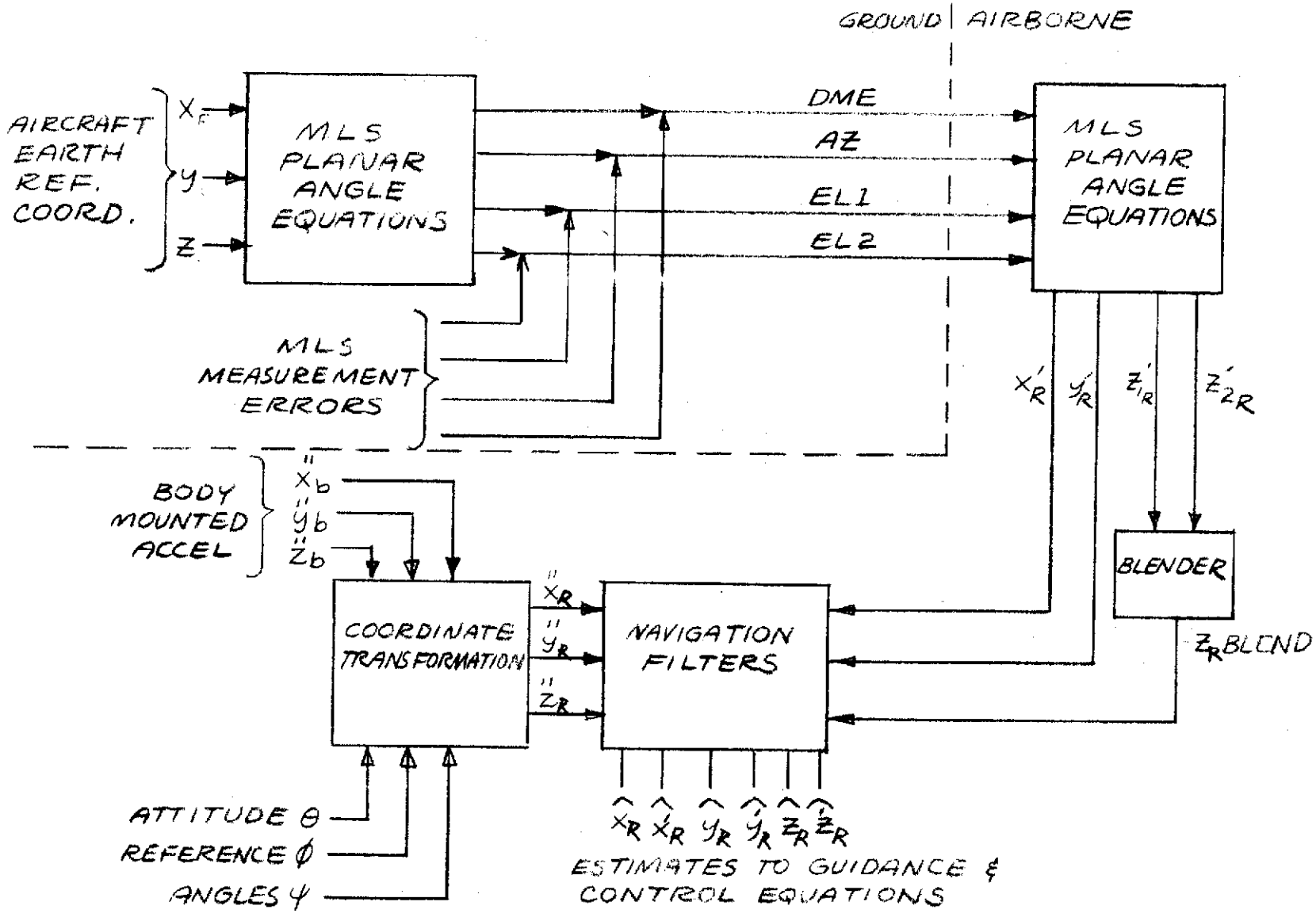

FIGURE 21-MLS SIGNAL GENERATION AND PROCESSING

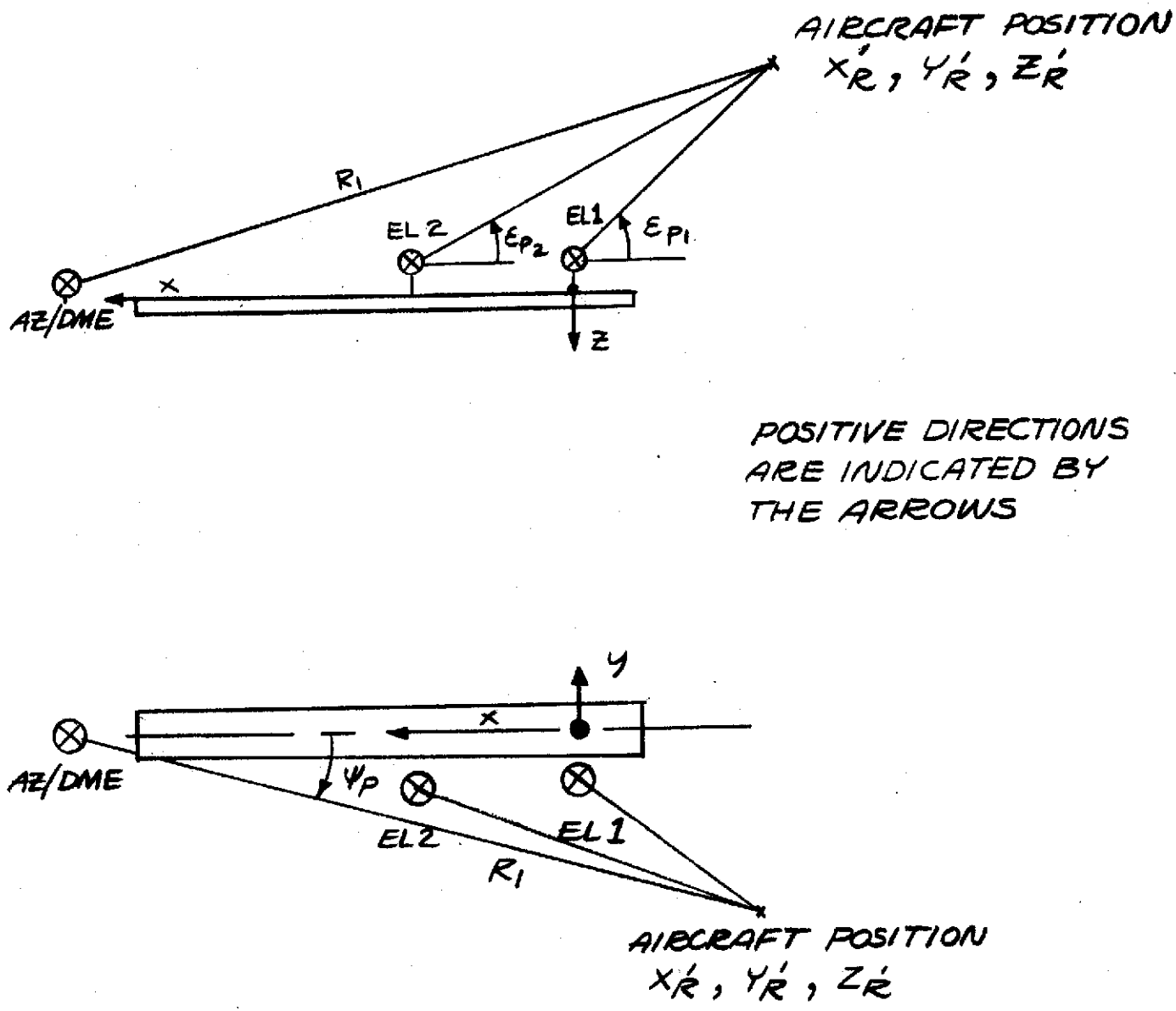

FIG. 22 GEOMETRY OF MLS NAVIGATION

$$X_R' = \frac{B - \sqrt{B^2 - AC}}{A}$$

$$Y_R' = (X_R' - X_{RA}) \tan \psi_p$$

$$Z_R' = X_R' \tan \varepsilon_{p_1} + Z_{RE}$$

WHERE

$$A = 1 + \tan^2 \psi_p + \tan^2 \varepsilon_{p_1}$$

$$B = X_{RA}(1 + \tan^2 \psi_p)$$

$$C = X_{RA} \cdot B - R_1^2$$

R_1 = DME SLANT RANGE

ε_{p_1} = PLANAR ELEVATION 1 ANGLE

ψ_p = PLANAR AZIMUTH ANGLE

(X_{RA}, Y_{RA}, Z_{RA}) = RUNWAY REFERENCED MLS AZIMUTH-DME SCANNER POSITION COORDINATES

LOCATION ASSUMPTIONS:

$X_{RE} = Y_{RA} = 0$; $Z_{RE1} = Z_{RA}$

FIG. 23 PLANAR ANGLE EQUATIONS TO CONVERT FROM MLS COORDINATES TO X, Y, Z COORDINATES

$$\tan \psi_p = \frac{Y_R}{X_R - X_{RA}}$$

$$\tan \varepsilon_{p1} = \frac{Z_R - Z_{RE1}}{X_R - X_{RE2}}$$

$$\tan \varepsilon_{p2} = \frac{Z_R - Z_{RE2}}{X_{RE2} - X_R}$$

$$R_1 = \left[(X_R - X_{RA})^2 + Y_R^2 + (Z_R - Z_{RA})^2 \right]^{\frac{1}{2}}$$

(Y_{RA} assumed 0)

$$h_2 = E \tan \varepsilon_{p2} - \frac{E^2}{2R_1} \tan^3 \varepsilon_{p2} - Z_{RE2}$$

WHERE

$$E = R_1 + X_{RE2} - X_{RA}$$

FIG. 24.- PLANAR ANGLE EQUATIONS TO CONVERT FROM RECTANGULAR POSITION COORDINATES TO MLS VARIABLES

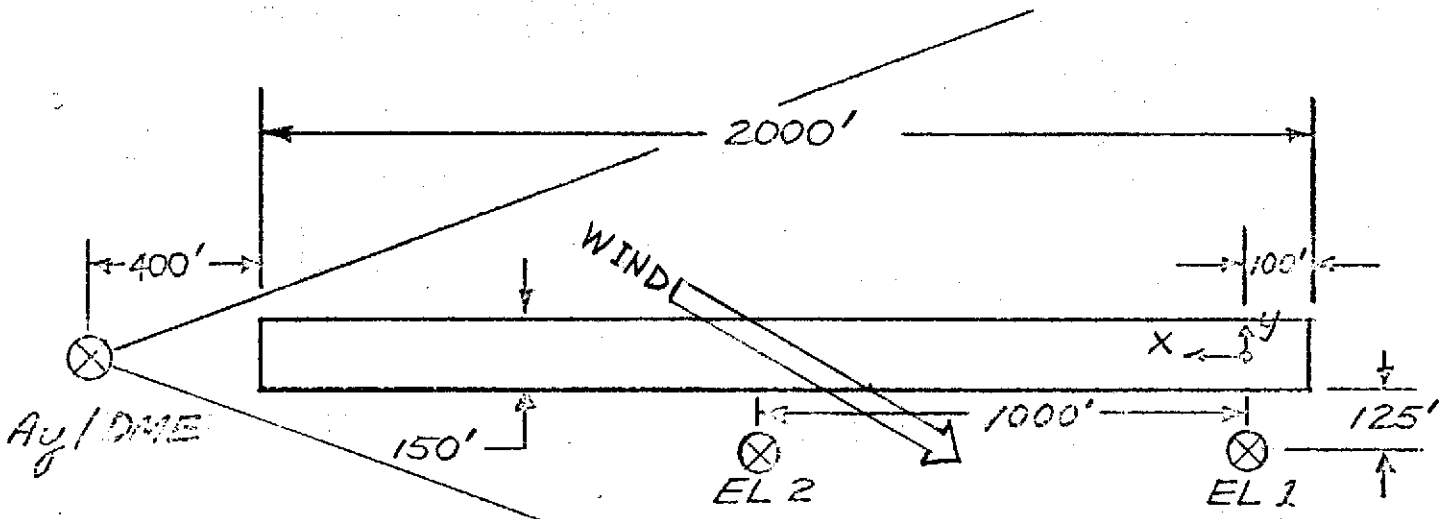

FIG 23 — STOLPORT GEOMETRY

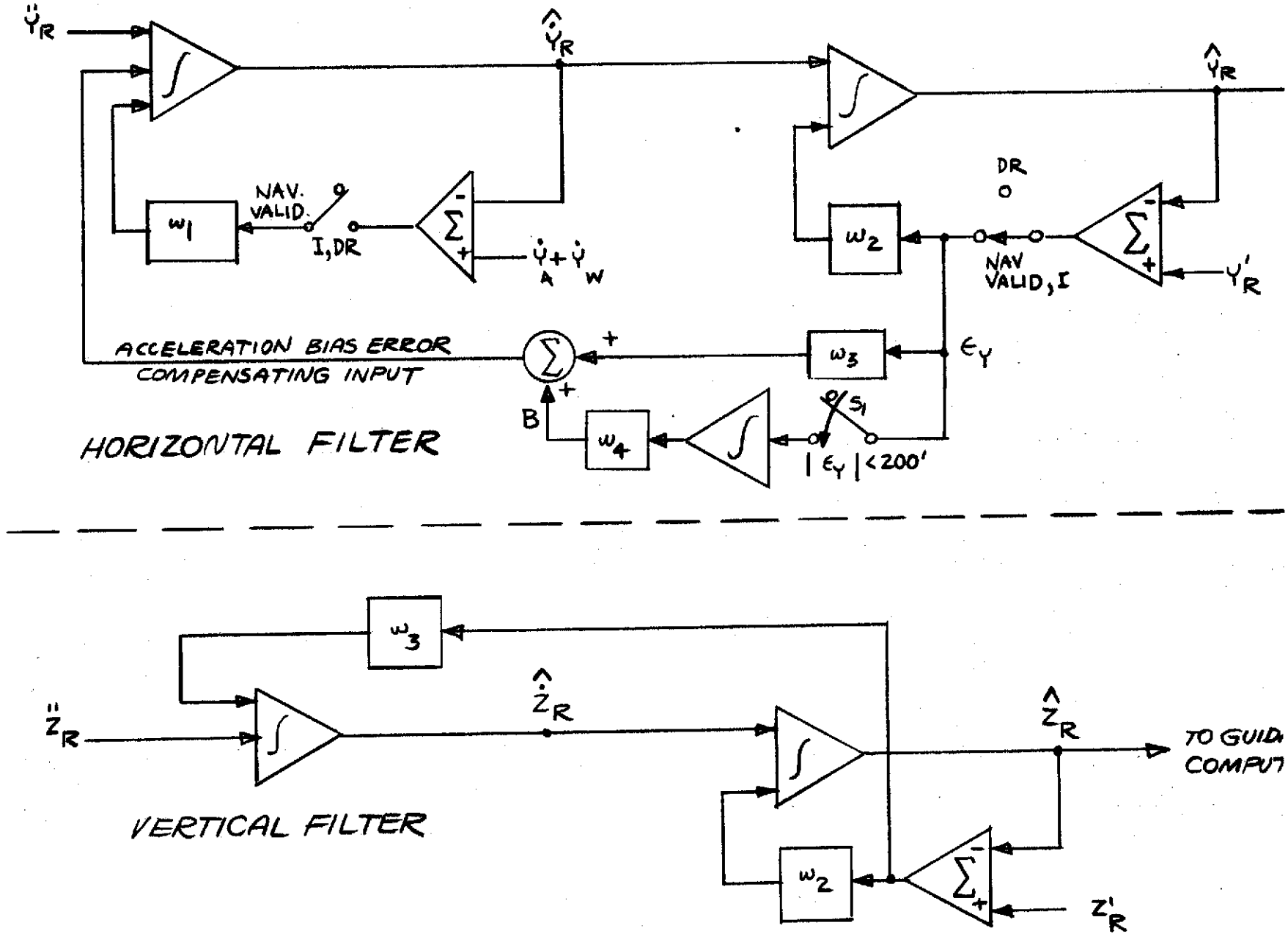

FIG. 26 – NAVIGATION FILTERS

	w_2	w_3	w_4
LOW GAIN	0.4	0.06	0.004
HIGH GAIN	1.2	0.54	0.108

(NOMINAL FREQUENCY)
(HIGH FREQUENCY)

TABLE 1 HORIZONTAL COMPLEMENTARY FILTER GAINS

	w_2	w_3
LOW GAIN	.67	.18
HIGH GAIN	2.0	1.62

(NOMINAL FREQUENCY)
(HIGH FREQUENCY)

TABLE 2 VERTICAL COMPLEMENTARY FILTER GAINS

	w_2	w_3	w_4	α
GAINS	1.5	0.75	0.125	0.5

TABLE 3 HORIZONTAL NON-COMPLEMENTARY FILTER GAINS

	w_2	w_3	α
GAINS	1.6	0.64	0.8

TABLE 4 VERTICAL NON-COMPLEMENTARY FILTER GAINS

FIGURE 27. - FILTER GAINS

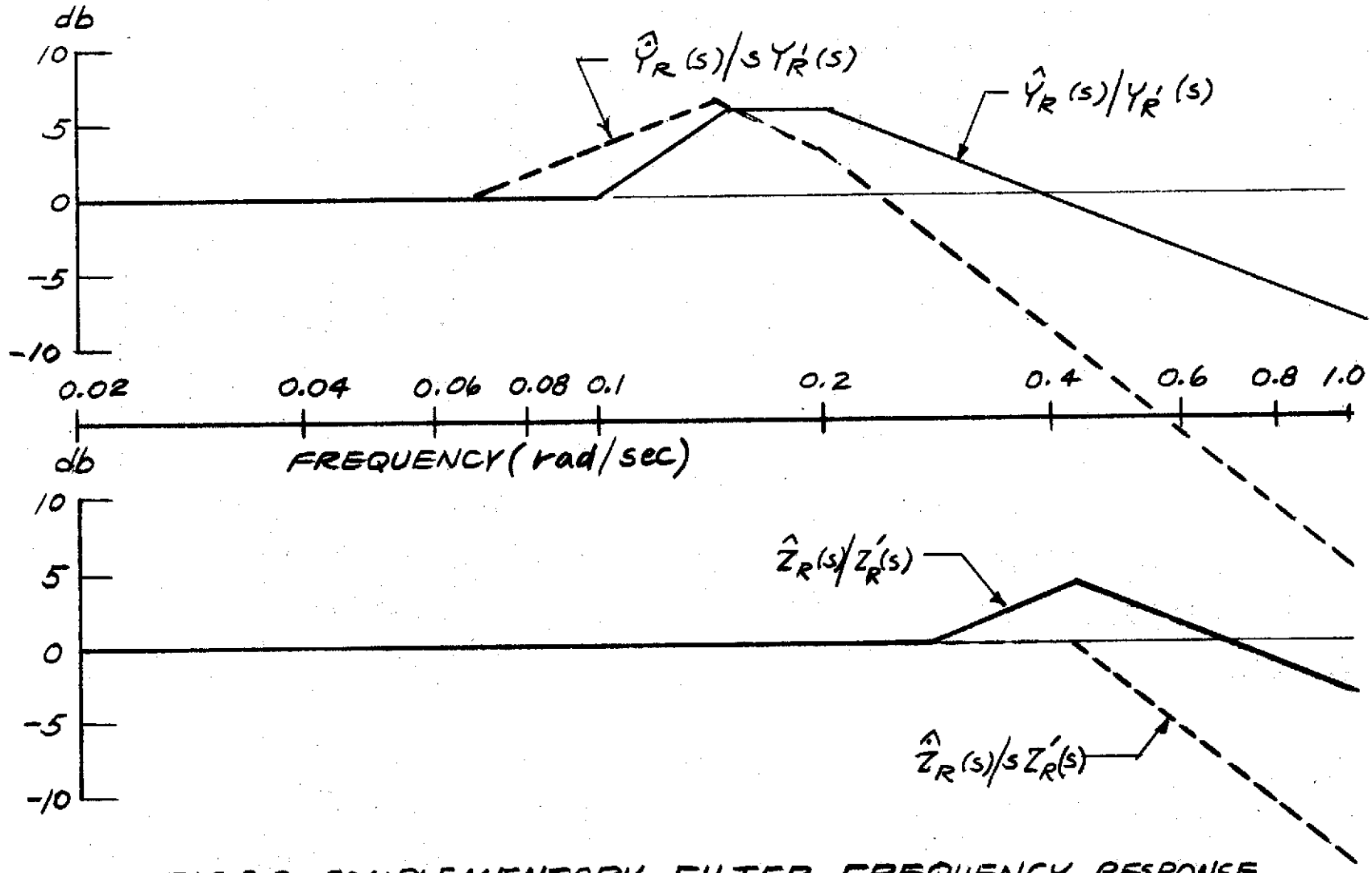

FIG 28 COMPLEMENTARY FILTER FREQUENCY RESPONSE CURVES FOR NOMINAL GAINS

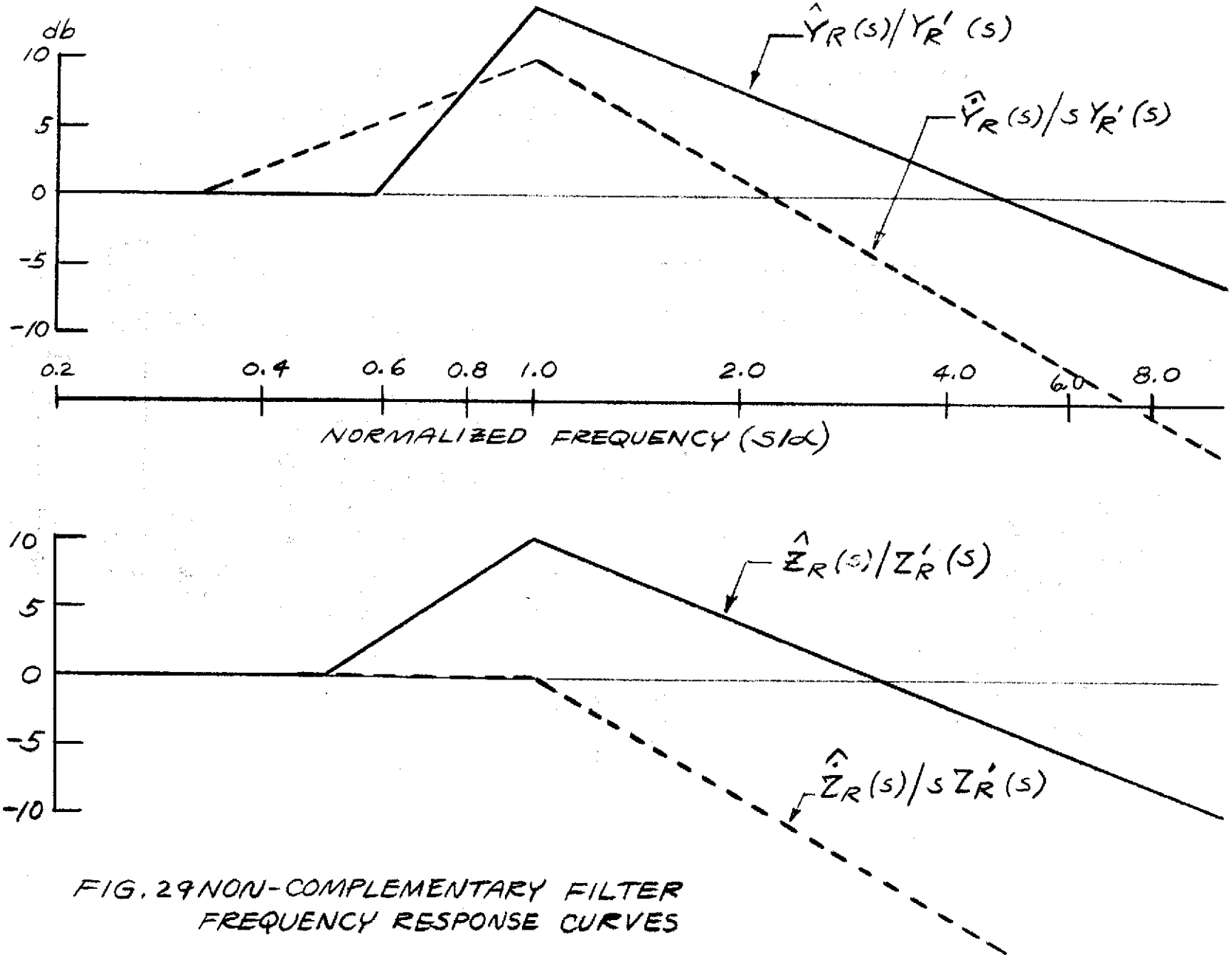

FIG. 29 NON-COMPLEMENTARY FILTER FREQUENCY RESPONSE CURVES

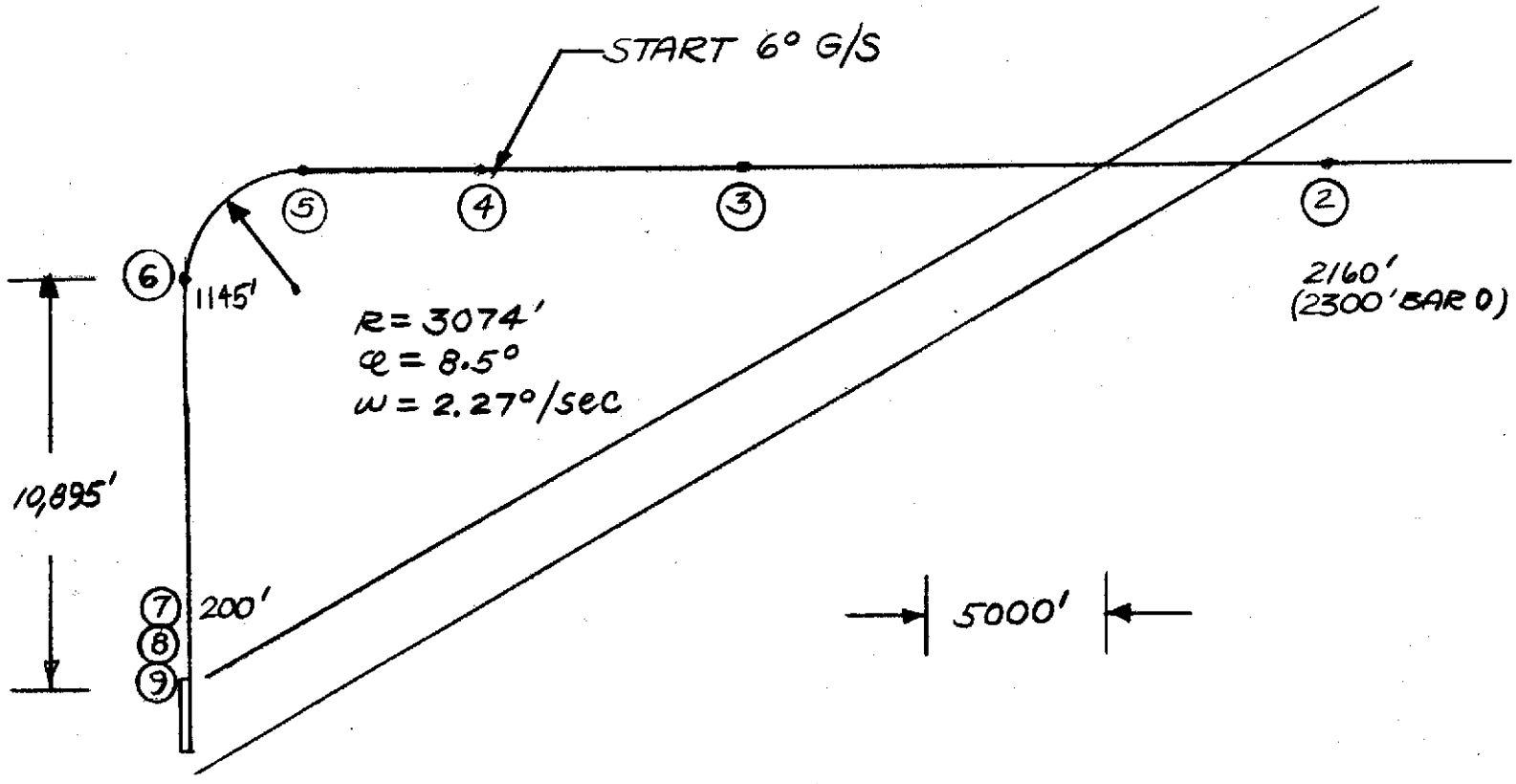

FIGURE 30.-90 DEGREE FLIGHT PATH (FPI)

FIGURE 31 - MLS FLIGHT PATH (FP1)

WAYPOINT	LOCATION		HEIGHT ABOVE RUNWAY (FT)	IAS (Knots)	G/S ANGLE (deg.)	TURN RATE (deg/sec)
	X (FT)	Y (FT)				
1	-13969	-38000		72.0	0	
2	-13969	-31000	2160	72.0	0	
3	-13969	-15000	2160	72.0	0	
4	-13969	-7898	2160	72.0	-6.0	
5	-13969	-3074	1653	72.0	-6.0	2.27
6	-10895	0	1145	72.0	-6.0	
7	-1903	0	200	72.0	-6.0	
8	-951	0	100	72.0	-6.0	
9	0	0				

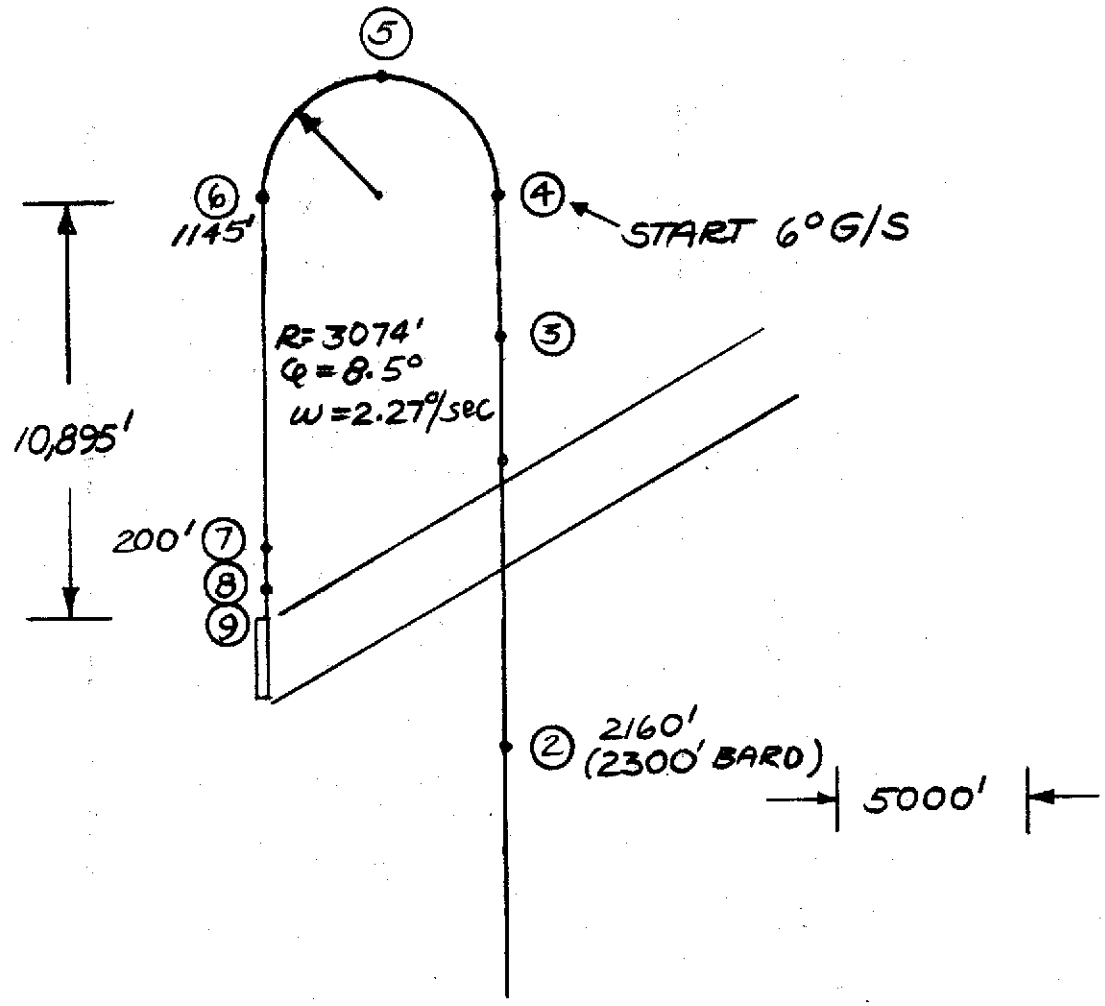

FIGURE 32.-180 DEGREE FLIGHT PATH (FP2)

FIGURE 33-MLS FLIGHT PATH (FP2)

WAYPOINT	LOCATION		HEIGHT ABOVE RUNWAY (FT)	IAS (Knots)	G/S ANGLE (deg.)	TURN RATE (deg/sec)
	X (FT)	Y (FT)				
1	10000	-6148	2160	72.0	0	
2	4000	-6148	2160	72.0	0	
3	-7000	-6148	2160	72.0	0	
4	-10895	-6148	2160	72.0	-6.0	2.27
5	-13969	-3074	1653	72.0	-6.0	2.27
6	-10895	0	1145	72.0	-6.0	
7	-1903	0	200	72.0	-6.0	
8	-951	0	100	72.0	-6.0	
9	0	0				

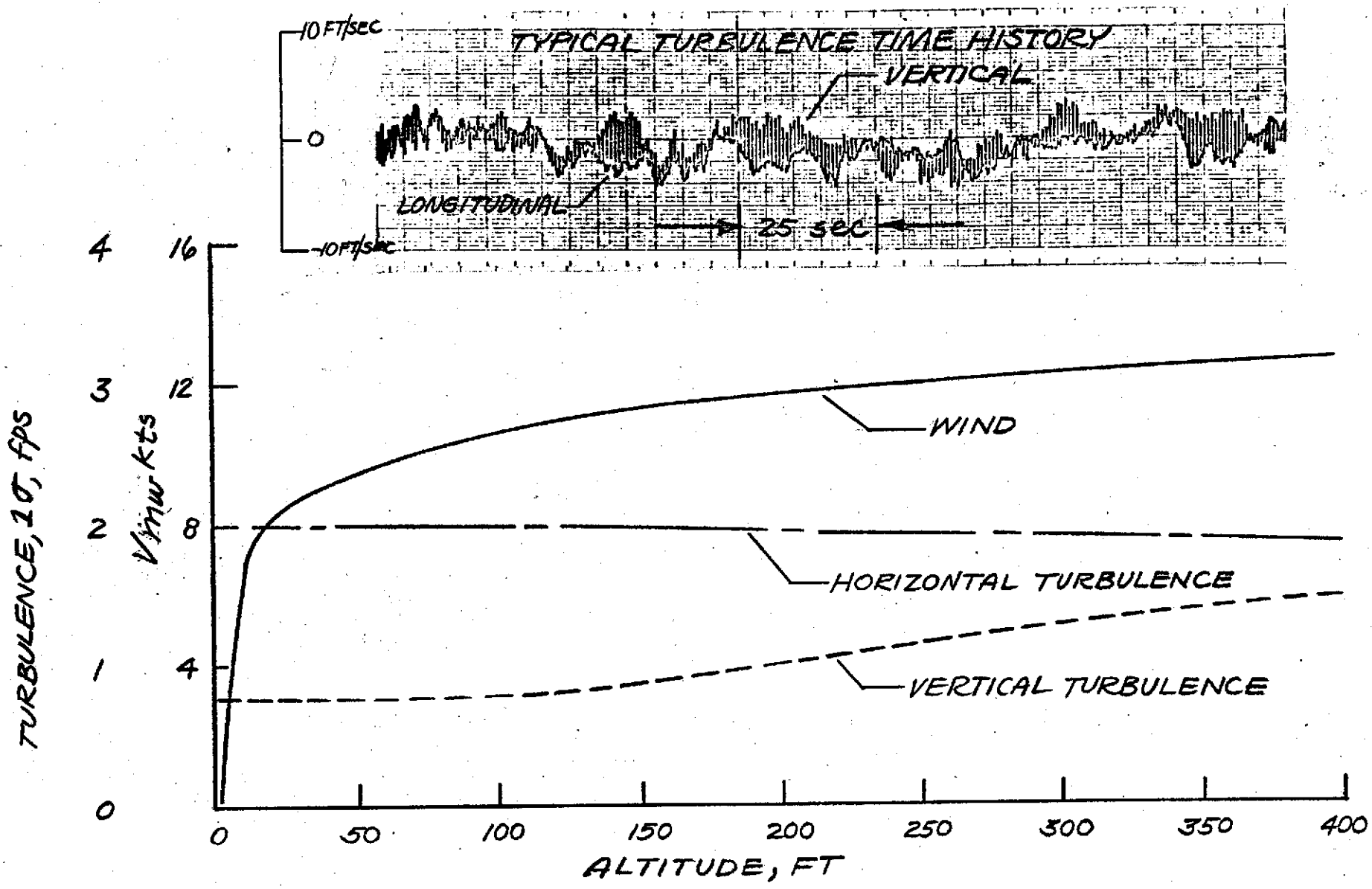

FIGURE 34.- ATMOSPHERIC DISTURBANCE MODEL

			BIAS	RANDOM (1σ)
CAT III ERRORS (RTCA)	A_Z	DEG	+0.124	0.112
	EL_1	DEG	+0.036	0.042
	EL_2	DEG	+0.034	0.032
	DME	FT	+ 20	20
CAT II ERRORS	A_Z	DEG	+0.3	0.2
	EL 1	DEG	+0.1	0.15
	EL 2	DEG	+0.1	0.15
	DME	FT	+100	100

FIG. 35 MLS ERROR COMBINATIONS

MLS RESOLUTIONS

SIGNAL	RANGE	RESOLUTION
DME	10 N. MILES	4 FEET
AZIMUTH	120° (± 60°)	0.003°
ELEVATION	20°	0.003°

FIGURE 36

FIG. 37

List of Symbols

Symbol	Definition	Dimension
h	altitude	ft.
$\dot{h}$	sink rate	ft/sec.
Δh	instantaneous altitude error from glide slope	ft.
$\ddot{z}_B$	vertical acceleration	ft/sec.^{2}
(x,y,z)	runway referenced position coordinate	ft.
$\ddot{Y}_B$	lateral acceleration	ft/sec.^{2}
VAK	A/C velocity	ft/sec.
$\ddot{X}_B$	longitudinal acceleration	ft/sec.^{2}
UBN	longitudinal turbulence	ft/sec.
WBN	vertical turbulence	ft/sec.
W_x	wind x component	ft/sec.
W_y	wind y component	ft/sec
θ	pitch angle	deg.
q	pitch rate	deg./sec.
ψ	heading angle	deg.
$\dot{r}$	yaw rate	deg./sec.
ϕ	roll angle	deg.
p	roll rate	deg./sec.
δ_w	wheel position	deg.
δ_r	rudder position	deg.
δ_e	elevator position	deg
δ_f	flap position	deg.

Symbol	Definition	Dimension
α	angle of attack	deg.
γ	flight path angle	deg.
β	side slip angle	deg.
$\dot{x}$	longitudinal velocity	ft/sec.
$\dot{y}$	lateral velocity	ft/sec.
GPIP	glide path interception point	—

A. FAA Auto Landing System Advisory Circular 20-57A for CAT II CTOL.

- 2σ Longitudinal Touchdown Dispersion = < 1500 ft total (need not be symmetrical).
- 2σ Lateral Touchdown Dispersion = < ±27 ft about R/W centerline. Attempting to scale these figures to a STOLport gives:
- 2σ Longitudinal STOL Touchdown Dispersion = < 700 ft total.
- 2σ Lateral STOL Touchdown Dispersion = < ±24 ft of centerline.

B. Interpretation of the FAA Criteria for Approval of CAT II Landing Weather Minima Advisory Circular AC 120-20 for ILS/CTOL 100 ft. Decision Height Window.

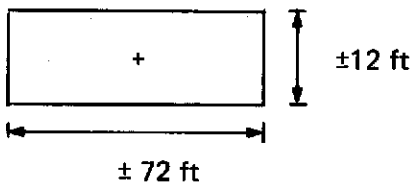

The values given for this window are interpreted to mean that the aircraft should be within the specified limits for at least 95% of the approaches attempted. With the assumption of a Gaussian distribution, the resulting vertical and horizontal 2σ errors become ±12 ft and ±72 ft, respectively.

C. ICAO Annex 10 ILS Specifications.

- CAT II Beam Centering = ±15 ft at the threshold (Interpreted as $\pm 2\sigma$)
- Restrict the aircraft deviations due to course bends (95% probability) to less than:

Category	Glideslope	Localizer
CAT I	±10 ft @ 100 ft	±30 ft @ 100 ft
CAT II	±4 ft @ 50 ft <2° incremental pitch	±15 ft threshold to 3000 ft <2° incremental roll
CAT III	Same as CAT II	Same as CAT II plus 2000 ft beyond threshold on runway

Fig. 38. CRITERIA.

D. RTCA-117 MLS Minimum Performance Table

2 σ	CAT I (150')	CAT II (50')	CAT III (T.D.)
Azimuth Bias	50'	32'	10'
Azimuth Random	26'	11'	9'
Elevation Bias	6'	1.2'	1.2'
Elevation Random	7'	1.4'	1.4'
DME Bias	300'	100'	20'
DME Random	----	----	---

Fig. 38 Concluded.

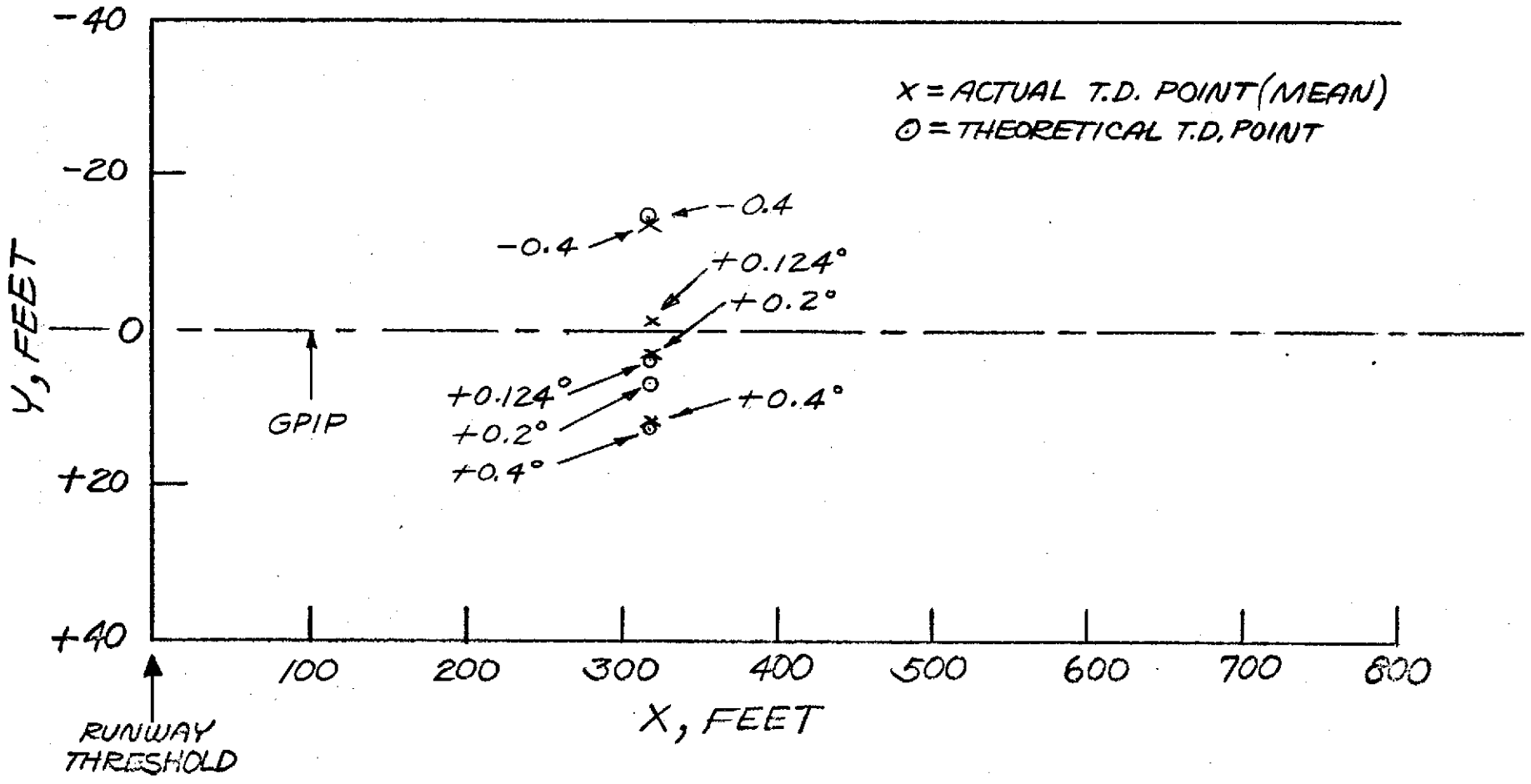

FIG. 39-EFFECT OF AZIMUTH BIAS ON LATERAL TOUCHDOWN DISPERSION

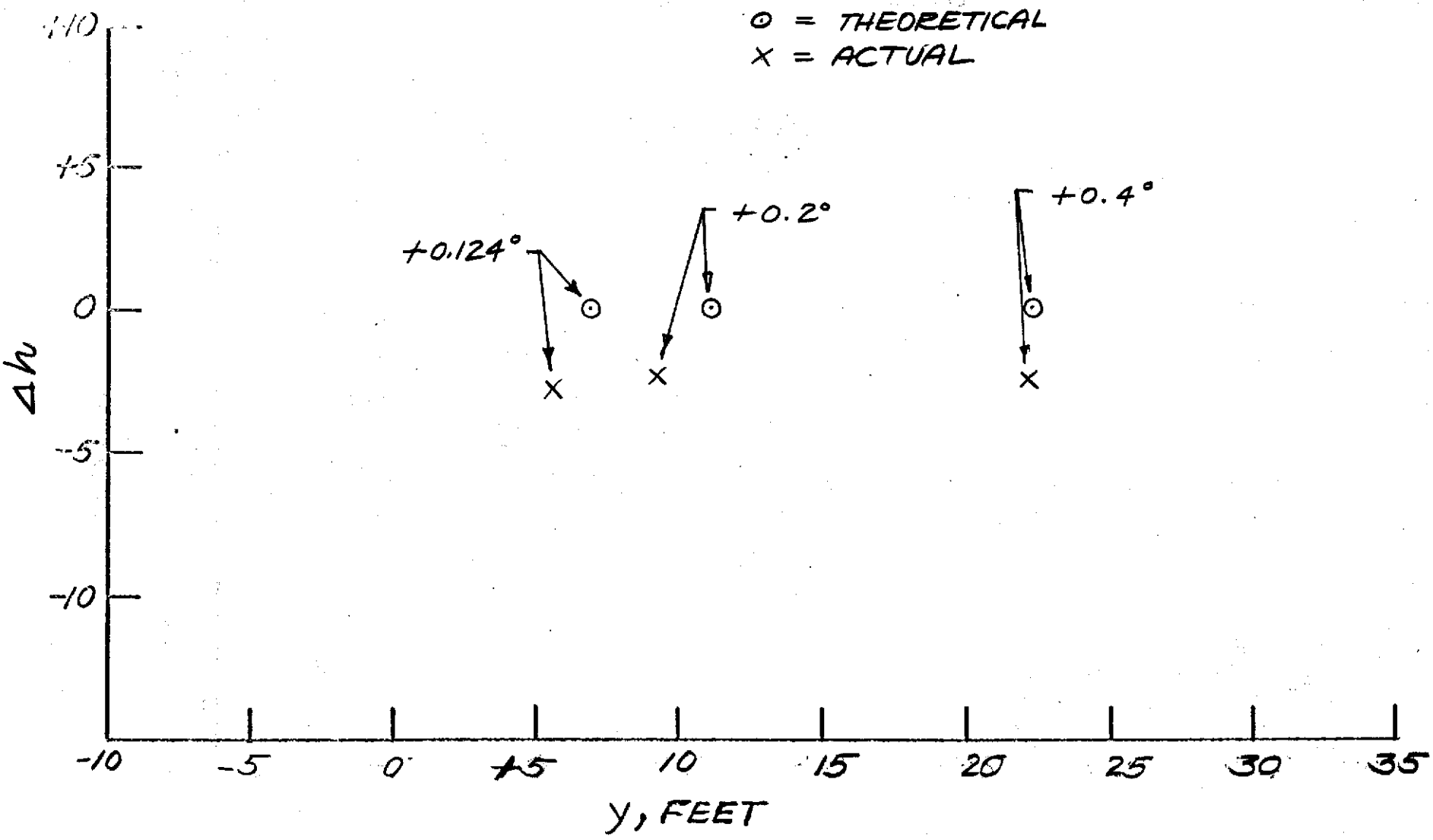

FIG. 40-EFFECT OF AZIMUTH BIAS AT 100 FEET ALTITUDE

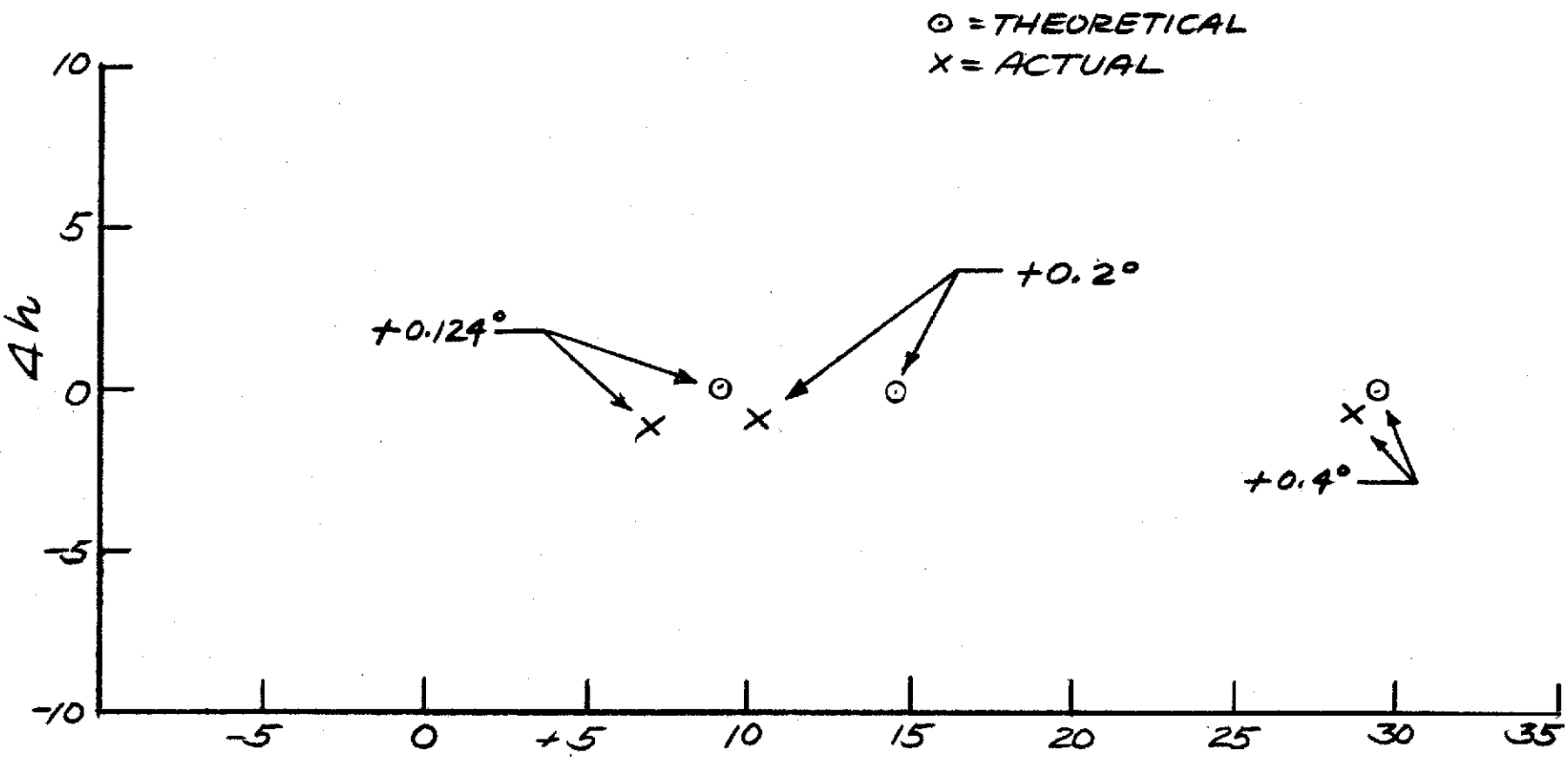

FIG. 41 - EFFECT OF AZIMUTH BIAS AT 200 FEET ALTITUDE

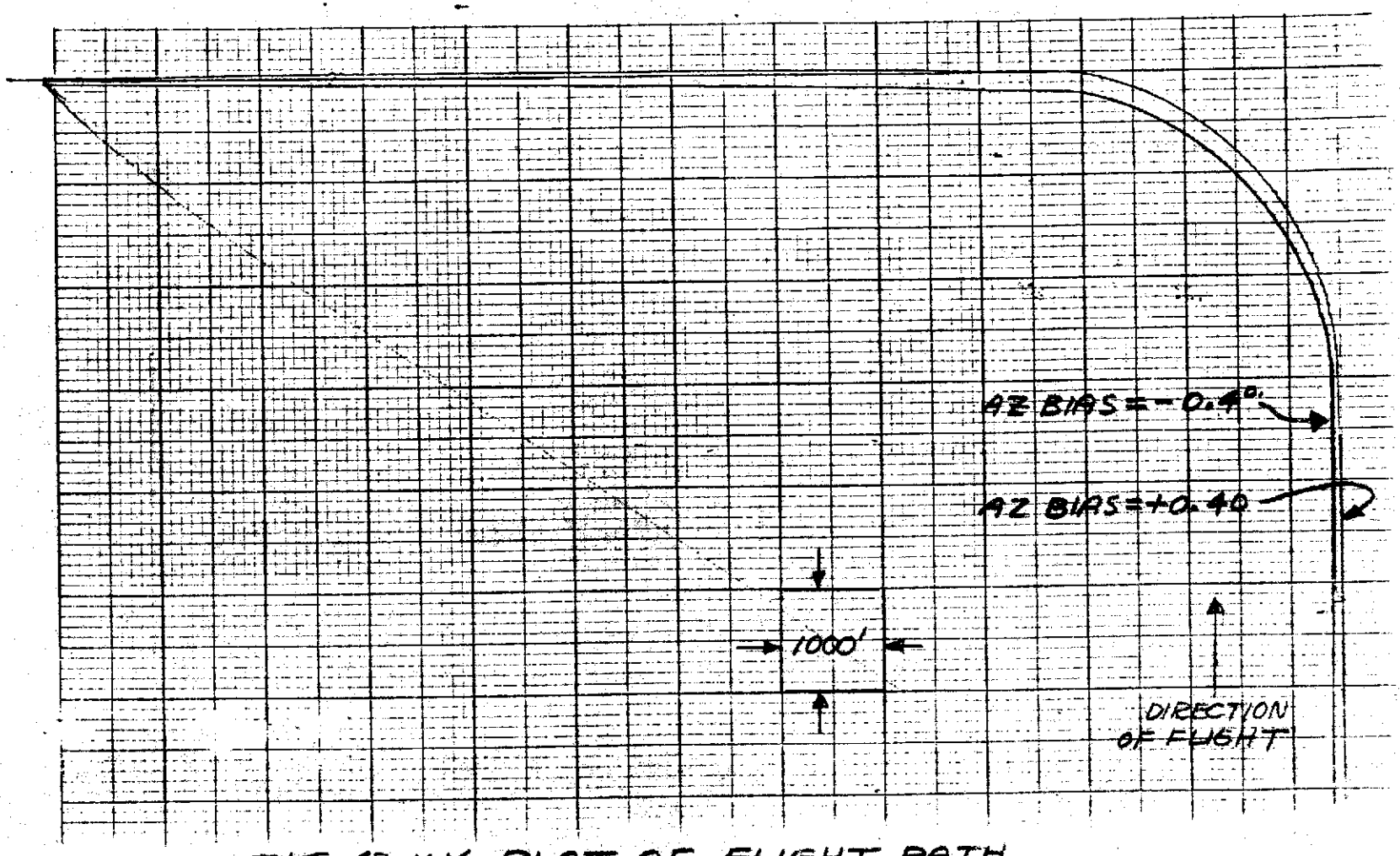

FIG. 42 X Y PLOT OF FLIGHT PATH
*1 WITH ± 0.4 AZIMUTH BIAS

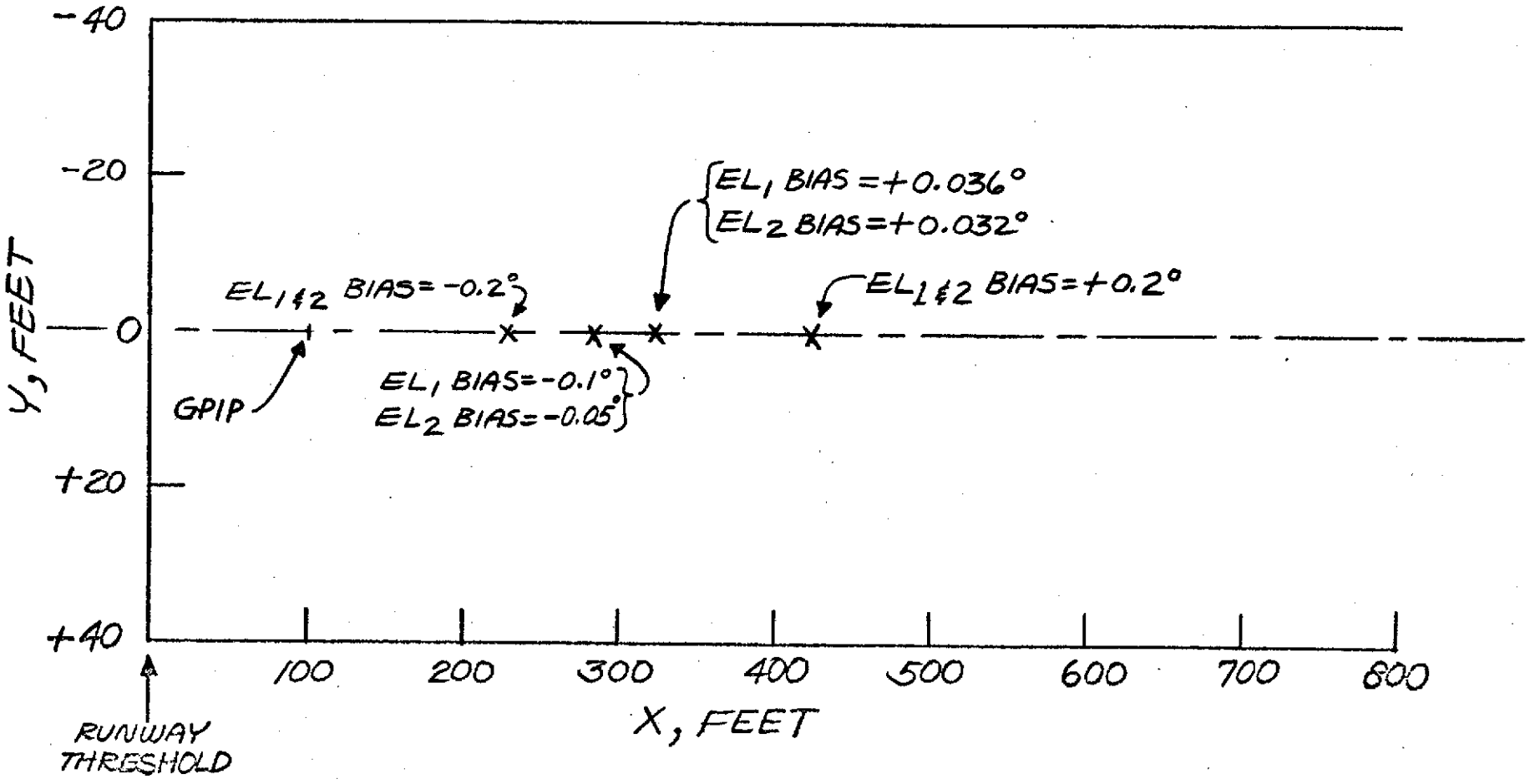

FIG. 43-EFFECT OF ELEVATION BIAS ON LONGITUDINAL TOUCHDOWN

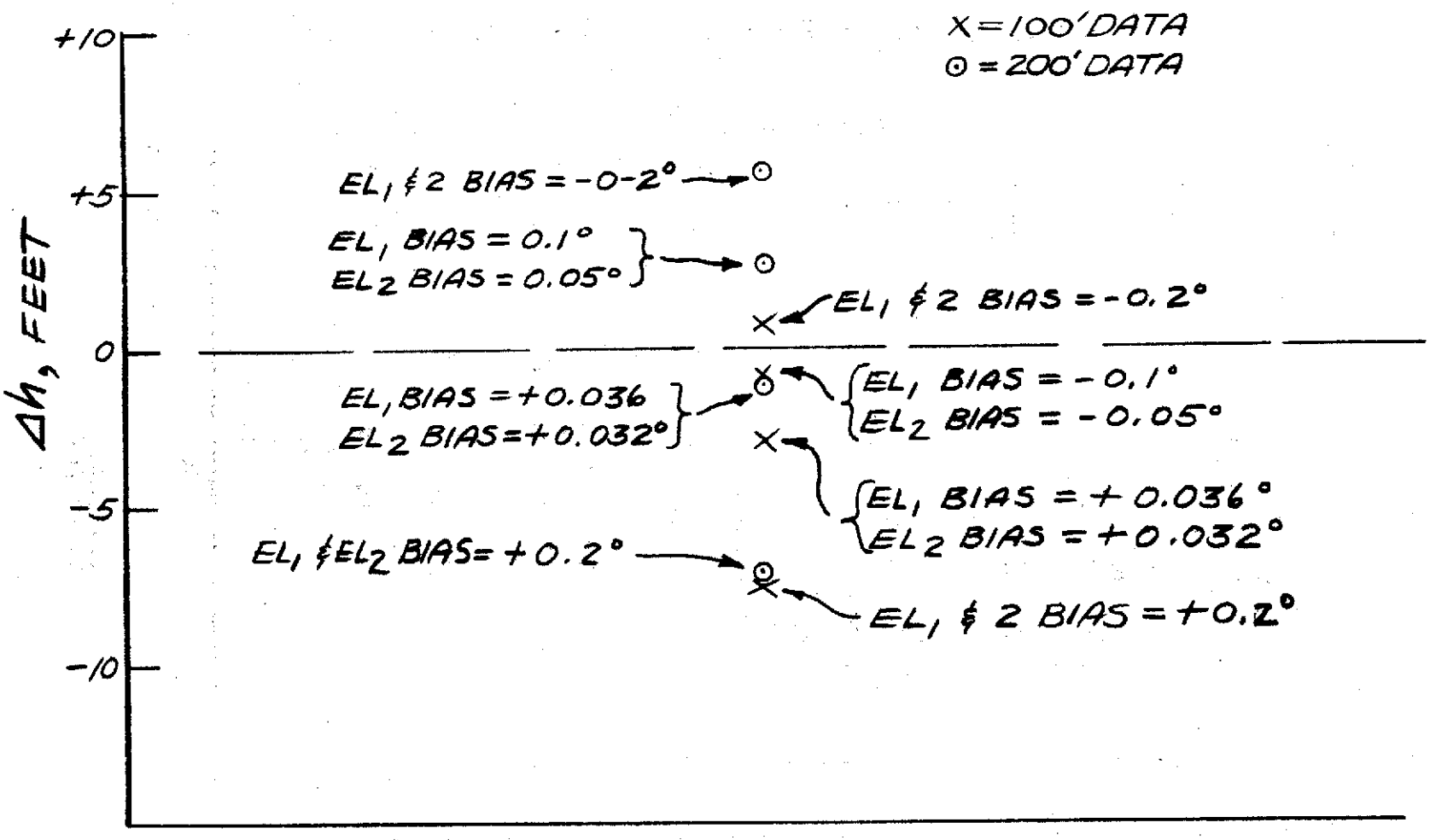

FIG. 44: EFFECT OF ELEVATION BIAS ON Δh AT 100 AND 200 FT ALTITUDES

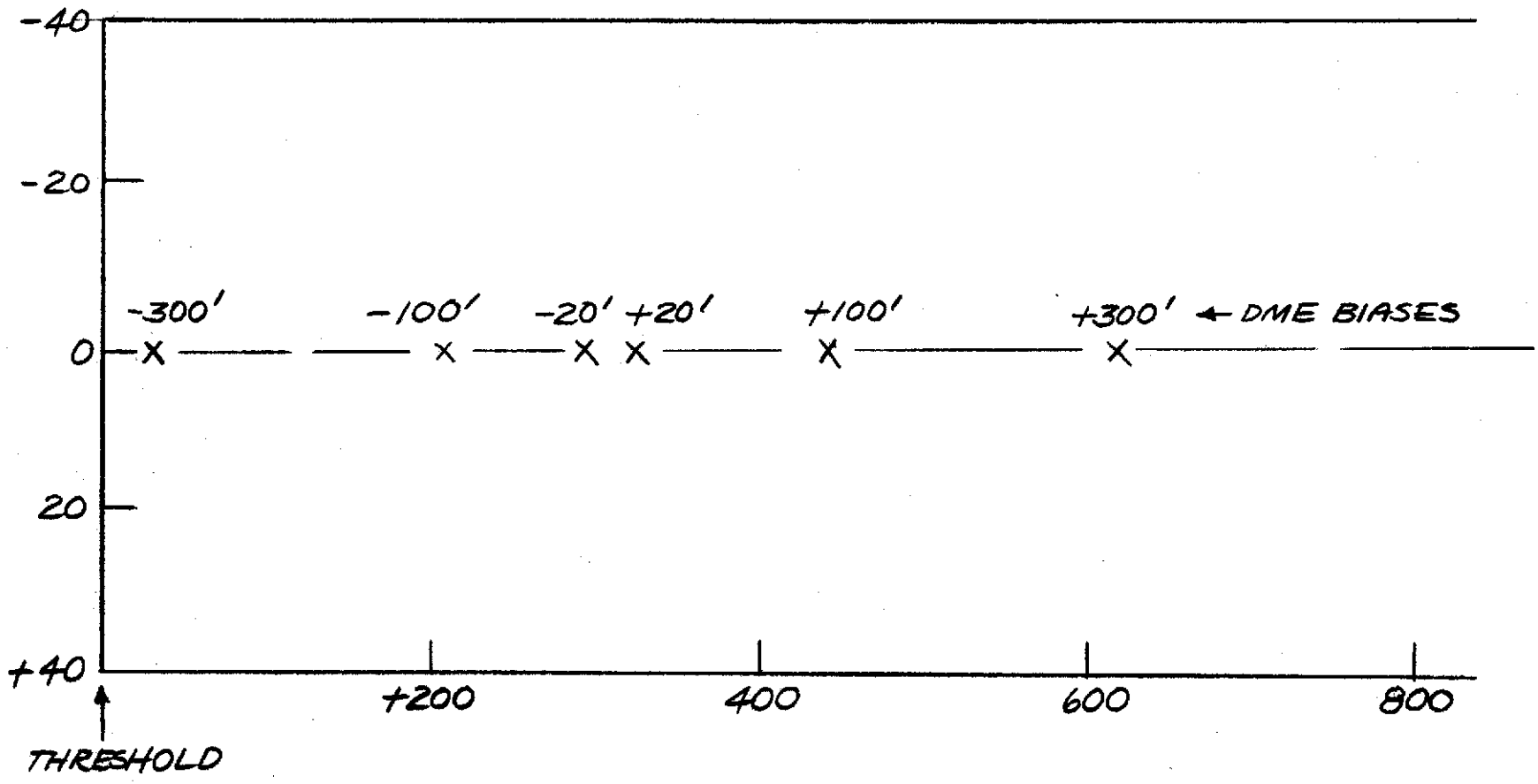

FIG. 45 - EFFECT OF DME BIAS ON LONGITUDINAL TOUCHDOWN DISPERSION

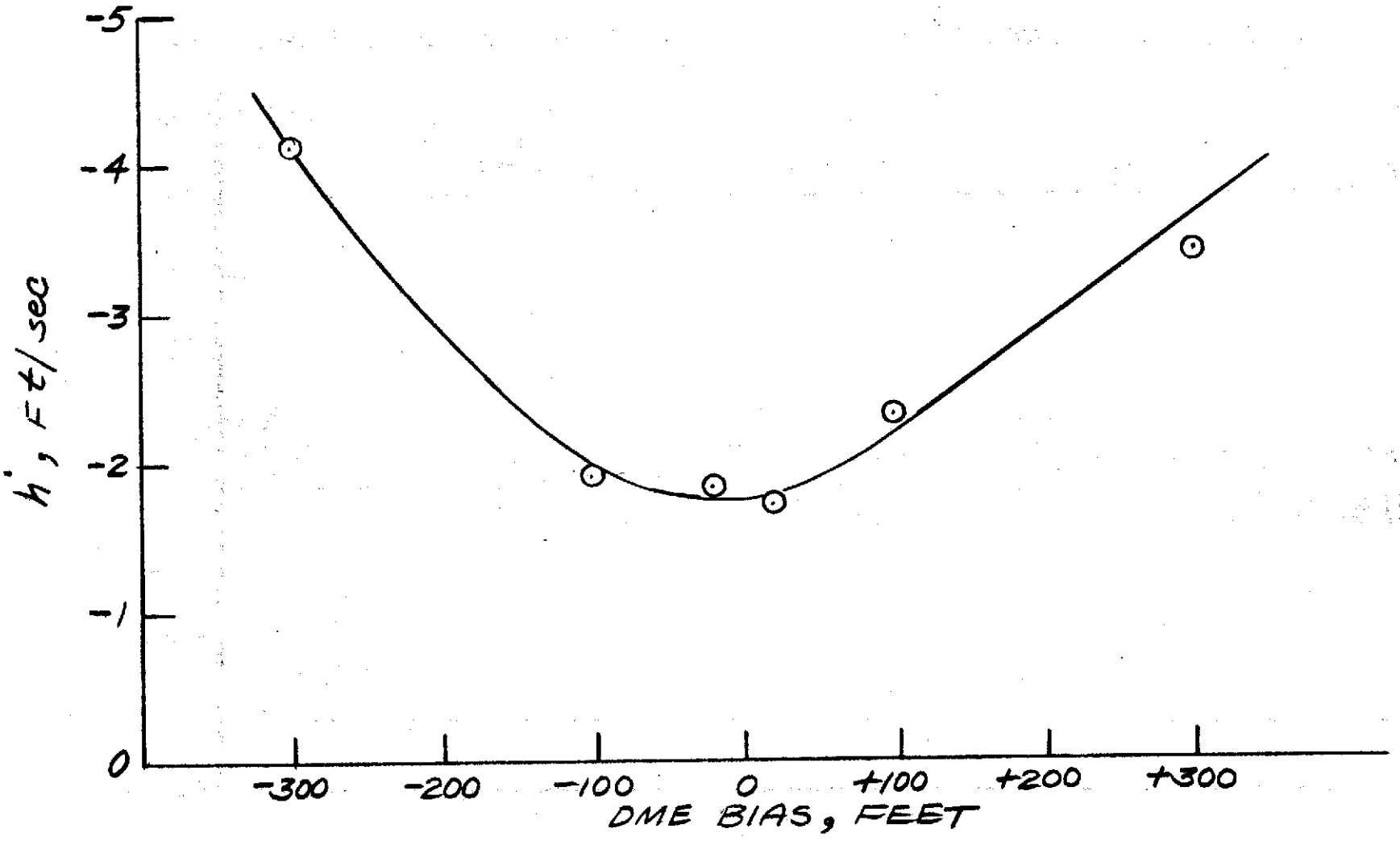

FIG. 46 - EFFECT OF DME BIAS ON SINK RATE AT TOUCHDOWN

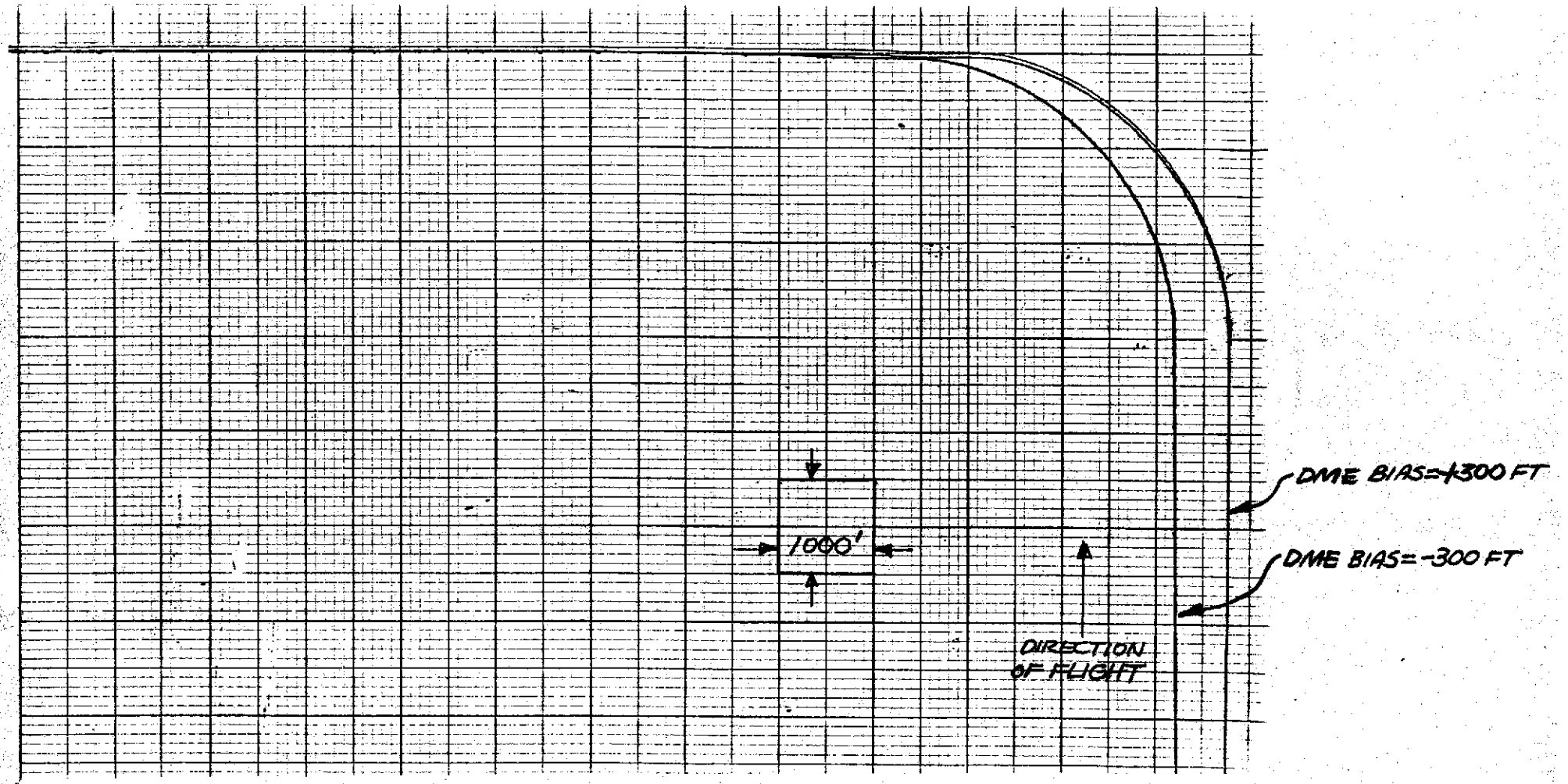

FIG. 47 X-Y PLOT OF FLIGHT PATH #1
WITH ± 300 FT. DME BIASES

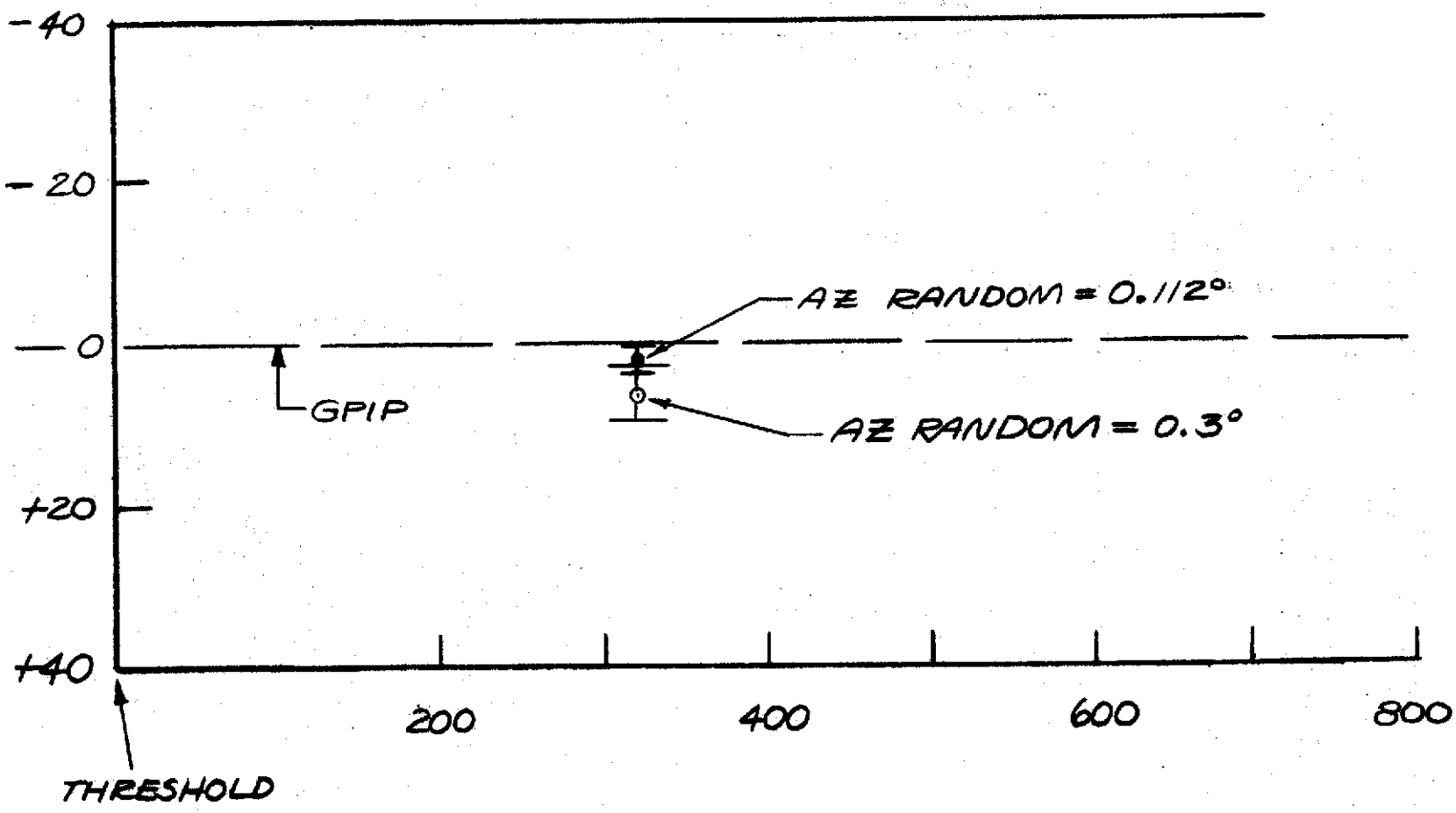

FIG. 48 EFFECT OF AZIMUTH RANDOM NOISE ON LATERAL TOUCHDOWN DISPERSION

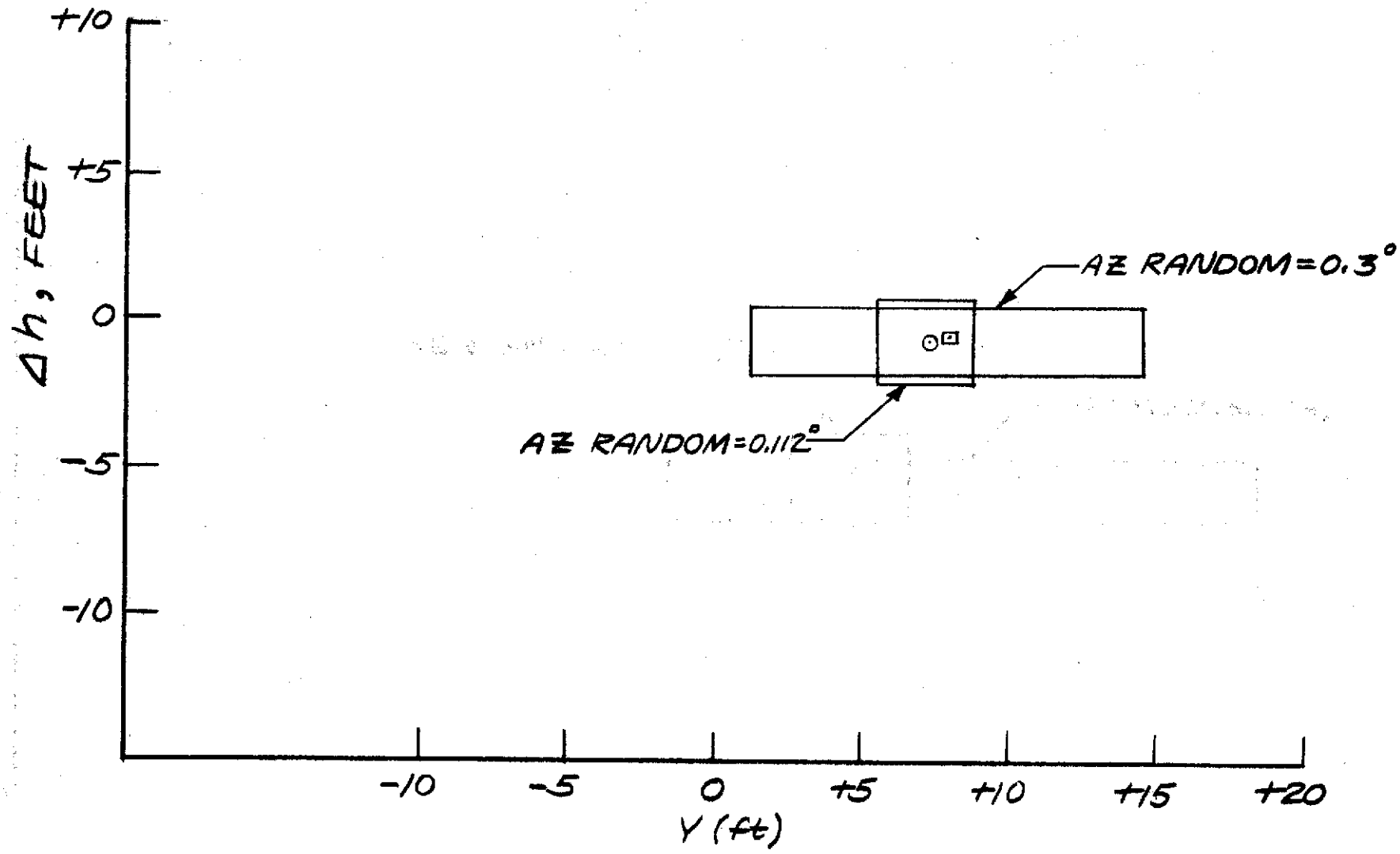

FIG. 19 - EFFECT OF AZIMUTH RANDOM NOISE AT 100 FT ALTITUDE

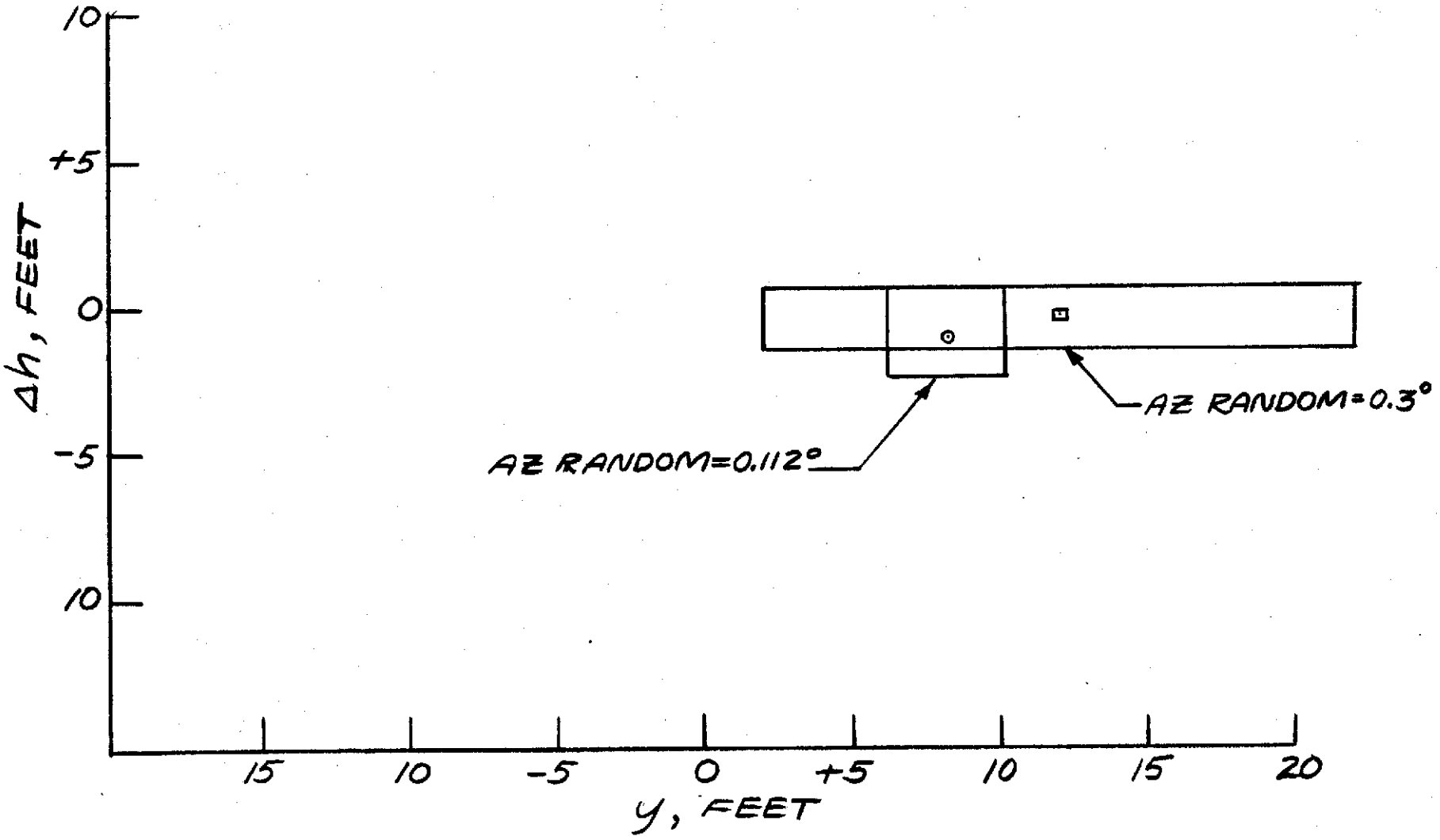

FIG.50 - EFFECT OF AZIMUTH RANDOM NOISE AT 200 FT ALTITUDE

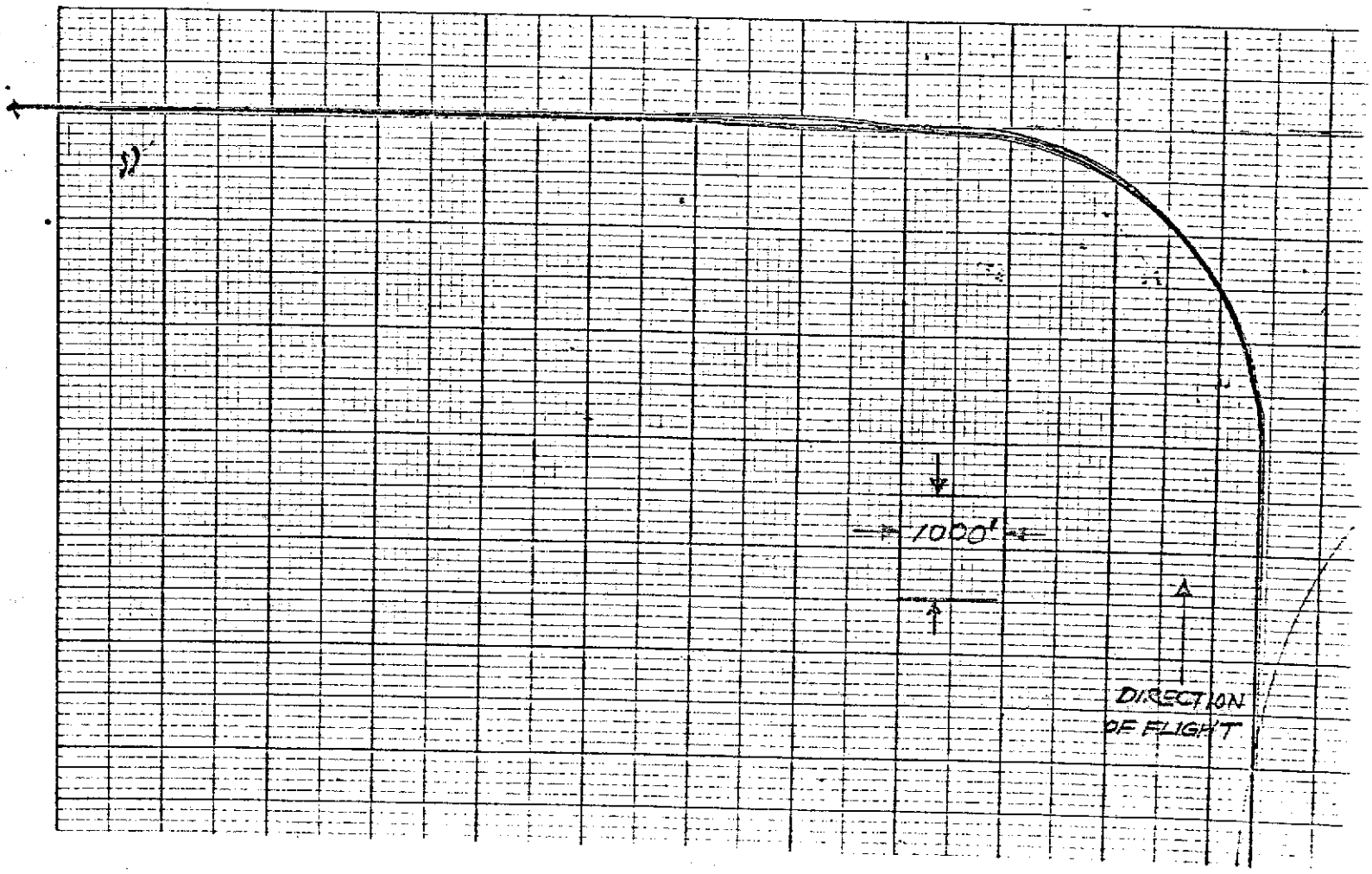

FIG. 51 X-Y PLOT OF FLIGHT PATH #1 WITH 0.3 AZIMUTH RANDOM NOISE (8 RUNS)

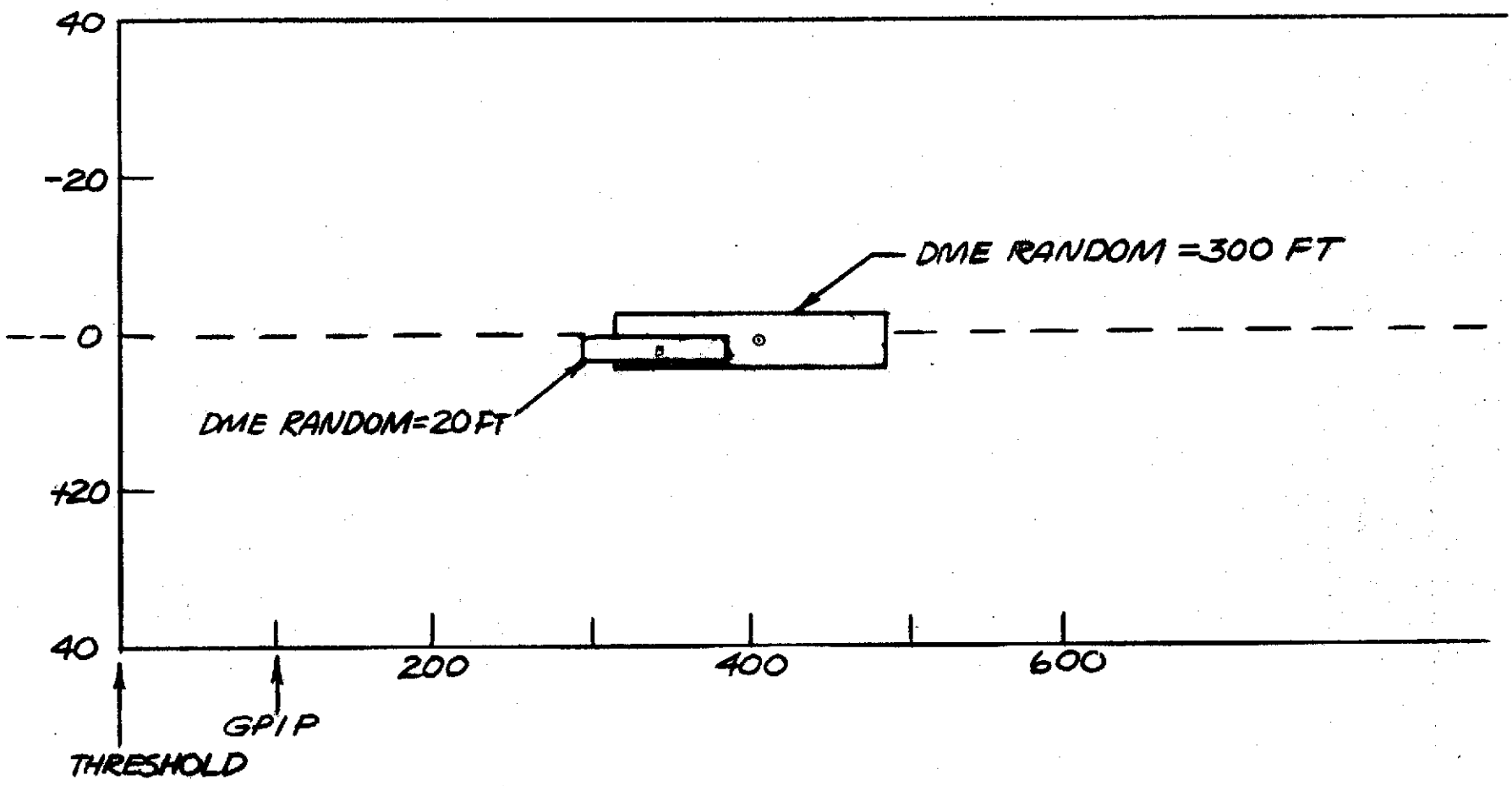

FIG. 52- EFFECT OF DME RANDOM NOISE ON TOUCHDOWN DISPERSION

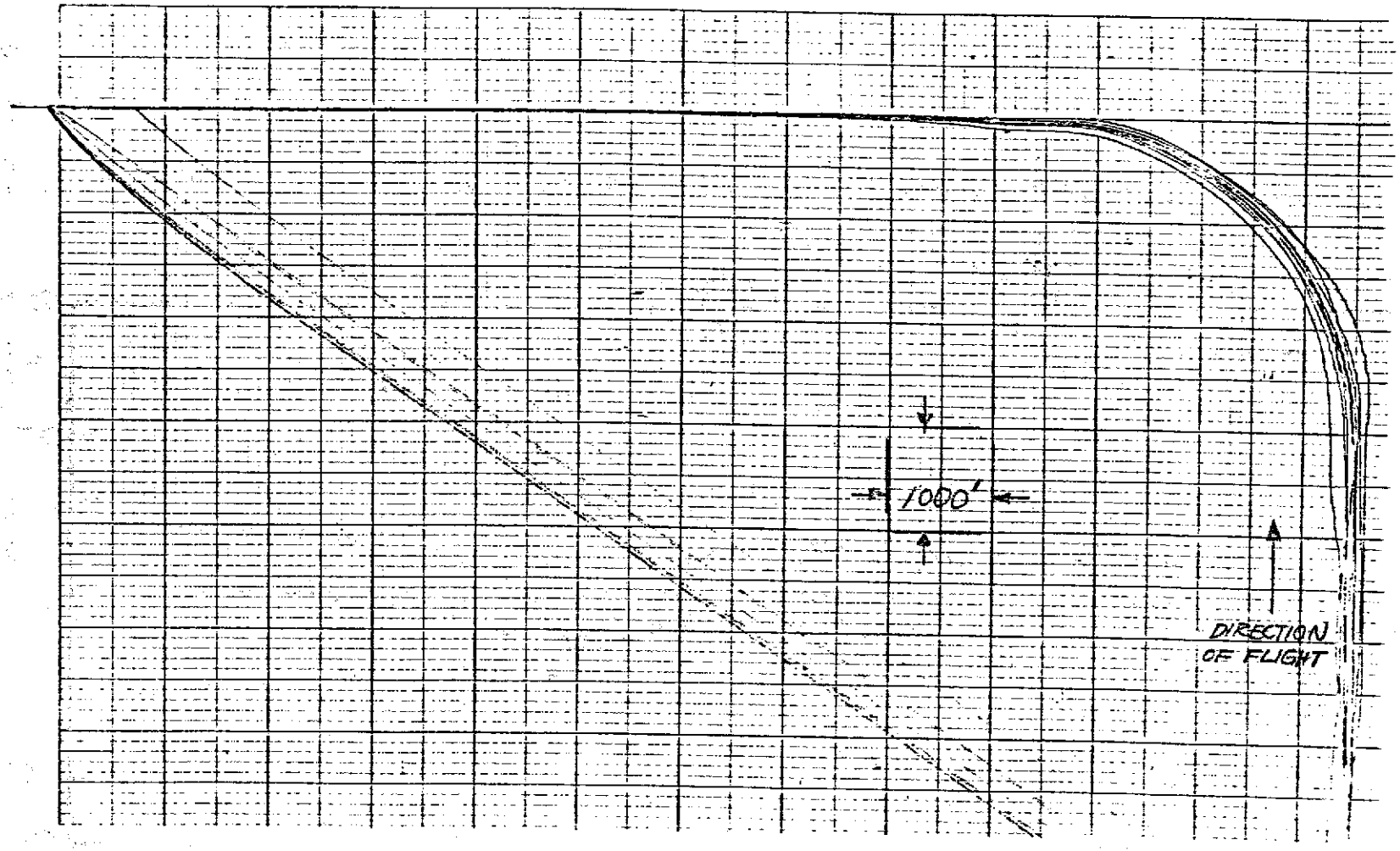

FIG. 53 X-Y PLOT OF FLIGHT PATH #1 WITH 300 FT. RANDOM DME NOISE (9 RUNS)

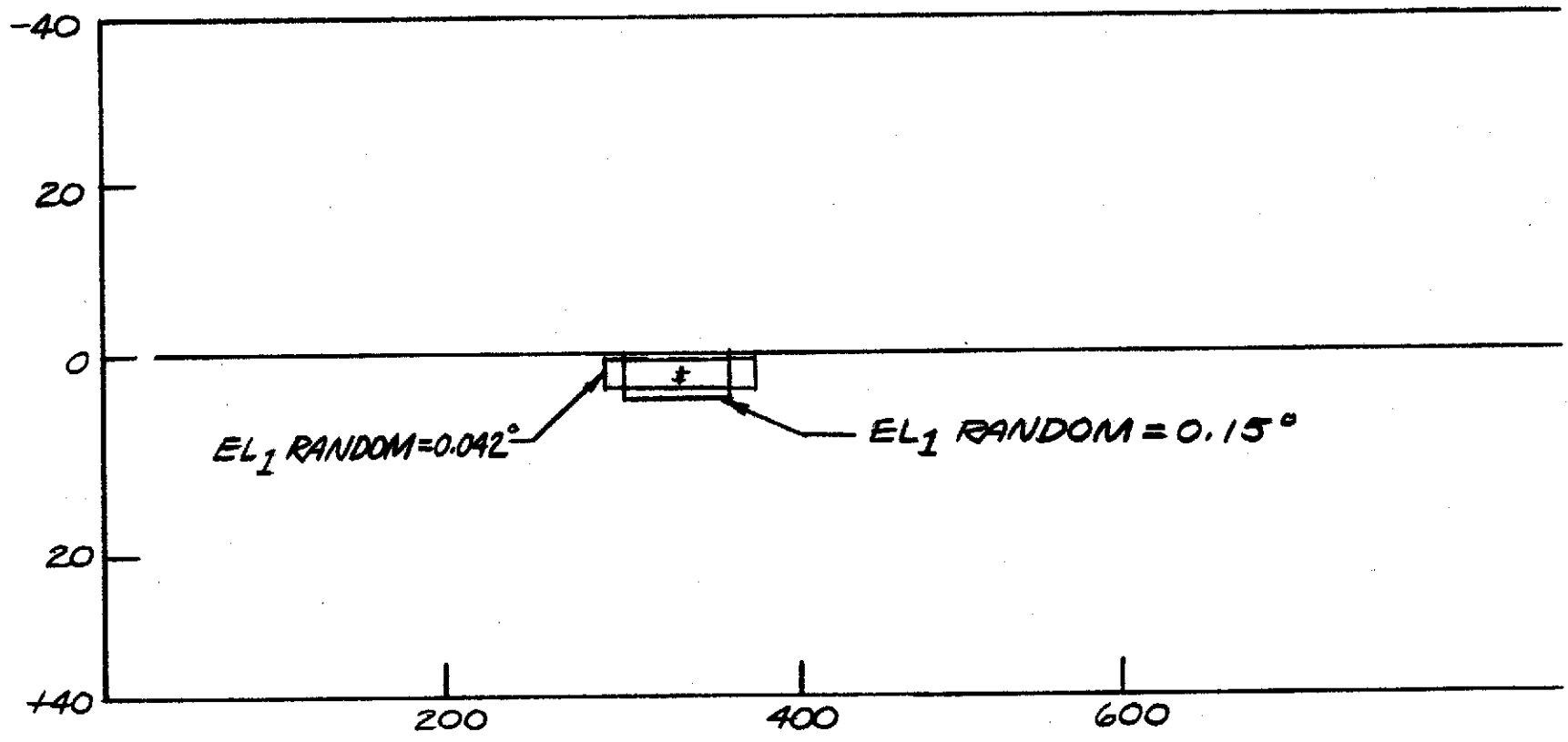

FIG.54- EFFECT OF EL_1 RANDOM NOISE ON TOUCHDOWN DISPERSION

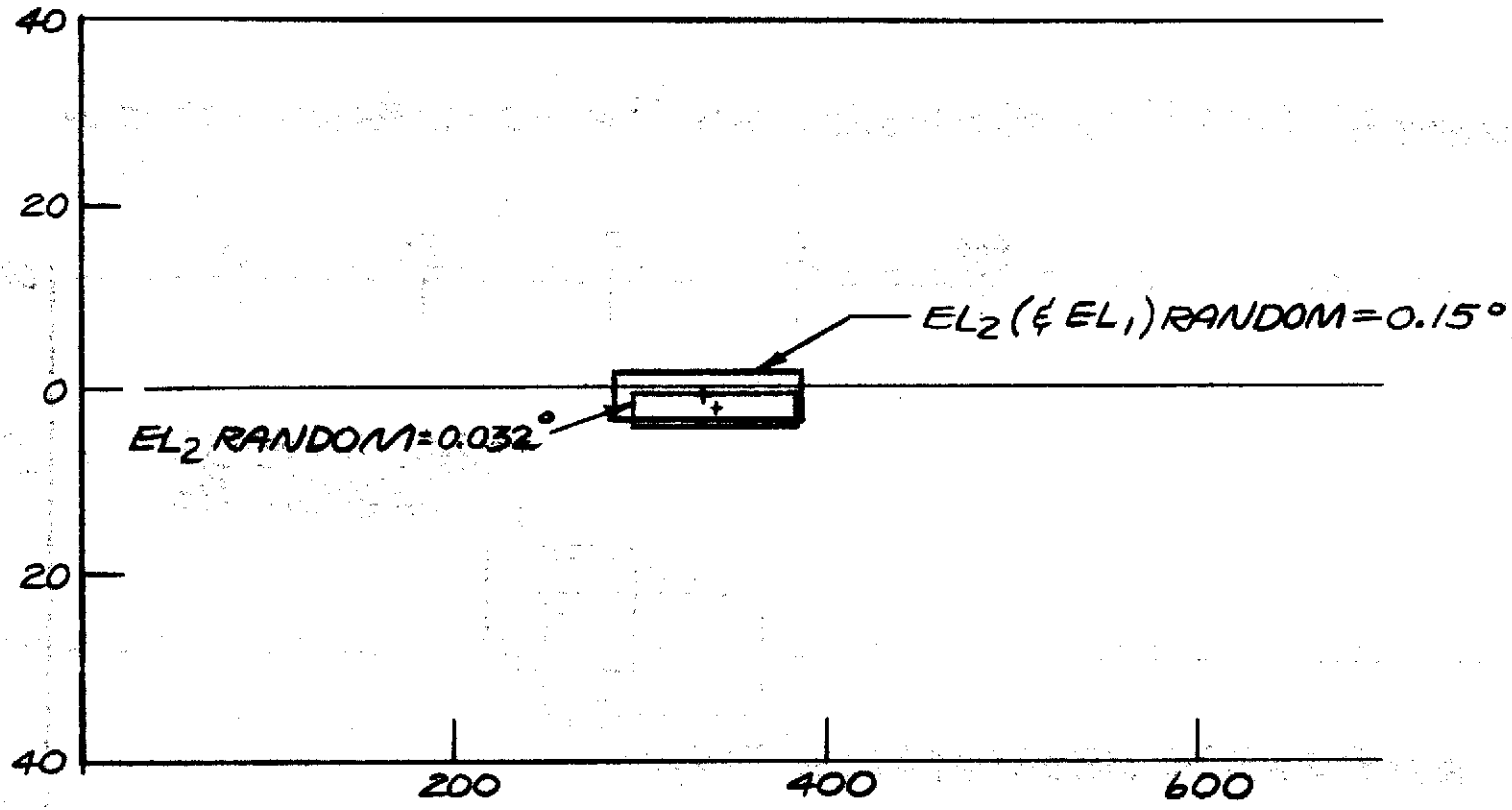

FIG. 55 - EFFECT OF EL_2 RANDOM NOISE ON TOUCHDOWN DISPERSION

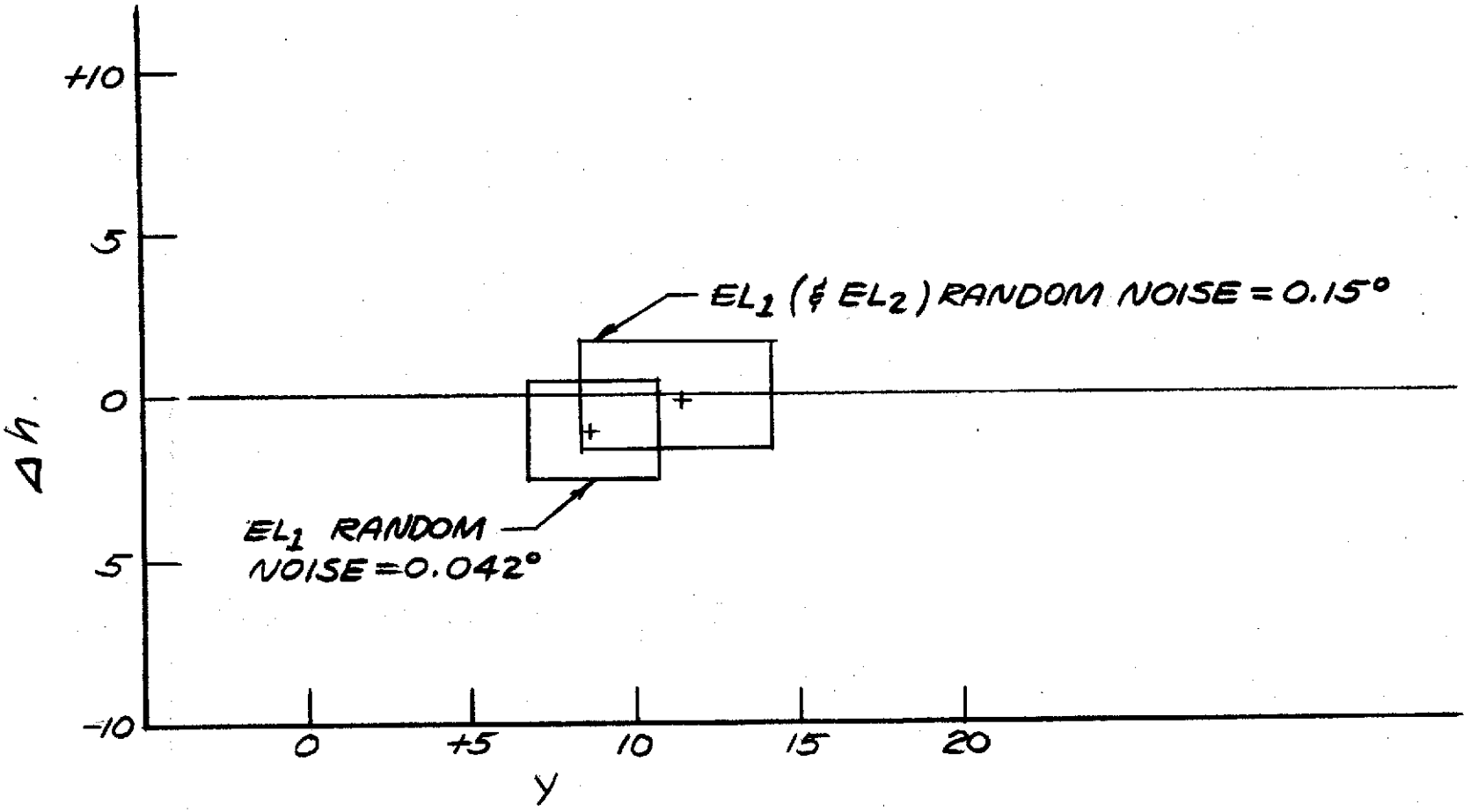

FIG. 56 - EFFECT OF EL_1 RANDOM NOISE AT 200 FT. ELEVATION

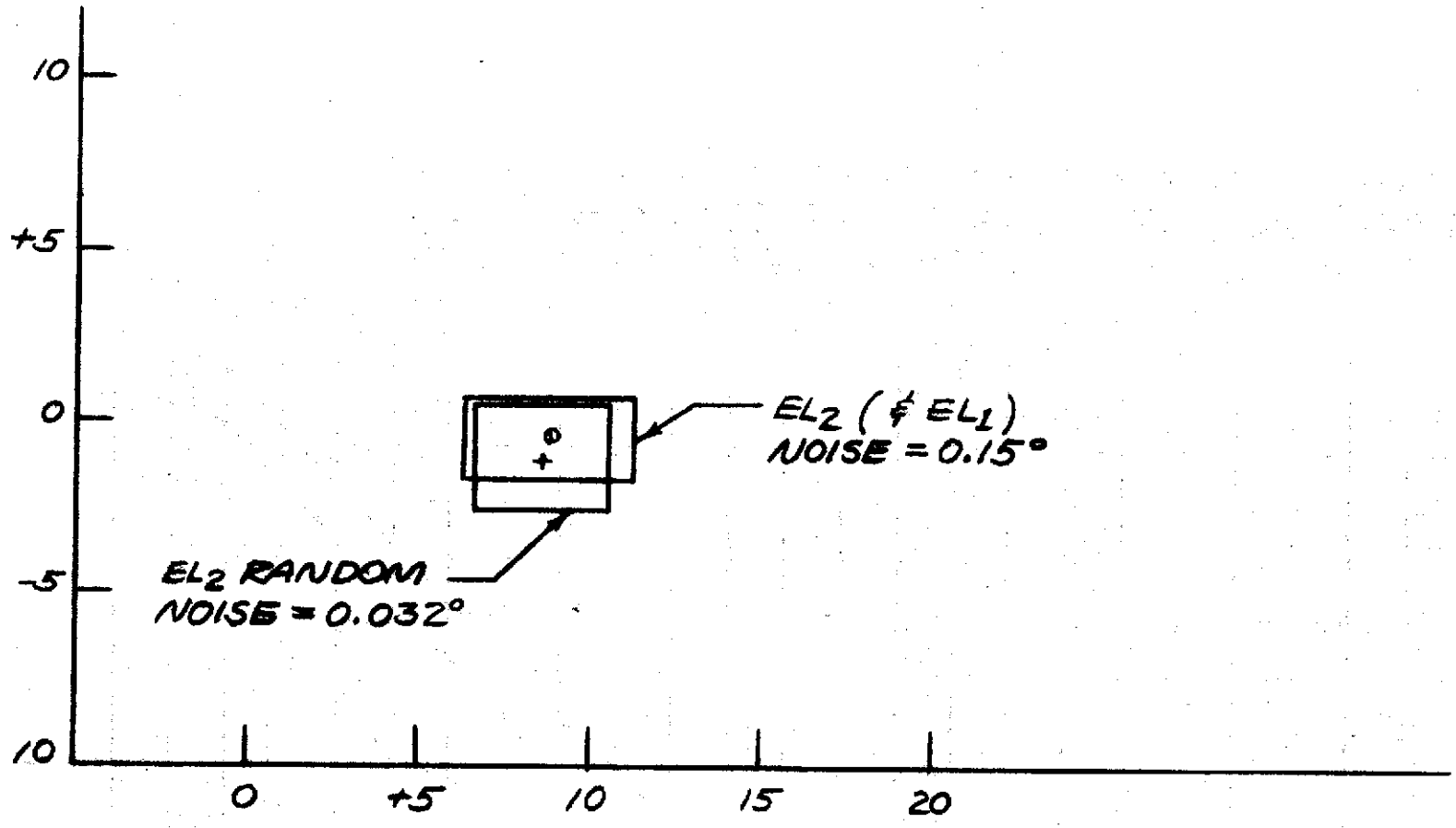

FIG. 57 - EFFECT OF EL_2 RANDOM NOISE AT 200 FT ELEVATION

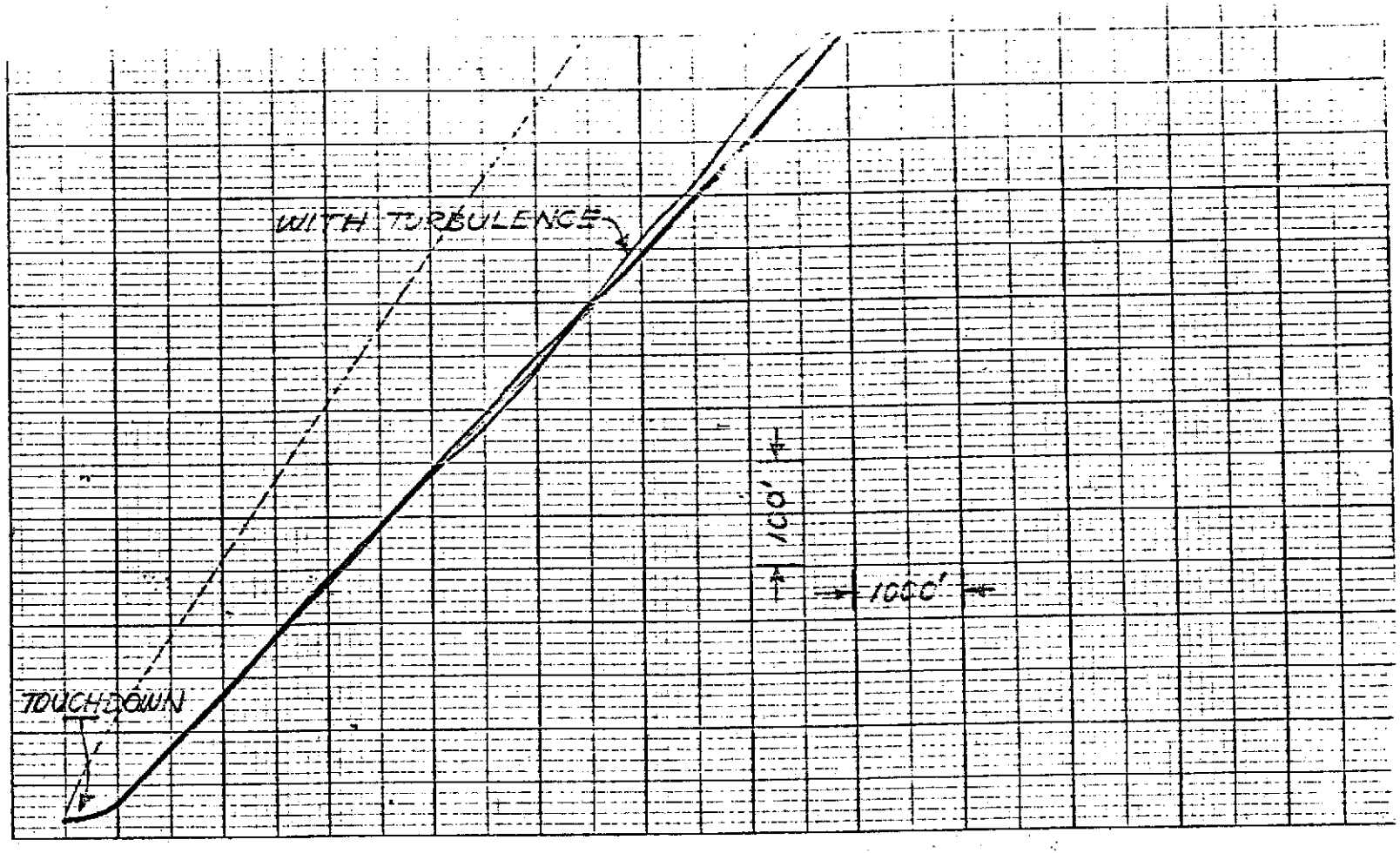

FIG. 58 GLIDESLOPE (X-Z) PLOT FROM 500 FT. ELEVATION WITH 0.15 EL_1 RANDOM NOISE & 0.032° EL_2 RANDOM (3 RUNS W/O TURBULENCE & 1 RUN WITH TURBULENCE)

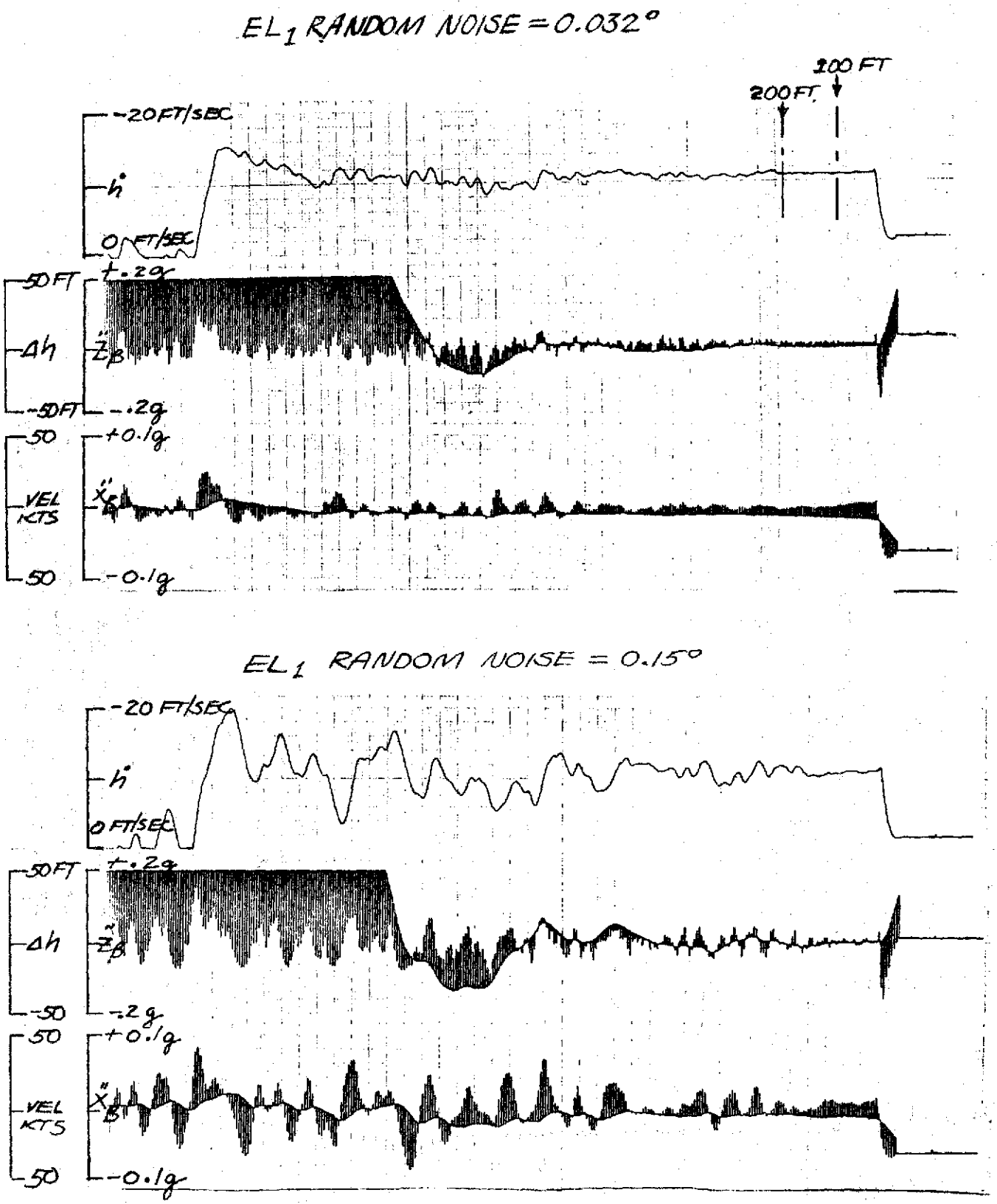

FIG. 58A EFFECT OF EL_1 RANDOM NOISE ON $\dot{h}$, Δh AND FORWARD VELOCITY (OTHERWISE CAT III ERRORS)

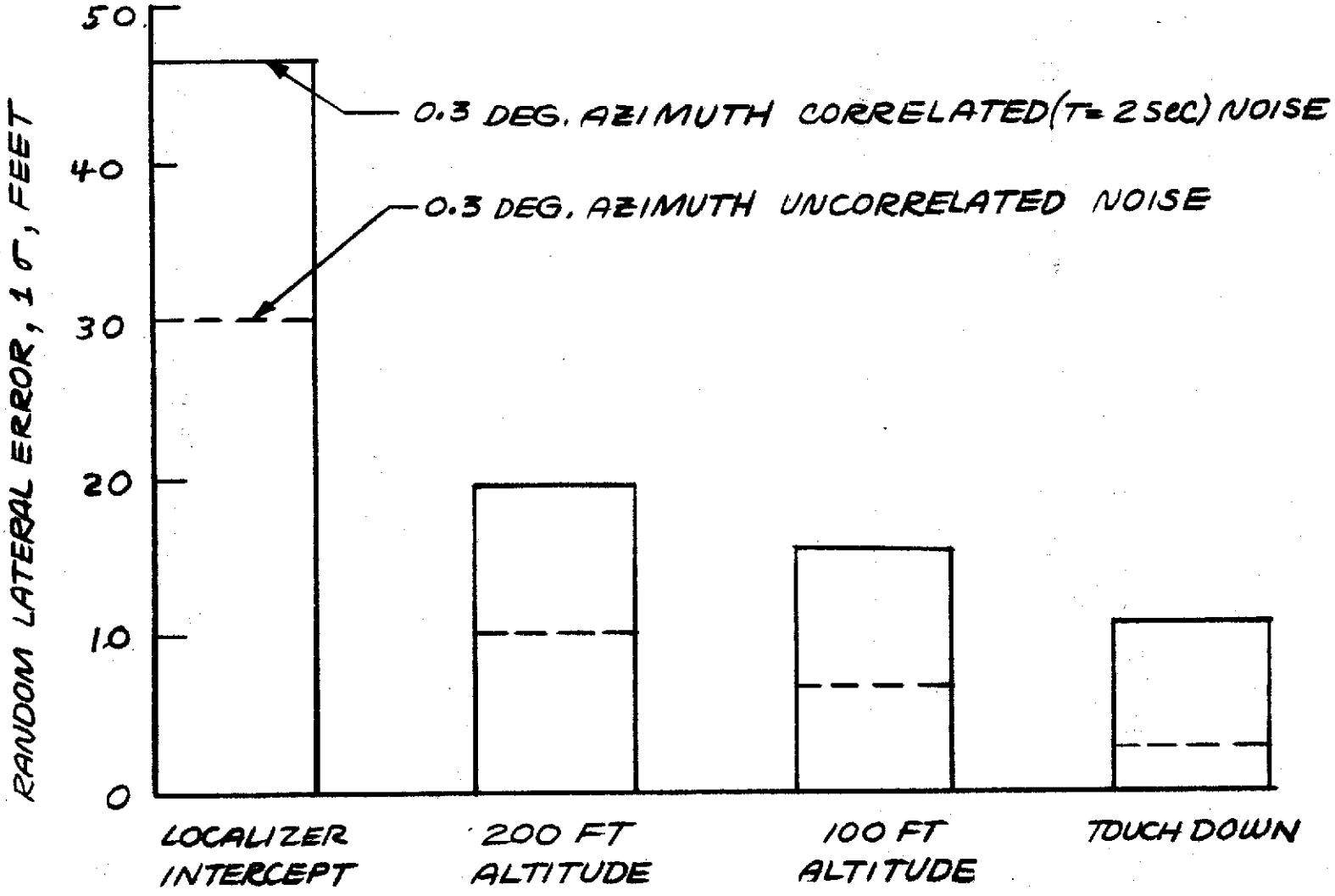

FIGURE 59. COMPARISON OF EFFECTS OF CORRELATED AND UNCORRELATED AZIMUTH NOISE ON LATERAL DISPERSION (OTHERWISE CAT III RANDOM AND BIAS CONDITIONS)

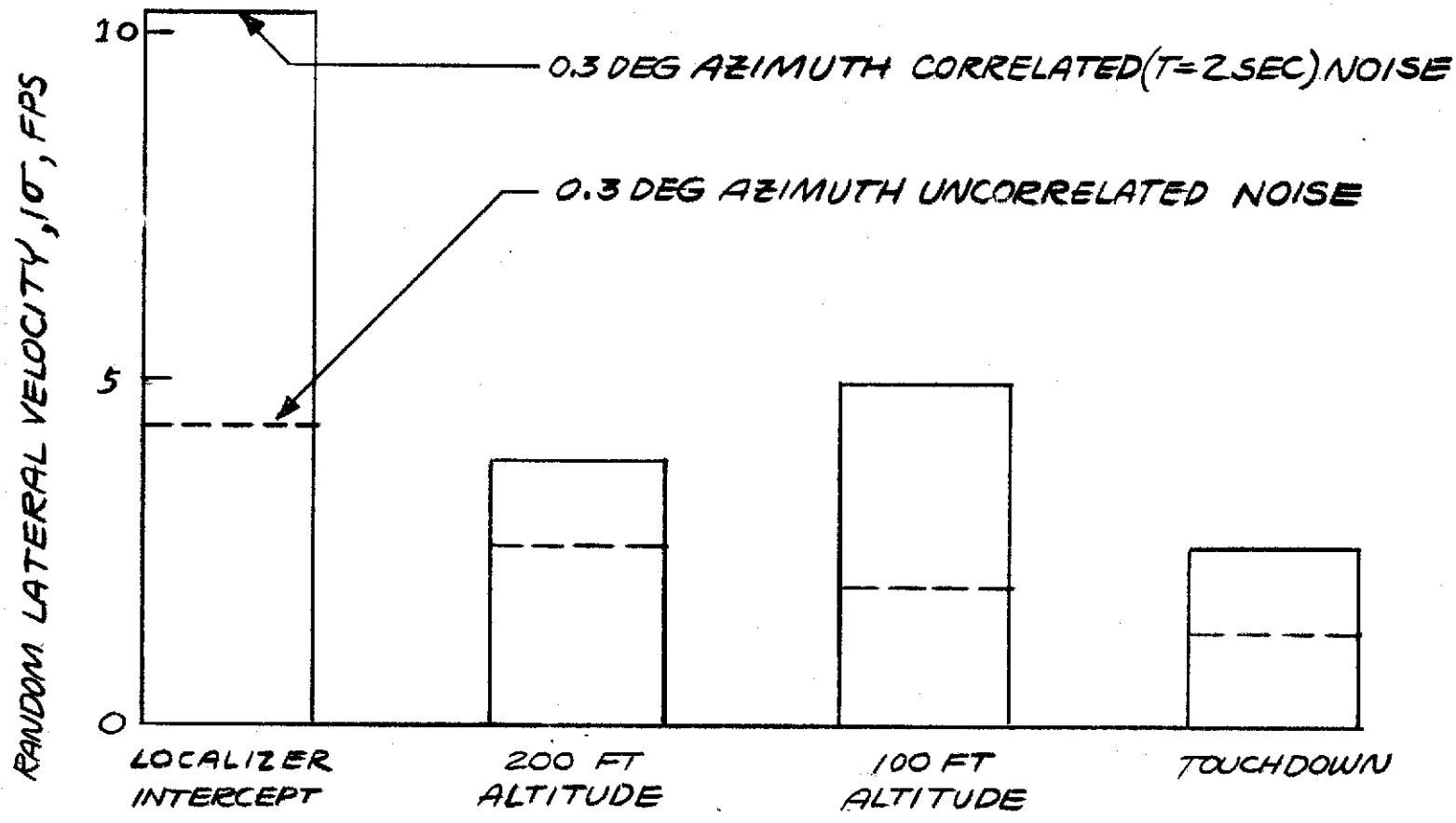

FIGURE 60 COMPARISON OF EFFECTS OF CORRELATED AND UNCORRELATED AZIMUTH NOISE ON LATERAL VELOCITY DISPERSION (OTHERWISE CAT III RANDOM AND BIAS CONDITIONS)

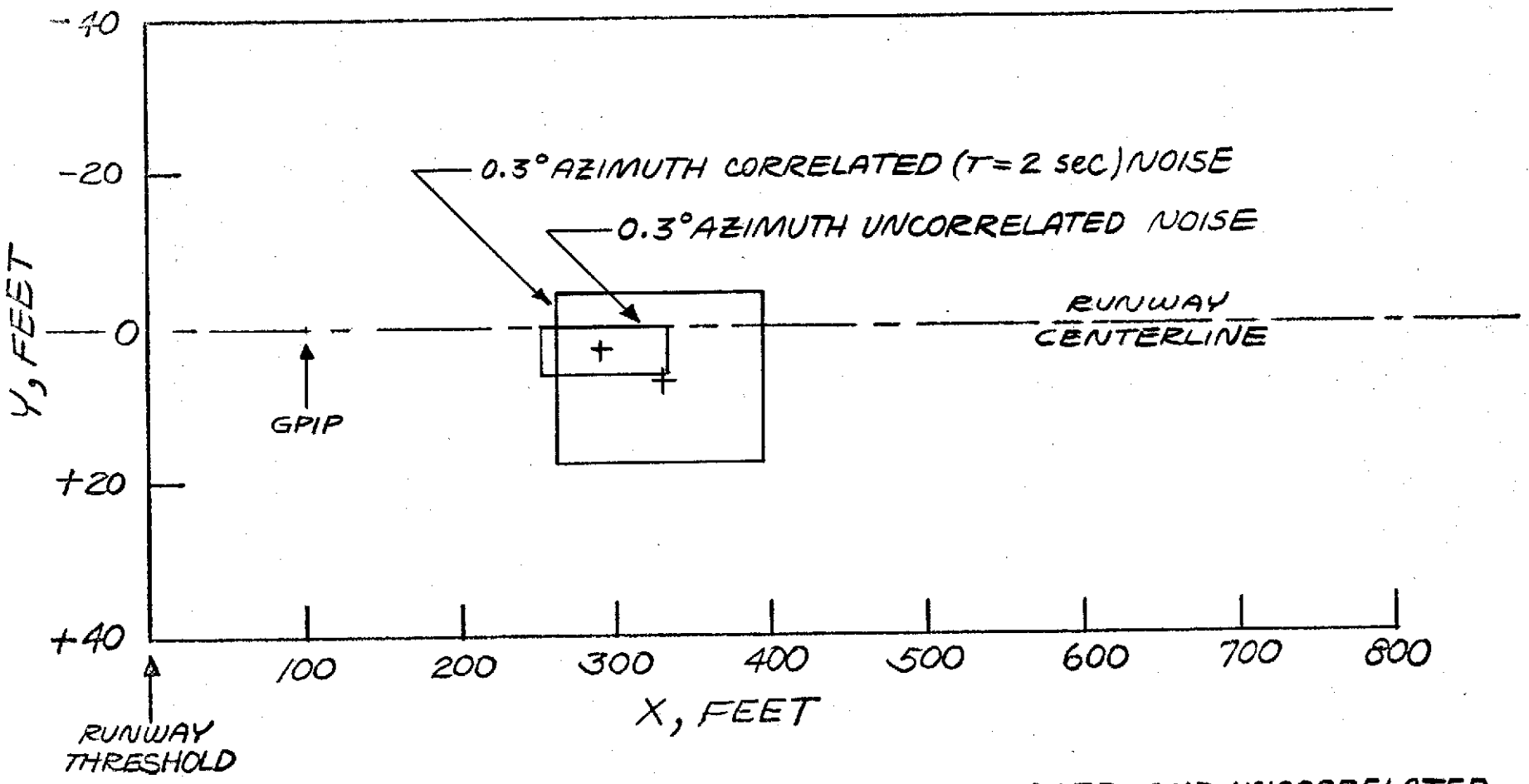

FIG. 61 COMPARISON OF EFFECTS OF CORRELATED AND UNCORRELATED AZIMUTH NOISE ON TOUCHDOWN DISPERSION (OTHERWISE CAT III RANDOM AND BIAS CONDITIONS)

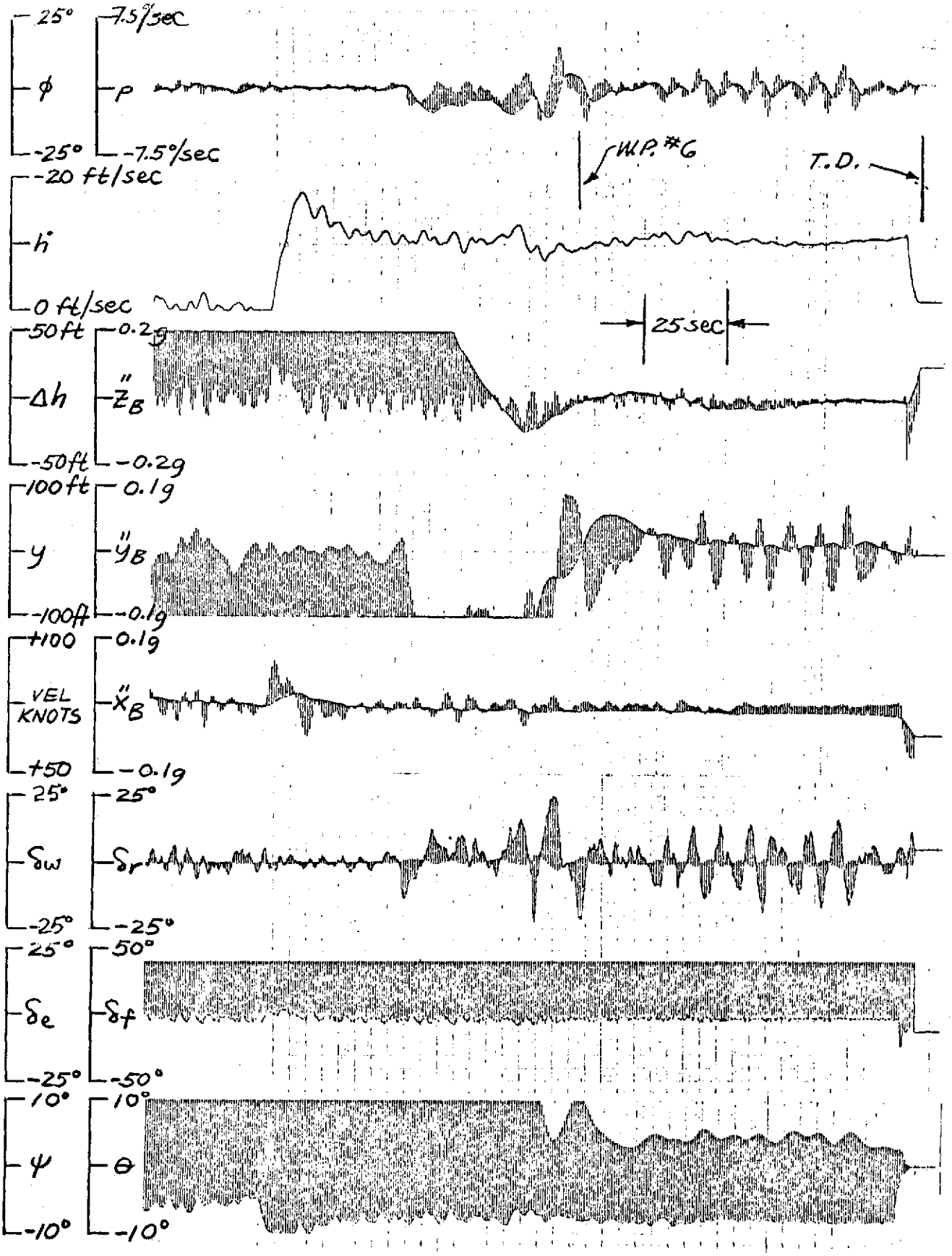

FIG. 62 SAMPLE TIME HISTORY OF EFFECT OF 0.3 DEG RANDOM AZIMUTH ERRORS — OTHERWISE CAT III RANDOM AND BIAS

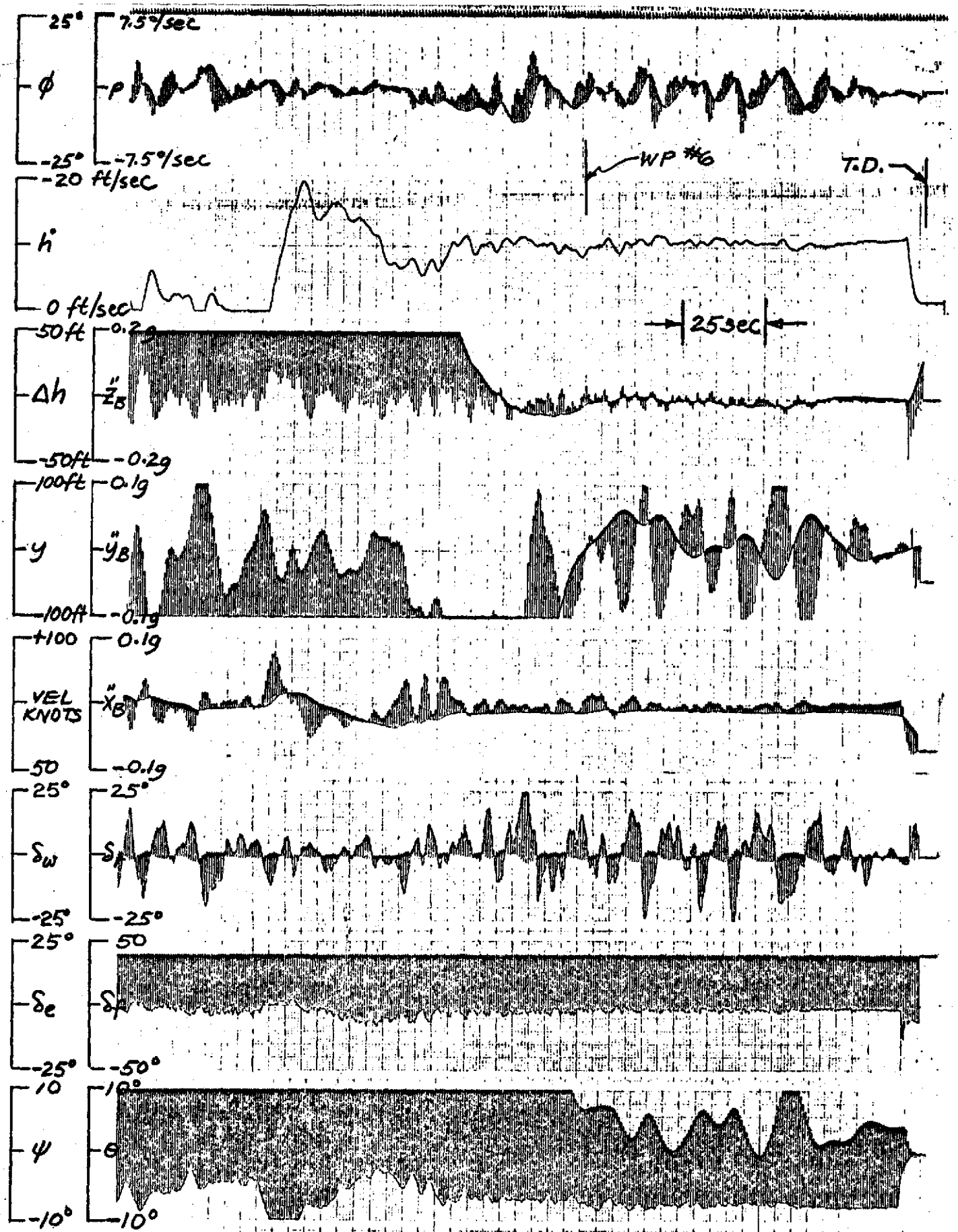

FIG. 63 SAMPLE TIME HISTORY OF EFFECT OF 0.3 DEG CORRELATED (τ = 2 sec) AZIMUTH NOISE - OTHERWISE CAT III RANDOM AND BIAS

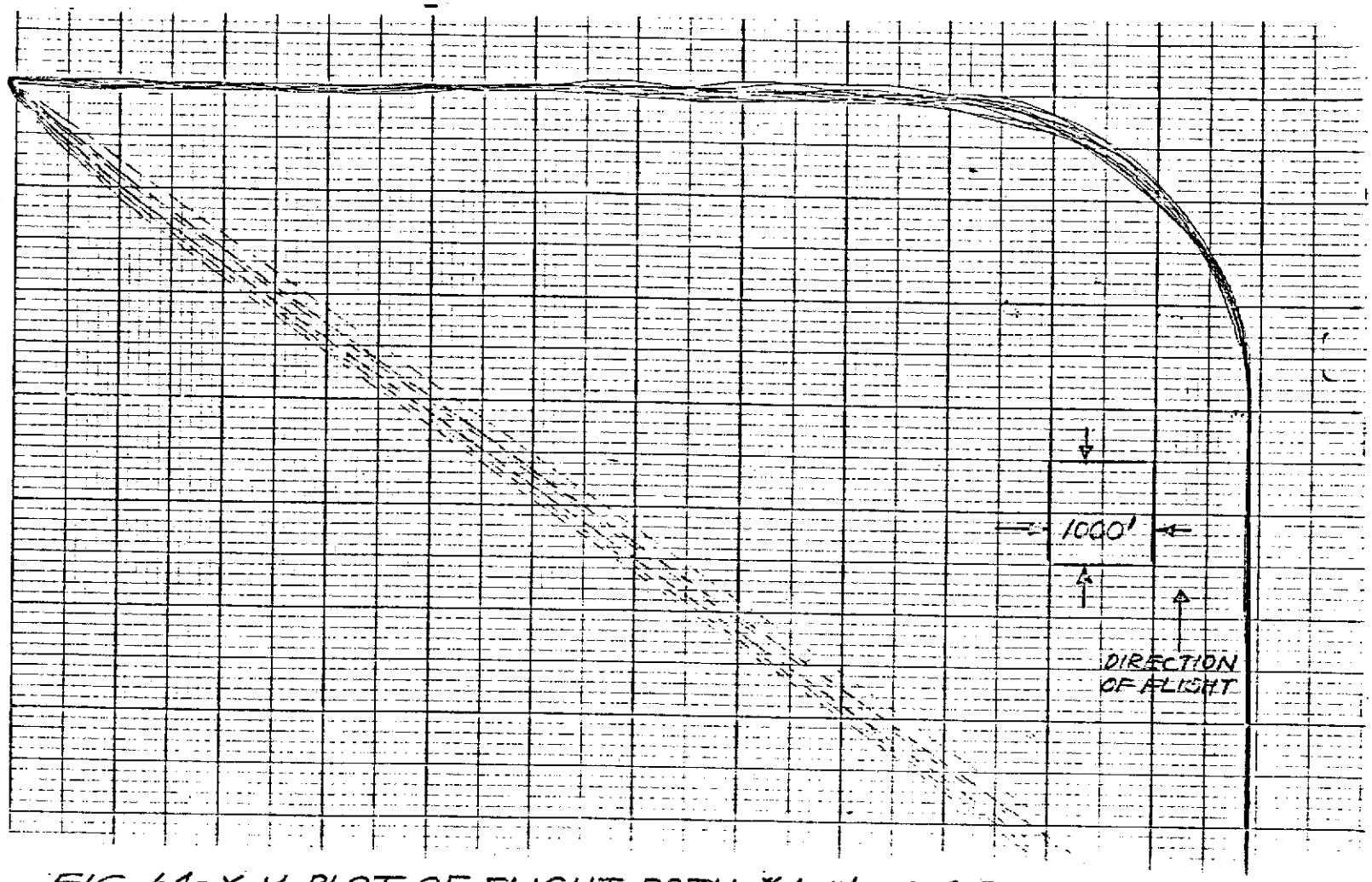

FIG. 64-X-Y PLOT OF FLIGHT PATH #1 WITH 0.3 DEG. AZIMUTH CORRELATED (T=2 SEC) NOISE [OTHERWISE CAT II RANDOM AND BIAS (10 RUNS)]

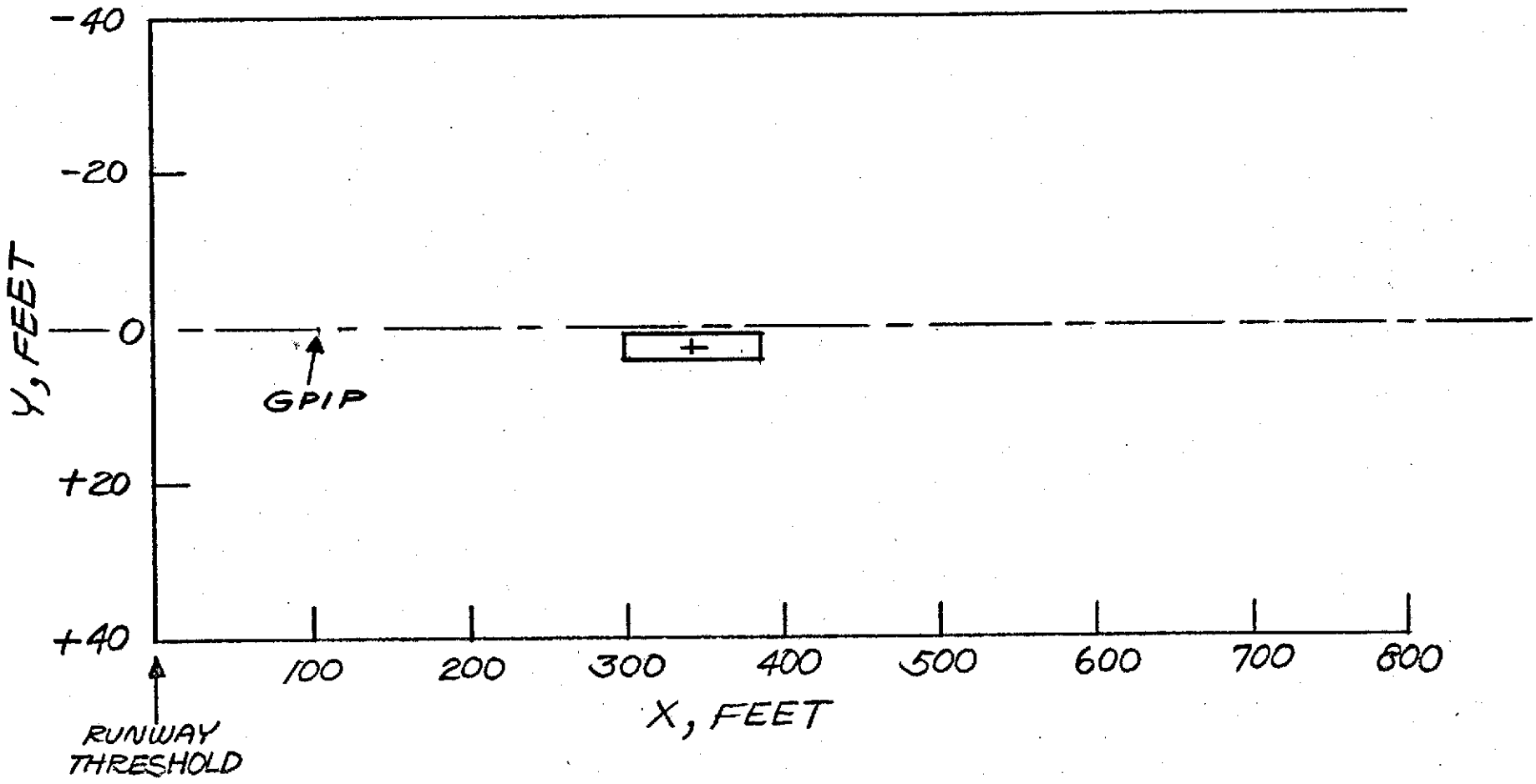

FIG. 65- EFFECT OF CAT III RANDOM and BIAS ERRORS ON TOUCHDOWN DISPERSION - NO TURBULENCE

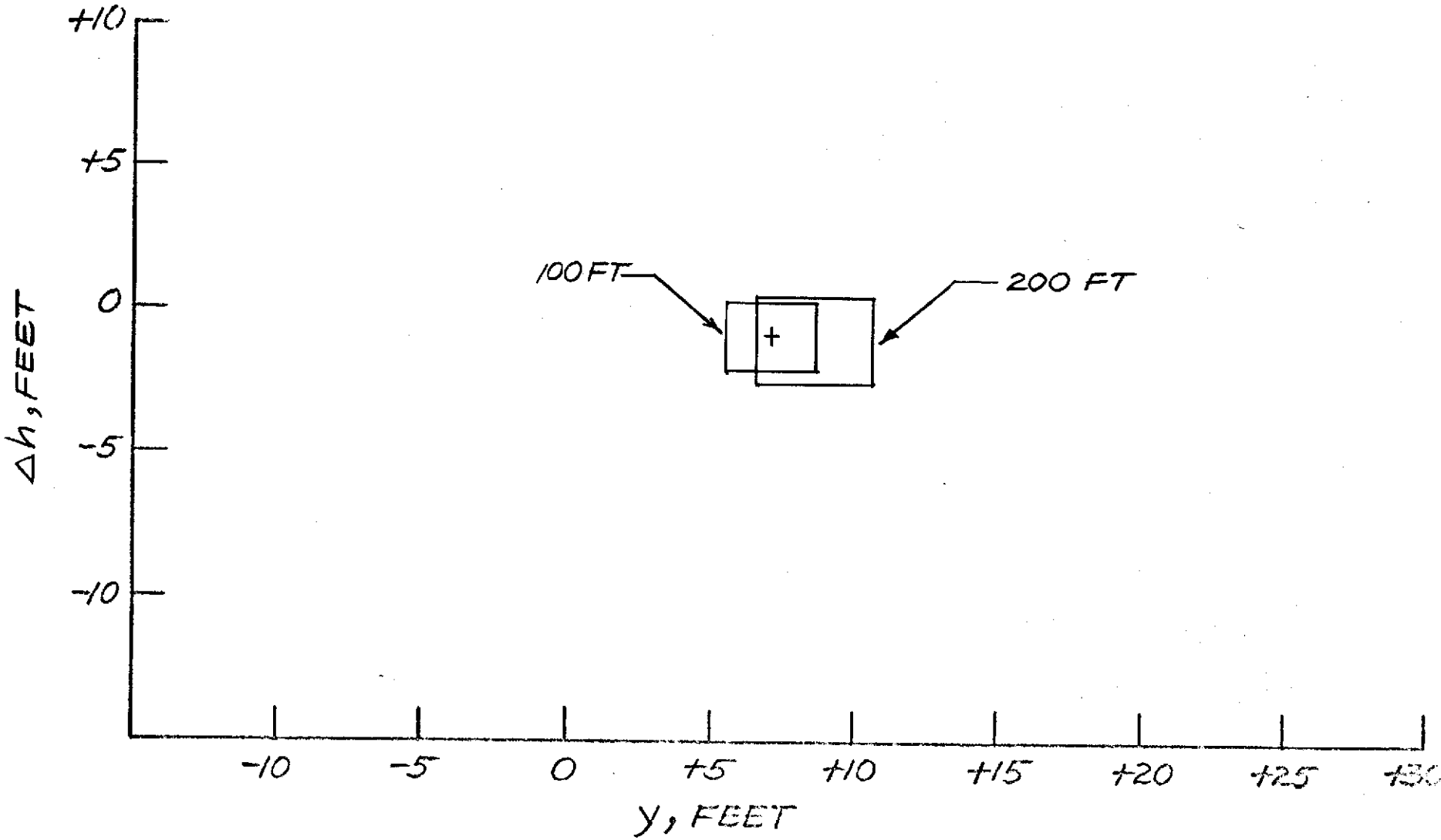

FIG. 66 – EFFECT OF CAT III RANDOM and BIAS ERRORS ON DISPERSION AT 100 FT and 200 FT ALTITUDES – NO TURBULENCE

FIG. 67 SAMPLE TIME HISTORY OF CAT III RANDOM and BIAS ERRORS – NO TURBULENCE

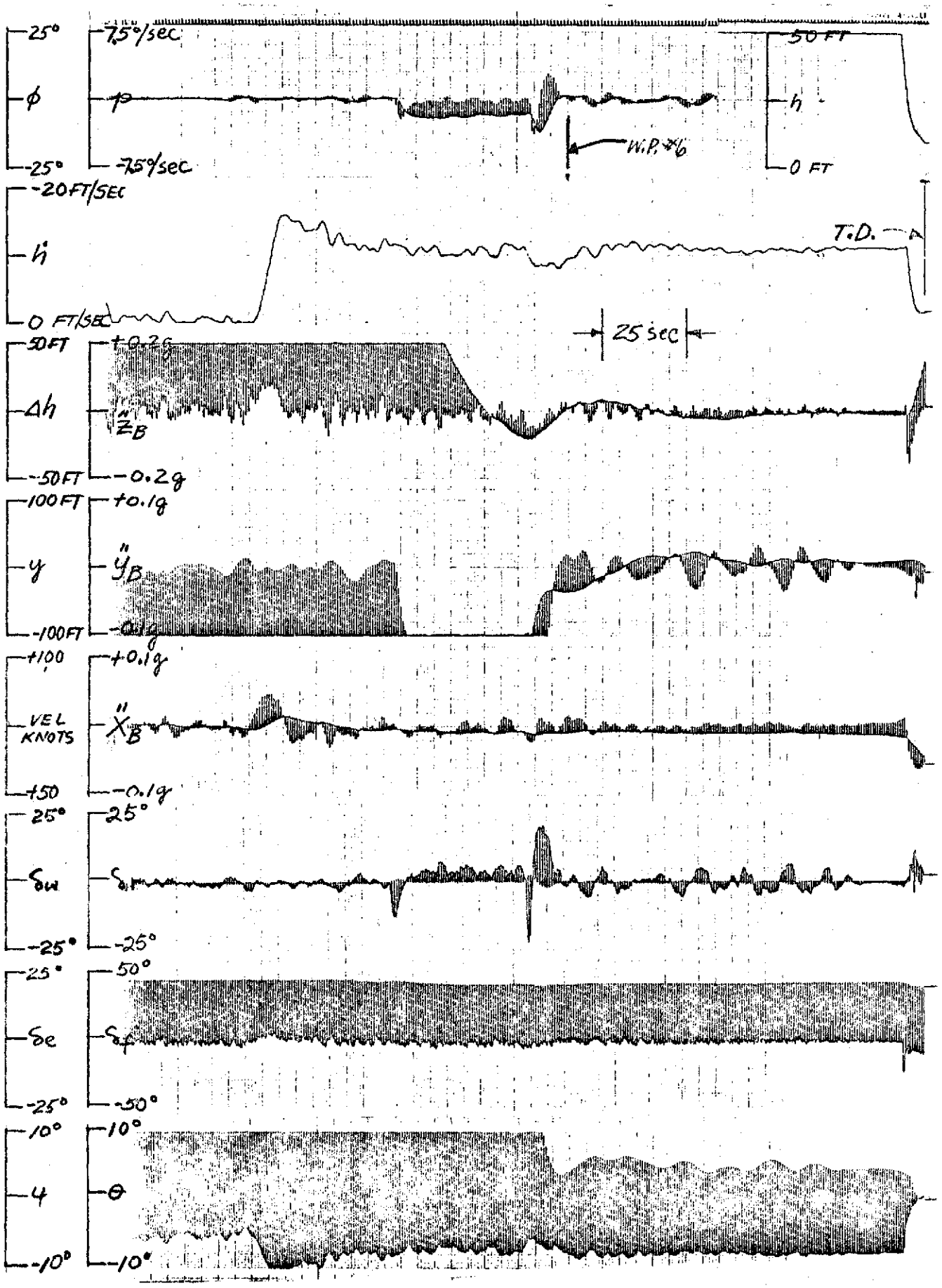

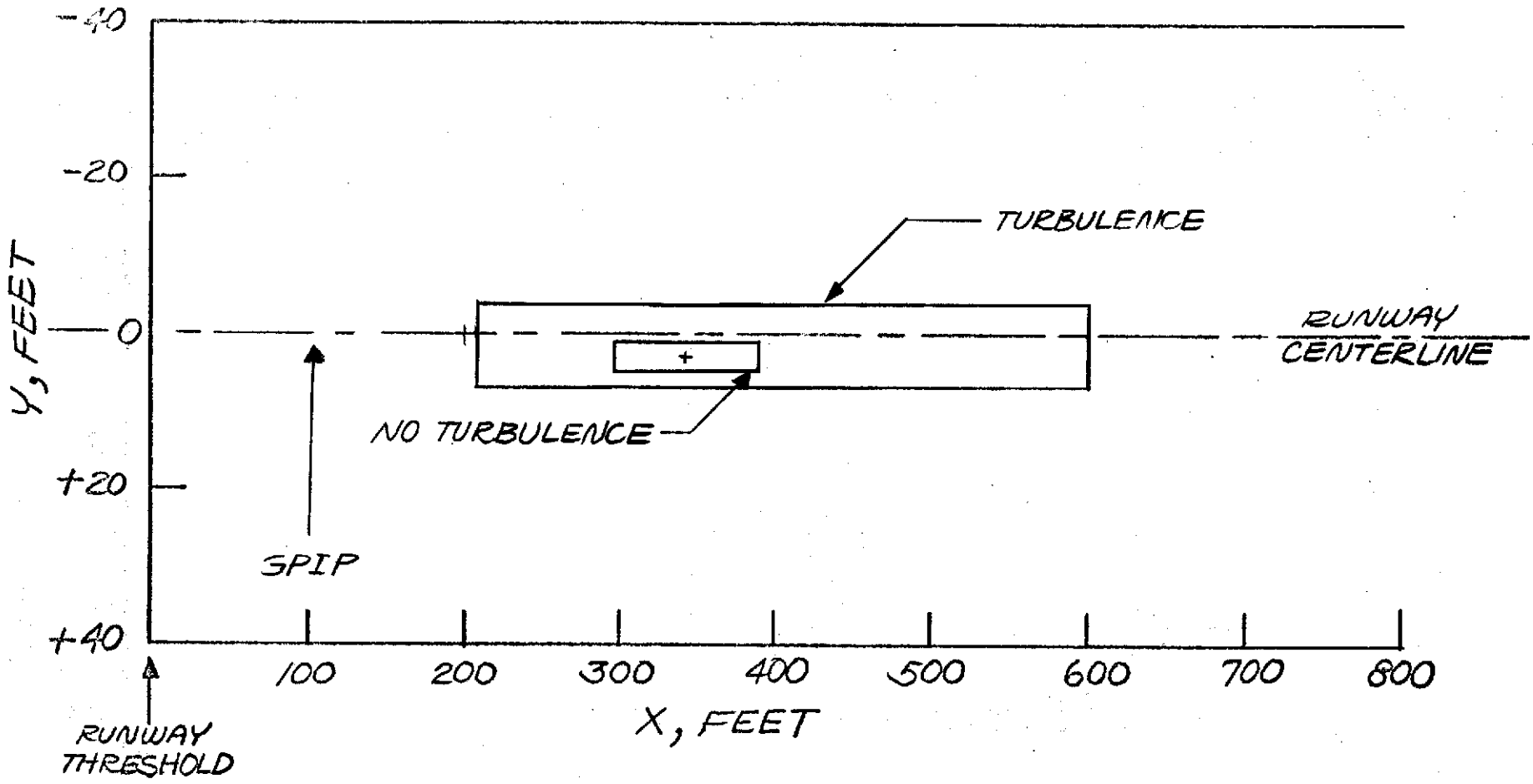

FIG. 68 – COMPARISON OF TOUCHDOWN DISPERSIONS WITH and WITHOUT TURBULENCE – CAT III RANDOM & BIAS ERRORS

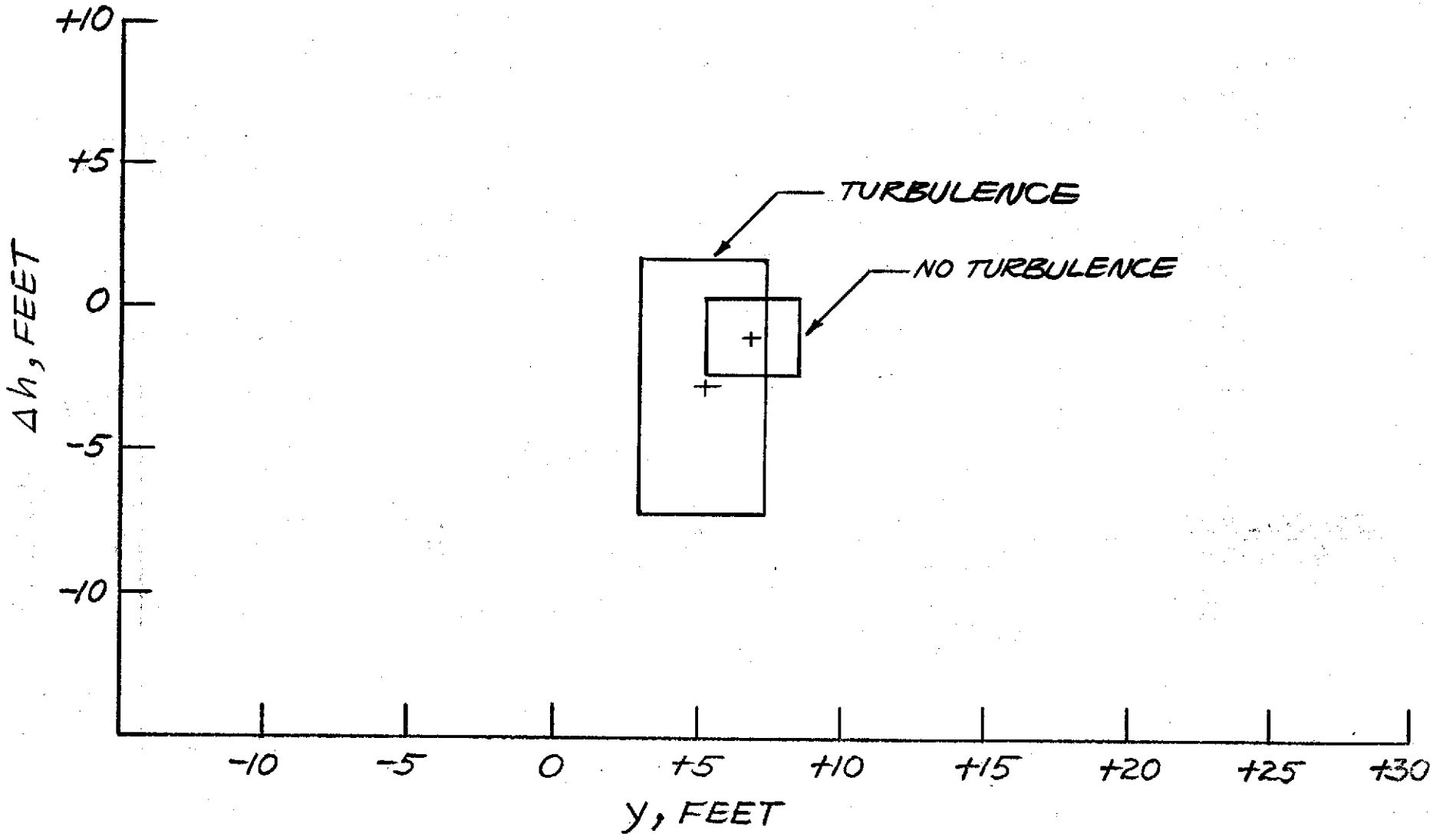

FIG.69 - COMPARISON OF DISPERSIONS AT 100 FT ALTITUDE WITH & WITHOUT TURBULENCE - CAT III RANDOM & BIAS ERRORS

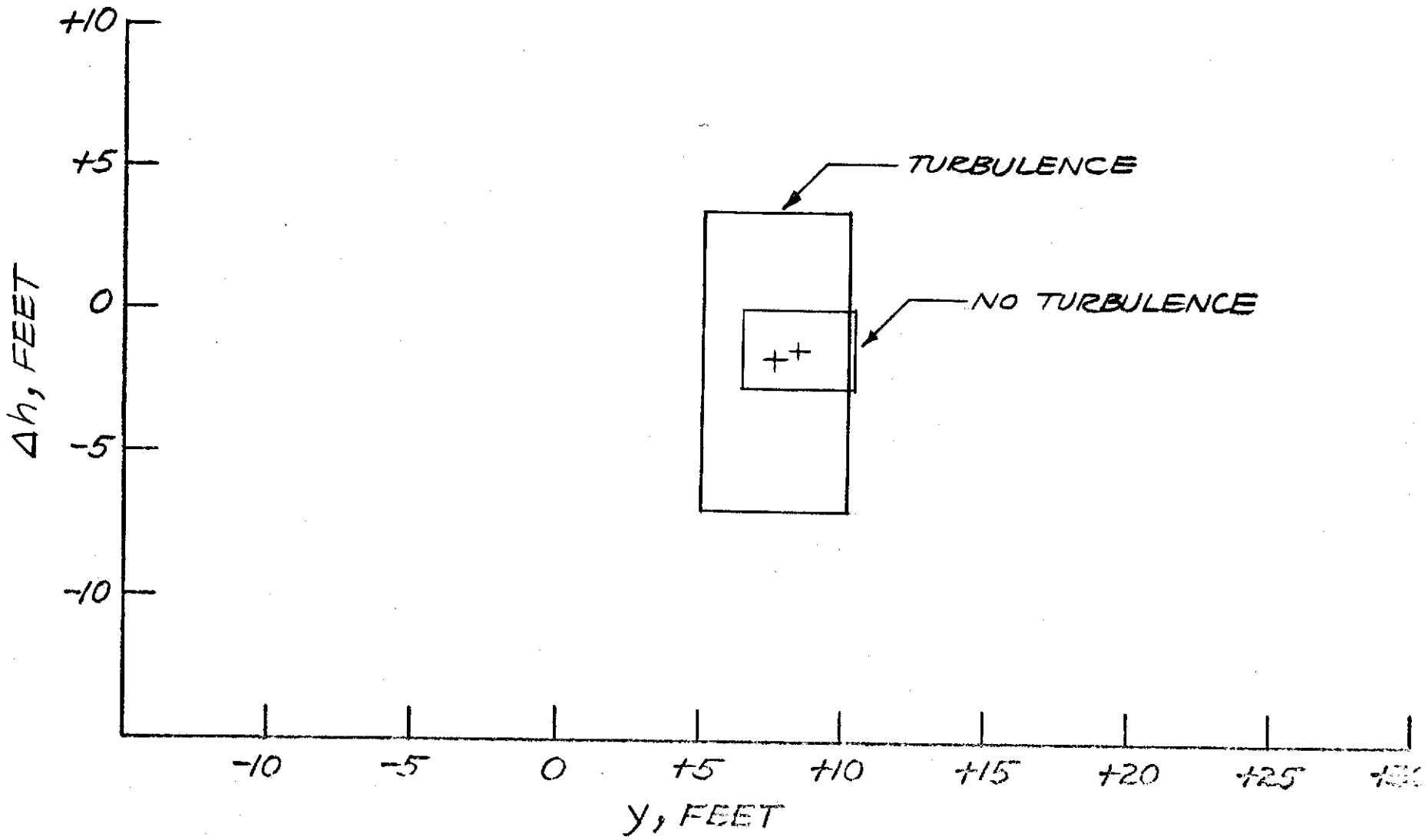

FIG. 70 - COMPARISON OF DISPERSIONS AT 200 FT. ALTITUDE WITH AND WITHOUT TURBULENCE - CAT III RANDOM and BIAS ERRORS

FIG. 71 SAMPLE TIME HISTORY OF CAT. IIIB RANDOM and BIAS ERRORS WITH TURBULENCE

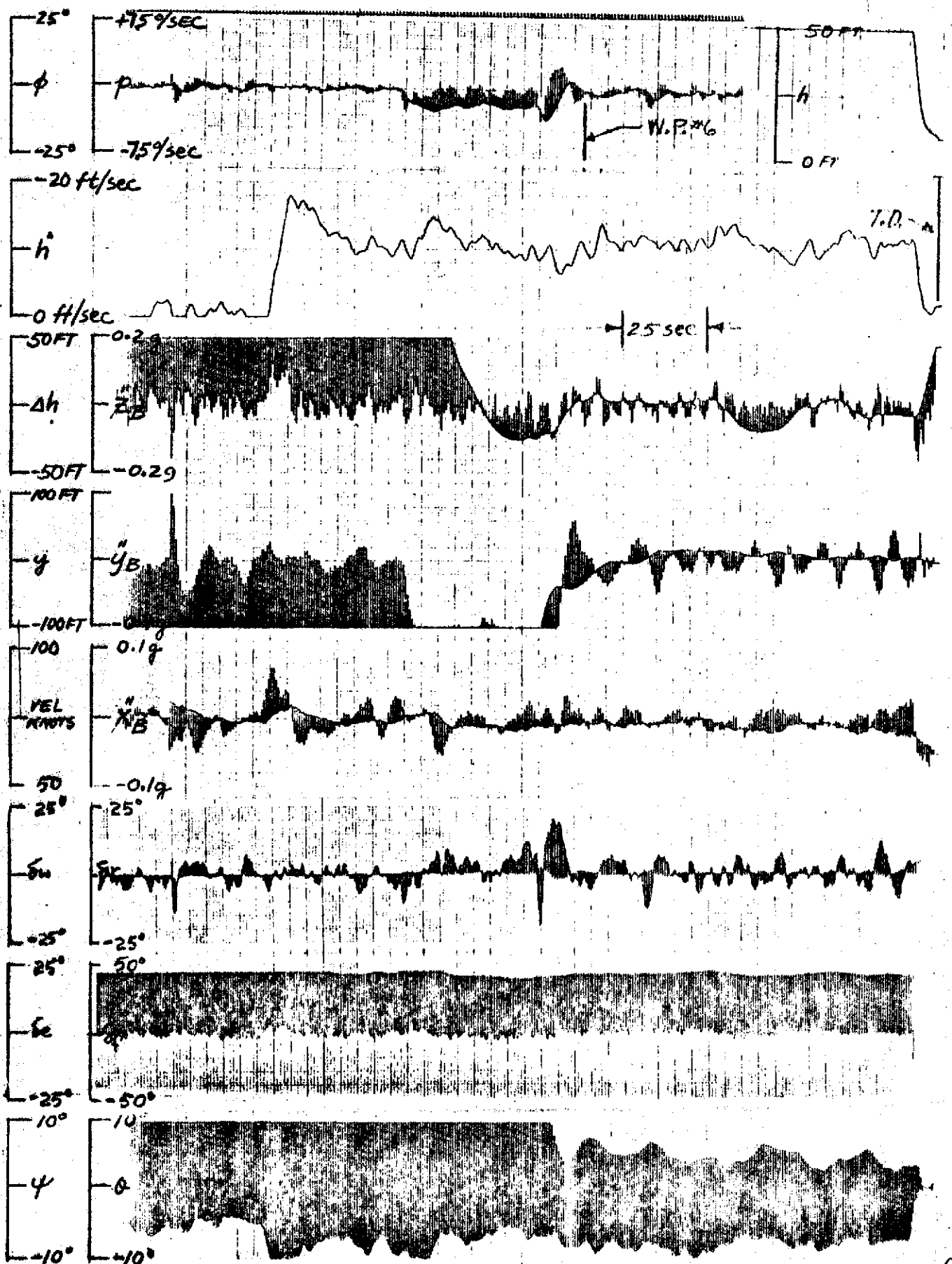

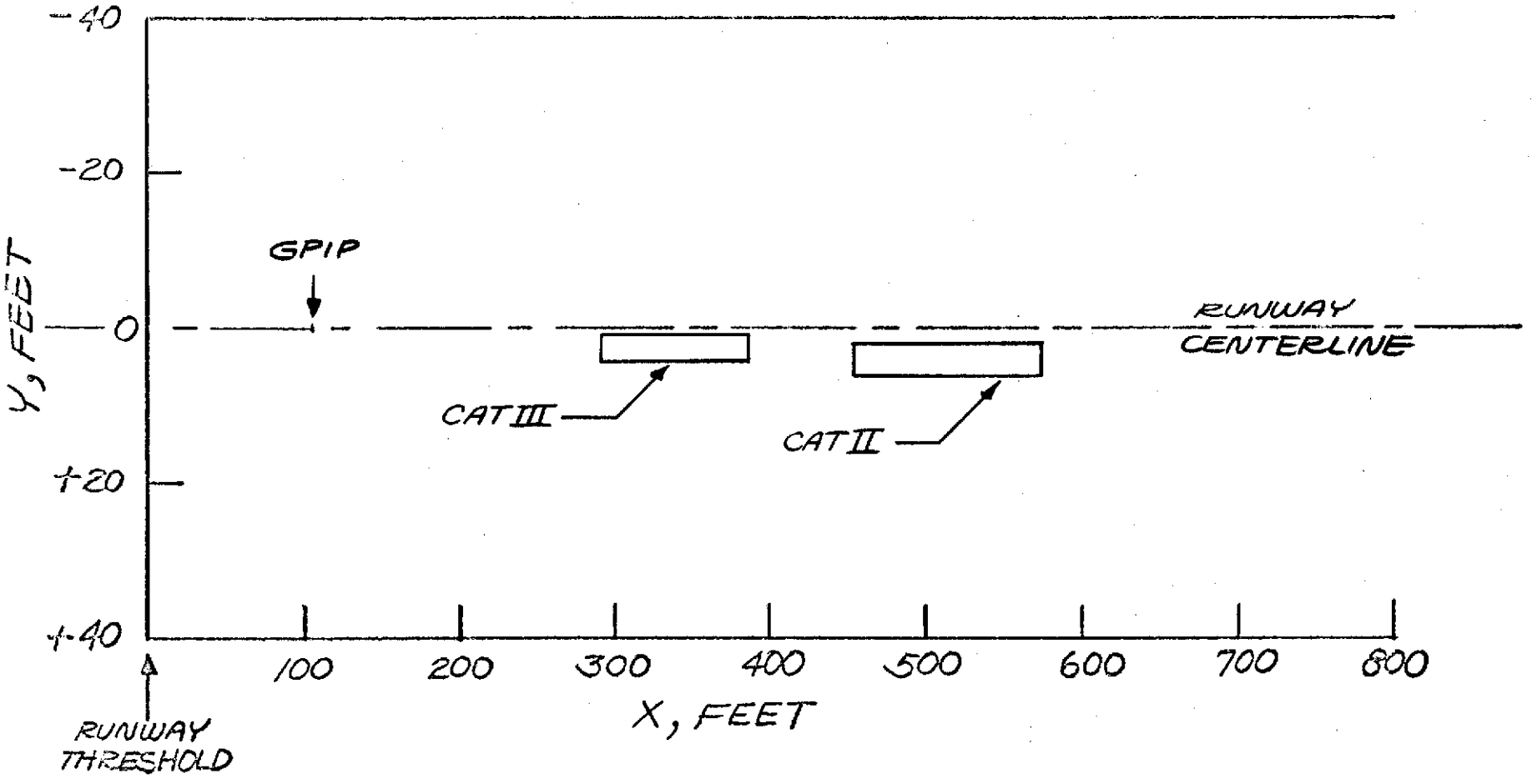

FIG. 72.-COMPARISON OF TOUCHDOWN DISPERSIONS WITH CAT II and CAT III RANDOM and BIAS ERRORS - NO TURBULENCE

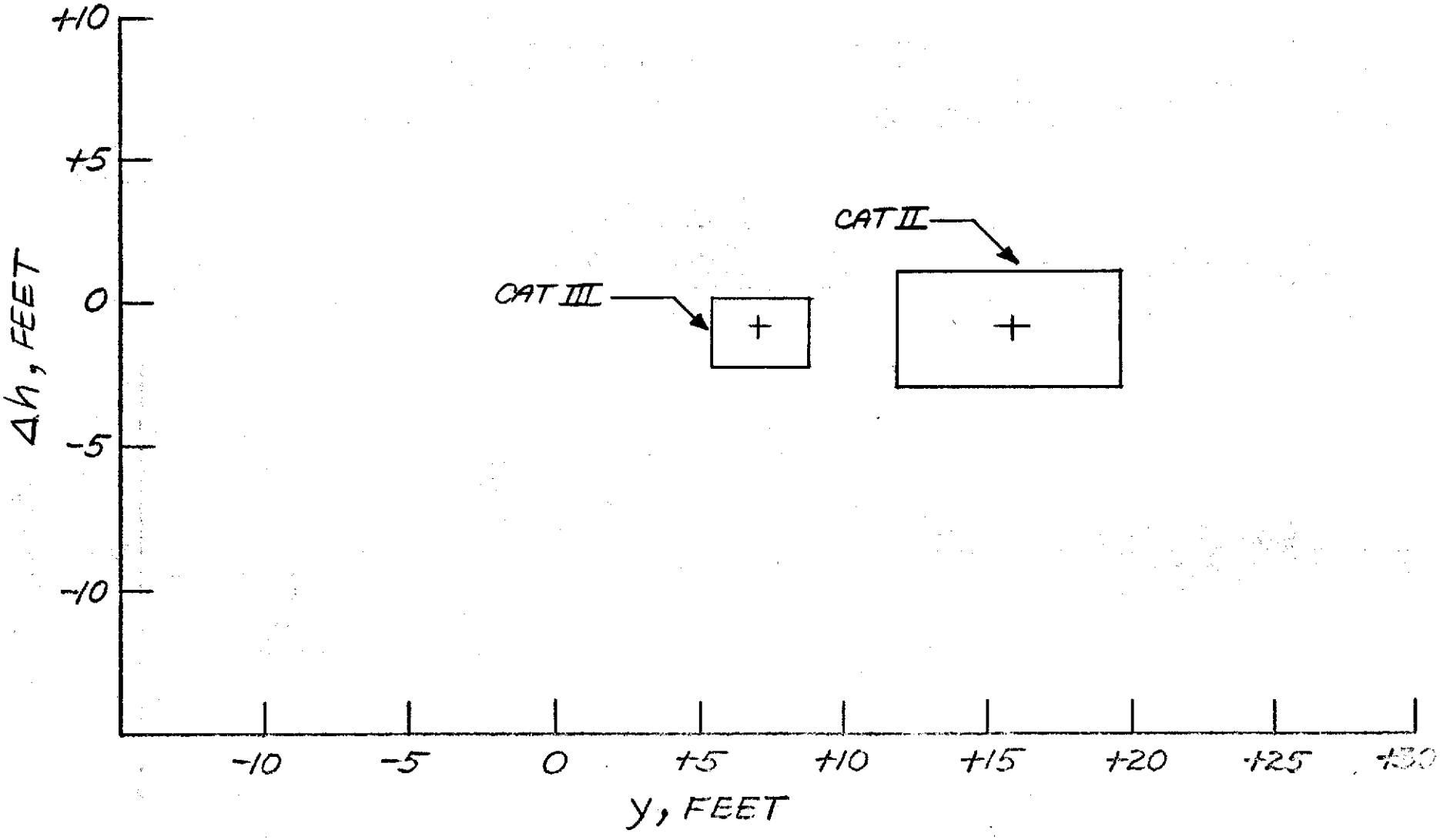

FIG. 73 - COMPARISON OF DISPERSIONS AT 100 FT ALTITUDE WITH CAT II and CAT III RANDOM and BIAS ERRORS - NO TURBULENCE

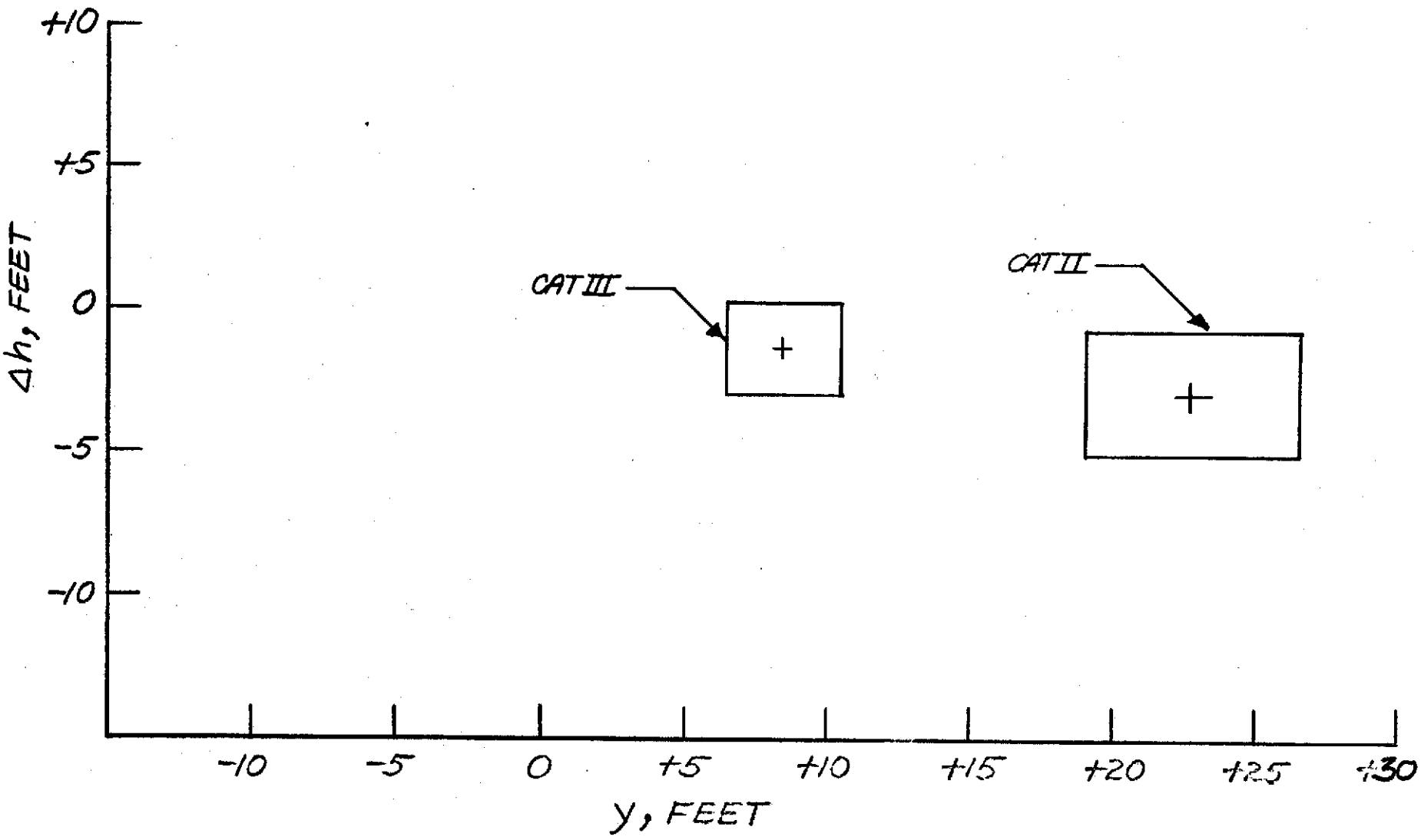

FIG. 74 COMPARISON OF DISPERSIONS AT 200 FT ALTITUDE WITH CAT II and CAT III RANDOM and BIAS ERRORS - NO TURBULENCE

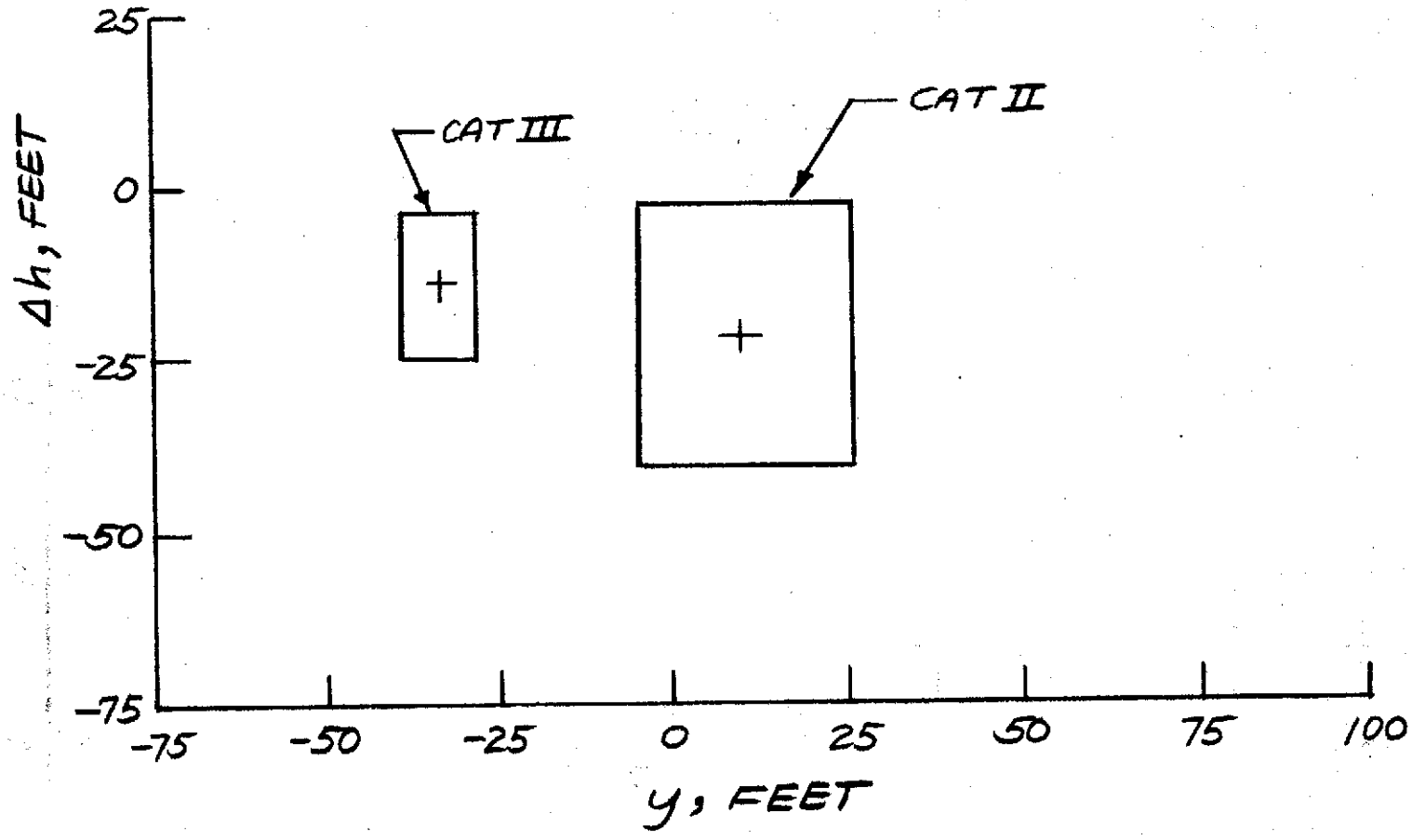

FIG. 75 COMPARISON OF DISPERSIONS AT THE LOCALIZER INTERCEPT WITH CAT II AND CAT III RANDOM AND BIAS ERRORS - NO TURBULENCE

FIG. 76 SAMPLE TIME HISTORY OF CAT II
RANDOM and BIAS ERRORS -NO TURBULENCE

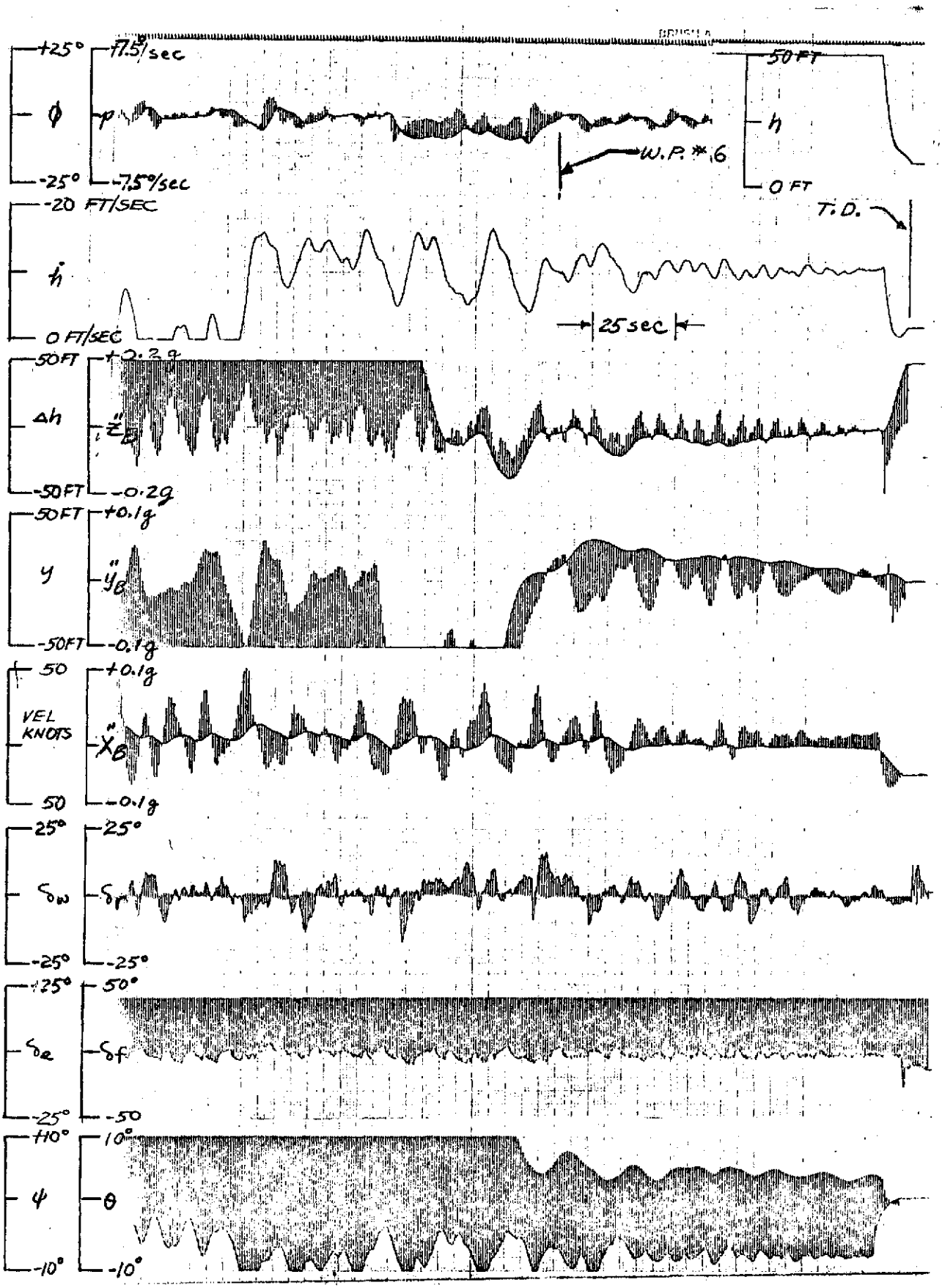

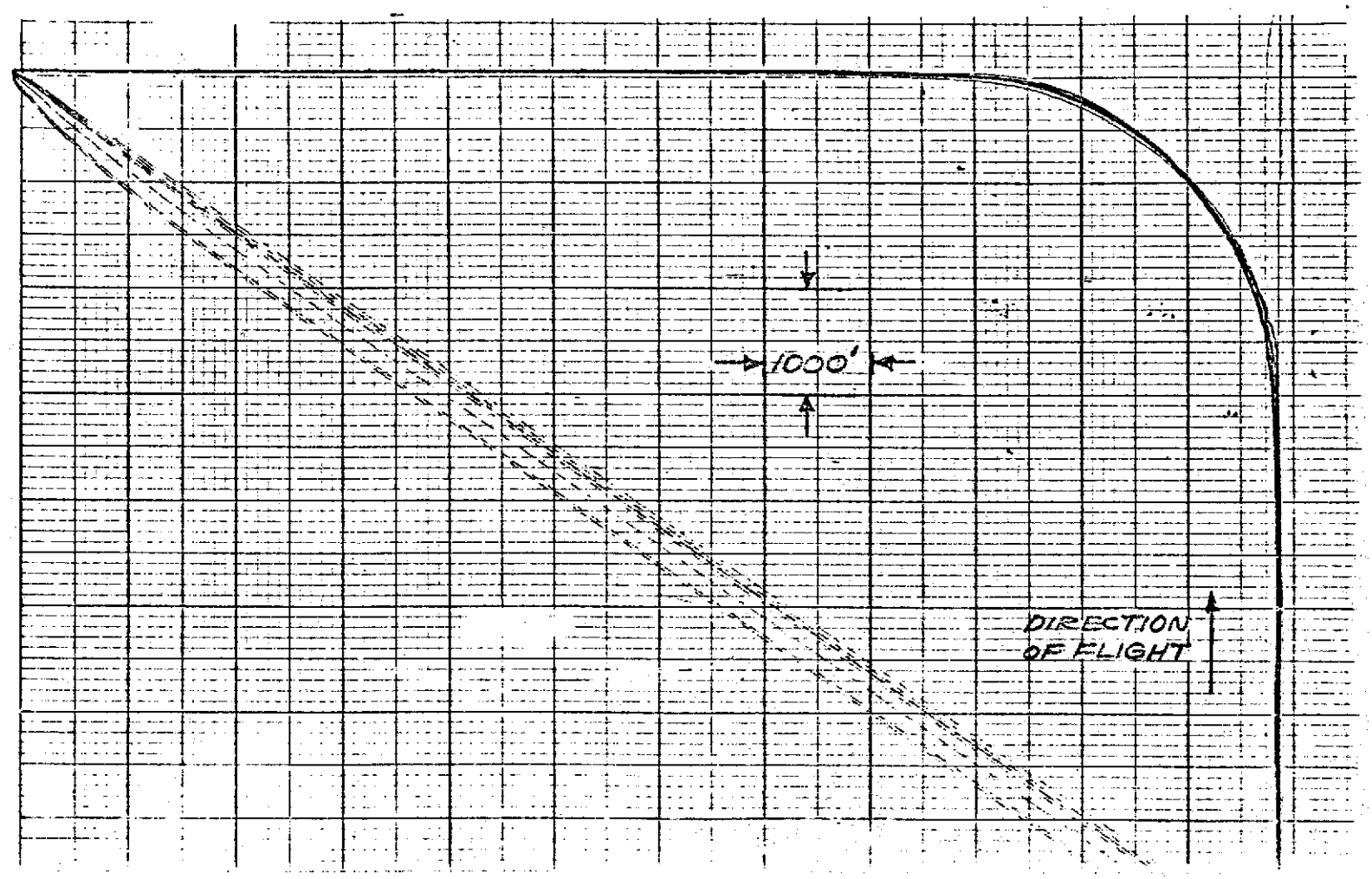

FIG. 77 X-Y PLOT OF FLIGHT PATH #1 WITH CAT II RANDOM AND BIAS ERRORS - NO TURBULENCE (9 RUNS)

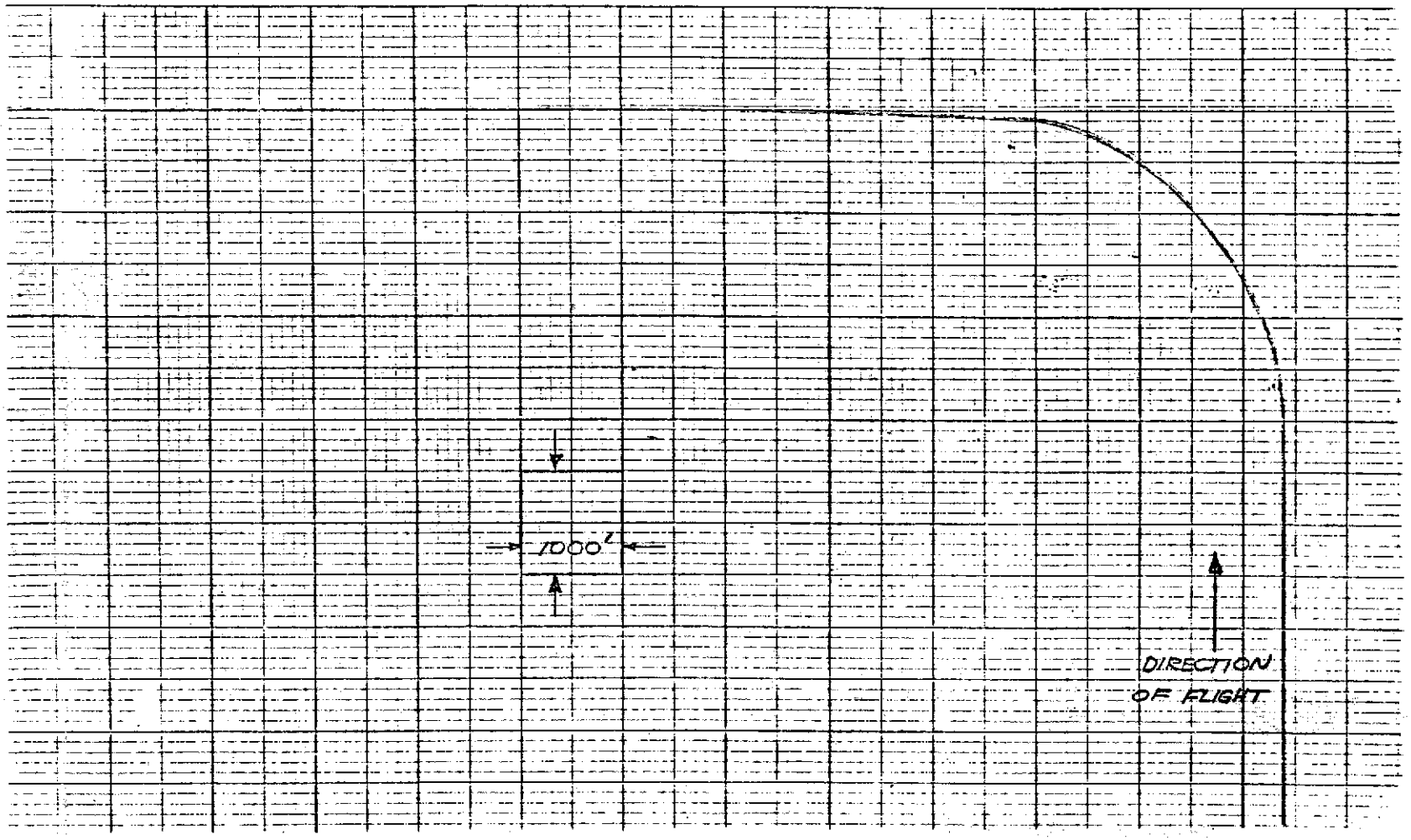

FIG. 78 X-Y PLOT OF FLIGHT PATH #1 WITH CAT III RANDOM AND BIAS ERRORS - NO TURBULENCE (11 RUNS)

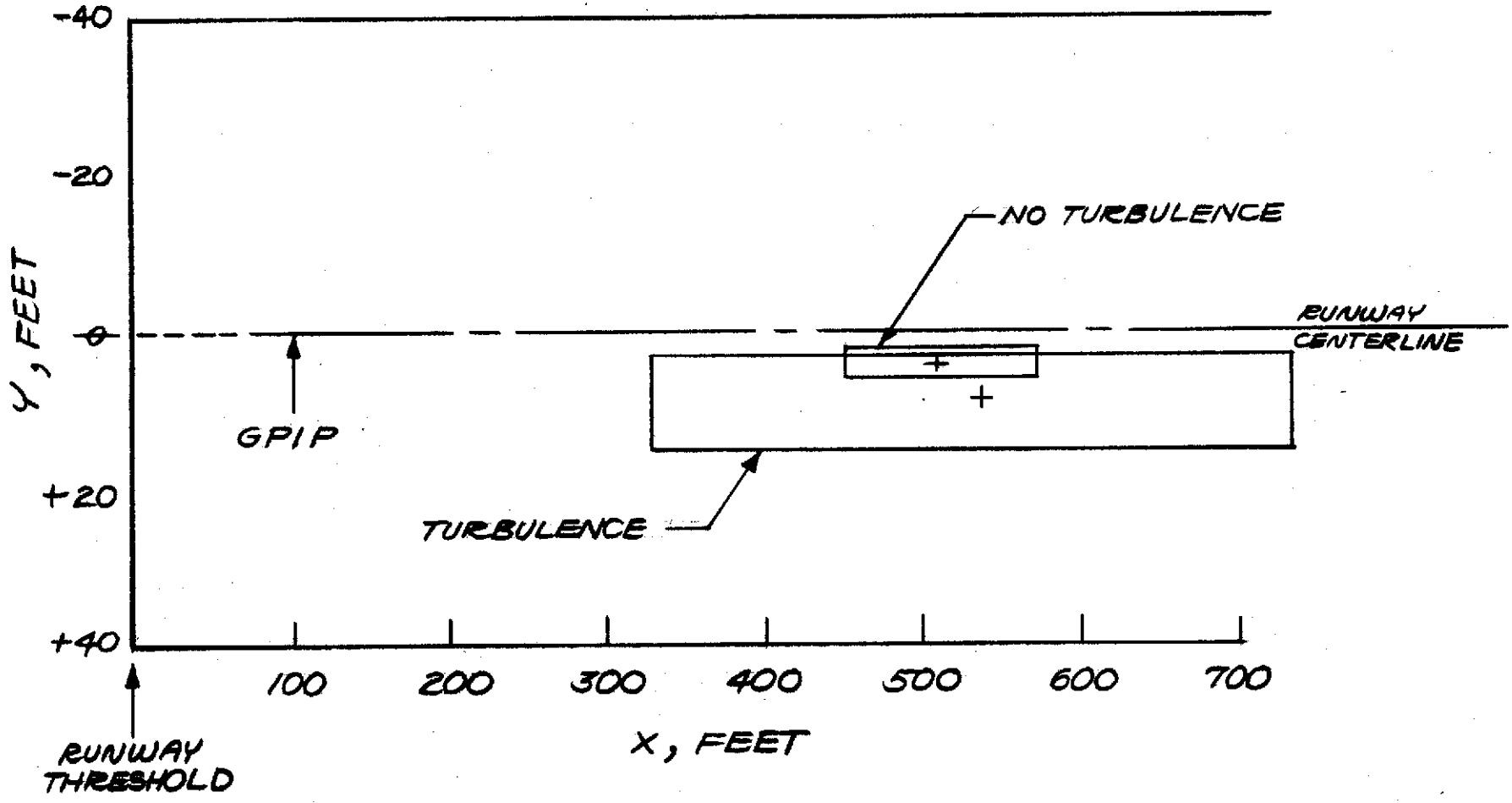

FIG. 79 COMPARISONS OF TOUCHDOWN DISPERSIONS WITH AND WITHOUT TURBULENCE [CAT II MLS RANDOM AND BIAS ERRORS]

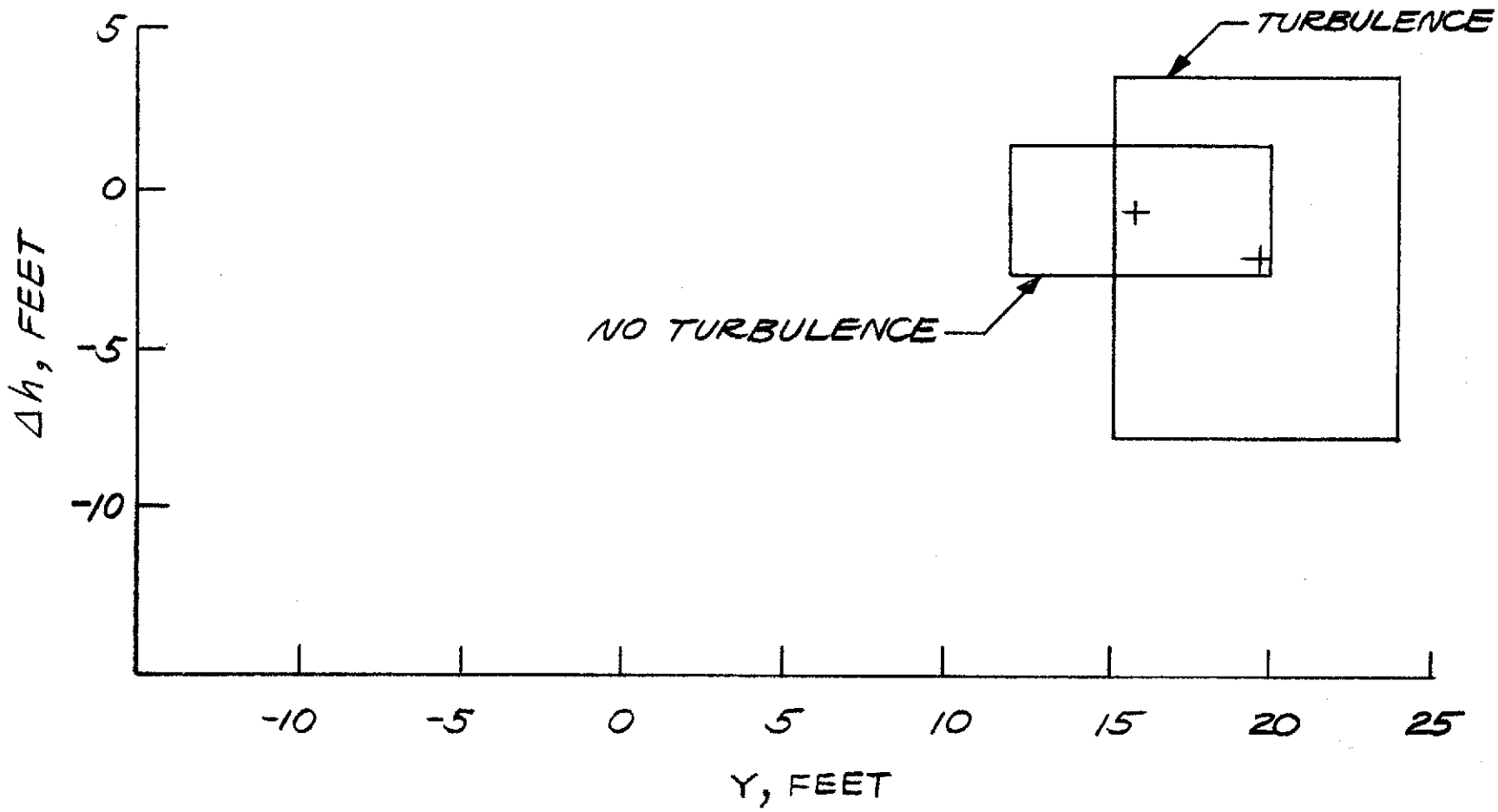

FIG. 80 COMPARISONS OF DISPERSIONS AT 100 FT ALTITUDE WITH AND WITHOUT TURBULENCE (CAT II MLS RANDOM AND BIAS ERRORS.)

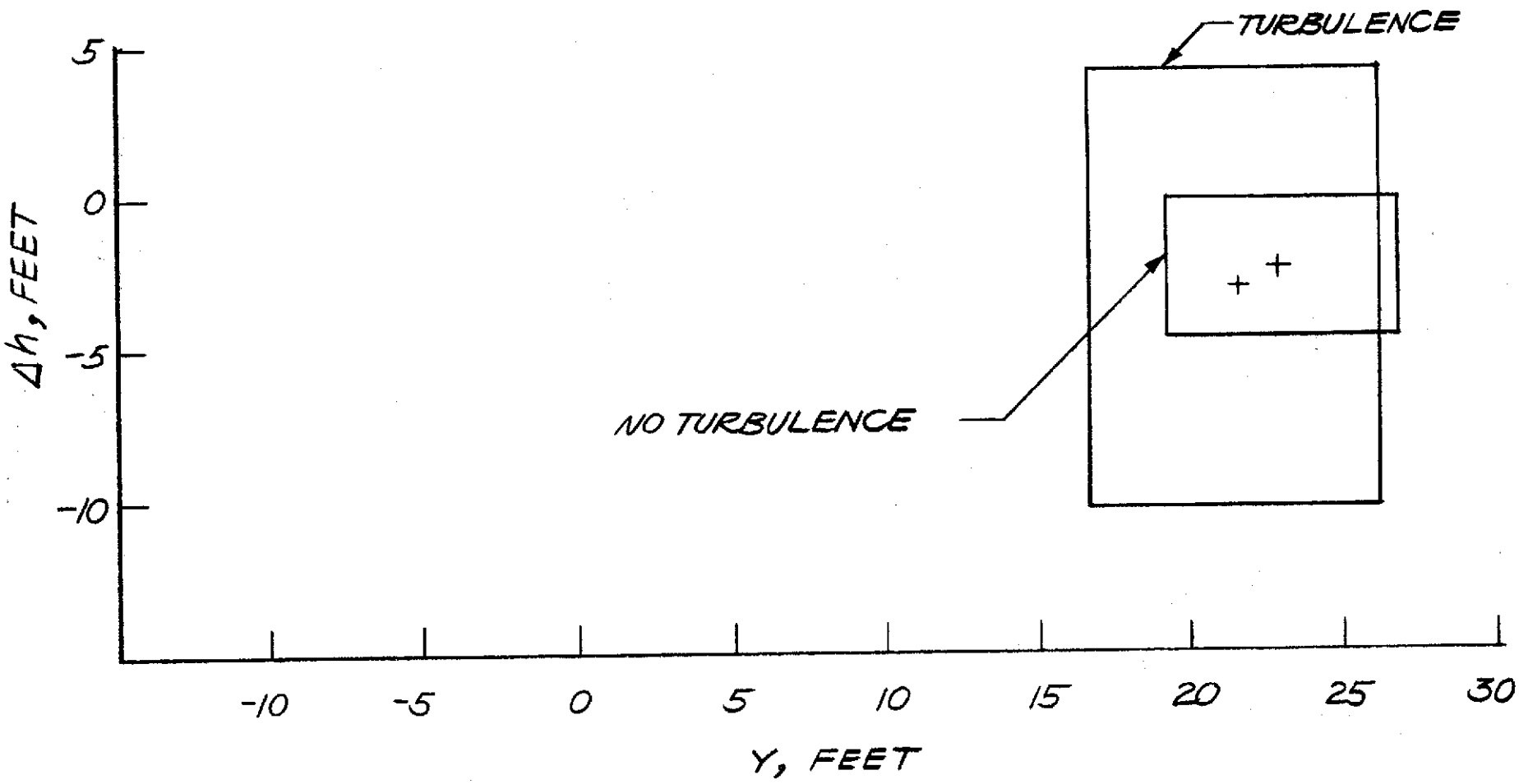

FIG. 81 COMPARISONS OF DISPERSIONS AT 200 FT. ALTITUDE WITH AND WITHOUT TURBULENCE (CAT II MLS RANDOM AND BIAS ERRORS)

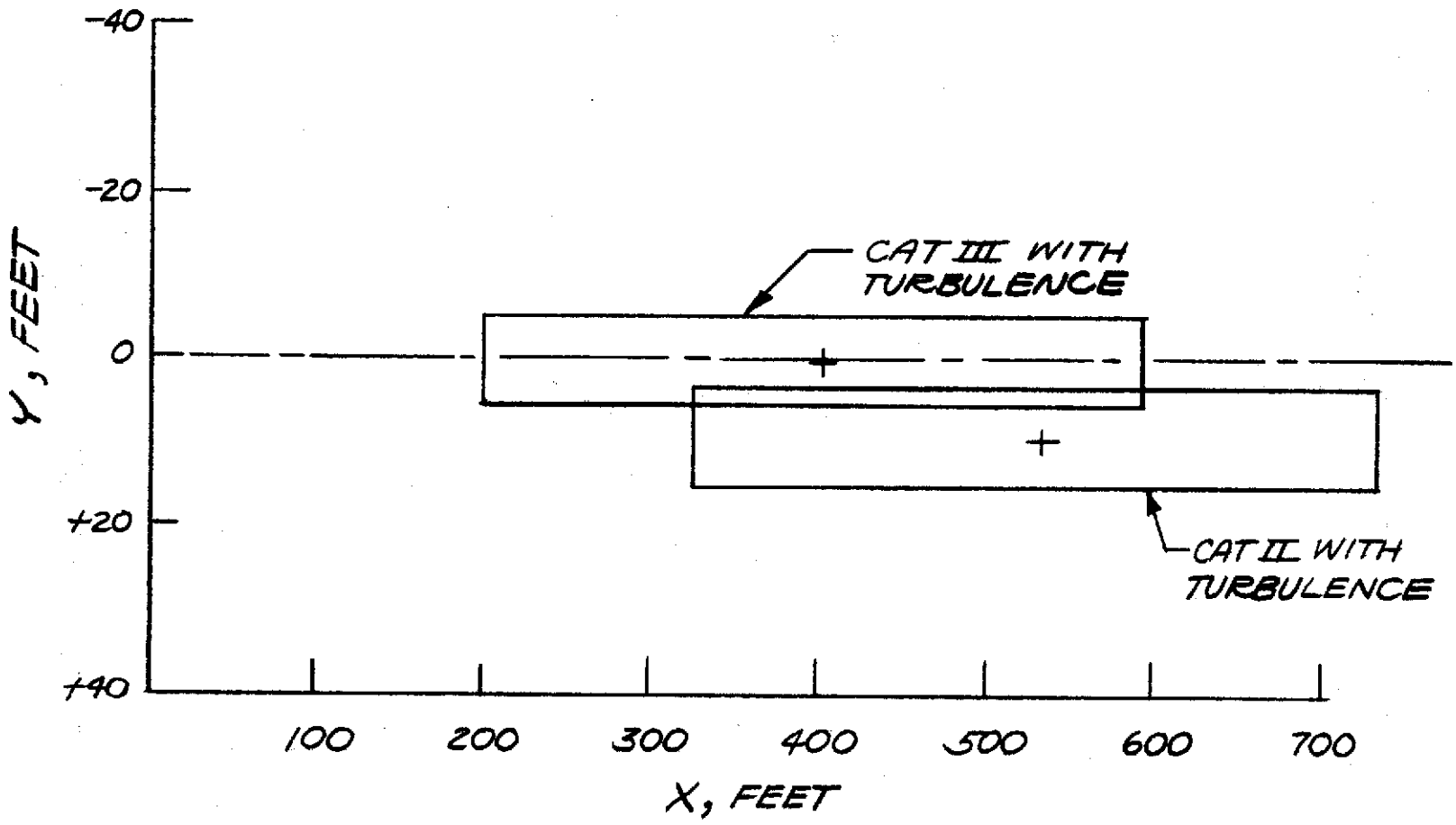

FIG 82 COMPARISONS OF TOUCHDOWN DISPERSIONS WITH TURBULENCE (CAT II AND CAT III RANDOM AND BIAS ERRORS)

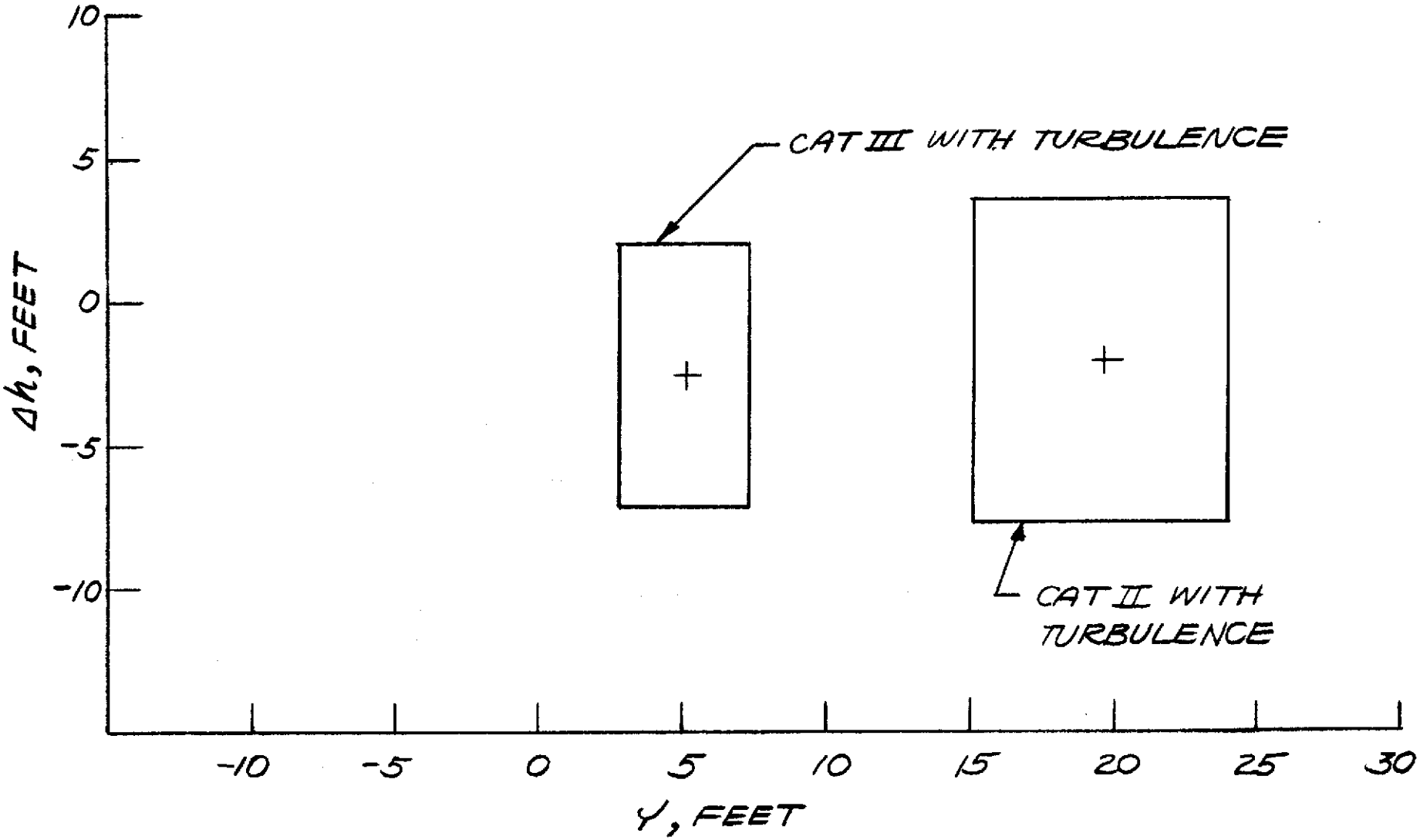

FIG 83 COMPARISONS OF DISPERSIONS AT 100 FT ALTITUDE WITH TURBULENCE (CAT II AND CAT III RANDOM AND BIAS ERRORS)

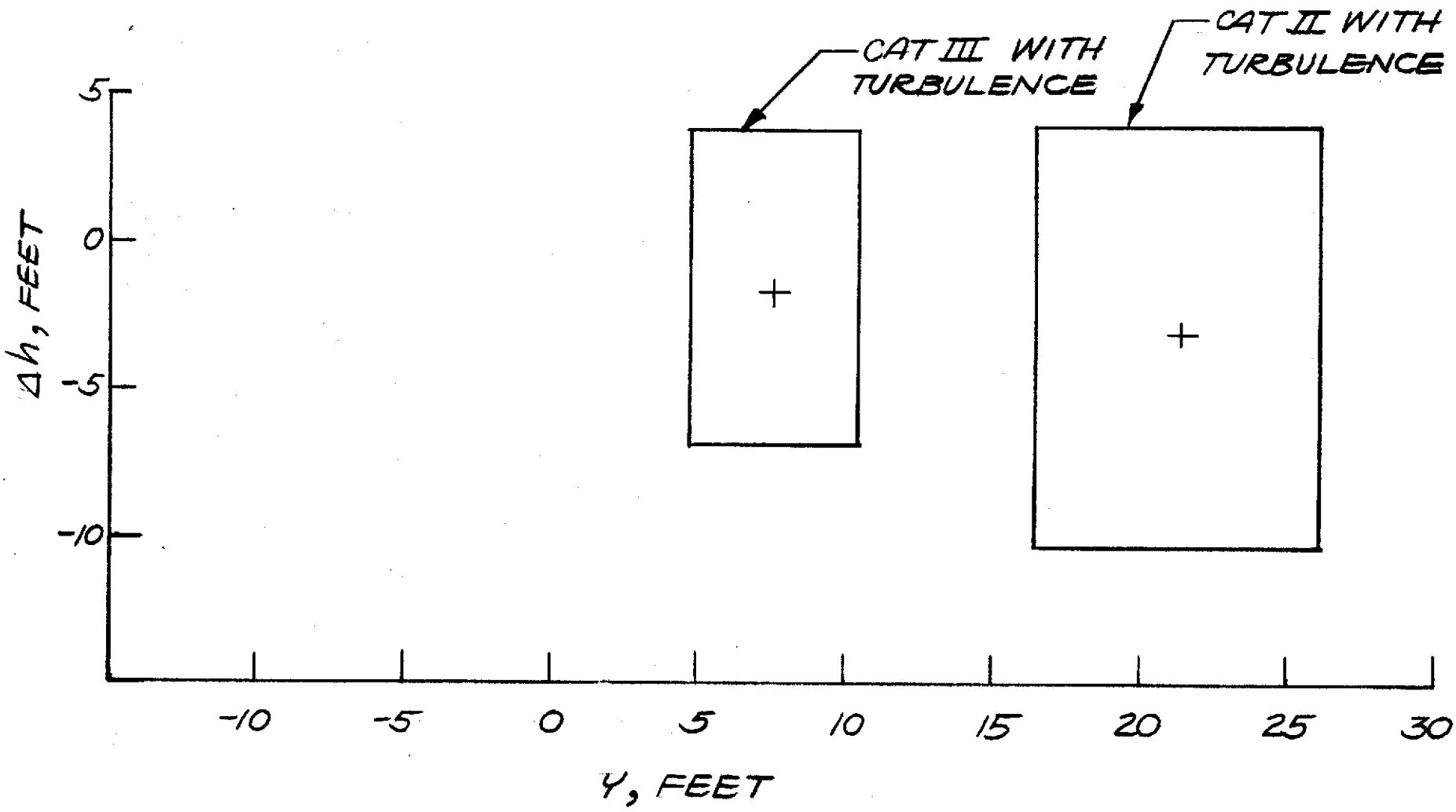

FIG. 83A. COMPARISONS OF DISPERSIONS AT 200 FT ALTITUDE WITH TURBULENCE (CAT II AND CAT III RANDOM AND BIAS ERRORS)

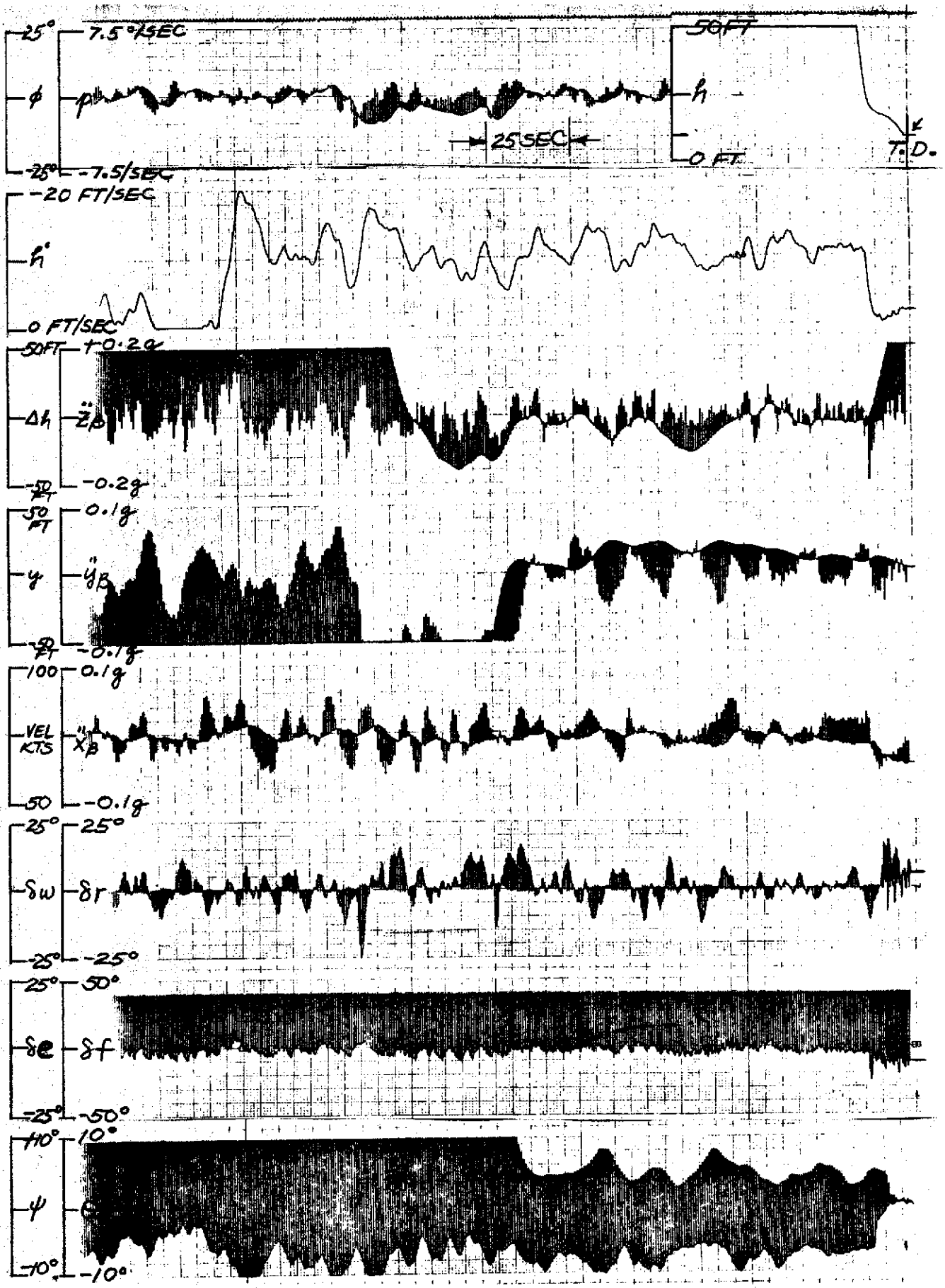

FIG. 83 B SAMPLE TIME HISTORY OF CAT II RANDOM AND BIAS ERRORS WITH TURBULENCE

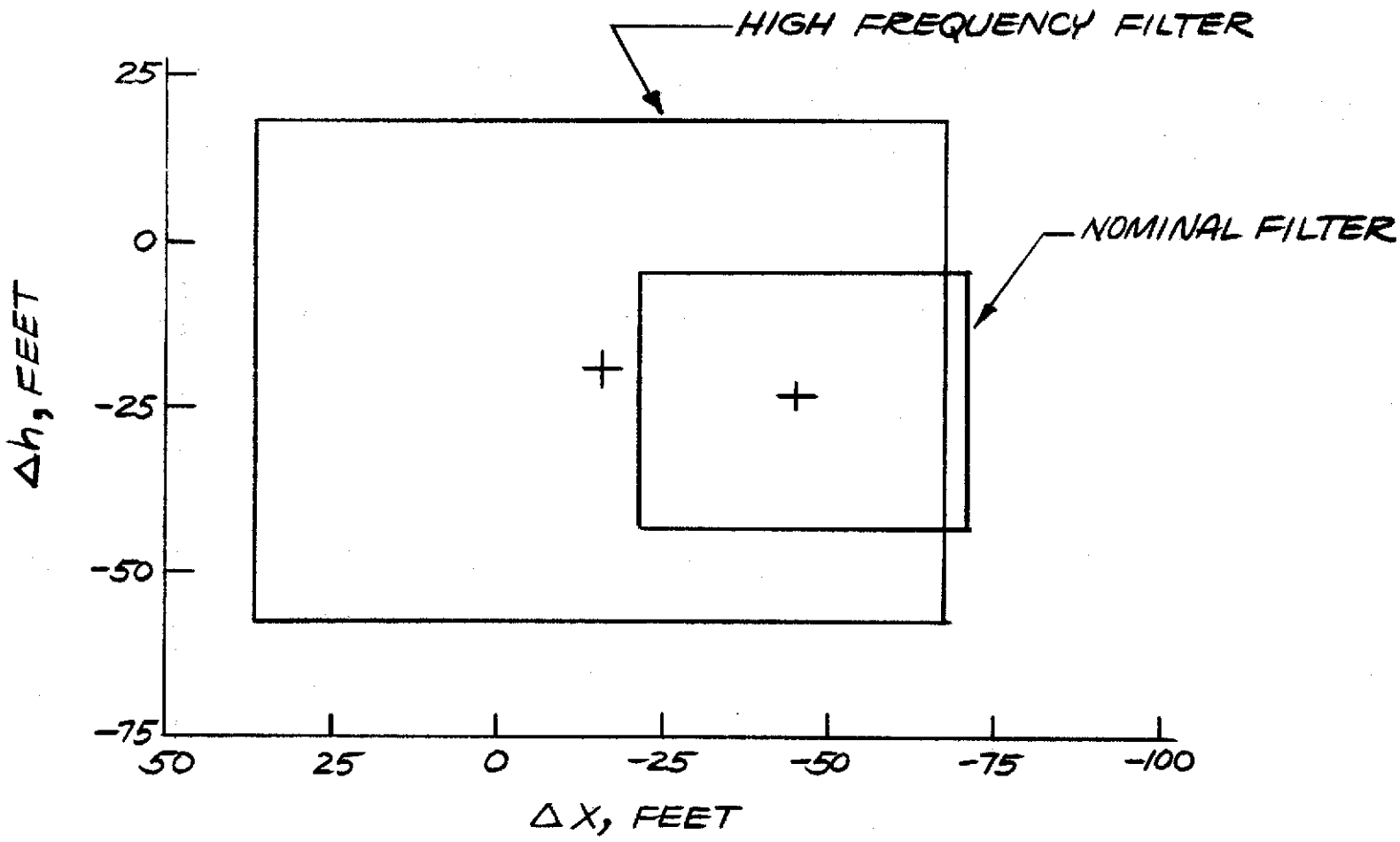

FIG. 84 EFFECT OF COMPLEMENTARY FILTER CUT-OFF FREQUENCY ON DISPERSION AT GLIDE PATH INTERCEPT POINT (CAT II RANDOM and BIAS)

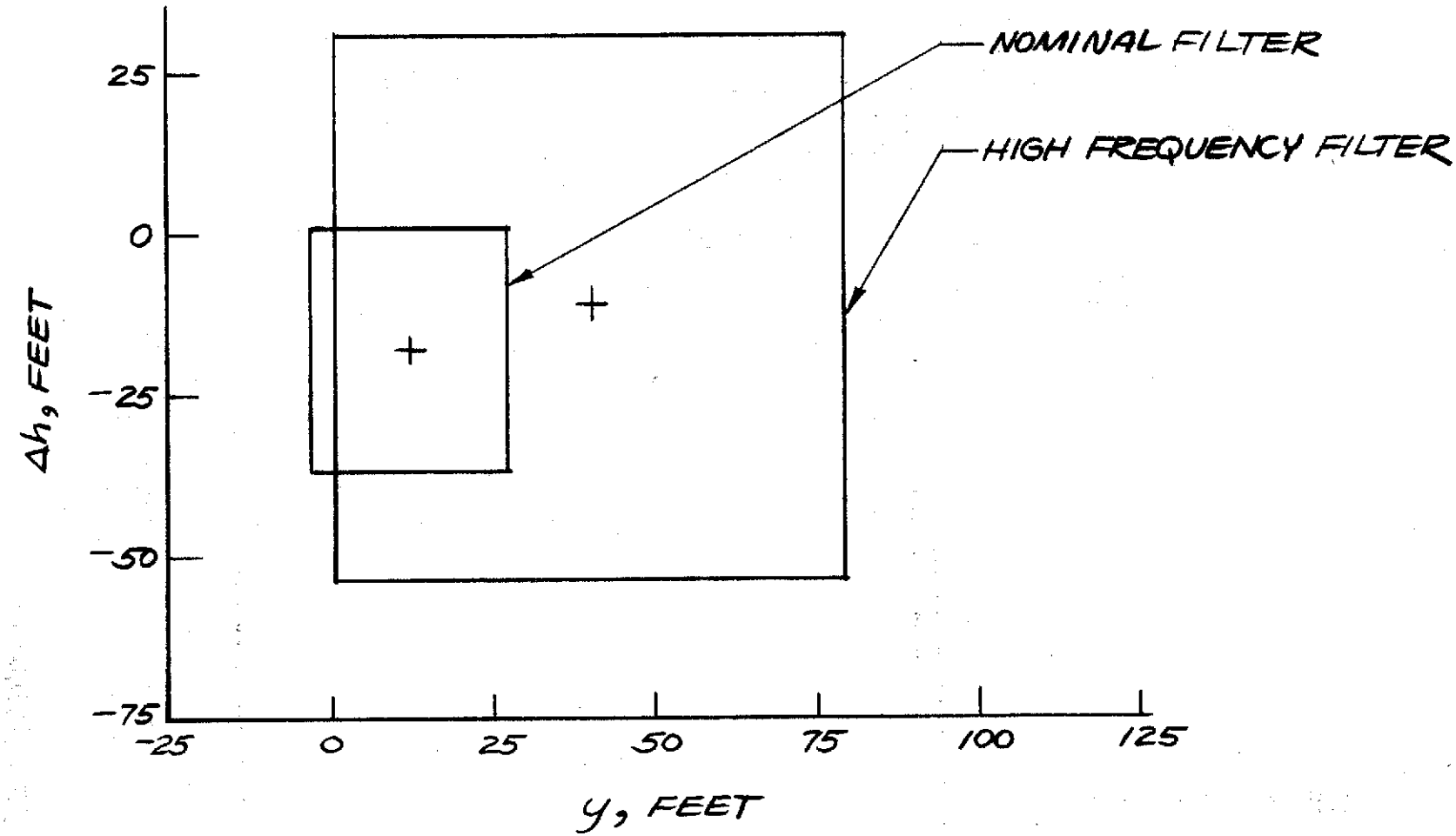

FIG 8 5 EFFECT OF COMPLIMENTARY FILTER CUT-OFF FREQUENCY ON DISPERSION AT RUNWAY INTERCEPT ALTITUDE (CAT II RANDOM AND BIAS)

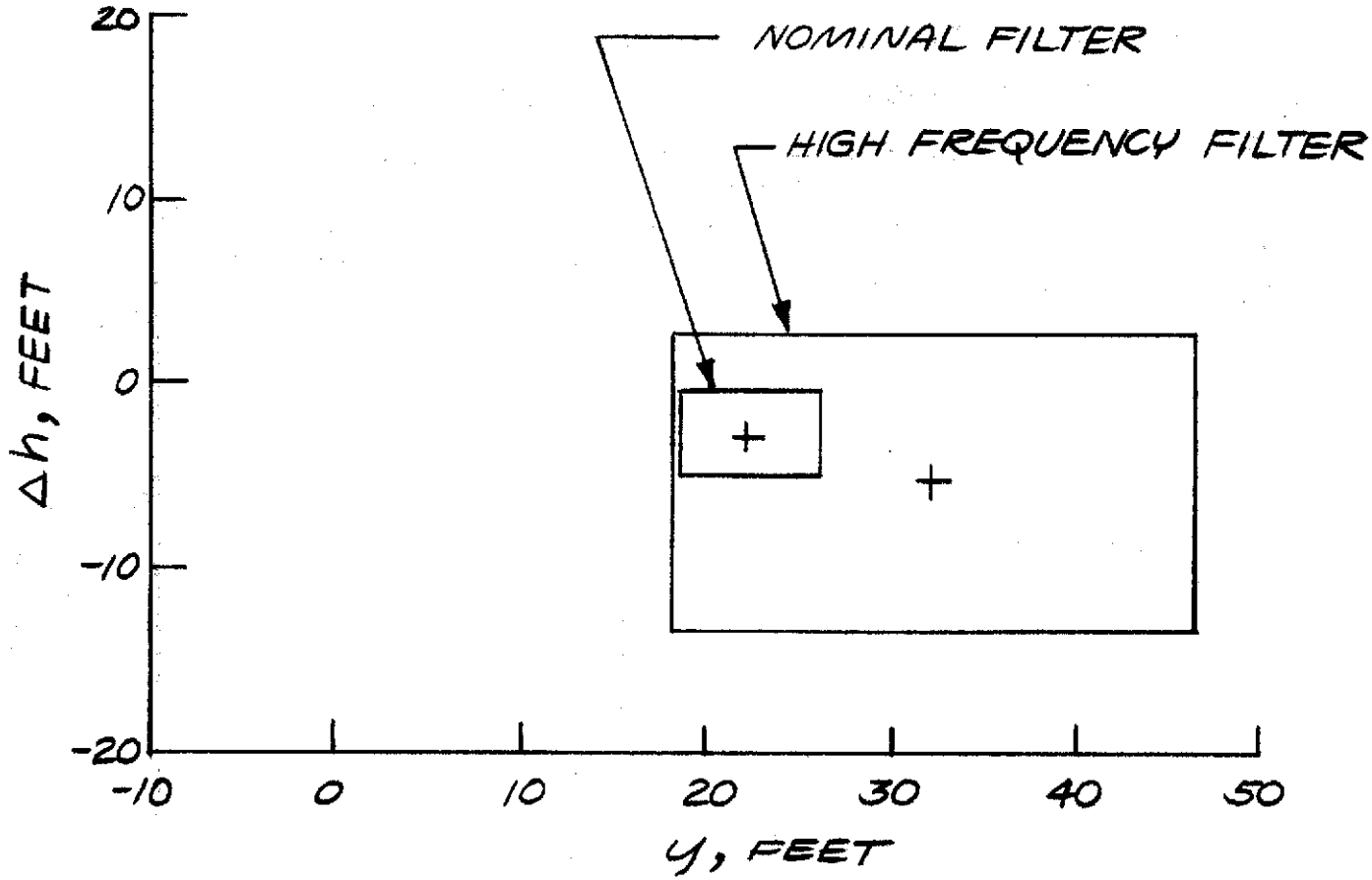

FIG. 86 EFFECT OF COMPLEMENTARY FILTER CUT-OFF FREQUENCY ON DISPERSION AT 200 FT ALTITUDE (CAT II RANDOM and BIAS)

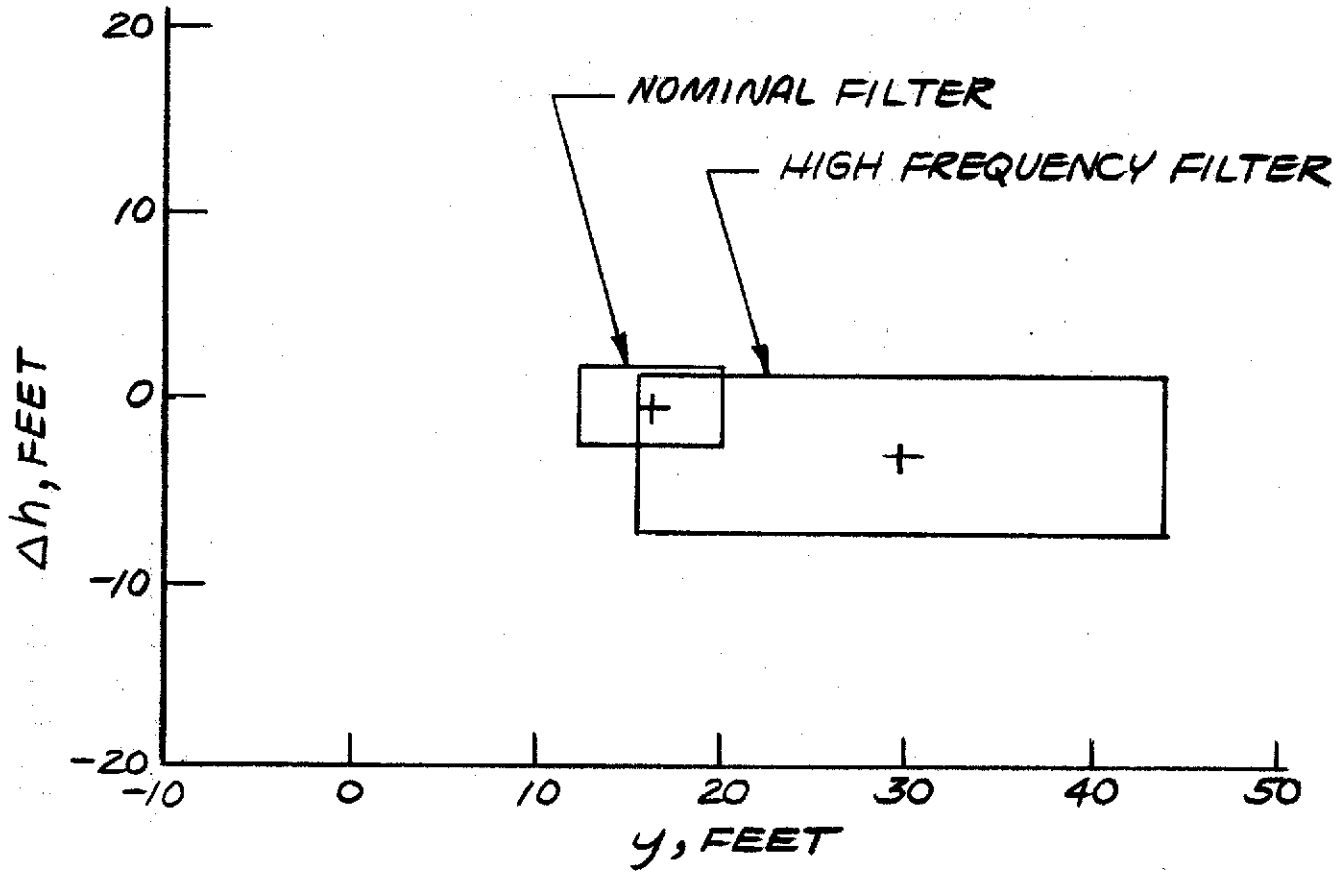

FIG. 87 EFFECT OF COMPLEMENTARY FILTER CUT-OFF FREQUENCY ON DISPERSION AT 100 FT ALTITUDE (CAT II RANDOM and BIAS)

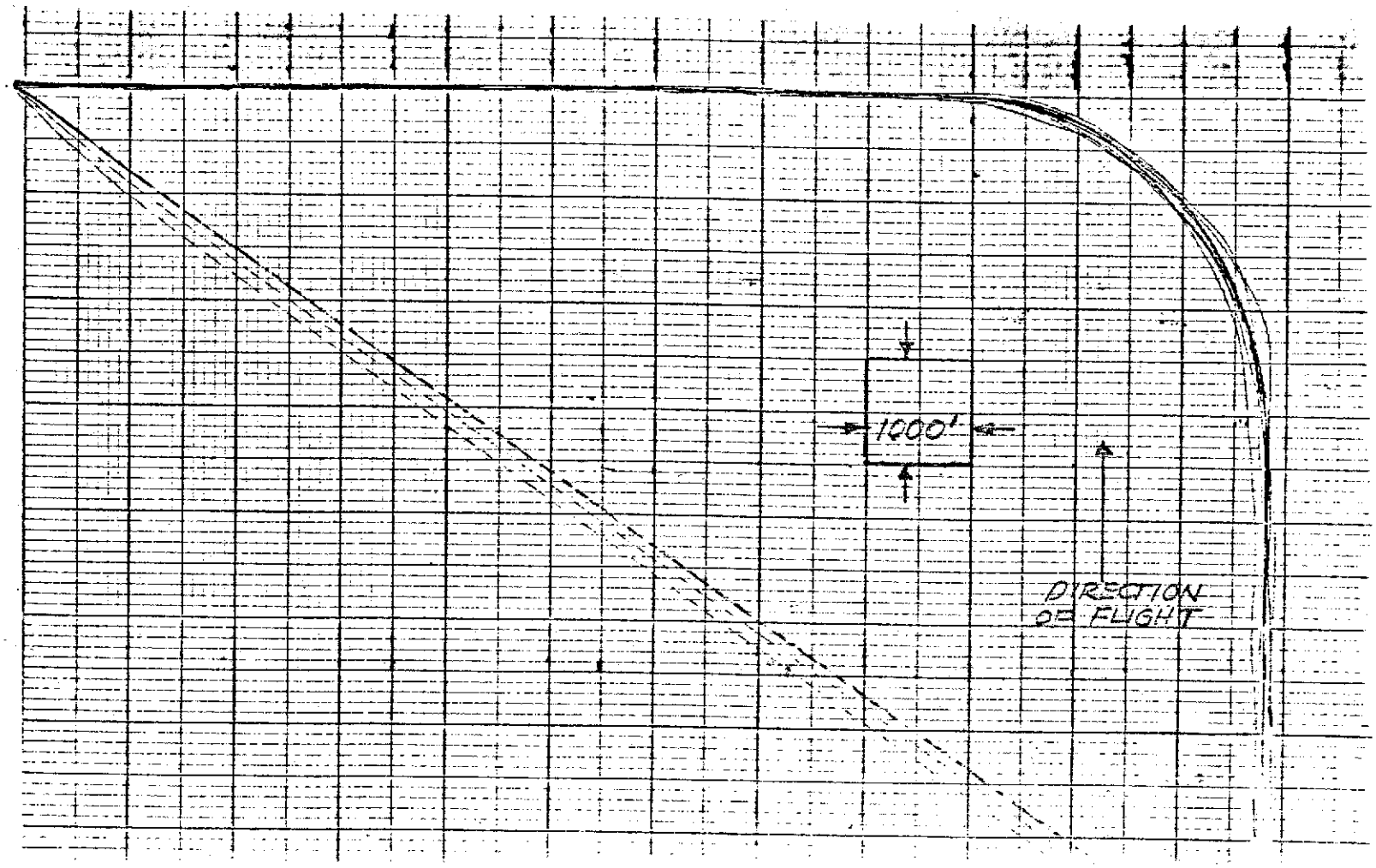

FIG. 88 X-Y PLOT OF SYSTEM WITH HIGH-FREQUENCY COMPLEMENTARY FILTER-CAT II RANDOM AND BIAS ERRORS (9 RUNS, 2 WITH TURBULENCE)

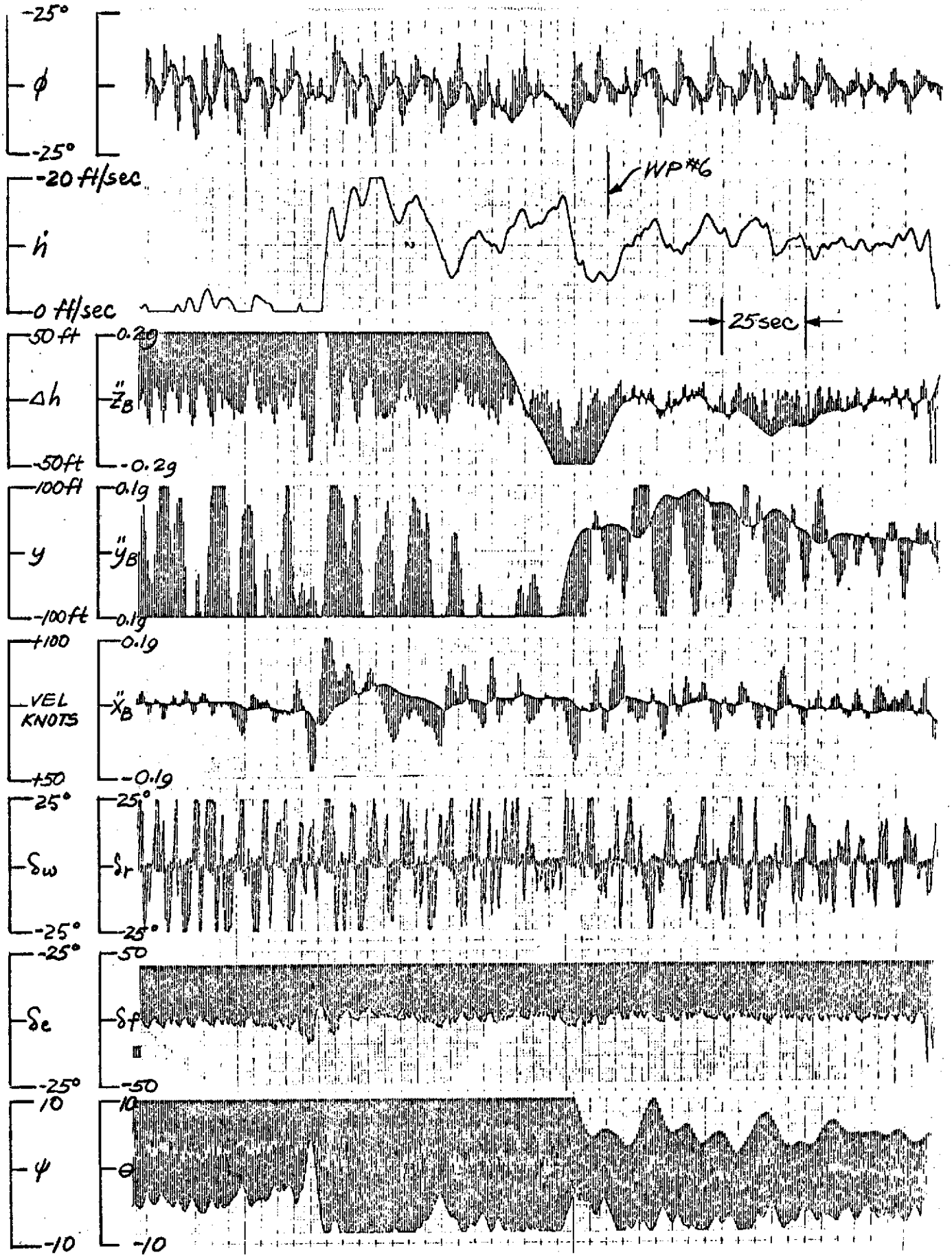

FIG. 89 SAMPLE TIME HISTORY OF EFFECT OF HIGH FREQUENCY FILTER WITH CAT II RANDOM AND BIAS ERRORS

FIG 90 SAMPLE TIME HISTORY OF SYSTEM WITH NON-COMPLEMENTARY FILTER WITH CAT III RANDOM & BIAS ERRORS - WITH TURBULENCE

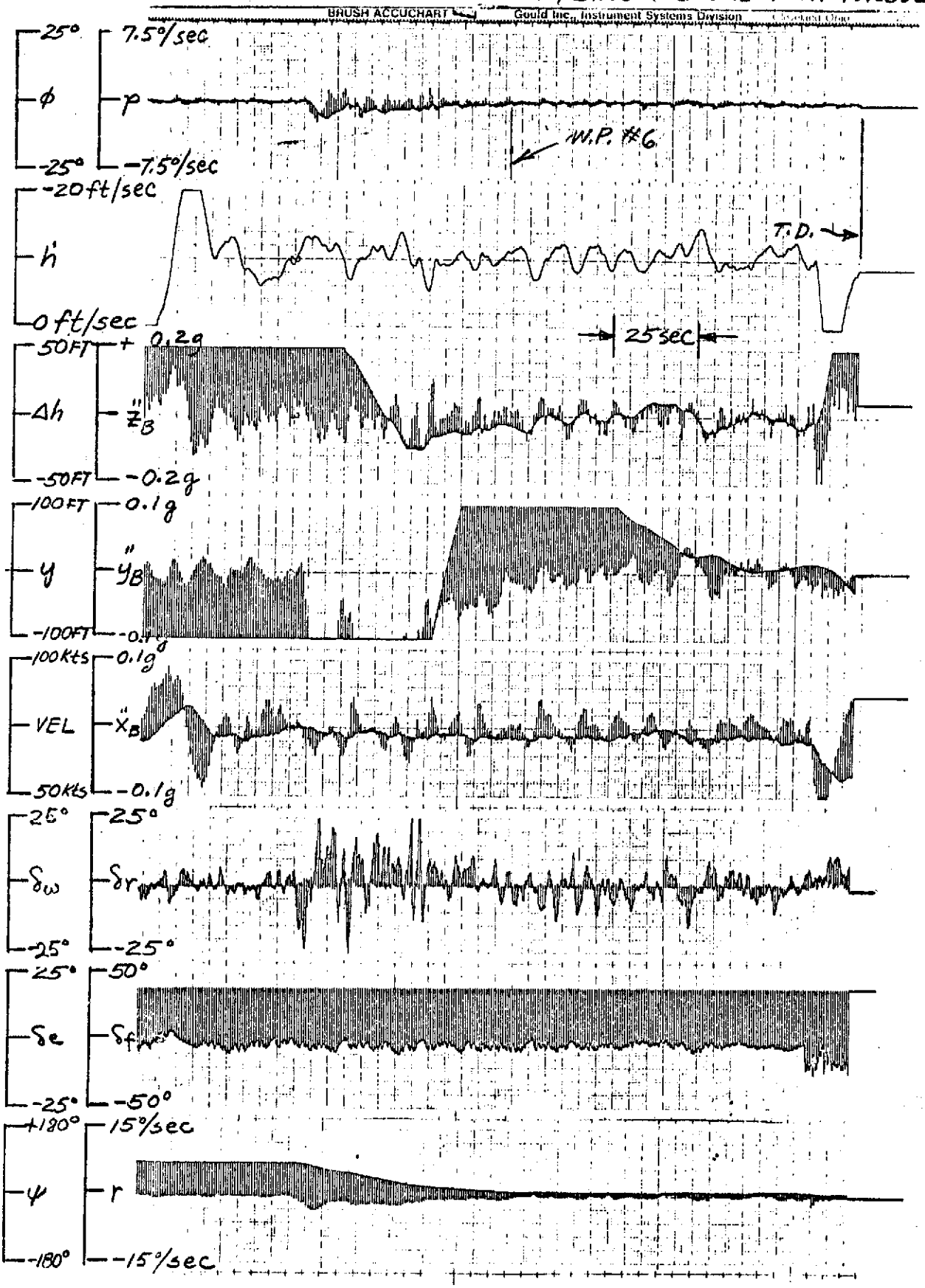

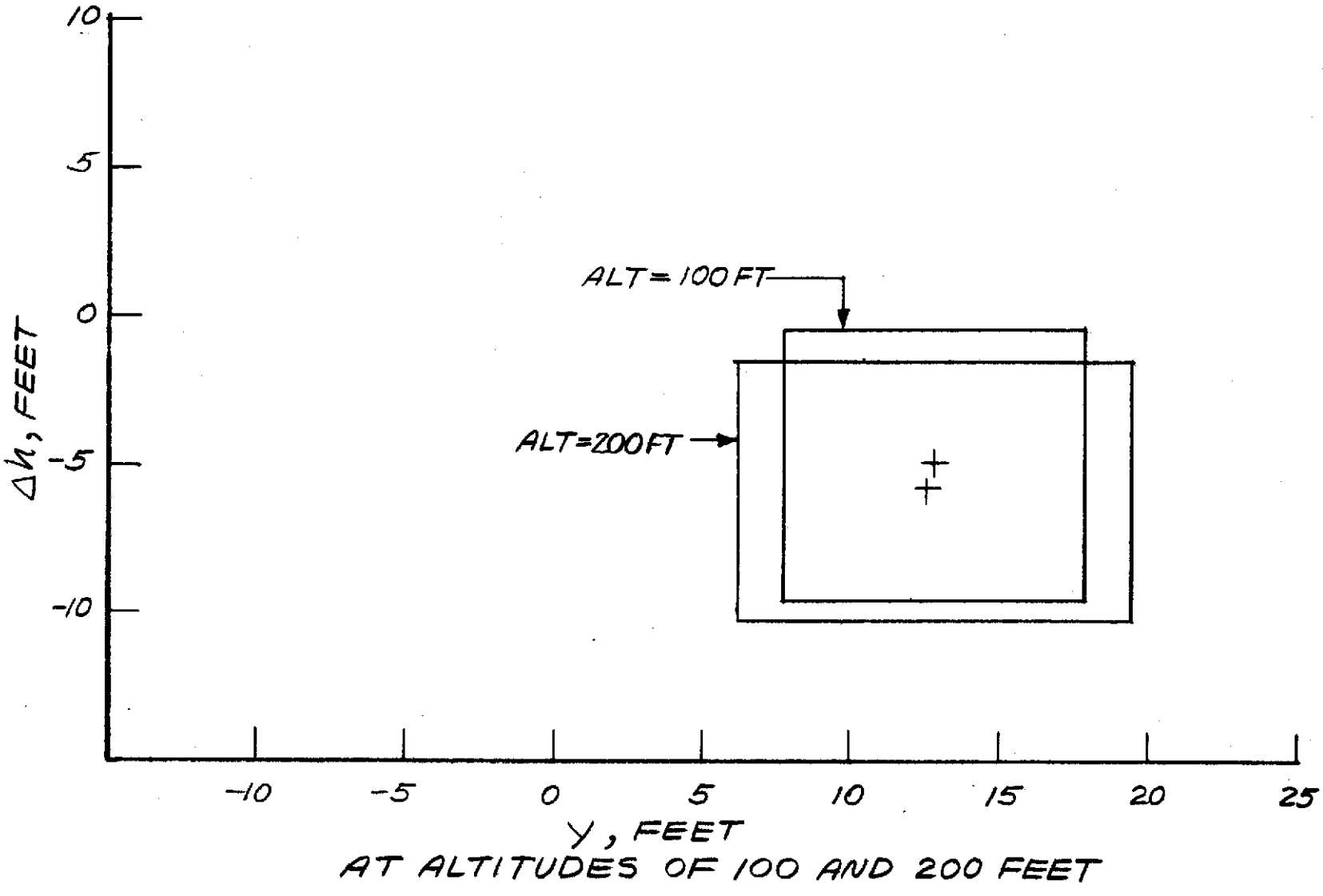

AT ALTITUDES OF 100 AND 200 FEET

FIG. 91A THE VERTICAL AND LATERAL DISPERSIONS WITH NON-COMPLEMENTARY FILTER

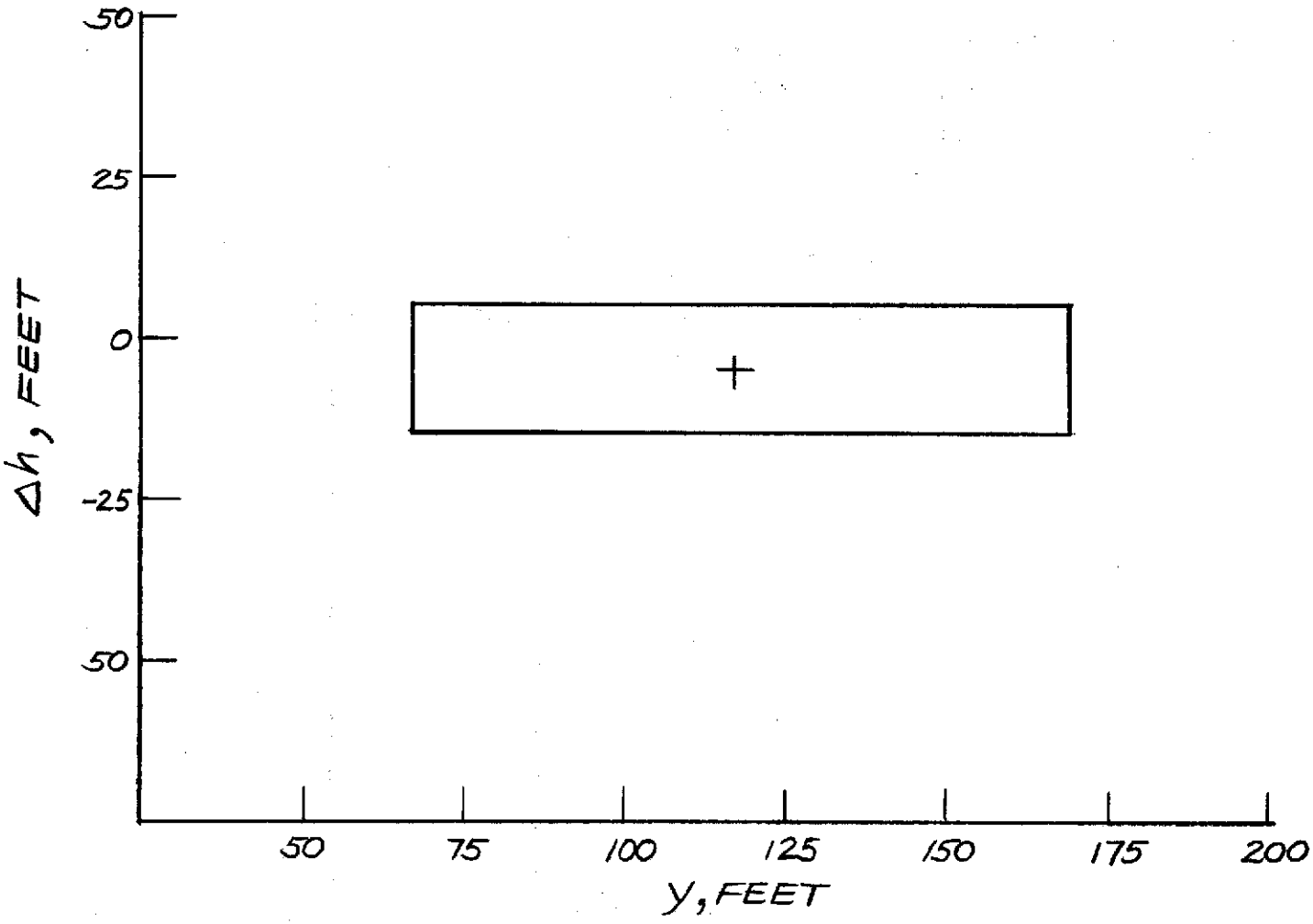

FIG. 91B - THE VERTICAL AND LATERAL DISPERSIONS WITH NON-COMPLEMENTARY FILTER.

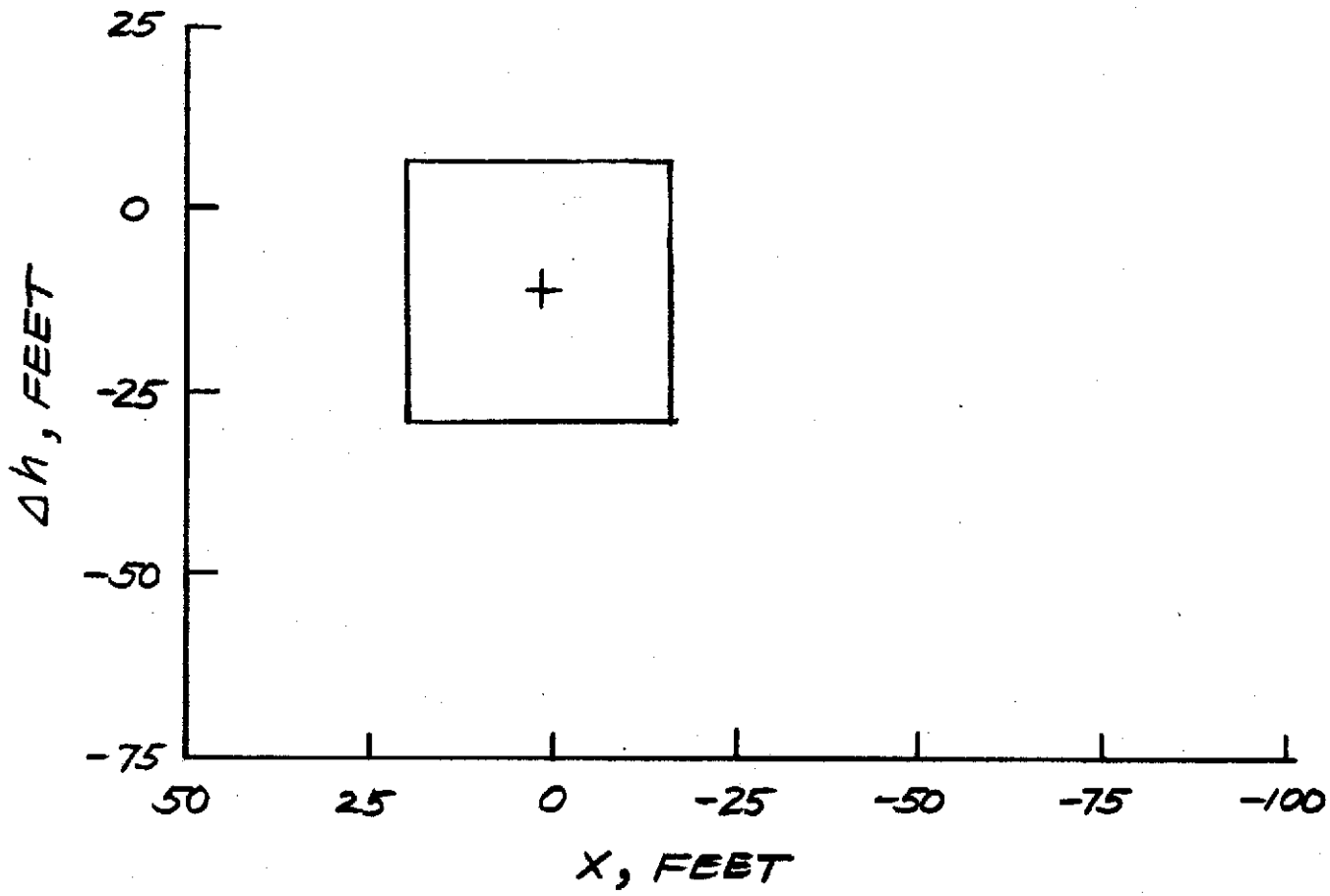

FIG. 92 THE VERTICAL AND LATERAL DISPERSIONS AT GLIDE SLOPE INTERCEPT WAY POINT (CAT III RANDOM AND BIAS NON-COMPLEMENTARY FILTER)

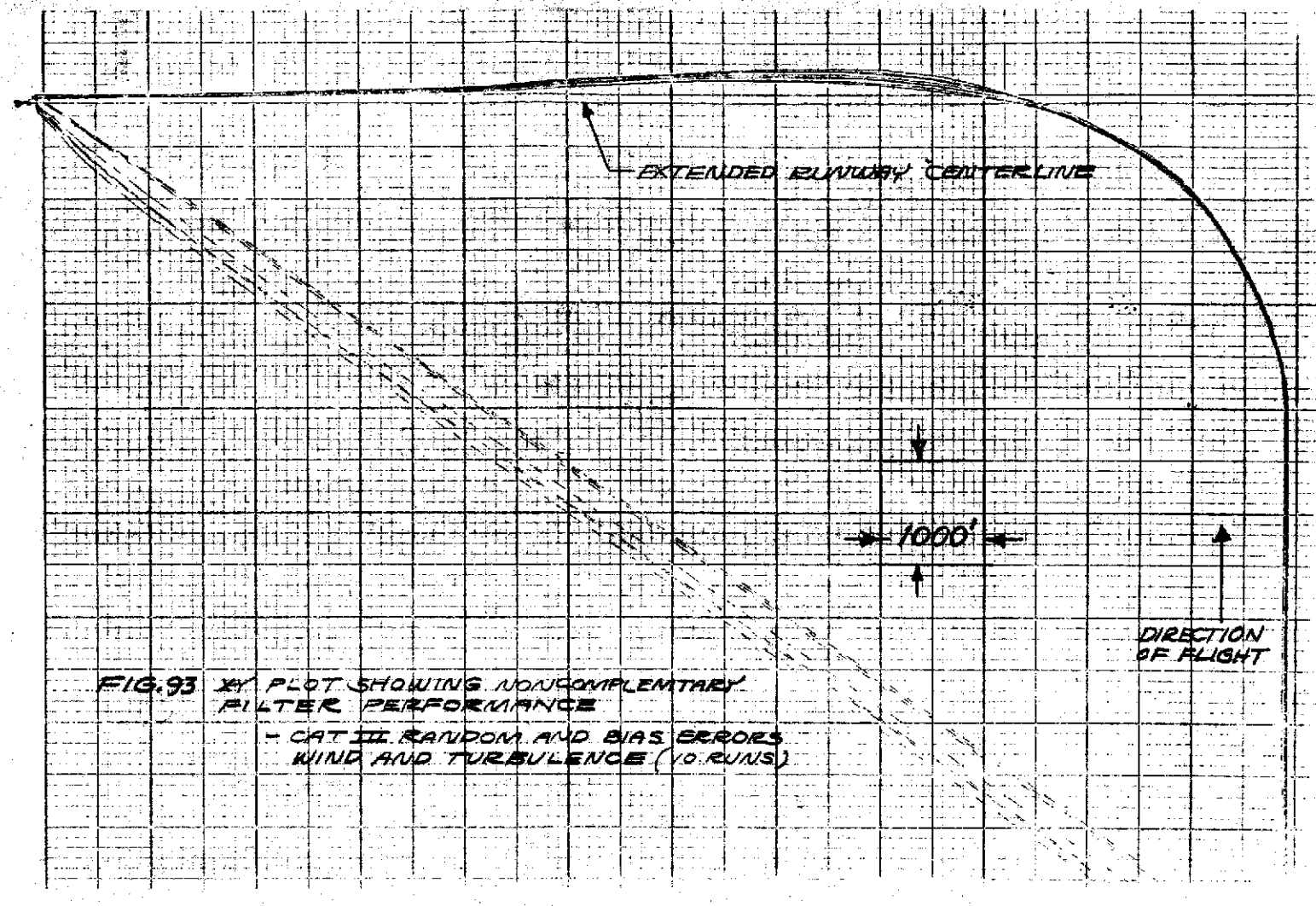

FIG. 93 XY PLOT SHOWING NONCOMPLEMTARY FILTER PERFORMANCE
- CAT III RANDOM AND BIAS ERRORS
WIND AND TURBULENCE (10 RUNS)

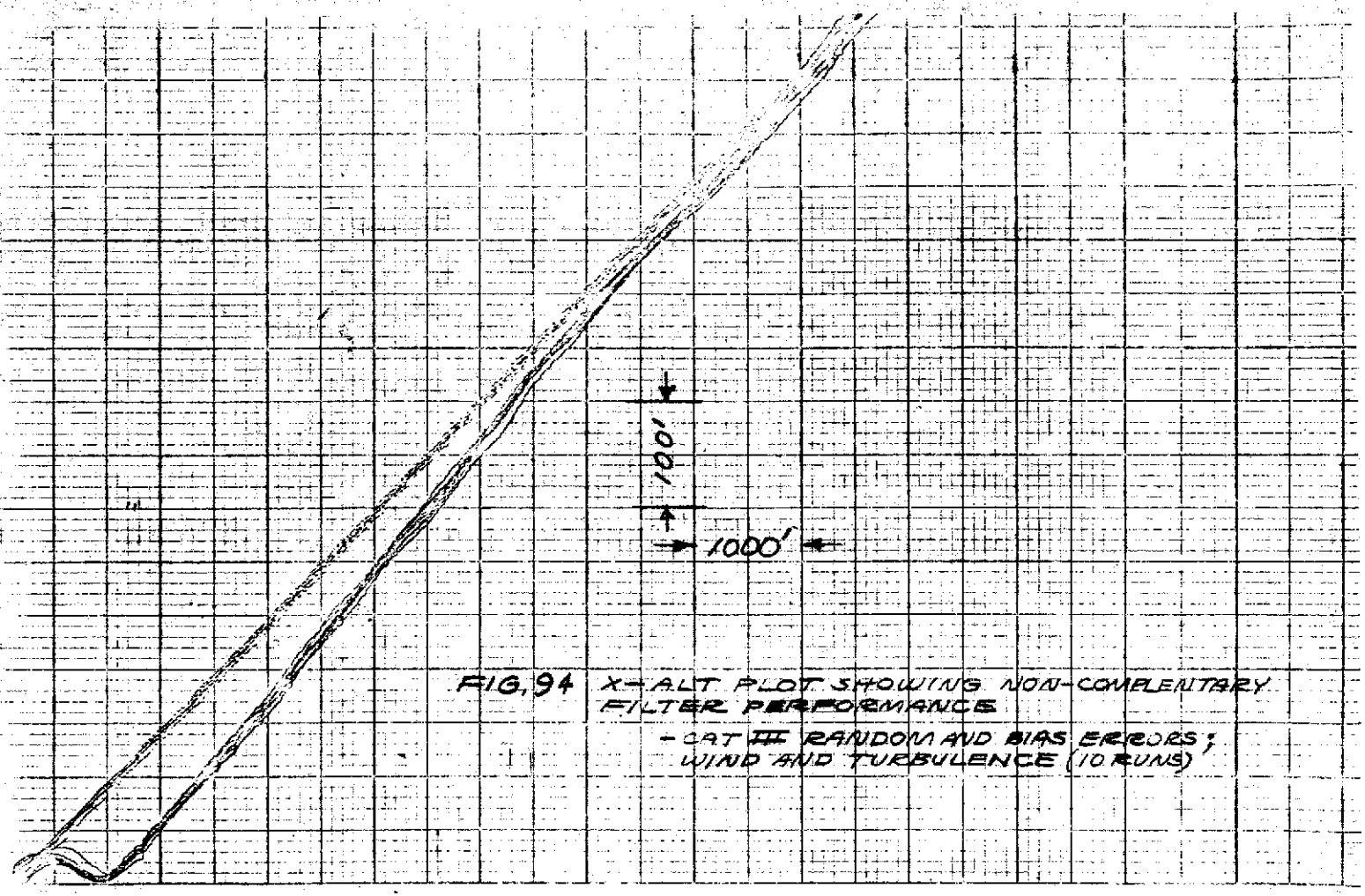

FIG. 94 X-ALT PLOT SHOWING NON-COMPLEMENTARY FILTER PERFORMANCE
- CAT III RANDOM AND BIAS ERRORS; WIND AND TURBULENCE (10 RUNS)

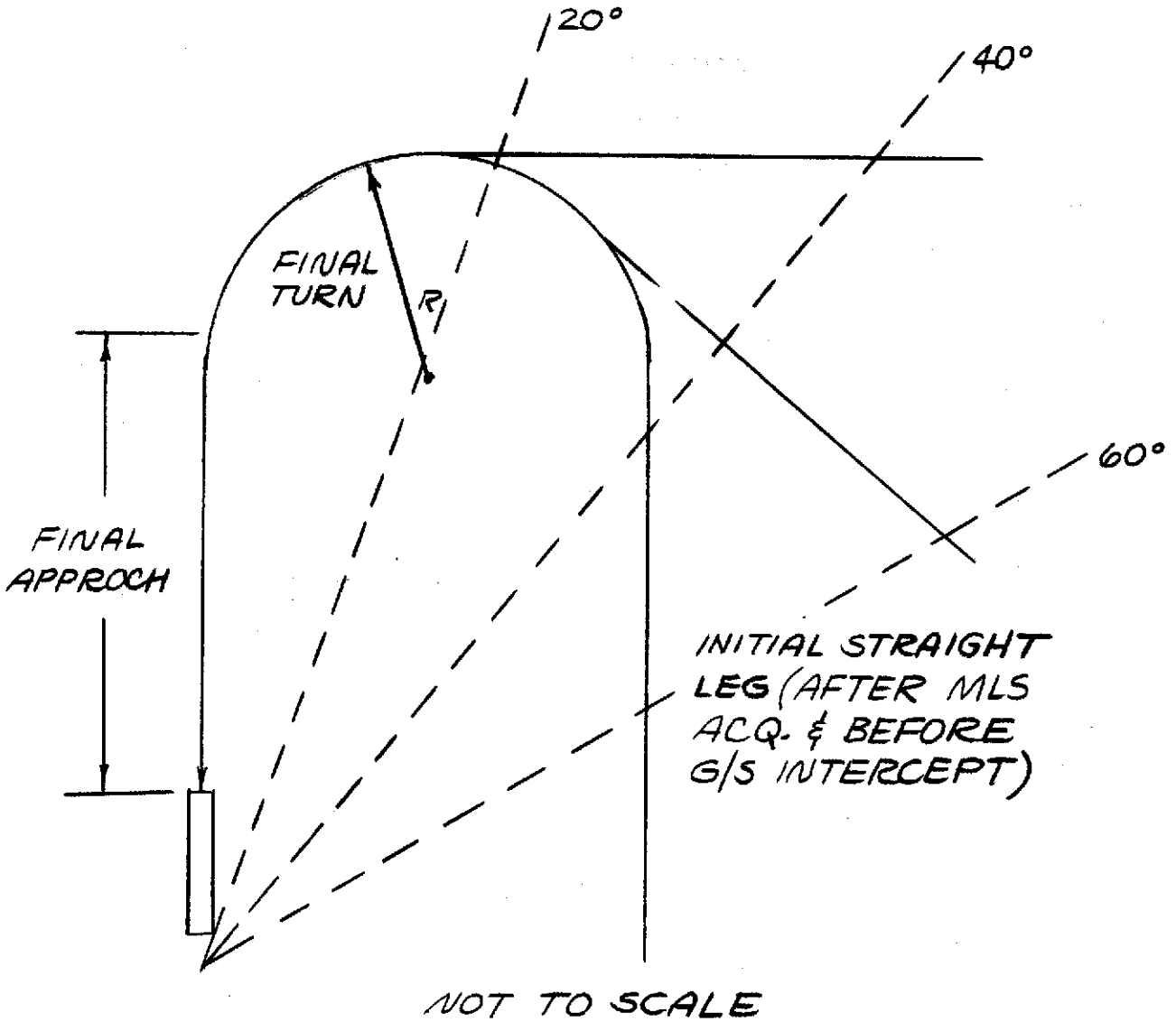

SUMMARY OF RECOMMENDATIONS OF REFERENCES 14 and 15

MIN. INITIAL STRAIGHT LEG – 3 to 6K ft.

MIN. RADIUS OF FINAL TURN – 3 to 4K ft.

MIN. FINAL APPROACH – 1.5 to 6K ft.

FIG. 95- COVERAGE ELEMENTS

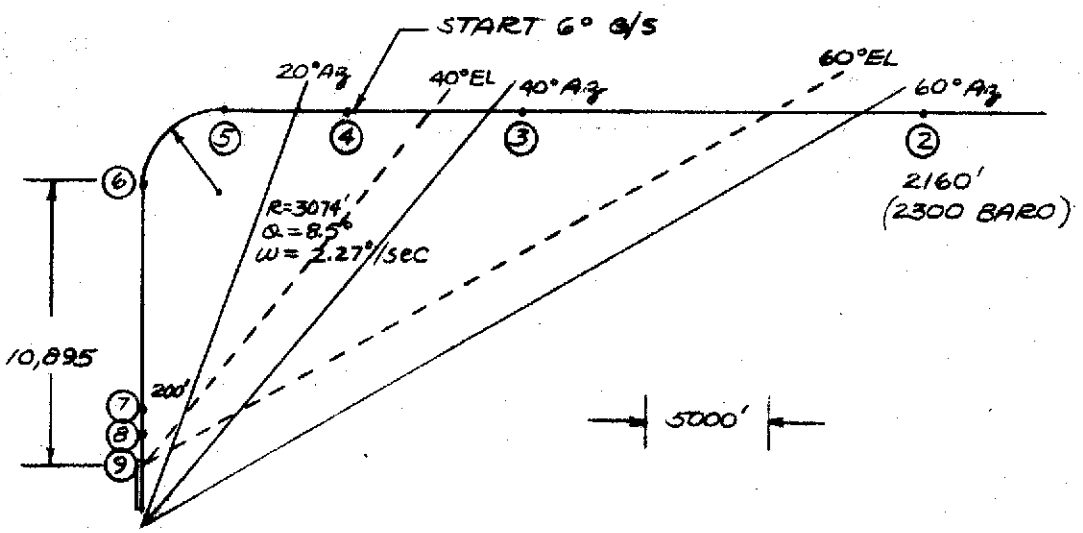

FIG. 96A – 90 DEGREE FLIGHT PATH (FP1)

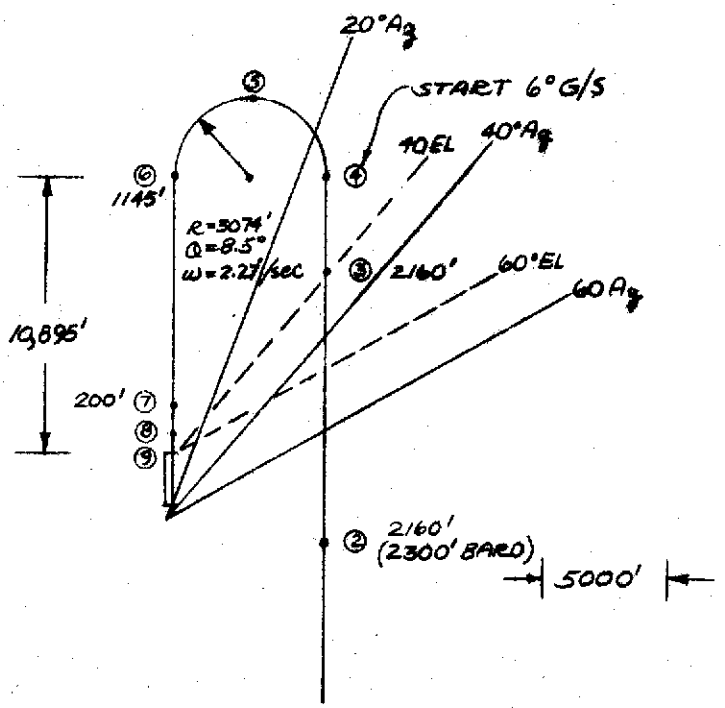

FIG. 96B – 180 DEGREE FLIGHT PATH (FP2)

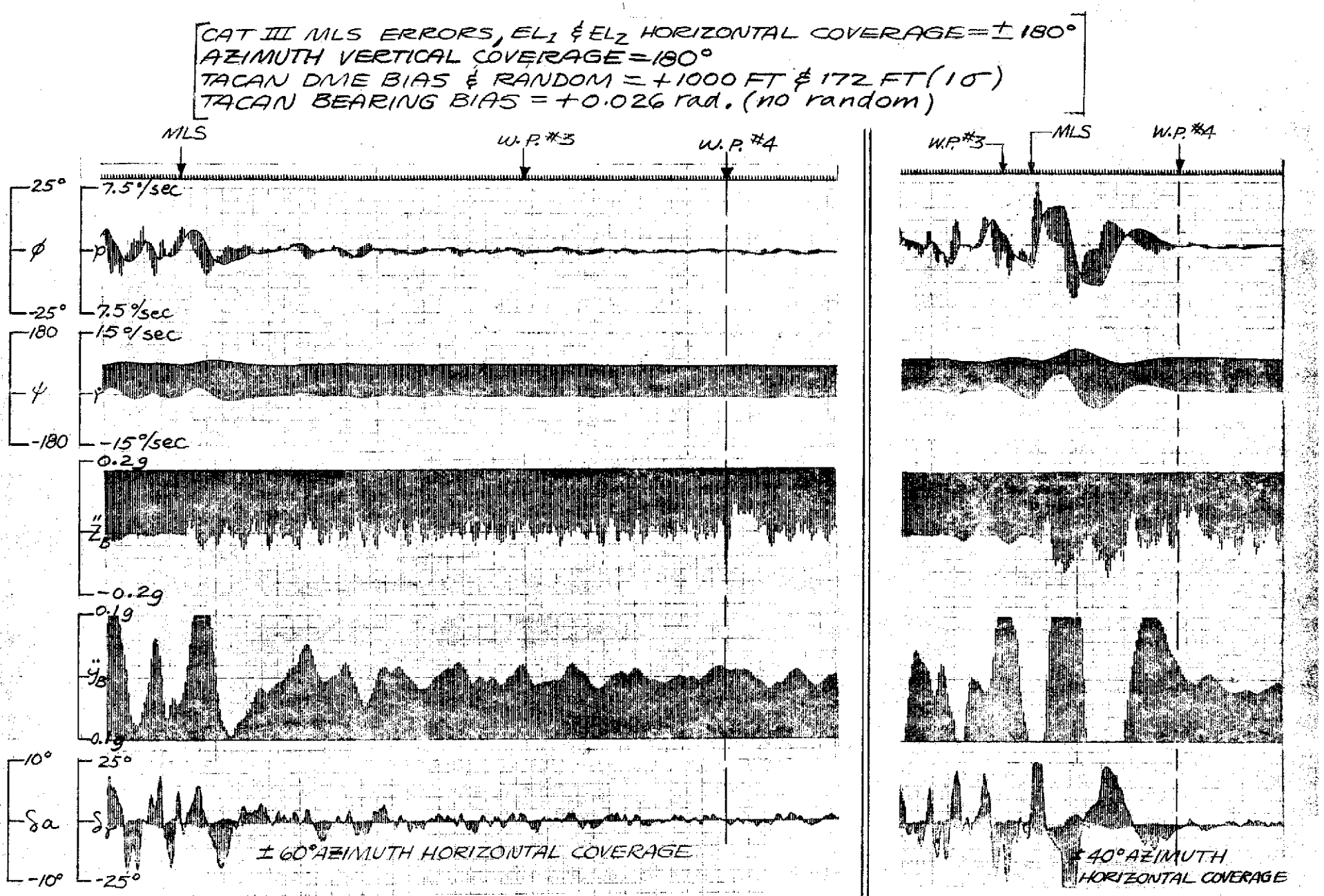

FIG. 97 - COMPARISON OF AIRCRAFT STABILITY AT THE INITIAL DESCENT POINT (W.P. # 4) WITH ± 60° AND ± 40° AZIMUTH HORIZONTAL COVERAGE - FLIGHT PATH # 1

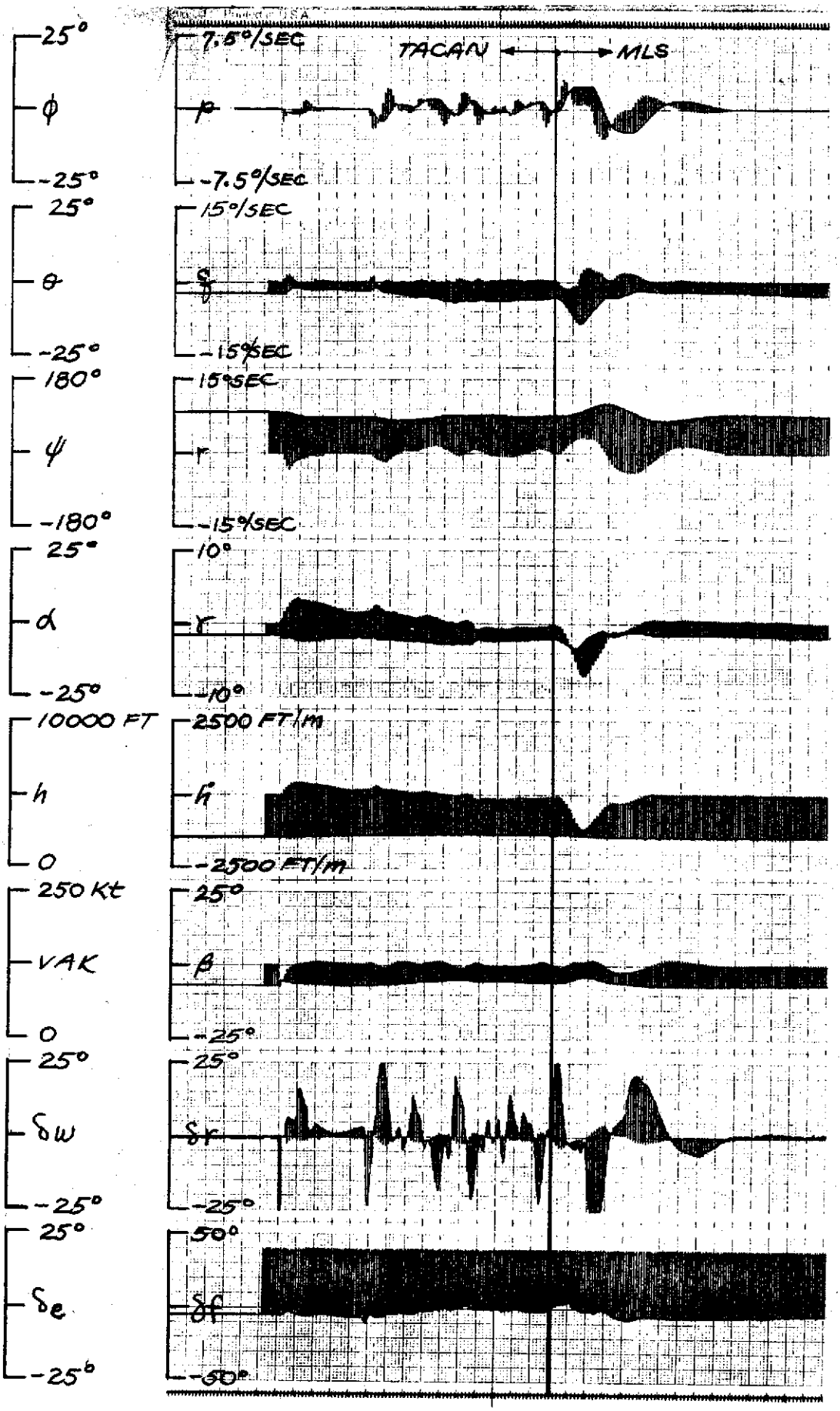

FIG. 97A SAMPLE TIME HISTORY SHOWING THE VERTICAL TRANSITION FROM TACAN TO MLS WITH 125 FT OF TACAN ALTITUDE ERROR. FP = 1
(CAT III MLS ERRORS, MLS Ag
HORIZ. COVER = ±60°, EL VERT COVER = 20°)

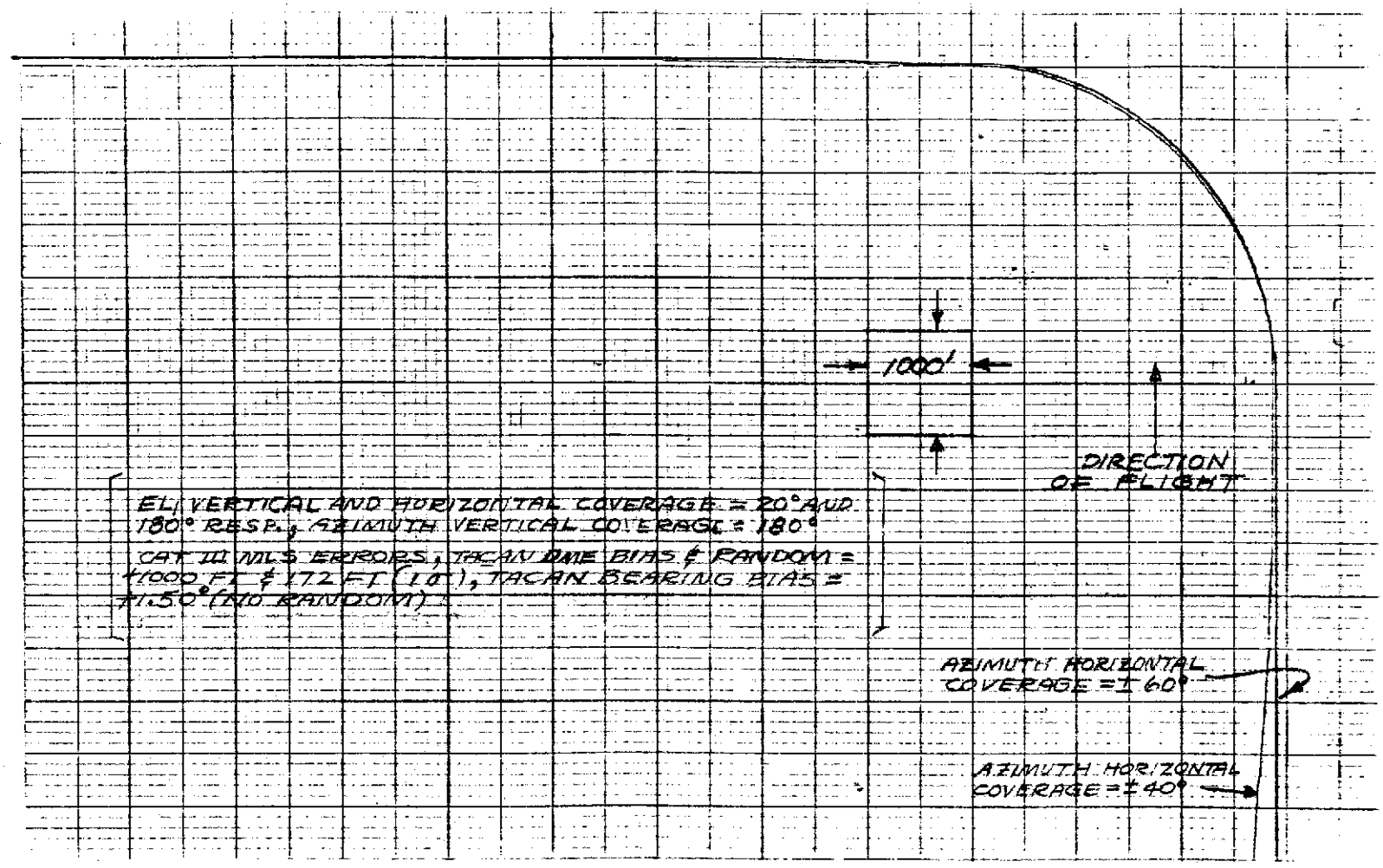

FIG. 98 X-Y PLOT OF FLIGHT PATH #1 WITH ± 40° AND ± 60° AZIMUTH HORIZONTAL COVERAGE

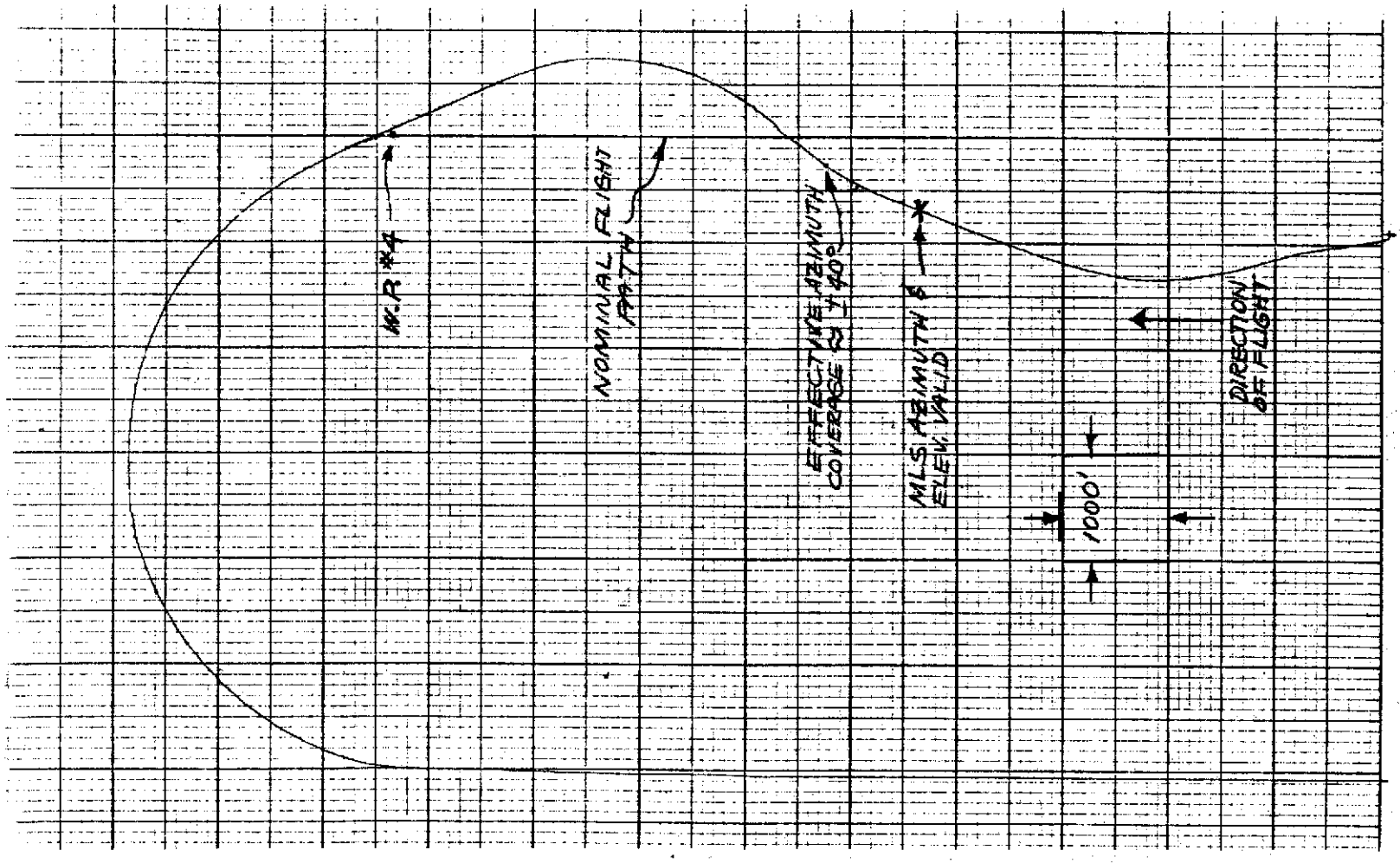

FIG. 99 X-Y PLOT SHOWING EFFECT OF 20° VERTICAL AND ±40° HORIZONTAL COVERAGE FOR FLIGHT PATH #2

AZIMUTH VERTICAL COVERAGE = 180°
EL, VERTICAL COVERAGE = 20°
NO MLS ERRORS
TACAN DME BIAS & RANDOM = +1000 FT. & 172 FT. (1σ),
TACAN BEARING BIAS = +1.50° (NO RANDOM)

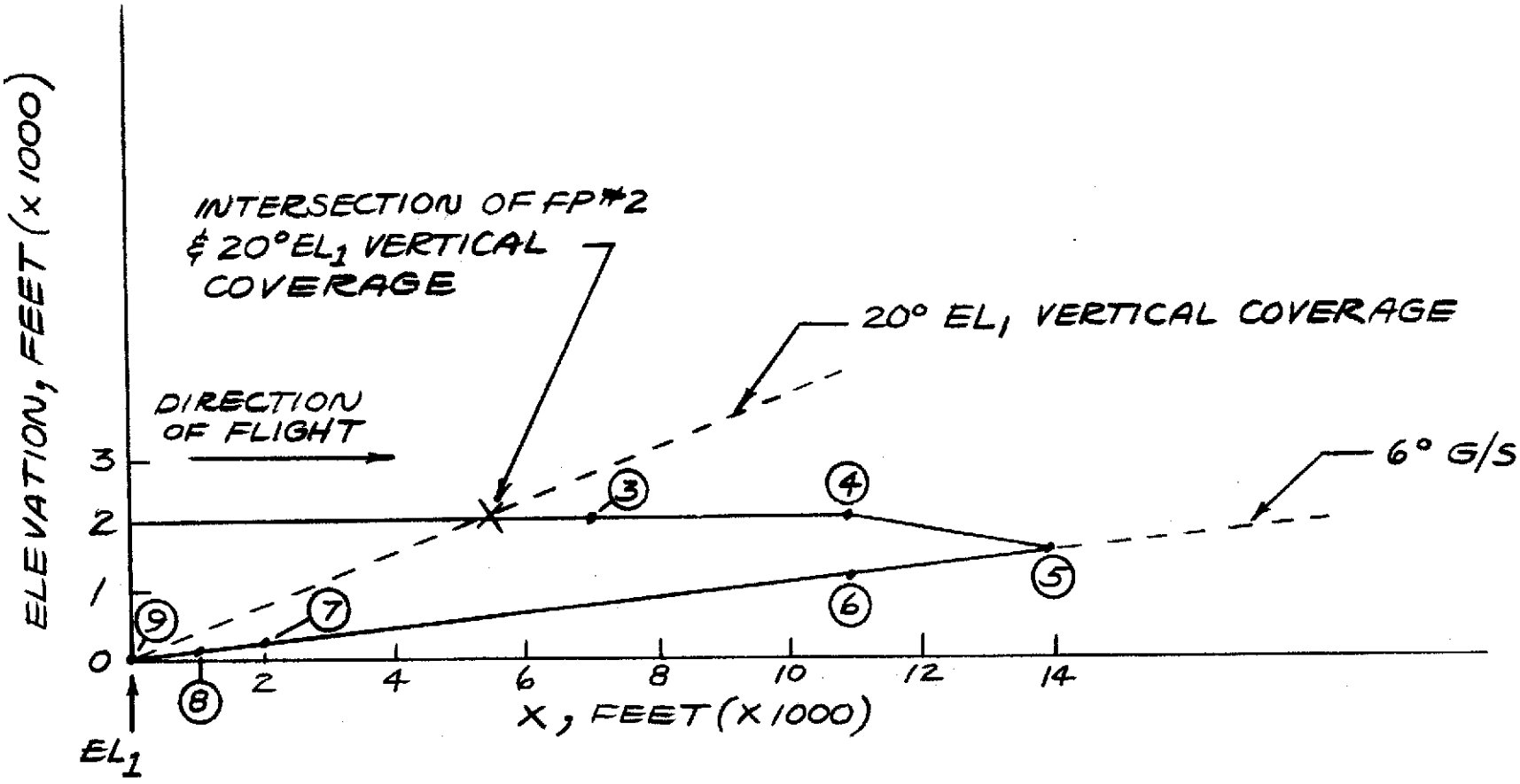

FIG. 100 – X VS ALTITUDE PLOT SHOWING THE INTERSECTION OF FLIGHT PATH #2 AND THE 20° EL_1 VERTICAL COVERAGE.

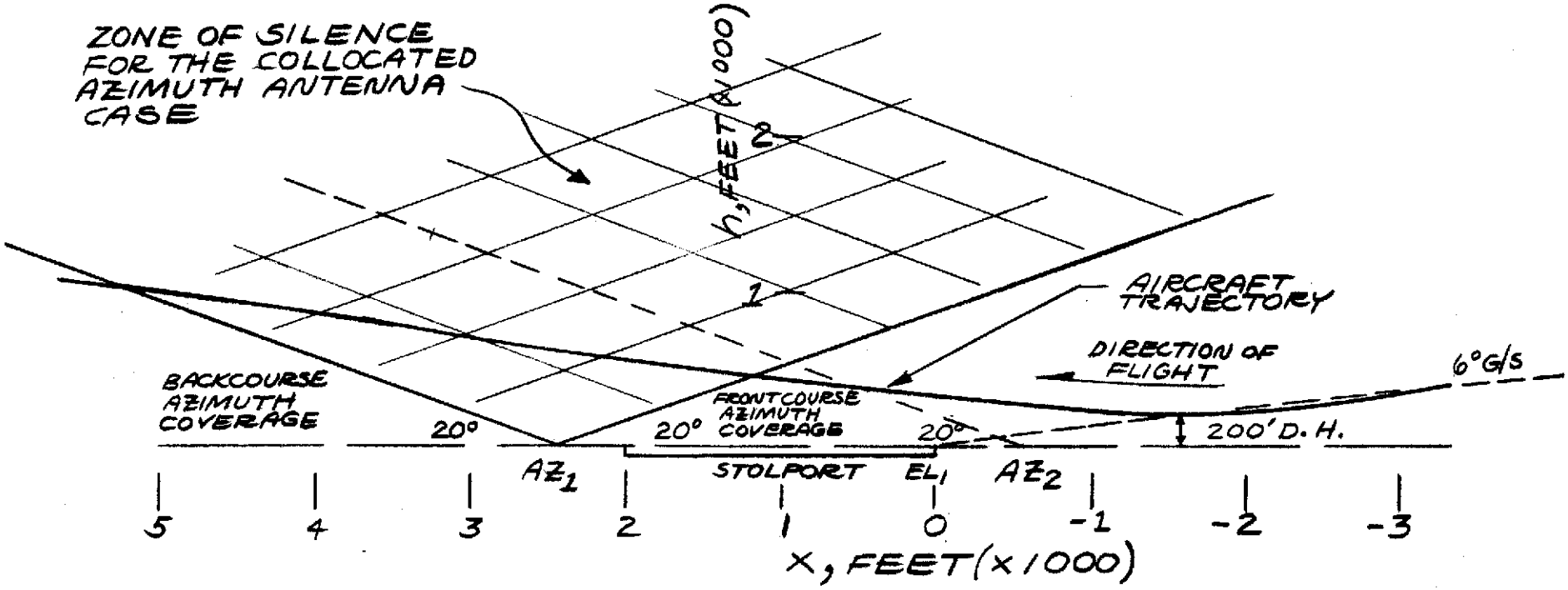

FIG. 101.-THE MLS ZONE OF SILENCE ENCOUNTERED WITH A POTENTIAL STOL STRAIGHT MISSED APPROACH AND COLOCATED AZIMUTH FRONT & BACKCOURSE ANTENNAS

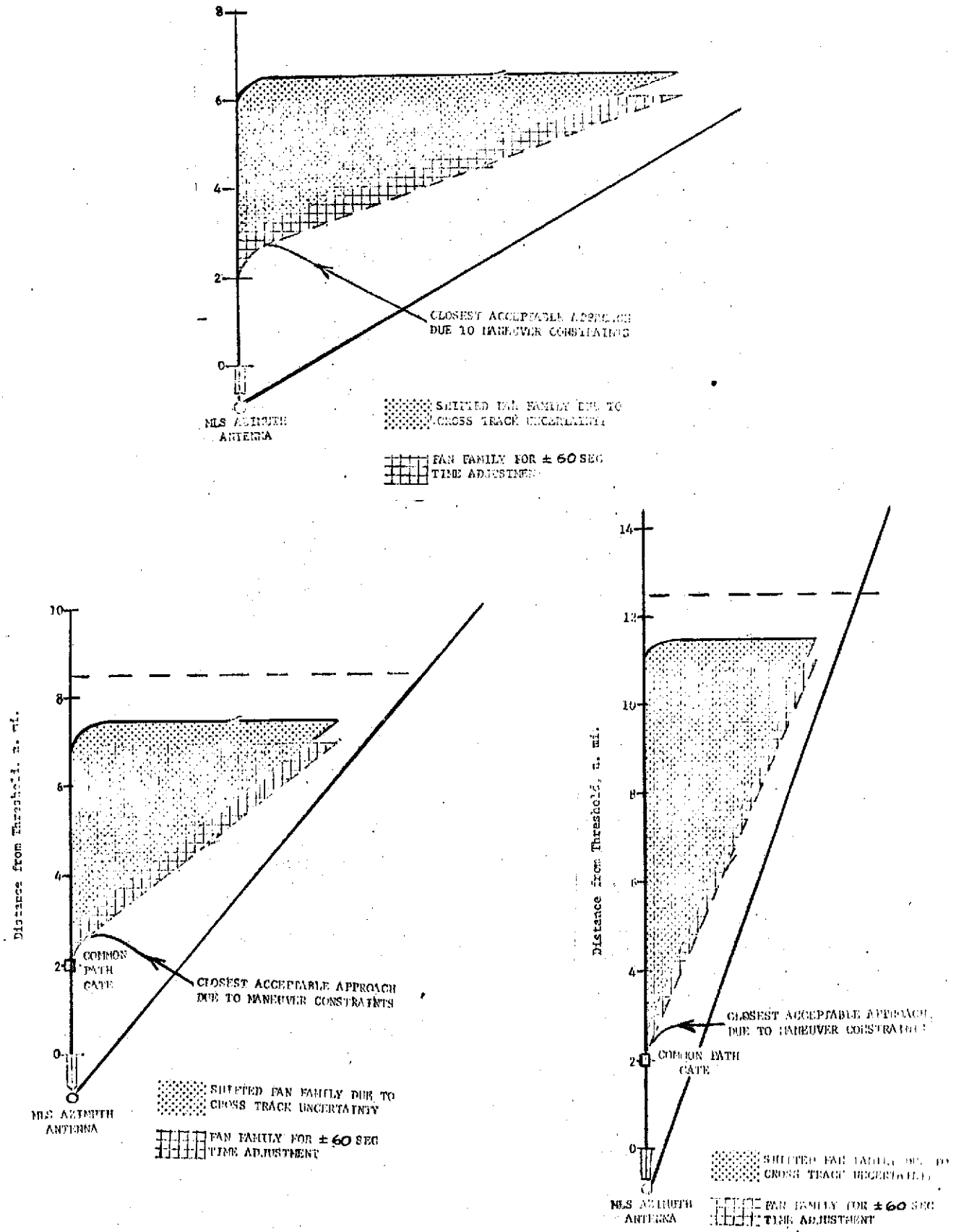

FIG. 102-MLS AIRSPACE REQUIRED FOR 60 SECOND FAN FAMILY WITH VARIOUS AZIMUTH COVERAGES

TABLE A-3. HOURLY CAPACITY FOR A LANDING APPROACH SPEED MIX OF 50% AT 80 kts., 25% AT 100 kts. AND 25% AT 110 kts.

Common Path Length (n.mi.) \ Separation at CPA** (n.mi.)	2.0	3.0
2	42.3	28.9
4	39.6	27.6
8	35.2	25.4

** Closest point of approach.

TABLE A-4. HOURLY CAPACITY FOR A LANDING APPROACH SPEED MIX OF 25% AT 80 kts., 37.5% AT 100 kts. AND 37.5% AT 110 kts.

Common Path Length (n.mi.) \ Separation at CPA** (n.mi.)	2.0	3.0
2	45.6	31.0
4	42.9	29.8
8	38.4	27.5

** Closest point of approach.

FIG. 103

FIG. 104 SAMPLE TIME HISTORY WITH ALL MLS DATA RATES = 5 Hz (INCLUDING EL_2)
[CAT III MLS ERRORS EXCEPT EL, # 2 RANDOM1 = 0.15°, NO TURBULENCE, NOMINAL COMPLENTARY FILTER]

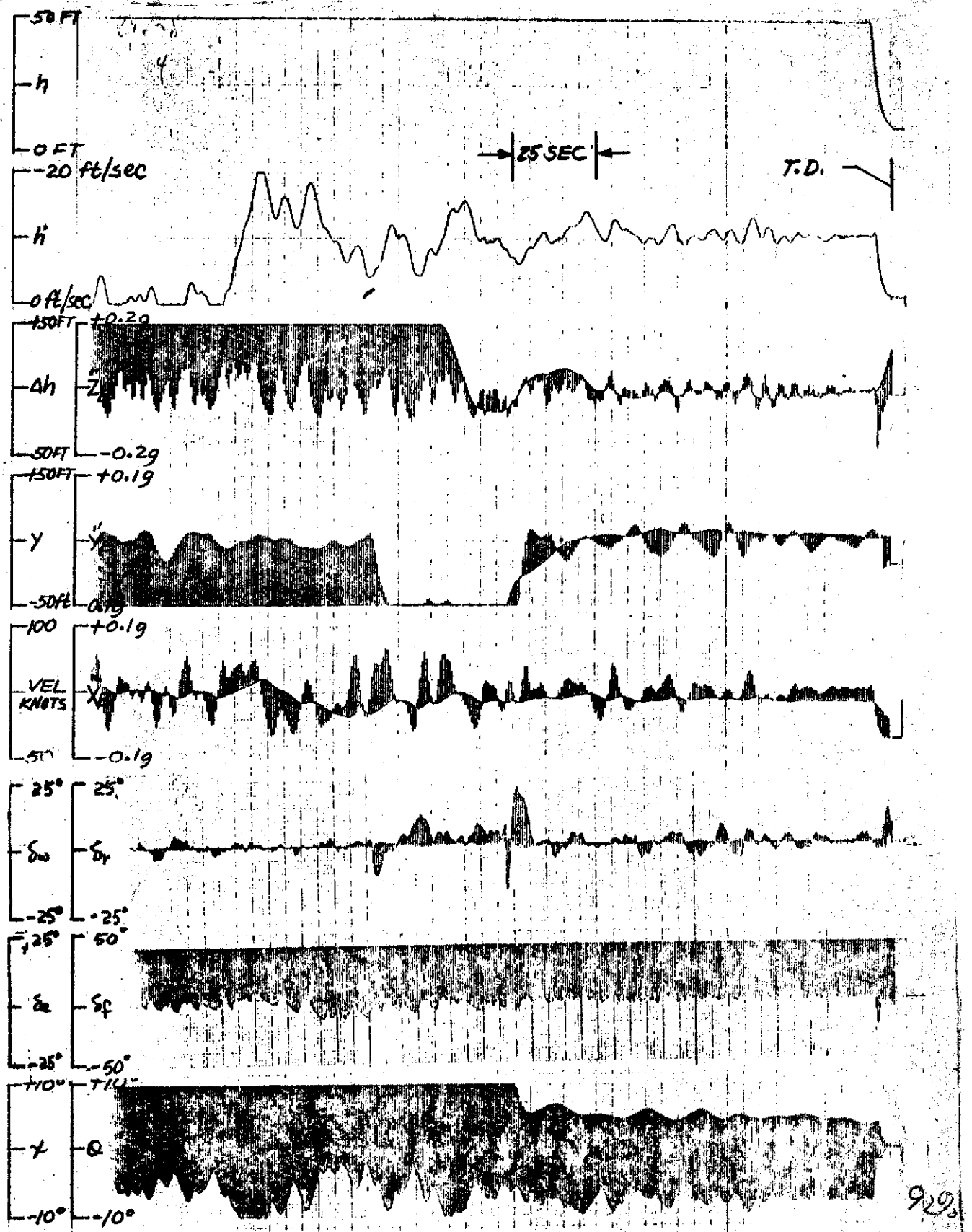

FIG. 105 SAMPLE TIME HISTORY WITH 5 Hz DATA RATE EXCEPT EL_2 = 10 Hz

[CAT III MLS ERRORS EL, & 2. RANDOM = 0.16°
NO TURBULENCE, NOMINAL COMPLEMENTARY FILTER]